Permafrost Carbon Stabilisation by Recreating a Herbivore-Driven Ecosystem

---

Torben Windirsch-Woiwode

Dissertation
zur Erlangung des akademischen Grades
“doctor rerum naturalium“
(Dr. rer. nat.)
in der Wissenschaftsdisziplin “Geochemie“

als publikationsbasierte Arbeit eingereicht an der
Mathematisch-Naturwissenschaftlichen Fakultät
Institut für Geowissenschaften
der Universität Potsdam
und dem
Alfred-Wegener-Institut Helmoltz-Zentrum
für Polar- und Meeresfoschung
Sektion Permafrostforschung

Disputation:	22.01.2024 in Potsdam-Golm
Hauptbetreuer:	Prof. Dr. Guido Grosse
Betreuer:	Prof. Dr. J. Otto Habeck
	Dr. Jens Strauss
Gutachter:	Prof. Dr. Guido Grosse
	Prof. Dr. Timo Kumpula
	Prof Dr. Christian Beer

Published online on the
Publication Server of the University of Potsdam:
https://doi.org/10.25932/publishup-62424
https://nbn-resolving.org/urn:nbn:de:kobv:517-opus4-624240

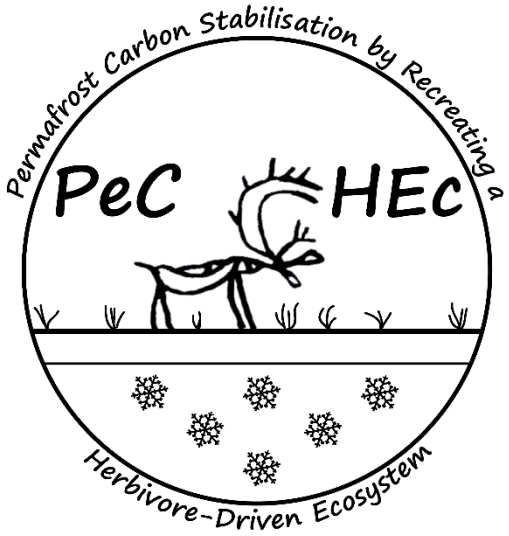

“Lives change worlds. People can save planets or wreck them. That’s the choice. Be the best of humanity.”

- 13th Doctor -

für Josephine und Jonne

Table of contents

ABSTRACT VI

ZUSAMMENFASSUNG VII

ABBREVIATIONS AND NOMENCLATURE IX

CHAPTER 1: INTRODUCTION 1

1.1 SCIENTIFIC BACKGROUND 1
1.1.1 ARCTIC GROUND 1
1.1.2 THE PHENOMENON OF PERMAFROST 1
1.1.3 ARCTIC NON-PERMAFROST AREAS 2
1.1.4 HYPOTHESIS 2
1.2 AIMS AND OBJECTIVES 3
1.3 METHODS 4
1.3.1 FIELD METHODS AND SAMPLING APPROACH 5
1.3.2 STUDY AREA SELECTION 5
1.3.3 LABORATORY METHODS 6
1.4 THESIS ORGANISATION 6

CHAPTER 2: LARGE HERBIVORES ON PERMAFROST – A PILOT STUDY OF GRAZING IMPACTS ON PERMAFROST SOIL CARBON STORAGE IN NORTHEASTERN SIBERIA 9

2.1 ABSTRACT 10
2.2 INTRODUCTION 11
2.3 STUDY AREA 14
2.4 METHODS 17
2.4.1 FIELD SAMPLING APPROACH 17
2.4.2 LABORATORY WORK 19
2.4.3 DATA ANALYSIS AND EXTERNAL DATA 20
2.5 RESULTS 20
2.5.1 VEGETATION ASSESSMENT 20
2.5.2 SEASONAL THAW DEPTH 21
2.5.3 CARBON PARAMETERS (TOC, TOC/TN RATIOS, AND $\Delta^{13}C$ RATIOS) 21
2.5.4 GRAIN SIZE DISTRIBUTION AND WATER CONTENT 23
2.5.5 STATISTICS AND CORRELATION ANALYSIS 24
2.6 DISCUSSION 25
2.6.1 EFFECTS OF GRAZING ON VEGETATION STRUCTURE AND PERMAFROST THAW 25
2.6.2 CARBON ACCUMULATION UNDER GRAZING IMPACT 28
2.6.3 METHODOLOGICAL LIMITATIONS OF THE PILOT STUDY 32
2.7 CONCLUSION 33
2.8 DATA AVAILABILITY STATEMENT 34
2.9 AUTHOR CONTRIBUTIONS 34
2.10 FUNDING 34
2.11 ACKNOWLEDGEMENTS 34
2.12 CONFLICT OF INTERESTS 35

CHAPTER 3: IMPACTS OF REINDEER ON SOIL CARBON STORAGE IN THE SEASONALLY FROZEN GROUND OF NORTHERN FINLAND: A PILOT STUDY 36

3.1 ABSTRACT 37
3.2 INTRODUCTION 37
3.3 STUDY AREA 39
3.4 METHODS 41
3.4.1 FIELD WORK 41

3.4.2 Laboratory analysis 43
3.4.3 Data analysis and calculations 44
3.5 Results 44
3.5.1 Core descriptions 44
3.5.2 Vegetation 46
3.5.3 Carbon parameters 46
3.5.6 Comparative data analysis 49
3.6 Discussion 52
3.6.1 Reindeer impact on soil carbon storage 52
3.6.2 Reindeer impact on vegetation 54
3.6.3 Reindeer impact on ground characteristics 54
3.6.4 SOC density and stocks across the Kutuharju station area 56
3.6.5 Methodological limitations of the pilot study design 56
3.6.6 Implications of the pilot study for future research 56
3.7 Conclusion 57
3.8 Data availability 57
3.9 Author contribution 57
3.10 Competing interests 57
3.11 Acknowledgements 57
3.12 Funding 58
Table 3-1 59
Table 3-2 61
Table 3-3 65

CHAPTER 4: LIPID BIOMARKER SCREENING TO TRACE RECENT LARGE HERBIVORE INFLUENCE ON SOIL CARBON IN PERMAFROST AND SEASONALLY FROZEN ARCTIC GROUND 66

4.1 Abstract 67
4.2 Introduction 67
4.3 Study area 70
4.4 Methods 71
4.4.1 Sampling approach 71
4.4.2 Laboratory analysis 73
4.4.3 Lipid biomarker indices 74
4.4.4 Statistics 75
4.5 Results 75
4.5.1 TOC 75
4.5.2 C/N ratio 76
4.5.3 Stable carbon isotope ratio 78
4.5.4 Absolute *n*-alkane concentration 78
4.5.5 Average chain length 78
4.5.6 Carbon preference index 79
4.5.7 Higher-plant alcohol index 79
4.5.8 Statistical results 79
4.6 Discussion 80
4.6.1 Effects of grazing intensity on biomarker signals 80
4.6.2 Effects of ground thermal regime on soil OM degradation 82
4.6.3 Impact of herbivory on permafrost OM storage 83
4.7 Conclusion 84
4.8 Acknowledgements 85
4.9 Competing interests 85
4.10 Author contribution 85
4.11 Funding 85
4.12 Data availability 86

CHAPTER 5: SYNTHESIS 88

5.1 Ecosystem changes under the impact of large herbivores 88
5.2 Grazing effects on soil organic matter decomposition 89
5.3 Feasibility of utilising herbivory in the Arctic 90
5.4 Research implications for successful planning and use of Arctic herbivory 91

REFERENCES 93

FINANCIAL AND TECHNICAL SUPPORT 104

APPENDIX 1

APPENDIX I ORGANIC CARBON CHARACTERISTICS IN ICE-RICH PERMAFROST IN ALAS AND YEDOMA DEPOSITS, CENTRAL YAKUTIA, SIBERIA 1
APPENDIX II WHAT ARE THE EFFECTS OF HERBIVORE DIVERSITY ON TUNDRA ECOSYSTEMS? A SYSTEMATIC REVIEW (ABSTRACT) 26
APPENDIX III SUPPLEMENTARY MATERIAL TO CHAPTER 2: LARGE HERBIVORES ON PERMAFROST – A PILOT STUDY OF GRAZING IMPACTS ON PERMAFROST SOIL CARBON STORAGE IN NORTHEASTERN SIBERIA 29
APPENDIX IV SUPPLEMENTARY MATERIAL TO CHAPTER 3: IMPACTS OF REINDEER ON SOIL CARBON STORAGE IN THE SEASONALLY FROZEN GROUND OF NORTHERN FINLAND: A PILOT STUDY 36
APPENDIX V SUPPLEMENTARY MATERIAL TO CHAPTER 4: A PILOT STUDY OF LIPID BIOMARKERS TO TRACE RECENT LARGE HERBIVORE INFLUENCE ON SOIL CARBON IN PERMAFROST AND SEASONALLY FROZEN ARCTIC GROUND 44
APPENDIX VI SUPPLEMENTARY MATERIAL TO APPENDIX IV: ORGANIC CARBON CHARACTERISTICS IN ICE-RICH PERMAFROST IN ALAS AND YEDOMA DEPOSITS, CENTRAL YAKUTIA, SIBERIA 51

ACKNOWLEDGEMENTS - DANKSAGUNG 56

Abstract

With Arctic ground as a huge and temperature-sensitive carbon reservoir, maintaining low ground temperatures and frozen conditions to prevent further carbon emissions that contribute to global climate warming is a key element in humankind's fight to maintain habitable conditions on earth. Former studies showed that during the late Pleistocene, Arctic ground conditions were generally colder and more stable as the result of an ecosystem dominated by large herbivorous mammals and vast extents of graminoid vegetation – the mammoth steppe. Characterised by high plant productivity (grassland) and low ground insulation due to animal-caused compression and removal of snow, this ecosystem enabled deep permafrost aggradation. Now, with tundra and shrub vegetation common in the terrestrial Arctic, these effects are not in place anymore. However, it appears to be possible to recreate this ecosystem locally by artificially increasing animal numbers, and hence keep Arctic ground cold to reduce organic matter decomposition and carbon release into the atmosphere.

By measuring thaw depth, total organic carbon and total nitrogen content, stable carbon isotope ratio, radiocarbon age, *n*-alkane and alcohol characteristics and assessing dominant vegetation types along grazing intensity transects in two contrasting Arctic areas, it was found that recreating conditions locally, similar to the mammoth steppe, seems to be possible. For permafrost-affected soil, it was shown that intensive grazing in direct comparison to non-grazed areas reduces active layer depth and leads to higher TOC contents in the active layer soil. For soil only frozen on top in winter, an increase of TOC with grazing intensity could not be found, most likely because of confounding factors such as vertical water and carbon movement, which is not possible with an impermeable layer in permafrost. In both areas, high animal activity led to a vegetation transformation towards species-poor graminoid-dominated landscapes with less shrubs. Lipid biomarker analysis revealed that, even though the available organic material is different between the study areas, in both permafrost-affected and seasonally frozen soils the organic material in sites affected by high animal activity was less decomposed than under less intensive grazing pressure. In conclusion, high animal activity affects decomposition processes in Arctic soils and the ground thermal regime, visible from reduced active layer depth in permafrost areas. Therefore, grazing management might be utilised to locally stabilise permafrost and reduce Arctic carbon emissions in the future, but is likely not scalable to the entire permafrost region.

Zusammenfassung

Mit dem arktischen Boden als riesigem und temperatursensiblen Kohlenstoffspeicher ist die Aufrechterhaltung niedriger Bodentemperaturen und gefrorener Bedingungen zur Verhinderung weiterer Kohlenstoffemissionen, die zum globalen Klimawandel beitragen, ein Schlüsselelement im Kampf der Menschheit, die Erde weiterhin bewohnbar zu halten. Vorangehende Studien ergaben, dass die Bodenbedingungen in der Arktis während des späten Pleistozäns im Allgemeinen kälter und dadurch stabiler waren, als Ergebnis eines Ökosystems, das von großen pflanzenfressenden Säugetieren und weiten Flächen grasartiger Vegetation dominiert wurde - der Mammutsteppe. Gekennzeichnet durch hohe Pflanzenproduktivität (Grasland) und geringe Bodenisolierung aufgrund von Kompression und Schneeräumung durch Tiere, ermöglichte dieses Ökosystem eine tiefreichende Entwicklung des Permafrosts. Heutzutage, mit der vorherrschenden Tundra- und Strauchvegetation in der Arktis, sind diese Effekte nicht mehr präsent. Es scheint aber möglich, dieses Ökosystem lokal durch künstliche Erhöhung der Tierbestände nachzubilden und somit den arktischen Boden kühl zu halten, um den Abbau von organischem Material und die Freisetzung von Kohlenstoff in die Atmosphäre zu verringern.

Durch Messungen der Auftautiefe, des Gesamtgehalts des organischen Kohlenstoffs und Stickstoffs, des stabilen Kohlenstoff-Isotopenverhältnisses, des Radiocarbonalters, der *n*-Alkan- und Alkoholcharakteristika sowie durch Bestimmung der vorherrschenden Vegetationstypen entlang von Beweidungsgradienten in zwei unterschiedlichen arktischen Gebieten habe ich festgestellt, dass die Schaffung ähnlicher Bedingungen wie in der Mammutsteppe möglich sein könnte. Für durch Permafrost beeinflusste Böden konnte ich zeigen, dass eine intensive Beweidung im direkten Vergleich mit unbeweideten Gebieten die Tiefe der Auftauschicht verringert und zu höheren Gehalten an organischem Kohlenstoff im oberen Bodenbereich führt. Für im Winter nur oberflächlich gefrorene Böden konnte kein Anstieg des organischen Kohlenstoffgehalts mit zunehmender Beweidungsintensität festgestellt werden, höchstwahrscheinlich aufgrund von Störfaktoren wie vertikalen Wasser- und Kohlenstoffbewegungen, die nicht durch eine undurchlässige Schicht wie beim Permafrost begrenzt sind. In beiden Gebieten führte eine hohe Tieraktivität zu einer Umwandlung der Vegetation hin zu artenarmen, von Gräsern dominierten Landschaften mit weniger Sträuchern. Die Analyse von Lipid-Biomarkern ergab, dass das verfügbare organische Material zwar zwischen den Untersuchungsgebieten unterschiedlich war, aber sowohl in Permafrostgebieten als auch in saisonal gefrorenen Böden in Bereichen mit hoher Tieraktivität weniger stark zersetzt war als unter geringerer Beweidungsintensität. Zusammenfassend beeinflusst eine hohe Tieraktivität die Zersetzungsvorgänge in arktischen Böden und das thermische Regime des Bodens, was sich in einer reduzierten Tiefe der Auftauschicht in Permafrostgebieten widerspiegelt. Daher könnte das Beweidungsmanagement in Zukunft aktiv eingesetzt werden, um den Permafrost lokal zu

stabilisieren und gefroren zu halten sowie die Kohlenstoffemissionen in der Arktis zu verringern. Aufgrund der Größe der Fläche, die in der terrestrischen Arktis von Permafrost beeinflusst ist, wird ein solches Beweidungsmanagement aber nicht als Maßnahme auf die gesamte Permafrostregion ausgedehnt werden können.

Abbreviations and nomenclature

Notation	Meaning	Unit (if applicable related to SI units)
~	approximately	
°C	degree Celsius	*x* + 273.15 K
°E	longitudinal position in degrees east of the prime meridian	
°N	latitudinal position in degrees north of the equator	
A	stratigraphic unit of the Alas1 core (Appendix IV)	
ACL	average chain length; number of carbon atoms	
AD	Latin: anno Domini; in the year of the Lord	
B	field site in a drained thermokarst basin	
BD	bulk density	g * cm^{-3}
BP	before present (1950)	
bs	below surface	
cal yr BP	calibrated years before present	
CH_4	methane	
cm	centimetre	1 * 10^{-2} m
cm^3	cubic centimetre	1 * 10^{-6} m^3
C/N	ratio between TOC and TN	
CO_2	carbon dioxide	
CPI	carbon preference index	
DCM	dichloromethane: CH_2Cl_2	
DOI	digital object identifier	
e.g.	Latin: exempli gratia; for example	
et al.	Latin: et alii; and others	
eV	electronvolt	1.602176634 * 10^{-19} J
$F^{14}C$	modern fraction of ^{14}C	
Fig.	figure	
g	gram	1 * 10^{-3} kg
GC-MS	gas chromatography mass spectrometer	
GHG	greenhouse gas(es)	
Gt	gigaton	1 * 10^{12} kg
ha	hectare	1 * 10^4 m^2
HPA	higher plant alcohol index	
i.e.	Latin: it est; that is	
J	Joule	kg * m^2 * s^{-2}
K	Kelvin	
kg	kilogram	1 kg
kHz	kilohertz	
km	kilometre	1 * 10^3 m
km^2	square kilometre	1 * 10^6 m^2
m	meter	1 m
m^2	square meter	1 m^2
m^3	cubic meter	1 m^3
MeOH	methanol: CH_3OH	
min	minute(s)	60 s
mm	millimetre	1 * 10^{-3} m
MPa	mega Pascal	1 * 10^6 Pa
MS	mass specific magnetic susceptibility (Appendix IV)	10^{-8} m^3 kg^{-1}

MSTFA	N-Methyl-N-(trimethylsilyl)trifluoroacetamide; $C_6H_{12}F_3NOSi$	
n	number of samples	
NA	not available	
no.	number	
NSO	nitrogen-sulfur-oxigen compounds	
OM	organic matter	
Pa	Pascal	1 Pa
PCA	principal component analysis	
s	second	1 s
S-	field site on reindeer summer ranges	
SOC	soil organic carbon	
SMOW	standard mean ocean water	
ssp.	species (plural)	
T	temperature	°C
TC	total carbon	
TOC	total organic carbon	
TN	total nitrogen	
U	field site on a Yedoma upland	
vol%	per cent by volume	
VPDB	Vienna Pee Dee Belemnite	
W-	field site on reindeer winter ranges	
WIV	wedge ice volume	%
wt%	per cent by weight	
Y	stratigraphic unit of the YED1 core (Appendix IV)	
yr	year(s)	$3.1536 * 10^7$ s
$\delta^{13}C$	stable TOC isotope ratio	‰ vs. VPDB
$\delta^{18}O$	stable oxygen isotope ratio	‰ vs. SMOW
$\delta^{2}H$	stable hydrogen isotope ratio	‰ vs. SMOW
µA	microampere	$1 * 10^{-6}$ A
µg	microgram	$1 * 10^{-9}$ kg
µm	micrometre	$1 * 10^{-6}$ m
σ	sigma; standard deviation	

Chapter 1: Introduction

1.1 Scientific background

1.1.1 Arctic ground

The Arctic is the high-latitude region of the northern hemisphere, defined as the area north of the Arctic Circle at 66.5667 °N. The terrestrial parts of the Arctic are sparsely populated by humans and feature short summer and long and cold winter weather conditions. Apart from resource exploitation and forestry impacts, the various grounds of the Arctic regions are widely undisturbed by direct anthropogenic impacts. Climate warming shows dramatic effects and changes, especially on seasonal or perennially frozen ground (Fig. 1-1).

1.1.2 The phenomenon of permafrost

Perennially frozen ground called permafrost, defined as ground colder than 0 °C for at least two consecutive years (Van Everdingen 1998), is mainly a relic of the last Ice Age. The permafrost region – the area in which permafrost can be found – covers approximately 22 % of the Northern hemisphere's land surface (Obu *et al.* 2019). This frozen state allows for the storage of organic matter (OM) under conditions with slow to no decomposition, since the main driver behind decomposition is temperature-controlled microbial activity (Schuur *et al.* 2008). Current estimates for the amount of carbon stored in the permafrost region (including non-frozen areas) are 813 Pg within the top 3 m of ground (Palmtag *et al.* 2022) out of a global soil carbon pool of 2050 to 2800 Pg (Jackson *et al.* 2017, Strauss *et al.* 2021). With accelerated and sometimes abrupt thaw of permafrost deposits driven by global warming, this permafrost-stored carbon becomes gradually available for microbial decomposition. The ground releases carbon in the forms of CO_2 and CH_4 (Turetsky *et al.* 2019, Bowen *et al.* 2020). Therefore, one of the key aims of human actions against global warming should, besides stopping direct fossil fuel emissions (Abbott *et al.*

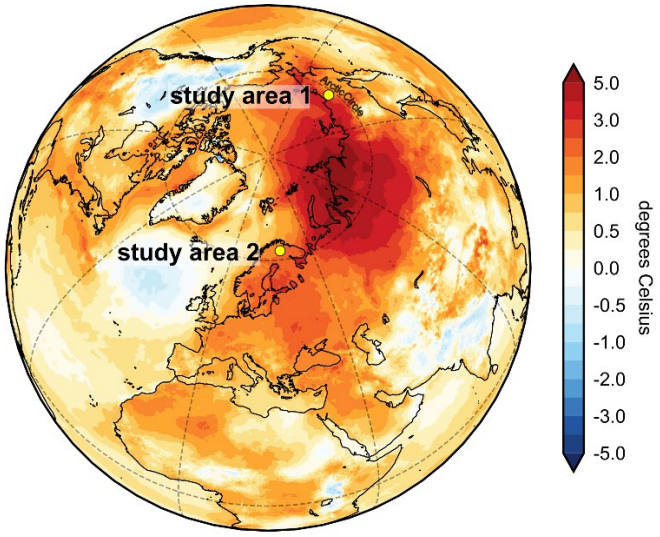

Figure 1-1 – surface temperature anomaly map for 2020 of the northern hemisphere, reference period 1981-2010; study areas used in this thesis are indicated by yellow dots; study area 1: Cherskiy, Siberia; study area 2: Kaamanen, Finland; map modified after Copernicus Climate Change Service, European State of the Climate.

2022), be the preservation of these frozen carbon deposits. Since the Arctic permafrost region faces amplified warming, up to four times the global average, this is a challenging effort.
The ground in areas affected by permafrost also contains a seasonally frozen/thawed top layer called the 'active layer', This layer thaws in the summer down to the 'permafrost table', below which the ground stays frozen year round. In winter, the active layer refreezes both from the cold winter air temperatures on top and from the frozen ground underneath. The active layer contains OM, which is available for microbial activity in summer. Further, the seasonally unfrozen conditions allow for vertical and lateral compound mobility, greenhouse gas (GHG) fluxes (mainly vertical), and lateral water movement on top of the impermeable permafrost table.

1.1.3 Arctic non-permafrost areas

Not all terrestrial Arctic areas contain permafrost beneath the surface. In northern Fennoscandia, for example, permafrost distribution is quite heterogeneous. In fact, the permafrost is 'sporadic' (10-50 % areal coverage) and 'isolated' (0-10 % areal coverage) (Obu et al. 2019) and exists mostly in mountain areas and in the form of frozen peat hills called 'palsas' (Gisnås et al. 2017). Warming air and ground temperatures threaten to decrease permafrost extent in the Arctic. With climate change, even the extent of 'continuous' (more than 90 % areal coverage) permafrost is decreasing, becoming 'discontinuous' (50-90 % areal coverage) in some areas. Consequently, the areal fraction non-permafrost is increasing. However, non-permafrost areas may still contain a top layer of seasonally frozen ground. In non-permafrost areas, the OM content therefore becomes available for microbial decomposition year-round, except for the top layer that still freezes in winter. Hence, permafrost degradation provides more available OM for the active global carbon cycle.

1.1.4 Hypothesis

In 1995, Zimov *et al.* (1995) published their findings of a prehistoric stable ecosystem in the cold environments of the high latitudes. This ecosystem called mammoth steppe was characterised by vast grasslands and a high population density of large herbivorous mammals. These herbivores had two major effects on ground conditions: (1) they compressed the snow in winter, mitigating its insulating effect on the ground, and (2) they maintained the graminoid-dominated vegetation by trampling damage and selective browsing. Both activities led to a colder ground thermal regime, because cold winter temperatures were able to penetrate the ground more effectively as the snow was trampled down causing less insulation, and the graminoids did also not function like a wind shield/snow fence (Fig. 1-2). As another effect, graminoid-dominated vegetation is very productive and re-grows every year, fixating

carbon from the atmosphere and hence helping to maintain comparatively low atmospheric carbon levels (Zimov *et al.* 2012). With the disappearance of the mammoth and drastic climatic warming following the last Ice Age, vegetation shifted, creating the hardy and less productive tundra vegetation we see today. Along with ongoing shrubification (Mekonnen *et al.* 2021), both key effects of the mammoth steppe are no longer in place. Further, the process of shrubification helps warm the underlying ground by creating a buffer layer while trapping larger amounts of snow in the shrubs. This effect could be reduced by an intensified large herbivore presence through trampling, snow compression, and browsing (Pearson *et al.* 2013).

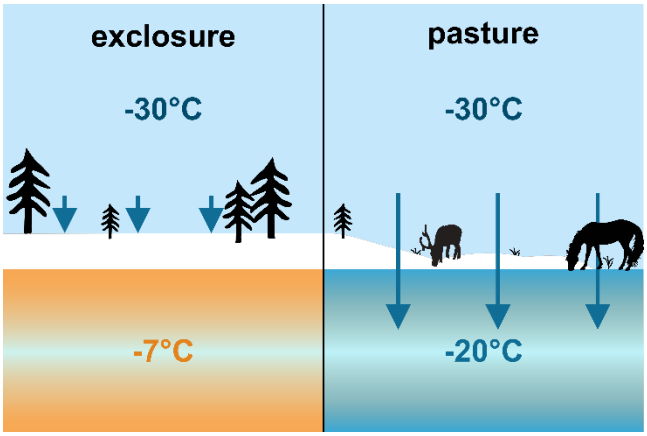

Figure 1-2 – Schematic comparison of the impact of large-herbivore grazing on winter soil temperatures; thick insulating snow results in warmer soil temperatures, whereas snow compaction, snow removal and vegetation changes induced by herbivory lead to colder ground conditions; temperatures provided are exemplary to illustrate the effects of snow compaction and removal.

Therefore, scientists hypothesised that recreating a grazing pressure similar to the Pleistocene in Arctic landscapes would again lead to colder ground conditions and hence reduced OM decomposition (Zimov 2005). It has already been shown that grazing reduces CH_4 emissions from permafrost while at the same time enhancing carbon cycling due to the altered vegetation composition (Fischer *et al.* 2022).

A crucial point is the season length, because relying on cold winter air temperatures to maintain cold ground temperatures only works if winter is much longer than summer. Further, graminoid-dominated vegetation provides only little insulation against warm summer temperatures.

In addition, the increased extent of seasonally frozen ground in the Arctic's permafrost-free areas requires testing this hypothesis for these environments as well. Seasonally frozen ground likely behaves differently under large herbivore impacts, especially for animal-introduced fertilization and compaction. Since the main season for animal-induced effects on the soil is during the summer months and under unfrozen conditions, these deposits can also be compared to grazed areas in temperate regions, where intensive grazing increases soil carbon (Mudge *et al.* 2011).

1.2 Aims and objectives

As reduced OM degradation should lead to higher soil carbon content, this should be measurable when comparing soil samples from comparable sites with different herbivore grazing intensities. The overall question is if large herbivore action increases soil carbon storage, and further if it provides fresh material for in-soil storage or reduces decomposition processes.

The detailed aims of this thesis are as follows:

1) Identifying the effects of large herbivore presence on Arctic permafrost-affected ground and its carbon stock
2) Investigating large herbivore effects on ground characteristics in Arctic seasonally frozen soils
3) Linking the findings of (1) and (2) to decipher the processes controlling organic carbon decomposition.

1.3 Methods

To answer these research aims, a variety of field and laboratory methods from sedimentology, biogeochemistry and organic geochemistry was applied. This includes several field campaigns to the Arctic in order to collect samples that were processes as described in figure 1-3.

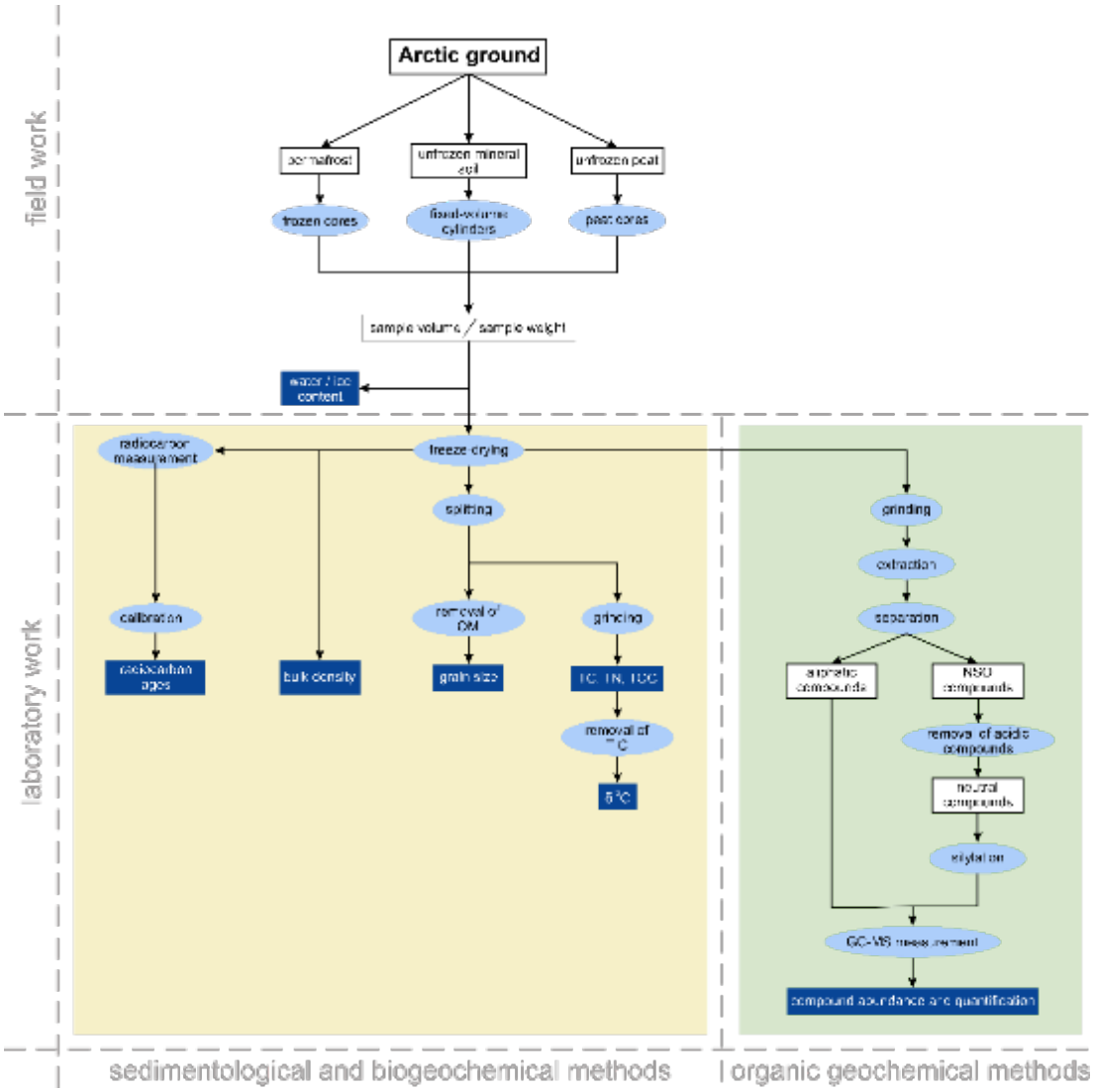

Figure 1-3 – Flow chart depicting the methods used in this thesis; white boxes indicate intermediate (sample) states, light blue highlights processes and treatments, dark blue indicates results; analysis of these results is not included in this figure.

1.3.1 Field methods and sampling approach

During the field campaigns, I encountered several deposit types that each required different sampling methods. Frozen ground was sampled using a portable Snow-Ice-Permafrost-Research-Establishment (SIPRE) auger to obtain intact soil cores. Unfrozen mineral soil deposits were sampled by excavating a soil profile down to the parent material. After cleaning the soil profile wall, samples were taken using stainless steel fixed-volume cylinders. Unfrozen peat deposits were sampled using an Eijkelkamp peat corer. The peat was subsequently subsampled in 5 cm increments. From all unfrozen deposits, biomarker subsamples were taken in the field using sterile and annealed glass jars that were frozen afterwards until further analysis in the laboratory. The aim was a continuous set of subsamples, but sampling locations within the soil column were shifted in unfrozen mineral soils to specifically capture individual soil horizons and visible shifts in material.

The sampling locations were selected for homogeneity of the soil but across different grazing intensities, covering a span from large herbivore exclosures to intensively used pasture areas. Along with grazing intensity, vegetation composition changed along these transects.

1.3.2 Study area selection

In order to find such grazing transects, sampling had to take place in areas with a known history of herbivory under controlled circumstances and with existing exclosure sites and in general known grazing intensities to test for the hypothesis of large herbivore impacts on soil carbon storage. For this, we selected the Pleistocene Park experimental area in the Kolyma river lowlands in northeastern Siberia (papers 1 and 3; chapters 2 and 4) and the Kutuharju Field Research Station premises near Kaamanen in northern Finland (papers 2 and 3; chapters 3 and 4) (Fig. 1-1). The grazing history under controlled conditions is depicted in figure 1-4.

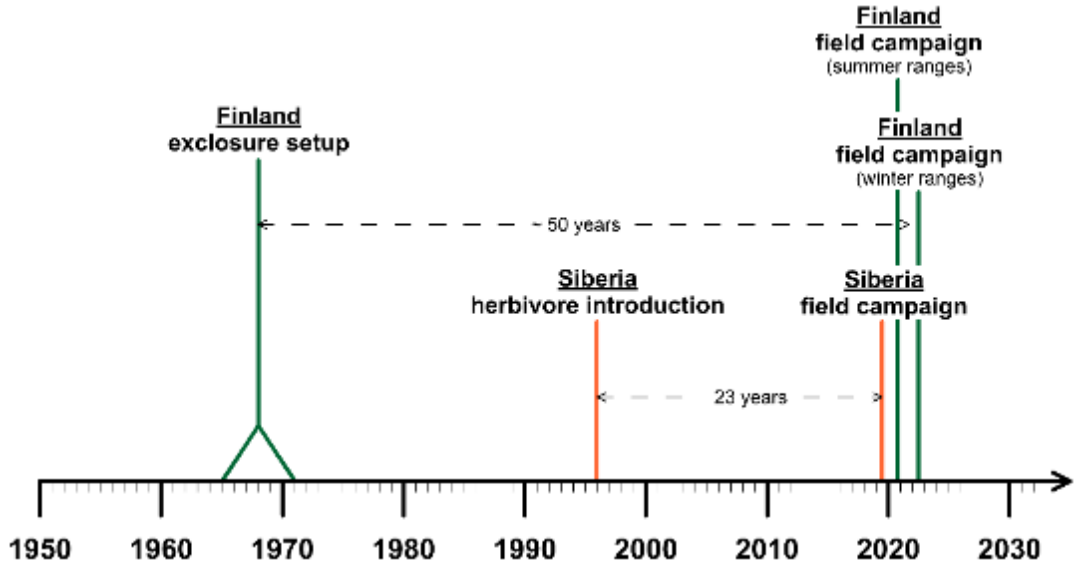

Figure 1-4 – Timeline of the controlled grazing history for both study areas, showing the time of (controlled) large herbivore introduction and the times of sampling; x-axis provides the calendar years in yr AD.

1.3.3 Laboratory methods

To determine the parameters shown in figure 1-3, the following methods were applied in the laboratory. Bulk density (BD) was derived from sample weight after freeze-drying with a Zirbus Sublimator 15, and sample volume, for all samples with known volume. Using the weight pre- and post-drying, the water content was calculated. Grain size distribution was measured for all mineral soil samples using a laser particle sizer (Malvern Panalytical MasterSizer 3000). Total carbon (TC) and total organic carbon (TOC) contents were measured via pyrolysis with an Elementar soliTOC cube. Total nitrogen (TN) content was determined using an Elementar rapidMAX N. The stable carbon isotope ($\delta^{13}C$) ratio of the TOC content was determined using a Delta V Advantage Isotope Ratio mass spectrometry supplement equipped with a Flash 2000 Organic Elemental Analyser. Results are reported in reference to the Vienna Pee Dee Belemnite standard (Coplen *et al.* 2006). Sample ages were determined by radiocarbon dating at the MICADAS facility at AWI (Mollenhauer *et al.* 2021). Ages were calibrated using the Calib 8.2 calibration software (Stuiver *et al.* 2021) applying the IntCal20 calibration curve (Reimer *et al.* 2020). For dating, macro-organic material was selected, if available. In other cases, the bulk sediment material was used.

Lipid biomarker analysis of the alcohol fraction and the *n*-alkane fraction was used as an OM quality proxy (chapter 4). For this analysis, lipids were extracted by accelerated solvent extraction (Dionex ASE 350) and subsequently the fractions were separated by medium pressure liquid chromatography (MPLC, Radke *et al.* (1980)) into aliphatic, aromatic and NSO compounds, and column chromatography using acidified columns for separation of the NSO fraction into alcohol fraction (neutral) and fatty acid fraction (acidic). For measurement using an ISQ 7000 Single Quadrupole Mass Spectrometer equipped with a Trace 1310 Gas Chromatograph, the alcohol fraction was silyllated using a 50:50 v/v mixture of DCM and MSTFA. Resulting spectrograms were analysed using the Xcalibur software.

For statistical data analysis, principal component analysis (PCA) was realised in the R software environment using the ‘stats’ package (R Core Team 2021).

1.4 Thesis organisation

This cumulative dissertation consists of several chapters.

In this chapter 1, an introduction into Arctic ground and permafrost is given. This chapter highlights the importance of research on stabilising mechanisms for Arctic soil carbon storage. It outlines the scientific questions and objectives and provides an overview of the methods used in this thesis.

Chapters 2 to 4 contain original research articles, either already published in peer-reviewed journals or currently under review (table 1-1). Chapter 2 shows the exemplary influence of large herbivores on ground characteristics in a Siberian permafrost environment (Windirsch *et al.* 2022a). In chapter 3, a similar approach on large herbivore influence on seasonally frozen

Arctic ground in northern Finland is presented (Windirsch *et al.* 2023c). Chapter 4 uses samples from both previous chapters and examines the degradation state of the OM in reference to herbivory using lipid biomarker analysis (Windirsch *et al.* under review). In chapter 5, the findings of the previous chapters are synthesised and discussed in a broader context, referring to the aims and questions raised in chapter 1.

Appending to these chapters is supplementary material which was originally submitted along the articles from chapters 2 to 4, as well as another publication on permafrost organic carbon storage from a haymaking area in Central Yakutia (appendix I) and the abstract of a systematic literature review article on herbivore diversity effects on tundra ecosystems (appendix II).

Table 1-1 – Overview of the publications contained in this thesis.

Chapter 2	*Large Herbivores on Permafrost – a Pilot Study of Grazing Impacts on Permafrost Soil Carbon Storage in Northeastern Siberia* Windirsch, T., Grosse, G., Ulrich, M., Forbes, B. C., Göckede, M., Wolter, J., Macias-Fauria, M., Olofsson, J., Zimov, N., and Strauss, J. (2022), Frontiers in Environmental Science 10, doi: 10.3389/fenvs.2022.893478
Chapter 3	*Impacts of Reindeer on Soil Carbon Storage in the Seasonally Frozen Ground of Northern Finland* Windirsch, T., Forbes, B. C., Grosse, G., Wolter, J., Stark, S., Treat, C. C., Ulrich, M., Fuchs, M., Olofsson, J., Kumpula, T., Macias-Fauria, M., and Strauss, J. (2023), Boreal Environment Research
Chapter 4	*A Pilot Study of Lipid Biomarkers to Trace Recent Large Herbivore Influence on Soil Carbon in Permafrost and Seasonally Frozen Arctic Ground* Windirsch, T., Mangelsdorf, K., Grosse, G., Wolter, J., Jongejans, L. L., and Strauss, J. (under review), Arctic Science
Appendix I	*Organic Carbon Characteristics in Ice-rich Permafrost in Alas and Yedoma Deposits, Central Yakutia, Siberia* Windirsch, T. Grosse. G. Ulrich, M., Schirrmeister, L., Fedorov, A. N., Konstantinov, P. Y., Fuchs, M., Jongejans, L. L., Wolter, J., Opel, T., and Strauss, J. (2020), Biogeosciences 17, doi: 10.5194/bg-17-3797-2020
Appendix II	*What are the effects of herbivore diversity on tundra ecosystems? A systematic review* Barbero-Palacios, L., Barrio, I. C., Axmacher, J. C. *et al.,* abstract, publication in preparation for submission to Environmental Evidence
Appendix III	Supplementary material to *Large Herbivores on Permafrost – a Pilot Study of Grazing Impacts on Permafrost Soil Carbon Storage in Northeastern Siberia* (chapter 2)
Appendix IV	Supplementary material to *Impacts of Reindeer on Soil Carbon Storage in the Seasonally Frozen Ground of Northern Finland* (chapter 3)
Appendix V	Supplementary material to *A Pilot Study of Lipid Biomarkers to Trace Recent Large Herbivore Influence on Soil Carbon in Permafrost and Seasonally Frozen Arctic Ground* (chapter 4)
Appendix VI	Supplementary material to *Organic Carbon Characteristics in Ice-rich Permafrost in Alas and Yedoma Deposits, Central Yakutia, Siberia* (appendix I)

Chapter 2: Large Herbivores on Permafrost – a Pilot Study of Grazing Impacts on Permafrost Soil Carbon Storage in Northeastern Siberia

Large Herbivores on Permafrost – a Pilot Study of Grazing Impacts on Permafrost Soil Carbon Storage in Northeastern Siberia

Windirsch, T.[1,2], Grosse, G.[1,2], Ulrich, M.[3,4], Forbes, B. C.[5], Göckede, M.[6], Wolter, J.[1,7], Macias-Fauria, M.[8], Olofsson, J.[9], Zimov, N.[10], and Strauss, J.[1]

[1]Alfred Wegener Institute Helmholtz Centre for Polar and Marine Research, Potsdam, Germany

[2]Department for Geosciences, University of Potsdam, Potsdam, Germany

[3]Institute for Geography, University of Leipzig, Leipzig, Germany

[4]German Federal Environment Agency, Dessau, Germany

[5]Arctic Centre, University of Lapland, Rovaniemi, Finland

[6]Department Biogeochemical Signals, Max Planck Institute for Biogeochemistry, Jena, Germany

[7]Institute of Biochemistry and Biology, University of Potsdam, Potsdam, Germany

[8]Biogeosciences Lab, School of Geography and the Environment, University of Oxford, England

[9]Department of Ecology and Environmental Science, Umeå University, Umeå, Sweden

[10]Northeast Science Station, Pacific Institute for Geography, Far-Eastern Branch of Russian Academy of Science, Chersky, Russia

Published in: Frontiers in Environmental Science, Volume 10, 2022

Citation: Windirsch, T., Grosse, G., Ulrich, M., Forbes, B. C., Göckede, M., Wolter, J., Macias-Fauria, M., Olofsson, J., Zimov, N., and Strauss, J.: Large herbivores on permafrost— a pilot study of grazing impacts on permafrost soil carbon storage in northeastern Siberia, Front. Environ. Sci. 10:893478, doi: 10.3389/fenvs.2022.893478, 2022.

2.1 Abstract

The risk of carbon emissions from permafrost is linked to an increase in ground temperature and thus in particular to thermal insulation by vegetation, soil layers and snow cover. Ground insulation can be influenced by the presence of large herbivores browsing for food in both winter and summer. In this study, we examine the potential impact of large herbivore presence on the soil carbon storage in a thermokarst landscape in northeastern Siberia. Our aim in this pilot study is to conduct a first analysis on whether intensive large herbivore grazing may slow or even reverse permafrost thaw by affecting thermal insulation through modifying ground cover properties. As permafrost soil temperatures are important for organic matter decomposition, we hypothesise that herbivory disturbances lead to differences in ground-stored carbon. Therefore, we analysed five sites with a total of three different herbivore grazing intensities on two landscape forms (drained thermokarst basin, Yedoma upland) in Pleistocene Park near Chersky. We measured maximum thaw depth, total organic carbon content, $\delta^{13}C$ isotopes, carbon-nitrogen ratios, and sediment grain size composition as well as ice and water content for each site. We found the thaw depth to be shallower and carbon storage to be higher in

intensively grazed areas compared to extensively and non-grazed sites in the same thermokarst basin. First data show that intensive grazing leads to a more stable thermal ground regime and thus to increased carbon storage in the thermokarst deposits and active layer. However, the high carbon content found within the upper 20 cm on intensively grazed sites could also indicate higher carbon input rather than reduced decomposition, which requires further studies including investigations of the hydrology and general ground conditions existing prior to grazing introduction. We explain our findings by intensive animal trampling in winter and vegetation changes, which overcompensate summer ground warming. We conclude that grazing intensity – along with soil substrate and hydrologic conditions – might have a measurable influence on the carbon storage in permafrost soils. Hence the grazing effect should be further investigated for its potential as an actively manageable instrument to reduce net carbon emission from permafrost.

2.2 Introduction

In the context of global climate warming, carbon emissions from Arctic permafrost regions have been identified as a key source of greenhouse gases (GHGs), further accelerating the permafrost carbon-climate feedback and increasing atmospheric warming (Schuur *et al.* 2015, Turetsky *et al.* 2019, Bowen *et al.* 2020). An estimated 1300 gigatons (Gt) of carbon are stored within the upper 3 m of ground in the permafrost region, of which approximately 1000 Gt are perennially frozen (Hugelius *et al.* 2014, Mishra *et al.* 2021). These 1300 Gt account for approximately 35 % of global soil carbon, with 2050 to 2800 Gt globally present in the top 3 m of non-permafrost regions (Schuur *et al.* 2015, Jackson *et al.* 2017, Strauss *et al.* 2021). With further Arctic warming now and in the future, deposits of organic-rich material embedded in permafrost are expected to become widely available for microbial decomposition and increased GHG production with permafrost thaw (Schuur *et al.* 2008).

In general, there are processes leading to carbon accumulation in permafrost areas, such as deposition of organic-rich sediments (via aeolian or fluvial transport, Chlachula (2003); Huh *et al.* (1998)), increased in situ biomass accumulation (via increased plant growth, Schuur *et al.* (2008)), cryoturbation (Kaiser *et al.* 2007), and animal influence via faeces. This last one is linked to increased plant growth by providing easily available nutrients (Grellmann 2002); moreover, the disturbance of the surface layer via trampling mixes fresh organic matter (OM) into the ground, providing additional OM input that adds to the previously permafrost-preserved OM.

Vegetation composition and snow conditions together play major roles in mediating Arctic surface, near-surface, and sub-surface temperature regimes by influencing the land surface energy budget, and thus the belowground carbon cycle. Both vegetation and snow can be heavily influenced by the presence of large herbivorous animals. Plant growth itself affects above and

below ground carbon storage as plants take up carbon dioxide from the environment, temporarily fixing carbon in their biomass, while plant litter and roots become components of the active layer of soils (the seasonal thaw layer on top of permafrost). Dense vegetation cover may cause relative ground cooling by reducing summer energy exchange by creating wind protection and a stable air layer between the ground's surface and the canopy (Zhang *et al.* 2013, Mod and Luoto 2016, te Beest *et al.* 2016). In winter, shrub vegetation effectively traps snow, leading to locally higher snow accumulation (Domine *et al.* 2016), hence insulation and therefore maintains relatively warm ground temperatures throughout winter (Sannel 2020). In contrast, graminoid vegetation facilitates ground cooling in winter, as it bends beneath accumulating snow, reducing the volume of air trapped beneath the snow (Blok *et al.* 2010). In summer, graminoid vegetation is also less insulating, leading to stronger ground warming underneath the canopy. However, this summer effect is offset by the vast difference between summer and winter seasonal length in the Arctic. In this way, graminoids contribute to a net cooling effect (Macias-Fauria *et al.* 2020). However, due to warming climate and an associated extension of the growing season, an increase in the establishment and growth of shrub vegetation has already been observed (Frost *et al.* 2013) and is projected to increase in the Arctic tundra regions (Zhang *et al.* 2013).

Previous studies have reported on the effect of herbivore - mainly reindeer - presence on carbon storage in tundra biomes (Olofsson 2006, Falk *et al.* 2015, Olofsson and Post 2018, Ylänne *et al.* 2018). Those investigations mainly focused on the above-ground biomass changes and concluded that the effects of grazing-associated vegetation changes from shrubs to graminoid vegetation enhance soil carbon sequestration and might help reduce soil carbon emissions. In contrast to these findings, Monteath *et al.* (2021) challenge the idea of a rewilding strategy – reintroducing and promoting (semi-) wild animals – against Arctic carbon emissions, stating that cause and consequence in herbivore extinction and Arctic shrubification are unclear. While their macrofossil analysis suggests that extinction was a consequence of habitat loss in a warming climate, leading to shrub expansion and vegetation shifts, a study using ancient DNA analysis found the opposite (Murchie *et al.* 2021). Modeling studies have tried to quantify the impact of large herbivores on permafrost soil carbon storage (Zimov *et al.* 2009, Beer *et al.* 2020). These modeling exercises and predictions have, however, not yet been tested in the field.

Some researchers have proposed to actively exploit these processes and properties in order to preserve permafrost and limit permafrost carbon emissions as a consequence of a warming climate. The establishment of sufficiently large numbers of herbivores as ecosystem engineers could intensify grazing and trampling pressure in today's tundra and forest-tundra landscapes (Olofsson and Post 2018, Beer *et al.* 2020). During the late Pleistocene, the mammoth steppe

was characterised by highly productive grasslands with high grazing pressure by large herbivores. Olofsson *et al.* (2004) and Zimov (2005) suggested that grazing and trampling in the Arctic reduces shrub abundance. This could help to shift shrubifying tundra ecosystems towards grass and forb dominated ecosystems similar to the mammoth steppe in terms of productivity and thermal insulation properties. Such a vegetation shift is also suggested to cause an albedo increase and hence lower latent and sensible heat fluxes due to overall reduced energy input (te Beest *et al.* 2016). In winter, dense populations of large herbivores may also affect the insulation effect of snow on the ground by trampling down or removing the dense snow cover in their search for forage, leading to enhanced refreezing of the ground (Fig. 2-1) (Beer *et al.* 2020).

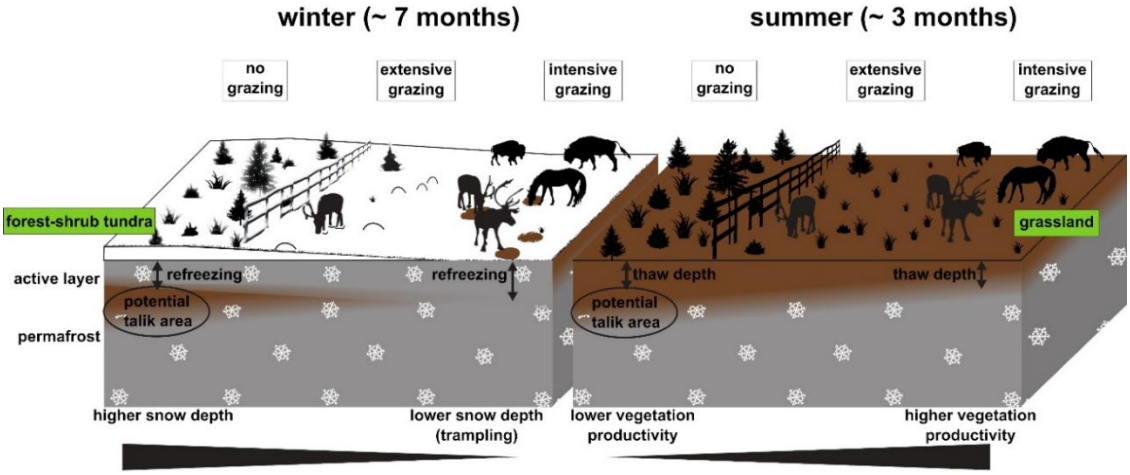

Figure 2-1 – Graphical representation of the Pleistocene Park hypothesis (Zimov 2005); Left: during winter time (~60% of the year), a greater number of large animals trample down and/or partly remove the snow cover, facilitating the full refreezing of the active layer; as the active layer refreezes in winter in the graminoid-dominated areas, thawing is reduced compared to non-grazed tundra and forest areas; Right: during summer time (~30% of the year), a greater number of animals enhances a vegetation shift from shrubby towards graminoid-dominated, increasing vegetation productivity but also ground warming by disturbing the heat insulation layer; since the ground under intensive grazing impact is colder and is fully refrozen at the beginning of summer, overall thaw depth is smaller in these areas by the end of summer.

The Pleistocene Park project, near Chersky in northeastern Siberia, aims to re-establish a megaherbivore-driven system via rewilding of the forest-tundra with greater numbers of modern large and cold-adapted herbivores. These include, among others, musk oxen, Yakutian horses, Kalmyk cattle, bison, and reindeer. With this study focusing on sites in Pleistocene Park, we aim to identify the effects of dense and functionally diverse herbivory pressure on an ice-rich Arctic permafrost landscape. Therefore, we compare belowground carbon and sediment characteristics at five sites in two landscape units with different grazing intensities. We hypothesise that a high large herbivore density and hence intensive grazing and trampling reduces decomposition of preserved OM by reducing ground temperatures. Our work constitutes a pilot study that opens the path for further field-based multi-proxy and multi-disciplinary approaches.

2.3 Study area

Our study area, Pleistocene Park, is located in northeastern Siberia in the floodplains of the Kolyma River, approximately 100 km inland from the Arctic Ocean (Fig. 2-2) (Fuchs *et al.* (2021)). The landscape is characterised by thermokarst lakes, drained thermokarst basins with different depths, and uplands of late-Pleistocene ice- and organic-rich permafrost deposits (i.e. Yedoma; (Schirrmeister *et al.* 2011, Palmtag *et al.* 2015). Climate in this region is characterised by large temperature amplitudes (average of -33 °C in January; average of 12 °C in July) with a mean annual temperature of -11 °C (Göckede *et al.* 2017). Annual precipitation is 197 mm; March is the driest month (7 mm) and August receives the most precipitation (30 mm). The main seasons for precipitation are summer and autumn (Göckede *et al.* 2017). The prevailing deposit types are Yedoma and thermokarst deposits (Veremeeva *et al.* 2021) with the latter covering approximately 58 % of the land area in regions with high Yedoma coverage, and up to 96.4 % in regions with low Yedoma deposit occurrence. These deposits are interspersed with marshes, river valleys, and deltas (Veremeeva *et al.* 2021). Vegetation within the thermokarst basins generally varies with the local wetness gradient and to some extent with grazing intensity. *Carex appendiculata* tussocks dominate in shallow water around lake margins. In frequently flooded areas, tall grasses (e.g. *Calamagrostis langsdorfii*) grow up to 70 cm high, which is a little higher than in surrounding areas (Corradi *et al.* 2005). Seasonal flooding typically occurs after snow melt during the spring freshet, temporarily refilling the drained thermokarst basins and covering sampling site B3 (Fig. 2-2).

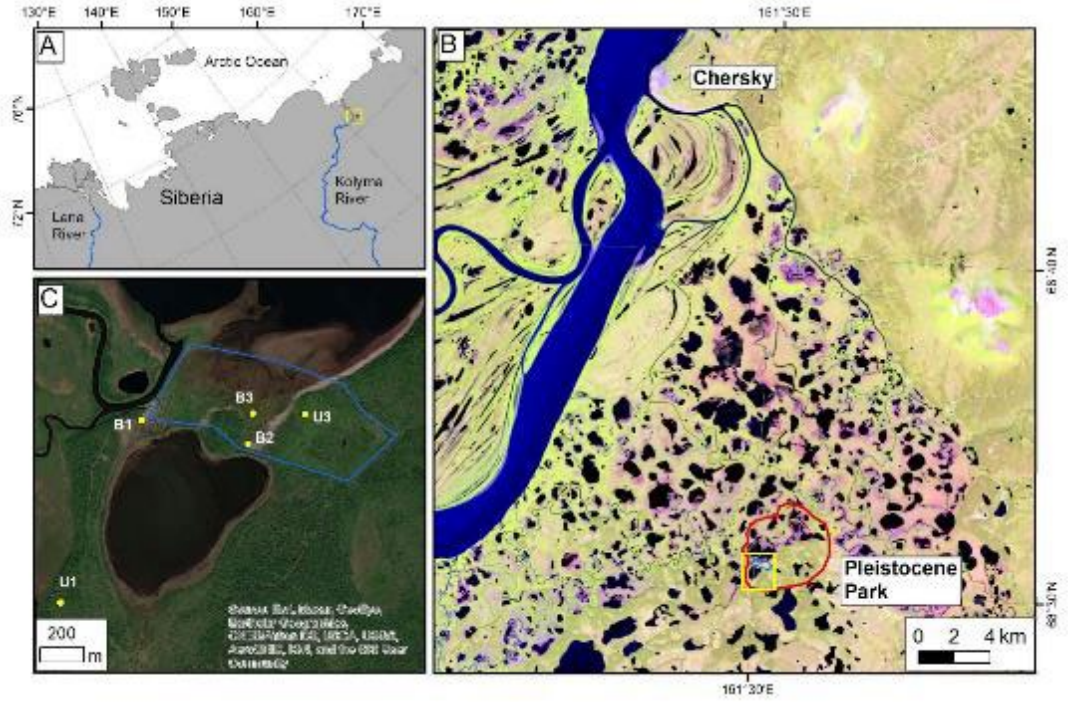

Figure 2-2 – Location of the study area in northeastern Siberia marked with a yellow frame (A). In the Landsat-8 satellite image (band combination of shortwave infrared 1 - near infrared - red, 2019-07-04) of panel (B) the red line marks the area of Pleistocene Park south of Chersky; the yellow frame indicates the location of the field study sites shown in (C). Panel (C) shows a high resolution GeoEye satellite image (2018-07-21; ArcGIS Online base map provided by the Environmental Systems Research Institute, ESRI) with Pleistocene Park fences (blue) and sampling sites labelled as B, indicating drained basin sites, and U, indicating Yedoma upland sites; numbers indicate the grazing intensity of each site, from 1 (no grazing) to 3 (intensive grazing).

Here, graminoids (mainly *Poaceae*) make up the main vegetation type and show signs of animal grazing (Fig. 2-3 B3). A driftwood belt was present towards the outer basin margins (between B3 and B2 in our study area). The sampling site B2 is located on the elevated reaches of a basin and is characterised by extensively grazed lower-growing graminoid-dominated (*Poaceae*) vegetation with occasional forbs (Fig. 2-3 B2). Towards the edge of the basin, drier ground is covered with dense trees and shrubs (*Larix* spp., *Salix* spp.) up to 2.5 m height, which grow into forests in some places (Fig. 2-2, west of B3 and B2). Sampling site B1 is located on the edge between the basin and the upland and represents a non-grazed surface. It is characterised by grasses (e.g. *Beckmannia syzigachne*, *Hordeum jubatum*), forbs (e.g. *Saxifraga* spp.), *Equisetum* spp., and low-growing shrubs (e.g. *Salix* spp.) (Fig. 2-3 B1). This site was covered in *Larix* forest until deforestation in 2015. A mix of dwarf and taller shrubs (e.g. *Salix* spp.), forbs, and grasses is found on the Yedoma uplands, where sites U3 and U1 are located (Fig. 2-3 U3). Shrubs reach a height of up to 2.5 m. The lower vegetation features diverse forbs, grasses, and *Equisetum* spp. reaching 10 to 20 cm in height.

The Pleistocene Park project was started in 1996 as a large-scale and long-term ecosystem change experiment (Zimov 2020). For this experiment, a large number of Yakutian horses, Kalmykian cattle, reindeer, bison, and musk oxen as well as moose, sheep, yaks, and European bison – all large and cold-adapted herbivores – were gradually introduced into a 40-ha fenced area, which stretches across tundra and forest-tundra vegetation over a landscape characterised by Yedoma uplands and partially drained thermokarst basins. Today, this 40-ha area is the heartland of a 160 km^2 fenced park that constitutes a unique experimental site for examining rewilding impacts on Arctic ecosystems (Macias-Fauria *et al.* 2020). The presence of these animals - and some man-made interventions such as removal of trees to build fences on the periphery of the park - has already transformed most of the previous tundra vegetation into grassland, while forest areas are developing towards more open vegetation. However, responses in soil property changes from surface effects, especially below the active layer, are slow , so these deep deposits are most likely not yet influenced by animal activity after a 23-year time period. Long-term studies on GHG emissions have been conducted in nearby areas of Pleistocene Park. For instance, Göckede *et al.* (2017), (2019) investigated the carbon and energy budgets of tundra wetlands and regime shifts related to drainage disturbance on a nearby floodplain of the Kolyma River. They found that an undisturbed wetland, similar to the non-grazed wetlands in the Pleistocene Park area, acted as a moderate annual sink for CO_2, and as a moderate source for CH_4. Both carbon and energy cycles were shown to be highly sensitive to shifts in hydrology. Our sites and therefore results are very similar to their study sites as vegetation, sediment, and climate are the same, based

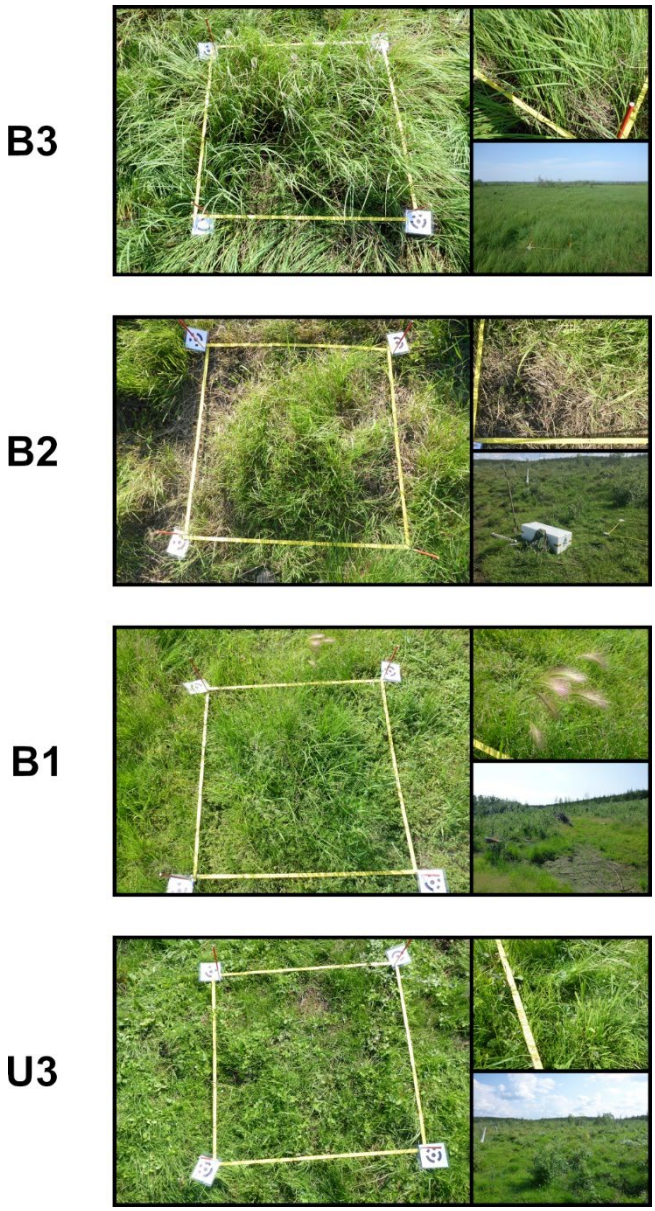

Figure 2-3 – Vegetation photos of the study sites sampled in July 2019; each site comprises a 1 by 1 m plot photo (left), a vegetation detail photo (top right) and a landscape photo (bottom right).

on the close distance of the locations. A recent study by Fischer *et al.* (2022) found similar results as close as 10 m from our B3 site.

2.4 Methods

2.4.1 Field sampling approach

The sampling sites were chosen based on their grazing intensity, which was identified by long-term monitoring of animal preferences for grazing sites and additional observations over several days at the start of the field campaign in July 2019. We applied a space-for-time approach to compare apparently similar sites selected within the same landscape units that ideally only differed by grazing intensity, instead of long-term monitoring of non-grazed sites along with gradual herbivore introduction. For this pilot study with limited field time, we decided to prioritise the number of herbivore treatments and landscape positions investigated over the number of replicates within a given treatment and site in order to allow a preliminary analysis of a larger range of site conditions. We implemented a nomenclature scheme for our study sites that provides information on the landscape type (B for thermokarst basin or U for Yedoma upland) and the grazing intensity (3: intensive grazing; 2: occasional grazing; 1: no grazing). Five sites were selected to cover these different site characteristics. We sampled one soil core per site during our field campaign (Fig. 2-2): B3 was an intensively grazed site in a wet area of a thermokarst basin; B2 was an extensively grazed site within the thermokarst basin, close to the fence of Pleistocene Park; B1 was a non-grazed site within the thermokarst basin, just outside the park's fence; U3 was an intensively grazed site on a Yedoma upland; and U1 was a non-grazed site on a Yedoma upland. “Intensive grazing” and “occasional grazing” are relative terms in this context, with “intensive” referring to a daily presence of feeding animals over several hours throughout each day and “occasional” describing an occasional animal presence with feeding occurring along animal tracks. Location details are provided in table 2-1.

Table 2-1 – Sampling site locations and characteristics.

site	latitude (°N)	longitude (°E)	grazing intensity	main vegetation type	flooding regime	active layer depth (July 2019) [cm bs]	total core length [cm]	main sediment material
B1	68.512167	161.496278	no grazing	graminoids, forbs and shrubs	occasional	80	127	silt, peat layer (85 - 115 cm bs)
B2	68.511111	161.508528	occasional	graminoids and forbs	occasional	51	108	clayish silt
B3	68.512694	161.508750	intensive	graminoids	seasonal	38	110	clayish silt
U1	68.504469	161.488390	no grazing	NA	none	NA	72	silt
U3	68.512778	161.514611	intensive	graminoid-rich tundra and shrubs	none	53	114	clayish silt

In this setup, the area outside the fence was defined as an exclosure with no access for the park's animals. We chose our sampling sites so that the three B sites were located in the same drained thermokarst basin, and the two U sites were located on the same Yedoma upland complex. The goal was to choose sites with similar properties so the animal influence was the main variable and differences between all other characteristics were minimised. Unfortunately, site B1 was experimentally deforested in 2015, prior to our study, which resulted in an unavoidable environmental difference that may have impacted soil composition at this site. The main impact is most likely soil compaction of the active layer due to the use of heavy machines. Also, flooding regime (seasonal or occasional) is different between our sites and might have some effect on the soils. Since animal trampling as well as defecation and browsing always occur where animals graze, in the following we will use the term "grazing" to indicate all animal activity including trampling, defecation, and foraging. Each site is exposed to the same grazing pressure year-round, as there are no separate summer and winter ranges, enabling us to study the net effect of the animals' winter and summer impacts.

Firstly, we prepared a visual description of the surroundings at each sampling site, including the main vegetation type. We identified and sampled the most abundant vegetation species and estimated their coverage based on one by one m plots (Fig. 2-3).

Secondly, we removed the active layer using a spade, until we hit permafrost. We measured the thaw depth and sampled the soil profile by using fixed-volume steel cylinders with a volume of 250 cm^3. Due to very wet ground conditions, we were not able to collect cylinder samples at the intensively grazed site B3, where the ground was saturated from the surface to the frozen

ground (38 cm). Instead, we cut blocks 8 to 10 cm high (see also Windirsch *et al.* (2021b) for exact sample dimensions) out of the soil profile using a knife. The organic top layer was sampled separately at all sites.

Thirdly, we used a Snow Ice and Permafrost Research Establishment (SIPRE) permafrost auger with an inner diameter of 7.6 cm in order to sample both the still-frozen parts of the active layer and the underlying permafrost. We reached maximum sampling depths of 110 cm below surface (bs) at B3, 108 cm bs at B2, 127 cm bs at B1, and 114 cm bs at U3 (Fig. S2-2 and S2-3). After drilling, soil samples and cores were individually wrapped in sterile plastic bags. All samples were brought in a frozen state to our laboratories for further analysis.

Due to high and dense shrub vegetation and therefore inaccessibility, we were not able to sample the U1 location during our summer field campaign. The Yedoma upland site outside the fence of Pleistocene Park was therefore sampled in the following winter with the SIPRE auger to a depth of 72 cm bs and was completely frozen at the time of extraction.

2.4.2 Laboratory work

In the laboratory the frozen cores were cut into approximately 5 cm samples according to stratigraphy using a band saw. Afterwards, all samples were freeze-dried (Zirbus Sublimator 15) and weighed pre- and post-drying for ice and water content determination (Mettler Toledo KERN FCB 8K0.1, accuracy ± 0.1 g). The dry samples were split into subsamples for biogeochemical and sedimentological analysis. In the following, the mean sample depth will be used to describe the position of each sample within the soil column.

The subsamples for biogeochemical analysis were homogenised using a planetary mill (Fritsch Pulverisette 5) and weighed into tin capsules and steel crucibles for measurement. We determined total carbon (TC), total nitrogen (TN), and total organic carbon (TOC) by combustion analysis using a vario EL III and a soliTOC cube (both Elemantar Analysensysteme). Afterwards, the carbon-nitrogen ratio (TOC/TN) was calculated from TOC and TN, giving information about the state of degradation and the source of the OM. TOC/TN ratios could not be calculated for samples with TN or TOC below the detection limit of 0.1 wt%.

OM for radiocarbon dating was taken from the dried original samples. For dating, the Mini Carbon Dating System (MICADAS) at the Alfred Wegener Institute Bremerhaven was used. We calculated the results in calibrated years before present (cal yr BP) using the calibration software Calib 8.2 and applying the IntCal20 calibration curve (Reimer *et al.* 2020, Stuiver *et al.* 2021).

We analysed the ratio of stable carbon isotopes and used it as a proxy for the degree of decomposition of the OM following Diochon and Kellman (2008). Soil $\delta^{13}C$ values differ between material sources and can distinguish between vegetation communities (Malone *et al.* 2018). Samples for $\delta^{13}C$ analysis were homogenised using a planetary mill, and subsequently treated with hydrochloric acid at 50 °C to remove carbonates. Measurements were done using a Delta

V Advantage Isotope Ratio mass spectrometer (MS) supplement equipped with a Flash 2000 Organic Elemental Analyser. Results are given in ‰ compared to the Vienna Pee Dee Belemnite (VPDB) standard (Coplen *et al.* 2006).

Finally, we determined grain size distribution within samples to check sediment substrate similarity. Therefore, OM was removed from the samples using hydrogen peroxide. Grain size distributions were subsequently measured using a MasterSizer 3000 (Malvern Panalytical).

2.4.3 Data analysis and external data

We determined the annual average number of freezing days (daily mean air temperature below 0 °C) over a period of nine years. For this we used data from 2009 to 2017 measured at the Chersky meteorological station (station RSM00025123). Data were obtained from the National Oceanic and Atmospheric Administration's National Climatic Data Center (NOAA NCDC) database.

In order to check for differences between intensively grazed and non-grazed sites, we combined our TOC data for intensive (B3 and U3) and non-grazed (B1 and U1) sites. We did this for the minimum active layer depth (38 cm at B3) to ensure similar conditions for all sites used. This left us with n = 11 samples for intensively grazed, n = 5 samples for occasionally grazed, and n = 10 samples for non-grazed sites. Since grazing intensities were artificially altered during the last few decades, we expect the most pronounced differences in the seasonally thawed layer, which corresponds to more recent periods. We visualised the distribution of TOC contents in the active layer in boxplots for intensive, occasional, and non-grazed sites of our study to explore possible differences in TOC content in relation to grazing intensity.

To identify correlations between TOC content, water or ice content, and sediment type (via mean grain size), we used principal component analysis (PCA). Data were initially normalised to values between 0 and 1. The PCA was conducted in the R environment using the "stats" package (R Core Team 2021).

2.5 Results

2.5.1 Vegetation assessment

At site B3 we found *Calamagrostis langsdorfii* as the only species in our one by one m plot with a coverage of more than 95 %. No other species was found underneath. *C. langsdorfii* reached a height of approximately 30 cm. At B2 *Poaceae* were dominant but could not be identified on a species level due to a lack of blossoms as well as herbivory damages (Fig. 2-3). Therefore, height could also not be recorded accurately. *Poaceae* covered approximately 70 % of our plot with small amounts of *Salix* ssp. in between (less than 10 % coverage). Close to our plot, *Salix* ssp. and *Larix* ssp. shrubs were present with a height of up to 2.5 m. Contrary

to the grazed sites, the predominant species at B1 was *Beckmannia syzigachne* with an approximate coverage of 65 % and an approximate height of 25 cm (Fig. 2-3). Underneath, low extents of *Saxifraga* ssp., *Equisetum* ssp. and low-growing *Salix* ssp. were found. After deforestation in 2015, no *Larix* ssp. were present. U3 featured a much lower-growing vegetation (up to 15 cm height), holding approximately 50 % of unidentified graminoids which could not be identified due to herbivory damages (Fig. 2-3). In between we found *Rubus* ssp. (15 to 20 %), *Saxifraga* ssp. (less than 5 %), *Salix* ssp. (less than 5 %), and some individuals of *Vaccinium* ssp. and *Arnica* ssp., which all lacked flowers and could therefore not be identified on species level. Towards the less intensively grazed upland areas, *Salix* ssp. shrubs up to 2.5 m in height grew with increasing density.

2.5.2 Seasonal thaw depth

We found that the seasonal thaw depth (July 2019) decreased with grazing intensity, giving a thaw depth of 38 cm below surface (bs) in B3, 59 cm bs in B2, and 85 cm bs in B1 with a semi-frozen zone between 80 and 85 cm bs. In U3, we measured a thaw depth of 53 cm bs. Since U1 was sampled in winter, we were not able to measure thaw depth at this site.

2.5.3 Carbon parameters (TOC, TOC/TN ratios, and $\delta^{13}C$ ratios)

At B3, TOC generally decreased from top to bottom with the highest value of 25.66 wt% at 20.25 cm bs and the lowest value of 1.18 wt% at 92.5 cm bs (Fig. 2-4). In contrast to this, TOC values for B2 peaked around the frozen-unfrozen interface with values between 4.89 wt% (21.25 cm bs) and 30.10 wt% (64 cm bs); the frozen part contained generally more TOC. The highest TOC values among all sites were found in a peat layer at B1 in the frozen core part, with a peak value of 52.80 wt% (92.5 cm bs). The unfrozen core part contained much less OC with values between 0.79 wt% (35.25 cm bs) and 9.65 wt% (3.75 cm bs).

At the U3 upland site, TOC was higher in the unfrozen core part with values between 3.52 wt% (11.25 cm bs) and 10.73 wt% (49 cm bs). In the frozen core part below, TOC values were rather homogeneous, varying between 1.01 wt% (103.5 cm bs) and 2.65 wt% (58.5 cm bs). In contrast to the previous sites, TOC at U1 was homogeneous throughout the core at values between 1.24 wt% (33 cm bs) and 2.54 wt% (27 cm bs) with a slight increase at the bottom to 4.50 wt% (71 cm bs).

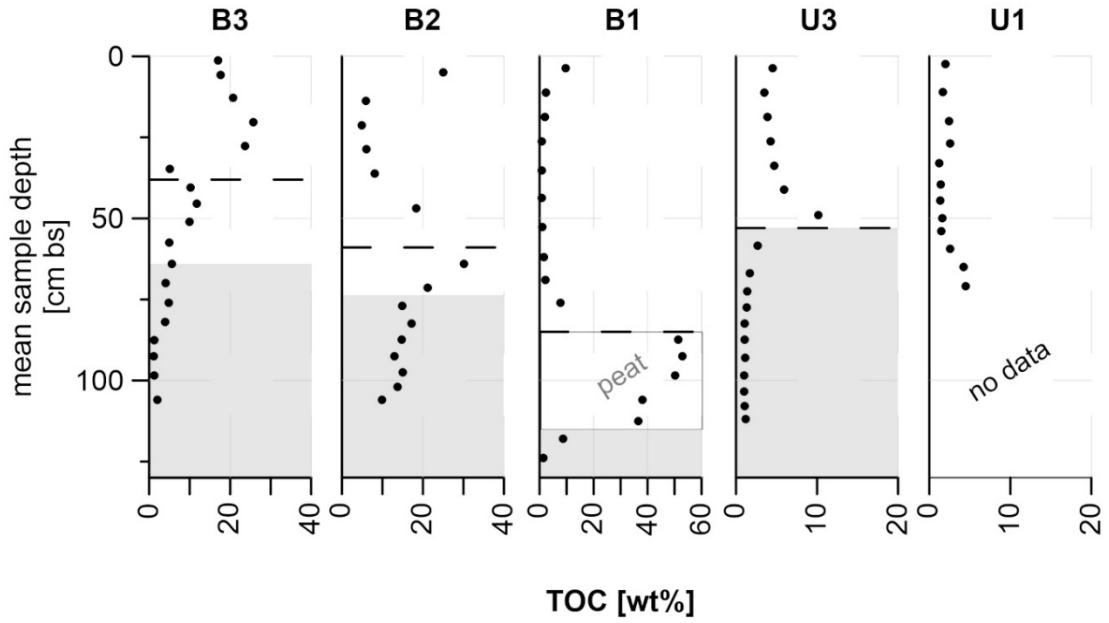

Figure 2-4 – Total organic carbon (TOC) values of all study sites; dashed lines mark the seasonal thaw depth measured in July 2019; gray areas are assumed to be permafrost based on cryostratigraphic characteristics; please note the different scales on the x-axes.

While TOC/TN ratios for B3 (range 12.68 to 25.96) and B2 (range 14.83 to 18.48) were similar (Fig. 2-5), values for B1 were higher, in the range of 16.94 to 24.90. In the upland sites, there was a strong contrast between U3 (11.40 to 29.19, mean of 17.75) and U1 (28.63 and 29.27) in TOC/TN ratios.

$\delta^{13}C$ values were also similar between the basin sites (B3: -30.63 ‰ vs. VPDB (uppermost sample) to -26.43 ‰; B2: -29.60 ‰ to -28.13 ‰; B1: -30.17 ‰ to -27.89 ‰) (Fig. 2-5). Upland sites showed higher $\delta^{13}C$ values in the range of -28.06 ‰ to -23.49 ‰. For full $\delta^{13}C$ values, please see figure S2-4 or the published data set (Windirsch *et al.* 2021b).

Radiocarbon dates were measured from samples at greater depth than the expected grazing influence. These data are provided in the supplementary table S2-1.

2.5.4 Grain size distribution and water content

The soil cores were silty overall and had relatively homogeneous grain size distribution (Fig. 2-6) across sites (Fig. S2-2 and S2-3). In B3, clay content decreased slowly with depth from 16.69 vol% at 76 cm bs to 7.50 vol% at 106 cm bs, while at the same time sand content increased from 3.46 vol% to 10.68 vol%. Clay content varied throughout B2 with a minimum of 14.16 vol% at 28.75 cm bs and a localised maximum of 22.17 vol% at 13.75 cm bs (Fig. 2-6). Sand content decreased with depth, starting at 12.73 vol% (5 cm bs) and reaching 2.43 vol% at the bottom (106 cm bs). In B1, clay content showed a peak value of 21.96 vol% at 76 cm bs, followed by a peat layer down to 106 cm bs with no grain size data available. Mean clay content for this core was 10.84 vol%. Sand content varied between 5.37 vol% (35.25 cm bs) and 11.31 vol% (43.75 cm bs) with two low values, 2.54 vol% at 52.75 cm bs and 2.22 vol% at 124 cm bs.

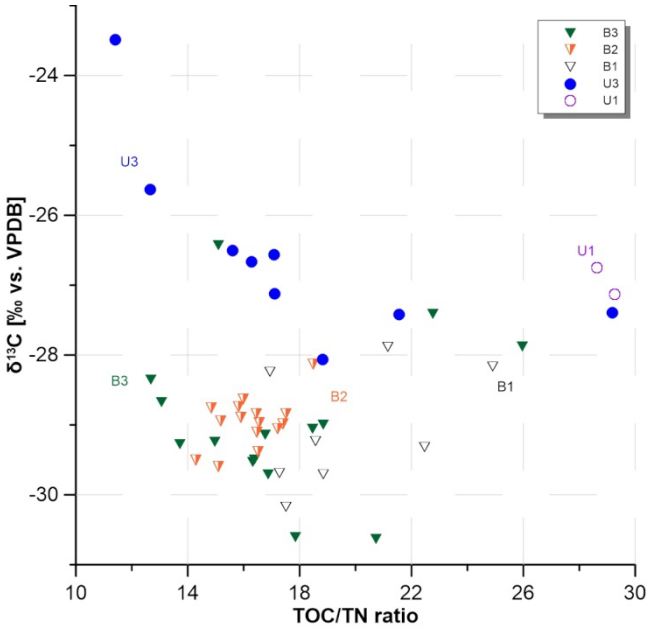

Figure 2-5 – Total organic carbon to total nitrogen (TOC/TN) ratios plotted against the stable carbon isotope ($\delta^{13}C$) ratios of all sampling sites.

U3 showed similar characteristics as B3 with clay content decreasing with depth (highest value 19.76 vol% at 49 cm bs, lowest value 6.34 vol% at 112 cm bs), while simultaneously the sand content increased to a peak value of 11.52 vol% at 103.5 cm bs (Fig. 2-6). Grain size composition for U1 showed no peaks, with clay contents between 8.03 vol% (71 cm bs) and 12.60 vol% (33 cm bs) and sand contents between 8.20 vol% (44.5 cm bs) and 14.01 vol% (71 cm bs).

The absolute water and/or ice content showed generally drier conditions in the frozen core of B3, with values fluctuating between 27.67 wt% (34.75 cm bs) and 78.59 wt% (1.25 cm bs). Similar characteristics were present in B2 (34.26 wt% at 28.75 cm bs to 71.10 wt% at 82.5 cm bs). In contrast, B1 showed large differences between the unfrozen upper part (17.19 wt% at 35.25 cm bs, 39.36 wt% at 3.75 cm bs) and the frozen lower part (39.59 wt% at 124 cm bs, 85.74 wt% at 112.5 cm bs).

U3 showed similar water content values at the top (32.00 wt% at 11.25 cm bs) and bottom (31.93 wt% at 112 cm bs) with higher values around the freezing interface (55.01 wt% at 49 cm bs) and lower values above and below that (22.11 wt% at 3.75 cm bs and 15.59 wt% at 87.5

cm bs). Water content in U1 was more stable, ranging between 25.63 wt% (39.5 cm bs) and 43.88 wt% (71 cm bs) with a similar value at the top (43.24 wt% at 2.5 cm bs).

The stable isotope characteristics of the pore water are shown in supplement figure S5.

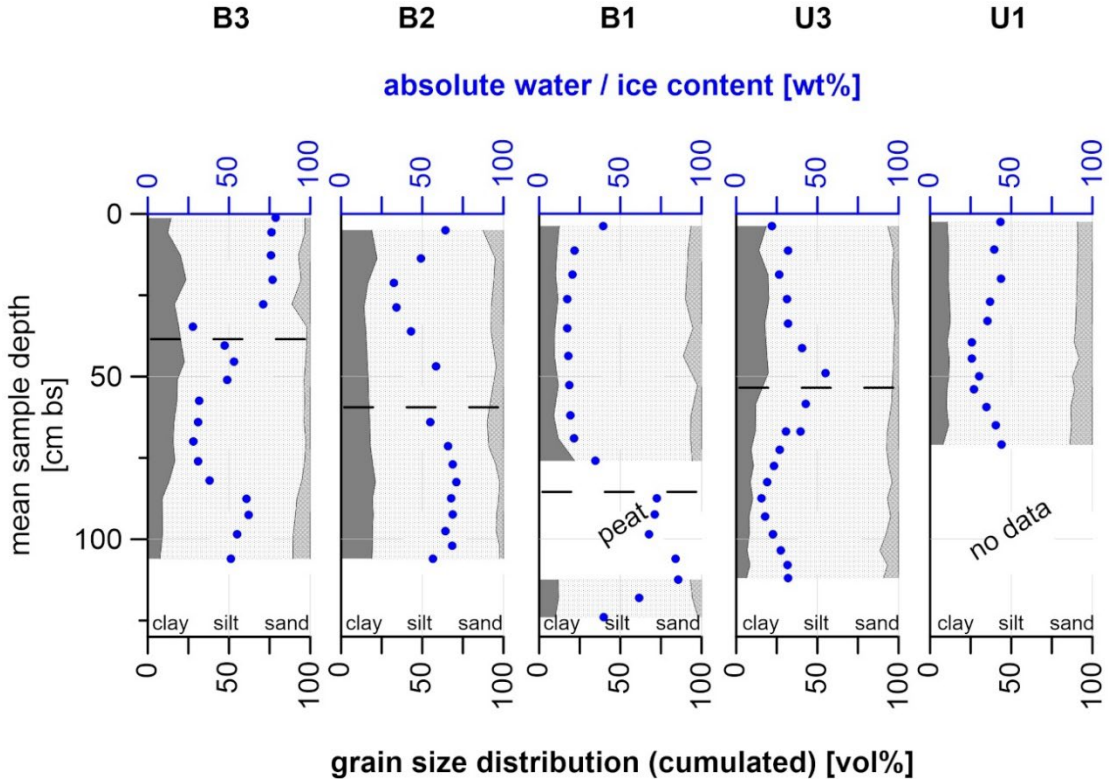

Figure 2-6 – Grain size distribution for all sampling sites plotted against depth; absolute water and/or ice content added in blue; dashed lines mark the seasonal thaw depth measured in July 2019.

2.5.5 Statistics and correlation analysis

The PCA revealed a positive correlation between water/ice content and TOC content (Fig. 2-7). While B3, B2, U3, and U1 tended to form clusters, B1 values were spread across parameters. For full PCA scores, see table S2-2 as well as figure S2-1.

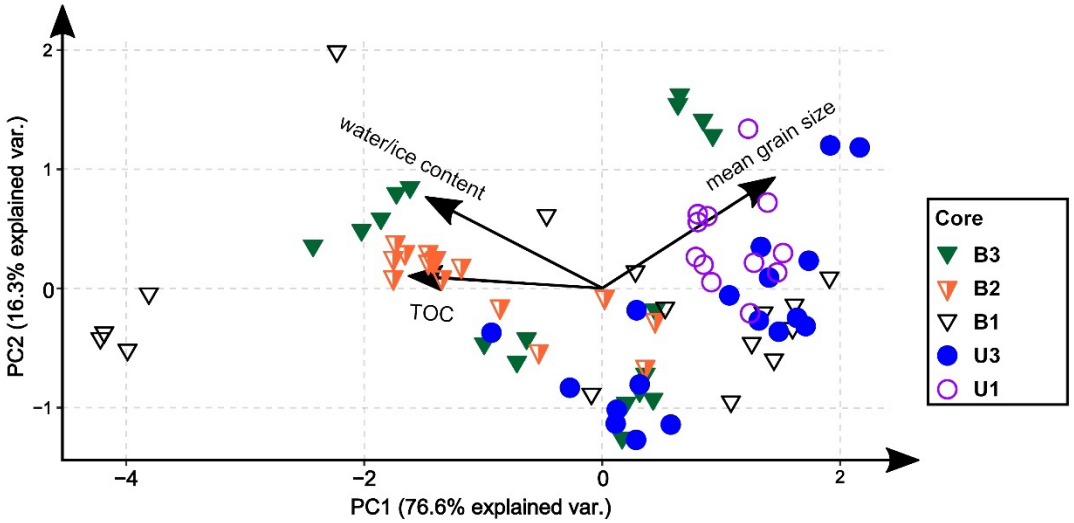

Figure 2-7 – Results of the principal component analysis (PCA) for variables total organic carbon (TOC), water/ice content, and mean grain size.

In figure 2-8 we visualised the range of the TOC values in the minimum active layer (depth 38 cm), grouped by grazing intensity (Fig. 2-8). TOC is clearly higher under intensive grazing compared to non-grazed sites, with no overlap except for outliers.

Due to potential dependency of TOC values within the unfrozen part of a core, and due to the small sample sizes, we did not test for statistical significance.

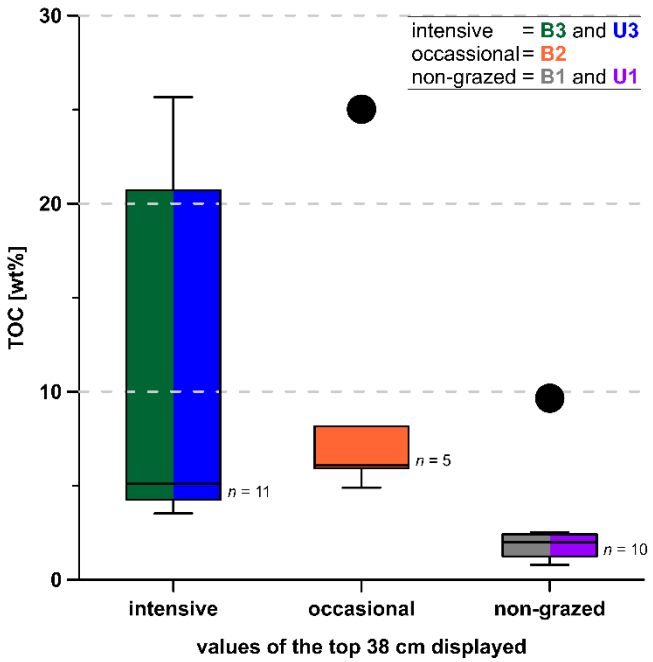

Figure 2-8 – Boxplots for total organic carbon (TOC) data of all samples from the uppermost 38 cm of all intensive, occasional, and non-grazed sampling sites; sites B3 and U3 are combined into the "intensive" boxplot, B2 is shown in the "occasional" boxplot, and B1 and U1 are combined into the "non-grazed" boxplot; the median is shown by the horizontal line within each box; box margins show the upper and lower quartile; whiskers mark minimum and maximum values; outliers (indicated by dots) are more than 1.5 box lengths away from box margins; colours indicate which sites are represented in which box.

2.6 Discussion

2.6.1 Effects of grazing on vegetation structure and permafrost thaw

For our studied cores we found that intensively grazed sites (B3, U3) were covered by generally shorter and sparser vegetation (Fig. 2-3 B3: grassland; Fig. 2-3 U3: shrubby grassland tundra), with taller grazing-resistant individuals in between, compared to occasionally or non-grazed sites (Fig. 2-3 B2: grasses and herbs, and B1: grasses, herbs and low shrubs). This could likely be a result of the reduction in shrub expansion through large herbivore action (Suominen and Olofsson 2000), while the differences in the

flooding regime between the sites promoting different vegetation types might also have an impact on this. The grazed sites located in the thermokarst basin (B3 and B2) were still flooded seasonally. The upland sites were generally better drained than the sites within the basin. We aimed to select representative sampling locations, based on overall vegetation and observed animal routes. However, we had limited information on representativeness in terms of soil type and wetness across this landscape. Still, we ensured that our study sites are comparable in terms of soil properties by measuring grain size composition of the soil material (Fig. 2-6). This revealed similar characteristics across sites with slight variations in clay and sand content, and silt contents ranging between 68 and 87 vol%, which shows that our sites are comparable in terms of physical soil properties.

Our results showed that the changes in vegetation height and structure correlated with large herbivore activity. This is in agreement with former studies in similar Arctic settings (Sundqvist *et al.* 2019, Skarin *et al.* 2020, Verma *et al.* 2020). However, the effects of seasonal flooding on vegetation composition and structure (sites B3 and B2) cannot be neglected. These differences in flooding regime marked a disparity between our sampling sites, since flooding at the basin sites B3 and B2 occurred seasonally or infrequently, while there are no records of any flooding for the other sites.

In our study area, shrubs were established on the upland before the introduction of large numbers of animals, and are now retreating, probably due to grazing pressure. While there are now higher shrubs at U3, there is a gradient in density of *Salix* ssp. shrubs towards less intensively grazed areas from individual shrubs to dense, forest-like coverage. At the edges of the drained thermokarst basin, shrubification took place on spots that could only be grazed occasionally (Olofsson *et al.* 2009) after the water level had retreated; the water retreated as the lake drained, allowing for incremental vegetation establishment. This leaves us with high soil wetness as another explanation for the absence of shrub vegetation (Martin *et al.* 2017). The clearing of the larch forest at the non-grazed site B1 four years prior to our study is also a plausible explanation for the limited shrub extent there.

The restricted grazing space within the fenced Pleistocene Park area led to a higher revisitation rate of animals to sites within the fence. This artificially increased grazing pressure led to the different vegetation structures observed inside and outside of the fence. Such shorter graminoid vegetation types are linked to grazing intensity (Forbes 2006). Monteath *et al.* (2021) found that the extinction of the Pleistocene megafauna was not responsible for causing an increase in shrubification, but rather that shrubification as a consequence of climate change during the early Holocene could have led to the extinction of megafauna as a result of habitat loss. However, modern rewilding approaches are planned and realised with recent herbivores capable of living in today's climate, though species composition might have to be adjusted continuously with warming conditions. Also, the cause and consequence in this setup are still

unclear, with opposite findings across studies, depending on the methods applied (Murchie *et al.* 2021). Numerous studies have found that contemporary herbivores were indeed capable of reducing shrub extent in Arctic environments on a local scale (Olofsson *et al.* 2009, Köster *et al.* 2015, Ylänne *et al.* 2018, Verma *et al.* 2020, Mekonnen *et al.* 2021). We found shallow thaw depths at intensively grazed sites and a much thicker active layer at the non-grazed B1 site. Generally, the increase in active layer thickness is associated with warming of the ground, influenced by summer temperatures, flooding, insulation from snow, and vegetation density and composition (Walker *et al.* 2003, Skarin *et al.* 2020, Magnússon *et al.* 2022). Therefore, as was stated by Zimov *et al.* (2012), the direct influence on these insulating factors could affect the active layer dynamics due to a stronger cooling of the ground in winter (Fig. 2-1). However, to determine any clear trends, repeated annual measurements of the thaw depth are needed.

Data from our basin sites showed that the more intensively grazed area featured smaller seasonal thaw depths in July 2019, compared to the occasionally or non-grazed sites (Fig. 2-4 and 2-9a). Keeping in mind the seasonal flooding at B3 and B2, one would expect greater thaw depths at these sites, since higher soil moisture promotes heat flow, and the relatively warm flood water adds heat to the soil as well (Magnússon *et al.* 2022). Examining the assumed permafrost table depth based on cryostratigraphic characteristics in the cores, we observed a contrary effect with an active layer depth of 61 cm bs under intensive grazing at B3, 74 cm bs under occasional grazing at B2, and 115 cm bs for the non-grazed B1 site. This supports our original hypothesis of grazing impacts being the main driver behind thaw depth differences, likely via vegetation changes.

At B3, the graminoid vegetation lay flat beneath the snow cover, offering little or no insulation. The snow itself was compacted by animal trampling, which further reduced the insulation properties of the snow cover. On the other hand, the forb undergrowth of the grassland at B2 provided slightly more resistance against the weight of the snow cover. Combined with less intensive trampling and, thus, a less compacted snow cover, the B2 sampling site was characterised by better winter insulation properties compared to B3. The *Salix* shrubs at B1 promoted localised snow trapping and a loose snowpack, both of which have been shown to provide effective insulation against cold winter air temperatures (Myers-Smith *et al.* 2011). Trampling was also missing in this non-grazed area. In addition to those surface conditions, the composition of the sediment itself could have contributed to a deeper active layer at site B1. From the grain size distribution data (Fig. 2-6) we saw that material among all studied sites was quite homogeneous (table 2-1). Exceptions were the sampling sites B1 and U1, which had a lower proportion of clay and were therefore generally dominated by coarser-grained material. High ice contents in the frozen part of the B1 core support the idea of an insulating effect of the peat layer that prevented the ground from thawing any deeper, but also helped to maintain the thick active

layer found here. This assumption implies that the peat layer worked as a heat flux barrier for the permafrost below, stopping summer thaw from the top, but also preventing bottom-up refreezing in winter. This could lead to present or future talik formation above the peat layer.
We were not able to compare thaw depths for the upland sites: the cryostratigraphically determined permafrost table depth of approximately 50 cm bs at U3 was, however, smaller than the active layer depths measured by Abramov *et al.* (2019) and Shmelev *et al.* (2021) for the close-by Mt. Rodinka site, located on a Yedoma upland with a mean active layer depth of 80 cm. Also evident in this study (Abramov *et al.* 2019) were smaller thaw depths, around 40 cm, for thermokarst basin sites featuring shorter vegetation in the Kolyma region , which is similar to our B3 site.
In our study, the reduced active layer thickness observed at the intensively grazed sites could also have originated from active layer compression by animal trampling, which would mean that even with shallower thaw depth the same amount of soil thawed. However, this last point cannot be tested with our data, since we were not able to measure bulk densities due to wet ground conditions and root structures. While such ground compaction is very common in peatlands (Batey 2009), the sandy silt soils that we found are only moderately compressible (Akayuli *et al.* 2013, Halcomb and Sjostedt 2019), especially as they were frozen throughout a major time of the year, making soil compaction a weak argument for the shallow active layer at intensively grazed sites. The regular flooding of the intensively grazed basin site, which usually leads to an increase in thaw depth (Magnússon *et al.* 2022), combined with the in fact shallower active layer found in our study when comparing to the non-grazed B1 site, suggests that the cooling effects induced by animal activity could be much larger than previously expected.

2.6.2 Carbon accumulation under grazing impact

We identified several variables that may be responsible for explaining differences in TOC between sites, including herbivory. Besides shorter graminoid vegetation types, other effects were also aligned with cooler temperature and/or less carbon degradation, such as soil moisture, as visualised by our PCA (Fig. 2-7). This coexisting influence of grazing and soil moisture should be tested in other locations. However, the contrast in TOC/TN ratios and $\delta^{13}C$ ratios (Fig. 2-5) of the studied deposits between intensive and non-grazed locations suggested that animal presence is affecting OM decomposition (if we assume a comparable OM source). But based on the differences in vegetation cover, we found that this contrast might also originate from different OM input as well as from different nitrogen input via the presence or absence of animal droppings. Since grazing alters the vegetation cover – assuming that in the absence of large herbivores the vegetation would be more homogeneous throughout the study area – the

observed strong differences in TOC/TN and $\delta^{13}C$ ratios have likely resulted from the differences in animal impact on the landscape. Grazing is, therefore, a reasonable explanation for the strong differences between sites, including TOC content.

Mean TOC was six times higher in the top 38 cm of B3 (minimum active layer depth) compared to B1, with intermediate values in B2 (Fig. 2-4 and 2-8). For the upland sites, mean TOC was twice as high under intensive grazing in those core sections lying within minimum active layer depth (38 cm, B3) compared to non-grazed cores. The effect was not visible in lower core parts, perhaps because of the relatively short time span of 23 years since intensified animal introduction into the area (Fig. 2-4). Instead, the TOC pattern in the frozen core parts was opposite to the higher TOC found in the active layer under intensive grazing influence. This suggests different pre-existing site conditions prior to herbivore introduction. The contrasting TOC pattern in the active layer suggests that animal grazing can help increase carbon storage in a relatively short time span (Fig. 2-9B) but grazing needs more time to affect deeper permafrost carbon storage apart from thermal stability, hence reduced thaw depth. Therefore, the TOC differences between sites were not significant when comparing the entire depth of the sampled cores. We explain this as a result of *i*) the TOC-rich peat layer found in B1 that shifts the TOC median value for non-grazed sites upwards, combined with *ii*) low TOC values in the frozen part of the intensively grazed sites which offset the high active layer TOC. Since the peat layer was found at 85 cm bs and dated to 4327 cal yr BP, we expect no connection to herbivory influence in a 23-year timespan, which is why we tested for significance in the active layer.

The significant differences in upper soil TOC between sites of intensive large herbivore presence (B3 and U3) and non-grazed sites (B1 and U1) agreed with the expected effects of grazing (Fig. 2-9B).

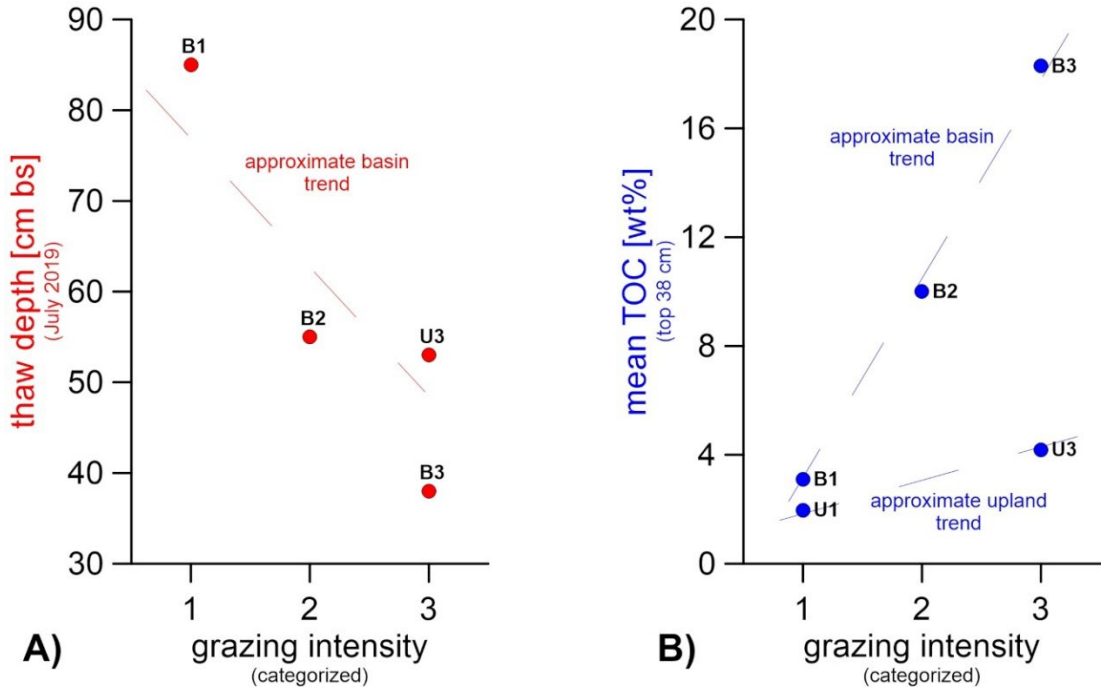

Figure 2-9 – Visualization of (A) thaw depth and (B) mean total organic carbon (TOC) of the uppermost 38 cm for all sampling sites, plotted versus grazing intensities 1 (no grazing) to 3 (intensive grazing); as site U1 was only sampled in winter, we do not have a summer thaw depth measurement for this site.

All organic carbon found in the upland areas showed higher $\delta^{13}C$ values (Fig. 2-5), which we interpreted as a result of colder, drier, and more compact ground conditions in the Yedoma deposits and therefore less OM decomposition, as well as differences in plant species, resulting in different $\delta^{13}C$ signals compared to the seasonally flooded and less compact ground of the drained thermokarst basin. Higher TOC/TN ratios in non-grazed sites indicated a different source material, originating from shrubby tundra, in comparison to grassland vegetation in occasionally and intensively grazed sites. However, these vegetation differences might originate from animal grazing impacts.

Above-ground carbon storage is also an important aspect of ecosystem carbon storage. Although we were unable to address above-ground carbon storage in this study, grazing activities of large herbivores have likely had an impact on above-ground biomass storage in vegetation by providing nitrogen fertilization via droppings. Mekonnen *et al.* (2021) stated that under intensified shrubification, shrubs take up large amounts of nutrients from the soil into the vegetation biomass. It is possible that CO_2 emissions from the soil might also be partially captured by this boosted plant growth and incorporated into plant biomass. However, nutrient availability is much more important for plant growth and hence carbon accumulation. Such nutrients become available when OM is decomposed, but the increased carbon accumulation by plant growth can to some extent offset the carbon losses associated with permafrost-stored OM decomposition (Keuper *et al.* 2012, Turetsky *et al.* 2020b). While shrub growth increases above-ground biomass, it generally leads to net ecosystem carbon losses via heterotrophic respiration (Phillips and Wurzburger 2019). The formation of grasslands, on the other hand,

increases above-ground carbon cycling as well, showing high productivity (Gao *et al.* 2016). While showing the highest respiration rates, soil carbon accumulation in wet Arctic grasslands is greatest when compared to other Arctic vegetation types (Bradley-Cook and Virginia 2018). This might be linked to the relative ease of grassland litter transfer into the soil, e.g. via animal trampling, as well as deeper root penetration of graminoids, compared to shrubby and sturdier vegetation (Wang *et al.* 2016). Based on this, we expect an increase in above-ground short-term carbon fixation in the more productive graminoid vegetation at intensively-grazed sites compared to non-grazed tundra sites, but cannot make any quantitative statements on this for our sites due to a lack of data regarding this matter. We summarise two points from our carbon data:

(1) In the upper part of the soil cores, TOC contents were higher in more intensively grazed sites, with a decrease with less grazing for both thermokarst-affected and Yedoma sites (Fig. 2-9B). As the soil and sediment characteristics of the non-grazed U1 Yedoma site matched findings from other Yedoma studies (Strauss *et al.* 2012, Jongejans *et al.* 2018, Windirsch *et al.* 2020c), we consider this as the pre-grazing Holocene state (i.e., not heavily grazed state). This suggests that intensive grazing for 23 years has already increased TOC amounts stored in the active layer by a factor of two (Fig. 2-4). At thermokarst sites, hydrology has an impact on TOC storage as well, which is seen in the strong correlation between TOC content and water content in the PCA (Fig. 2-7). However, a direct comparison to a pre-grazing state for our sites isnot possible.

(2) Intensively grazed areas displayed a shallower thaw depth (Fig. 2-9A). This was in line with the hypothesis that connected ground cooling effects with snow removal or snow compaction. These changes in snow properties can result from vegetation shifts towards graminoid communities, which trap less snow, as well as snow compaction by animal trampling. Also, here an active layer depth reduction could have happened in a rather short period of time. While TOC was significantly higher in the active layer in intensively grazed sites, the shallower thaw depths associated with these intensively grazed sites might contribute to stabilizing the underlying permafrost, hence preventing fossil permafrost-stored OM from degradation. However, our study cannot rule out influencing factors other than grazing adding to the trends illustrated in figure 2-9.

Even if we cannot quantify the landscape and its carbon storage with no artificially introduced herbivores, we can make some assumptions based on other studies' findings. These assumptions are hypothetical for our study area, but based on previously published studies. In a partially drained thermokarst basin within a Yedoma landscape, relatively warm soil conditions and hence a deep active layer would most likely be found in the drained basin (Windirsch *et al.* 2020c). Normally, the active layer would first become shallower after lake drainage, with less water content leading to reduced heat flux into the soil and making room for cold winter

air, and stabilise once tundra vegetation, shrubs, or even small trees re-establish, working as ground insulators in summer (Blok *et al.* 2010) in the absence of grazing. Over time, peat formation is likely to take place if wetness is still high, increasing carbon concentration and insulation effects on the underlying ground (Jones *et al.* 2012). In regularly flooded thermokarst basin areas, a graminoid vegetation holding vast extents of *Eriophorum* spp. will likely develop, while dry basin areas will normally feature *Salix* spp. shrubs (Regmi *et al.* 2012). On the surrounding uplands we expect a generally homogeneous appearance of soil carbon and vegetation, where differences are controlled by local parameters. These controls include differences in cryostratigraphy, substrate, and water availability, among others. On uplands we expect to find tundra vegetation, most likely with increasing shrubification throughout the last decades. Moreover we expect forested areas on those uplands with differing thaw depth between vegetation types and a thick but stable active layer beneath forests (Stuenzi *et al.* 2021). A deepening active layer is likely to occur underneath tundra as a result of global climate warming, which also increases shrubification (Wilcox *et al.* 2019) and therefore snow trapping. While shrubification may shield the ground from further summer thawing, the contrasting seasonal lengths of summer and winter may come into effect, reducing summer thaw but preventing winter refreezing at the same time. These literature-based qualitative scenarios suggest that the grazing impacts observed in our study, especially as regards alterations in vegetation and thaw depth, might represent a major system change; this may also be true for the increase in carbon storage at the intensively grazed U3 upland site. Hence, larger scale grazing could potentially help to keep carbon in the ground and reduce natural carbon emissions from permafrost, although in no case would this be a substitute for decarbonizing the current industrialised society. Due to technical constraints, the efficacy of this landscape management tool should not be overestimated.

2.6.3 Methodological limitations of the pilot study

Due to the spatial and temporal limitations in the data we collected, we cannot unambiguously distinguish between previous conditions at our sites, and the overall herbivory impact on soil TOC. Soil carbon distribution as well as local environmental differences influencing thaw depth might have existed before herbivore introduction; this cannot be accounted for in our study. However, the presence of rather fresh material present in the seasonal thaw layer at sites B3 and U3 (table S2-1) suggested a link to modern disturbances (table S2-1), for which animal trampling, bioturbation, or cryoturbation all provide a valid explanation.

Despite results being consistent with the expected effects of grazing on ground temperature proposed by Zimov *et al.* (2012), the missing core replication of the present study combined with the expected spatial heterogeneity of active layer depths indicated that this interpretation needs further data for validation. Further, more replicated studies, potentially combined with spatially comprehensive modeling exercises, are advised along with monitoring of exclosure

sites with gradual herbivore introduction. Also a 23-year time period of herbivore activity is likely too short to affect deeper and permanently frozen deposits but mainly affects the active layer both in terms of chemical properties and thaw depth.

The larch forest clear cut at B1 marked a clear difference between our sampling sites, as stable boreal forest is known to protect permafrost against summer heat (Stuenzi *et al.* 2021), maintaining a deep but stable active layer. However, we still encountered the greatest seasonal thaw depth here. This greater thaw depth here agreed with the findings of relatively warmer but stable permafrost temperatures below forests in the Arctic and boreal region (Kropp *et al.* 2020) and was likely a relic of the previous forest-covered state. We found no sign of active layer refreezing. The thaw depth extended down to the peat layer, which started at 85 cm bs; the peat layer might have been functioning as a heat flux insulator both for summer thawing (from the top) and winter refreezing (from the bottom). Also, a detailed assessment of effects of different vegetation compositions typical for pastures in the Arctic on heat fluxes is needed. Ultimately, more studies and monitoring setups on the impact of large herbivore grazing on permafrost soil carbon storage are needed across the Arctic. Hence, we hesitate to draw universal conclusions on herbivory effects from our data, including the extension of these results to much larger regions.

2.7 Conclusion

We found evidence from our permafrost study sites that intensive grazing by large herbivorous animals might have contributed to keeping the soil cool and maintaining – or even slightly increasing – carbon storage in our studied permafrost sites over a 23-year time period. At the same time, annual thaw depth was found to be lower at intensively grazed sites. These changes of ground characteristics are likely a combined result of vegetation changes and snow insulation reduction, probably amplified by additional carbon input due to intense herbivore impacts. Vegetation appears to have changed from shrubby tundra to grasslands under herbivory impact in our study area. Differences in soil moisture seem to play a role at our sites as well, and further research on the hydrological conditions and connections at our sites is needed. To further investigate herbivory effects, it is necessary to sample grazing intensity transects at higher spatial and temporal resolution and replication and to repeat this approach in other permafrost areas as well. Also, more detailed monitoring approaches are needed, such as the setup of exclosure sites that allow for direct comparison of a range of sampled parameters with sites under the influence of different grazing intensities.

We conclude that intensified animal husbandry could locally contribute to stabilizing carbon storage in the active layer at non-forest permafrost sites, and might further preserve carbon stored in permafrost ground by maintaining a frozen state. This management practice may fit into a broader set of tools that could be used to mitigate the consequences of local permafrost

thaw in order to buffer climate change impacts. Answering the interesting question of whether such an approach could be scalable to larger regions was not part of our study.

2.8 Data availability statement

The datasets presented in this study can be found in online repositories. The datasets presented are deposited with the PANGAEA data repository, accessible using https://doi.org/10.1594/PANGAEA.933446 (Windirsch *et al.* 2021b).

2.9 Author contributions

TW, GG, MU, and JS designed the study. TW conducted field and laboratory work, prepared the graphics, and led the writing of this manuscript. TW, GG, MU, and JS analysed and interpreted the laboratory results. GG designed the maps used in this study. BF, MM-F, and JO provided expertise on herbivory and herbivore-environment interactions. JW contributed expertise in vegetation classification and statistics. NZ and MG provided expertise on the area and local environment processes and characteristics as well as on the Pleistocene Park experiment. All authors contributed to compiling and editing the manuscript.

2.10 Funding

The field campaign was carried out in the framework of the CACOON (Changing Arctic Carbon Cycle in the Coastal Ocean Near-Shore) project (#03F0806A (German Federal Ministry of Education and Research)) and as part of the PeCHEc (Permafrost Carbon Stabilization by Recreating a Herbivore-Driven Ecosystem) project funded by the Potsdam Graduate School. The authors received additional support from the Geo.X research network (SO_087_GeoX). Additional funding was provided by the CHARTER (Drivers and Feedbacks of Changes in Arctic Terrestrial Biodiversity) project (grant agreement ID 869471). We further acknowledge base funding provided by the Alfred Wegener Institute expedition funds, as well as support by the Open Access Publication Funds of Alfred-Wegener-Institut Helmholtz-Zentrum für Polar- und Meeresforschung.

2.11 Acknowledgements

We thank the Field Experiments & Instrumentation team at the Max Planck Institute for Biogeochemistry in Jena as well as Juri Palmtag for helping with the drilling campaign. We further acknowledge Dyke Scheidemann, Jonas Sernau, and Angelique Opitz (Carbon and Nitrogen Lab [CarLa]) as well as Mikaela Weiner and Hanno Meyer (Stable Isotope Lab) from AWI for assistance in the laboratory. We thank Christian Knoblauch (Universität Hamburg) for helping with TOC measurements. This study was supported by the Northeast Science Station team in Chersky, Sakha. We further thank J. Otto Habeck (Universität Hamburg) for his help in designing this study.

2.12 Conflict of interests

The authors declare no conflict of interests.

Chapter 3: Impacts of Reindeer on Soil Carbon Storage in the Seasonally Frozen Ground of Northern Finland: a Pilot Study

Impacts of Reindeer on Soil Carbon Storage in the Seasonally Frozen Ground of Northern Finland: a Pilot Study

Windirsch, T.[1,2], Forbes, B. C.[3], Grosse, G.[1,2], Wolter, J.[1,4], Stark, S.[3], Treat, C. C.[1], Ulrich, M.[5], Fuchs, M.[1], Olofsson, J.[6], Kumpula, T.[7], Macias-Fauria, M.[8], and Strauss, J.[1]

[1]Alfred Wegener Institute Helmholtz Centre for Polar and Marine Research, Potsdam, Germany

[2]Institute for Geosciences, University of Potsdam, Potsdam, Germany

[3]Arctic Centre, University of Lapland, Rovaniemi, Finland

[4]Institute of Biochemistry and Biology, University of Potsdam, Potsdam, Germany

[5]German Federal Environment Agency, Dessau-Roßlau, Germany

[6]Department of Ecology and Environmental Science, Umeå University, Umeå, Sweden

[7]Department of Geographical and Historical Studies, University of Eastern Finland, Joensuu, Finland

[8]Biogeosciences Lab, School of Geography and the Environment, University of Oxford, Oxford, England

Published in: Boreal Environment Research

3.1 Abstract

To test the effect of reindeer husbandry on soil carbon storage of seasonally frozen ground we analysed soil and vegetation properties in peatlands and mixed pine and mountain birch forests. We analysed sites with no grazing and contrasting intensities of grazing, and associated trampling, in Northern Finland. With a pilot study approach we optimised the study design to include several grazing class sites including grazing seasonality but omitting sample replication at one site. Soils were analysed for water content, bulk density, total organic carbon (TOC), total nitrogen, stable carbon isotopes and radiocarbon ages. We found that there was no significant difference between grazing intensities in terms of TOC, but that TOC mainly depended on the soils' TOC content present prior to intensive herbivory introduction. In contrast, understory vegetation was visibly transformed from dwarf shrub to graminoid-dominated vegetation with increasing grazing and trampling intensity. Also, we found a decrease in bulk density with increasing animal activity on soil sites, which most likely results from named vegetation changes and therefore different peat structures.

3.2 Introduction

Due to global warming, high-latitude regions are experiencing rapid warming, which has the potential to emit substantial amounts of carbon from previously either seasonally or perennially frozen organic material (OM) stored below ground (Hugelius et al. 2014, Schuur et al. 2015). With rising soil temperatures, microbial decomposition of OM accelerates (Davidson and Janssens 2006, Walz et al. 2017). Also, following recent global climate modelling approaches, high-latitude soil temperatures will further increase, thus shortening the freezing season as well as reducing permafrost extent, with more subarctic and low Arctic areas losing perennially

frozen ground conditions (IPCC 2021). In seasonally frozen soils, the frozen season is also shortened due to climate warming and increasing snowfall (Venäläinen et al. 2001).

Large grazing herbivores exert two important effects on soil temperatures both during and outside the growing season. First, large herbivores are assumed to have stabilised cold ground conditions during the late Pleistocene (Zimov et al. 1995) by altering the vegetation structure both via grazing and trampling (Tuomi et al. 2021). Especially a reduction in vegetation height has been shown to alter the temperature regime (Olofsson et al. 2004, Zimov 2005). At very high intensities, grazing by large herbivores may reduce shrub growth in favour of grasslands, which increases albedo hence reducing heat fluxes and overall energy input (te Beest et al. 2016). A similar effect on vegetation is known from anthropogenic disturbances (Forbes et al. 2001). Second, large herbivores compress and partially remove the snow cover in winter. In this way, large herbivores again promote ground cooling, since this reduction of insulation allows for cold winter air temperatures to reach the ground (Beer et al. 2020).

Adding to this, pasture areas have been shown to act as a carbon sink in temperate climate (Mudge et al. 2011), which is most likely a result of increased vegetation productivity linked to grassland establishment by intensive grazing, compared to former tundra vegetation.

With herbivores promoting lower ground temperatures by above-named processes, in permafrost areas, OM degradation is slowed down by maintaining a perennially or at least seasonally frozen state of soil OM (Macias-Fauria et al. 2020, Windirsch et al. 2022a). Yet, the mechanisms by which herbivores influence soil carbon storage are likely different in non-permafrost areas, where soil temperatures are lower under grazing during winter, but higher under grazing during summer (Fig. 3-1) (Olofsson et al. 2004, Macias-Fauria et al. 2008, Stark et al. 2015). In permafrost areas, this effect is mainly observed in the seasonal thaw layer on top of the permafrost called active laver. However, in Fennoscandia this seasonal thaw layer is most often not present, simply due to the absence of permafrost. Instead, unfrozen or seasonally frozen peat soils make up approximately 18.1 % of the land surface of Finland (Tanneberger et al. 2017), where this study was carried out, and are preferred by reindeer for pasture sites. This allows us to assume that the pasture effects proposed by Mudge et al. (2011) take place here as well. Especially changes in vegetation by reindeer grazing are present in Fennoscandia (Maliniemi et al. 2018).

For this study, we hypothesise that more intense animal activity leads to snow compaction and vegetation changes, which both reduce ground insulation, promoting winter cooling of the ground and hence reducing OM decomposition, hence increasing soil carbon storage with grazing intensity in a similar way as for perennially frozen soils (Windirsch et al. 2022a) (Fig. 3-1). In detail, we aim to assess the effects of reindeer presence on soil organic carbon storage in a northern boreal landscape with seasonally frozen ground. We aim to answer

whether combined reindeer grazing and trampling increase soil carbon storage in a cold region. Further we aim to decipher under which grazing intensity (from exclosures to pastures) the shifts in carbon storage occur. For this, we sampled as many sites as possible, spanning over five different grazing intensities and two grazing seasons, as a first assessment of possibly detectable changes.

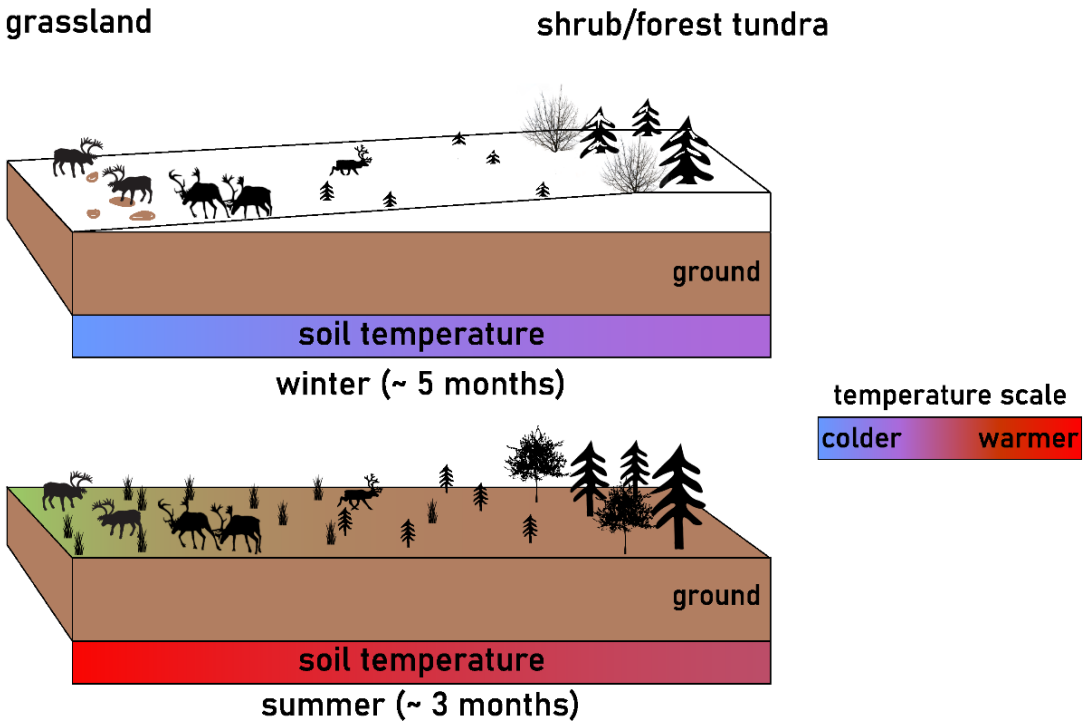

Figure 3-1 – Schematic overview of our hypothesis stating that increased herbivore activity reduces snow height by trampling, and induces vegetation changes towards grasslands, overall reducing snow trap mechanisms; this promotes cooling of the ground in winter and reduces OM degradation, leading to higher carbon levels stored in pasture substrates; approximate season length taken from Ruosteenoja *et al.* (2011).

3.3 Study area

We conducted this pilot study in Inari municipality in Northern Finland. The study area varies between 185 and 370 m above sea level (Paoli et al. 2018). The landscape was shaped by glaciation during the last ice age and became ice-free approximately 9000 years ago. Glacial features such as eskers and moraines provide relief in the valley areas between mountain ranges. As a result of former glaciation, the ground consists of sandy sediments and gravel deposits which are typical glacial remnants at ground level. Fine material (silt, loess) is washed out during, or removed by, aeolian processes after glacial melt (Derbyshire and Owen 2018). The area is characterised by vast pine (*Pinus sylvestris*) and mountain birch (*Betula pubescens* ssp. *czerepanovii*) forests, interspersed with lakes and peat mires characterised by graminoids and shrubby vegetation. Mountain birch consists of short-statured, shrub-like multi-stemmed growth forms. Evergreen dwarf shrubs dominate the understorey vegetation (e.g. *Empetrum nigrum* ssp. *hermaphroditum*, *Vaccinium vitis-idaea*, *Calluna vulgaris* and *Linnaea borealis*) (Oksanen and Virtanen 1995, Maliniemi et al. 2018). The deciduous dwarf shrubs *Vaccinium*

myrtillus and *Betula nana* are also common. *Deschampsia flexuosa* is the most common graminoid species. The ground layer is dominated by the bryophytes *Pleurozium schreberi* and *Dicranum* spp. and ground lichens *Cladonia rangiferina*, *Cladonia arbuscula* and *Cladonia* spp. (Oksanen and Virtanen 1995). The climate in our study area is typically subarctic and continental, with January as the coldest month (mean air temperature of -13.1 °C) and July as the warmest (mean air temperature of 13.9 °C). Mean annual air temperature was 0.1 °C from 2008 to 2020 (monthly observation data of the weather station at Inari Kaamanen, Finnish Meteorological Institute, 2021). Annual precipitation sums up to 458.4 mm, based on monthly averages, and is highest in July with 69.2 mm (Finnish Meteorological Institute, 2021).

The herding of semi-domesticated reindeer (*Rangifer tarandus tarandus*) has been the prevailing form of land-use in the study area for centuries (Löf et al. 2022). The livelihood originally adapted to long seasonal migrations between nutrient-rich coastal areas in Norway during summer and continental lichen-rich mountain areas in Finland, Sweden and Norway during winter (Oksanen and Virtanen 1995). Since the 1880's, reindeer herding has been practised within separate reindeer herding cooperatives, many of which have established a pasture rotation system separating winter and summer ranges with fences (Kumpula et al. 2011). Reindeer select their feeding sites based on forage availability and insect avoidance, and favour peatlands for foraging during summer (Bezard et al. 2015, Horstkotte et al. 2022). Semi-dry and dry mountain birch forests are used for foraging especially in early and late summer (Bezard et al. 2015).

In this study, we selected a total of 21 sites from the Kutuharju Field Research Station and the Muotkatunturi reindeer herding cooperative. Out of these sites, 18 were located on the premises of the Kutuharju Field Research Station, and three in the reindeer summer ranges of the Muotkatunturi herding co-operative (Fig. 3-2) (Windirsch et al. 2021).

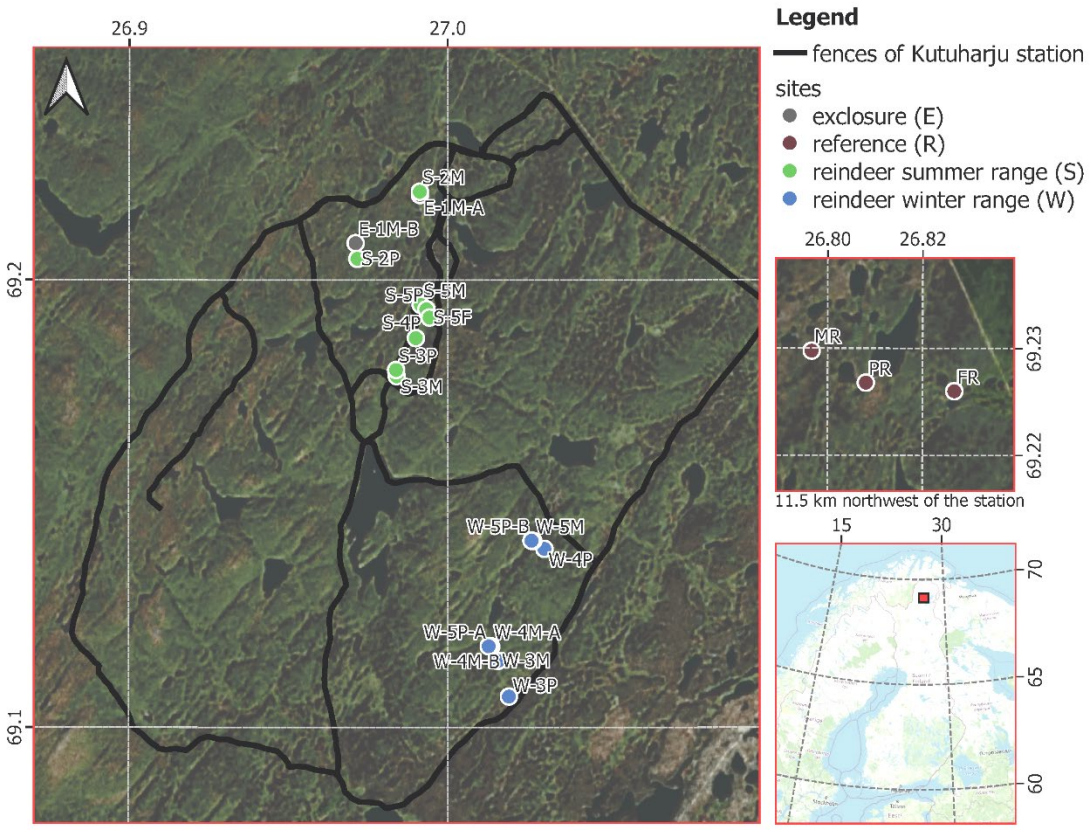

Figure 3-2 – Satellite imagery and topographic map of the study sites; left: satellite image of the sampling locations on the Kutuharju station premises; right top: satellite image of the sampling locations outside the research station in the Muotkatunturi herding district; right bottom: study area location map (red square); basemap provided by ESRI and OSM.

The Kutuharju Field Research Station spans across 44.6 km^2 (Fig. 3-2) and consists of peatlands (16.9 %, 7.5 km²) and mineral soil deposits (77.0 %, 34.4 km²), interspersed with lakes (4.6 %, 2.1 km²) and rocky terrain without soil formation (1.5 %, 0.7 km²) (coverage based on National Land Survey of Finland (2021)). Approximately 170-200 animals are kept at the station after autumn slaughter, resulting in an average reindeer density of 4.4 reindeer/km^2. The area is separated into four fenced areas where the animals roam during different seasons (early summer, all summer, late summer, winter). The surrounding area outside the station's fences is part of the reindeer summer ranges of the Muotkatunturi reindeer herding co-operative, which has an area of 2580 km² with a reindeer stock of maximum 6800 individuals, leading to an average density of approximately 2.6 animals/km² (Finnish Reindeer Herders' Association 2022).

3.4 Methods

3.4.1 Field work

In order to detect the long-term effects of reindeer grazing on soil carbon storage, we applied a space-for-time approach, in which we selected presumably similar sites, in terms of soil type,

influenced by different grazing intensities, instead of monitoring one site for a longer time period while gradually introducing herbivory. We did so in a pilot study design that aimed at sampling a high number of individual sites to gain a detailed overview over a large area.

We selected sites to cover all five grazing intensities that we were able to identify: control sites entirely without grazing, sites along reindeer migration routes (i.e., sites that the reindeer use for passage and which then experience occasional grazing pulses), and sites in the reindeer pastures (i.e., sites where the reindeer stay for long periods and which then experience long-term grazing and trampling). We selected our sites according to observed grazing intensity via animal numbers and visiting frequency over several days, as well as long-term observations made by the station and identified five different grazing intensities:

- no grazing (exclosure; intensity 1; 2 sites);
- occasional migration route (seasonal; intensity 2; 2 sites);
- daily migration route (seasonal; intensity 3; 4 sites);
- high-frequency daily migration route (seasonal; intensity 4; 4 sites);
- pasture or supplementary feeding site (seasonal; intensity 5; 6 sites) (table 3-1).

In addition, we sampled sites from the overall state present outside the research station premises (intensity 3; 3 sites) — which visually matched the migration route sites within the station premises. We accounted for this as the natural grazing state, where 'natural' refers to the common grazing intensity in the context of reindeer herding in Fennoscandia throughout history.

If there were several vegetation types present within one grazing intensity, we sampled each type. This resulted in 21 sites, out of which 18 were located on the premises of the Kutuharju Field Research station (Fig. 3-2).

In the site labels, the letters M (mineral soil), P (peat), and F (forest) are used to identify the individual sites by main characteristics. In this naming scheme, forest sites are also peat soils but covered by trees instead of open peatlands. The letter S marks sites from the Kutuharju station summer ranges, while W marks sites from winter ranges. R marks reference sites outside the station, E indicates exclosure sites. M and P are describing the soil type as either mineral soil or peat. At peat sites, we tried capturing the complete peat column and the first few cm of underlying mineral soil (Fig. S3-2 and S3-3). Winter ranges were sampled in June 2022, while summer ranges and reference sites were sampled in September 2020.

To avoid confounding factors such as soil erosion effects and soil moisture differences, we chose our sampling sites neither on hill tops nor steep slopes or valley bottoms, and avoided sites with ponding water or dried-up vegetation to make them as comparable as possible.

We retrieved peat cores with a Russian peat corer (50 cm sampling length, 530 cm^3). For mineral soil sites, soil profiles were excavated and sampled using fixed volume cylinders. Peat cores were subsampled in the field in 5 cm increments, while at mineral soil sites samples

were collected according to all visible soil horizons. Sampling with the peat sampler and fixed volume cylinders allowed us to determine the volume of each sub-sample, which later allowed us to calculate bulk densities. All samples were stored in Whirlpak sampling bags and kept cool throughout the transport to the laboratory.

On each site, we first visually assessed the main vegetation types (grassland, tundra, forest) by identifying the predominant species as well as the average height of each predominant species, both in the field and on pictures later on. We did this on 1 m² plots, in which centre we collected soil samples in the form of one soil core or soil profile afterwards. The plots were selected for not having trees, as tree roots would obstruct the soil sampling. However, we accounted for trees being present in the wider surrounding (approximately 10 by 10 m) to identify a site as either forest or open landscape. The dominance of vegetation species was estimated by the approximate area covered on the 1 m² plots. At many sites, we found one species each to cover more than 50 % of the plot. We did not aim to account for all species present, but the most abundant ones, to identify the main differences between plots.

3.4.2 Laboratory analysis

We determined the absolute water content of all samples by weighing (Mettler Toledo KERN FCB 8K0.1, accuracy 0.1 g) them pre- and post-freeze drying (Zirbus Sublimator 15) and related this to wet weight. Using the sample volumes calculated by the peat corer volume and sample thickness, we calculated the bulk density. Afterwards, samples were split into subsamples for biogeochemical and sedimentological analysis.

Using a planetary mill (Fritsch Pulverisette 5), samples for biogeochemical analysis were homogenised and weighed into steel crucibles for elemental analysis. Total organic carbon (TOC) and total nitrogen (TN) were determined by combustion, using a soliTOC cube and a rapidMAX N Elemental Analyser (both Elementar Analysensysteme). These parameters are reported in percentage by weight (wt%).

Carbon to nitrogen ratio (TOC/TN) was calculated from TOC and TN, used as a proxy for OM decomposition state by assuming a stable source (Strauss et al. 2015).

In order to have an indication on the quality and source of the organic matter, we analysed stable carbon isotope ratios ($\delta^{13}C$). For this, the previously homogenised samples were treated with hydrochloric acid at 50 °C for three hours to remove carbonates. After washing the sample acid free, we used a Delta V Advantage Isotope Ratio MS supplement equipped with a Flash 2000 Organic Elemental Analyser for isotope measurement. The resulting values are given in ‰ in relation to the Vienna Pee Dee Belemnite (‰ vs.VPDB) standard (Coplen et al. 2006).

In addition, we took OM for radiocarbon dating from selected samples from the dried original samples, and used the Mini Carbon Dating System (MICADAS) at Alfred Wegener Institute Bremerhaven (Mollenhauer et al. 2021). Results were calculated in calibrated years before

present (cal yr BP, meaning before 1950) using the calibration software Calib ver. 8.2 and applying the IntCal20 calibration curve (Reimer et al. 2020, Stuiver et al. 2021).
For sample reference, the mean sample depth is used for all soil parameters throughout this manuscript. Depth is given in cm below surface (cm bs).

3.4.3 Data analysis and calculations

We used a principal component analysis (PCA) comparing the top 30 cm of all our sites in terms of bulk density, TOC, $\delta^{13}C$ ratios, TOC/TN ratios and water content, categorised by grazing intensity, soil type (mineral soil or peat) and season of animal activity (summer, winter or no seasonality) to assess which measured parameters have the strongest effects within our dataset. For this, data were normalised between zero and one, using the following function:

$$function(x)[(x - \min(x))/(\max(x) - \min(x))]$$

where x is the dataset and min(x) and max(x) mark the minimum and maximum value of dataset x.
For the PCA we used "prcomp" on the normalised data. We chose the top 30 cm as grazing effects are usually most visible in the upper parts of a soil column.
All calculations were done in the R environment using the "stats" package (R Core Team 2021).
We further calculated weighted mean TOC values for the samples of the top 30 cm of each site, using Eq. 1

$$mean\ TOC = \frac{(h(sample\ A) \times TOC(sampleA)) + (h(sample\ B) \times TOC(sample\ B)) + \cdots}{30} \quad (1)$$

where h is the height as the vertical sample dimension in cm, TOC is the total organic carbon measurement value in percentage by weight, and 30 is the total depth that samples used in this calculation originate from, given in cm below surface.
Sampling gaps were interpolated from the adjacent sample. We did this for a more readable comparison across grazing intensities, soil types and seasonality.
For better comparability of our study sites, we also calculated soil organic carbon (SOC) stocks in kg m^{-2}, restricted to the top 30 cm due to large differences in sampling depth between sites. SOC was calculated using Eq. 2.

$$SOC[kg\ m^{-2}] = \frac{TOC\ [wt\%]}{100} \times bulk\ density\ [g\ cm^{-3}] \times sample\ height\ [cm] \times 10 \quad (2)$$

Due to small sample numbers within each grazing intensity, especially when differentiating between soil types, our dataset does not allow for significance testing of differences in soil parameters.

3.5 Results

3.5.1 Core descriptions

Almost all mineral soil profiles featured similar horizons, although with varying horizon thickness (Fig. 3-3 and S3-2). They consist of an organic layer on top, followed by an organic-rich soil layer in E-1M-B, MR, S-3M and W-3M. In W-5M, the organic top layer was compressed into the underlying soil (table 3-2). The organic-rich soil layer is followed by a pale, sandy eluvial horizon and an orange-reddish illuvial horizon (7.5YR ~ 5/8 on Munsell colour chart). At sites E-1M-A and W-4M-A and -B, the organic-rich soil layer was not found. Instead, the organic layer on top of the soil was directly followed by an eluvial horizon. Underneath, the eluvial horizon is followed by a yellowish (2.5Y 5/4) sand horizon down to the end of the profile. However, this layer was not reached at all mineral soil sites.

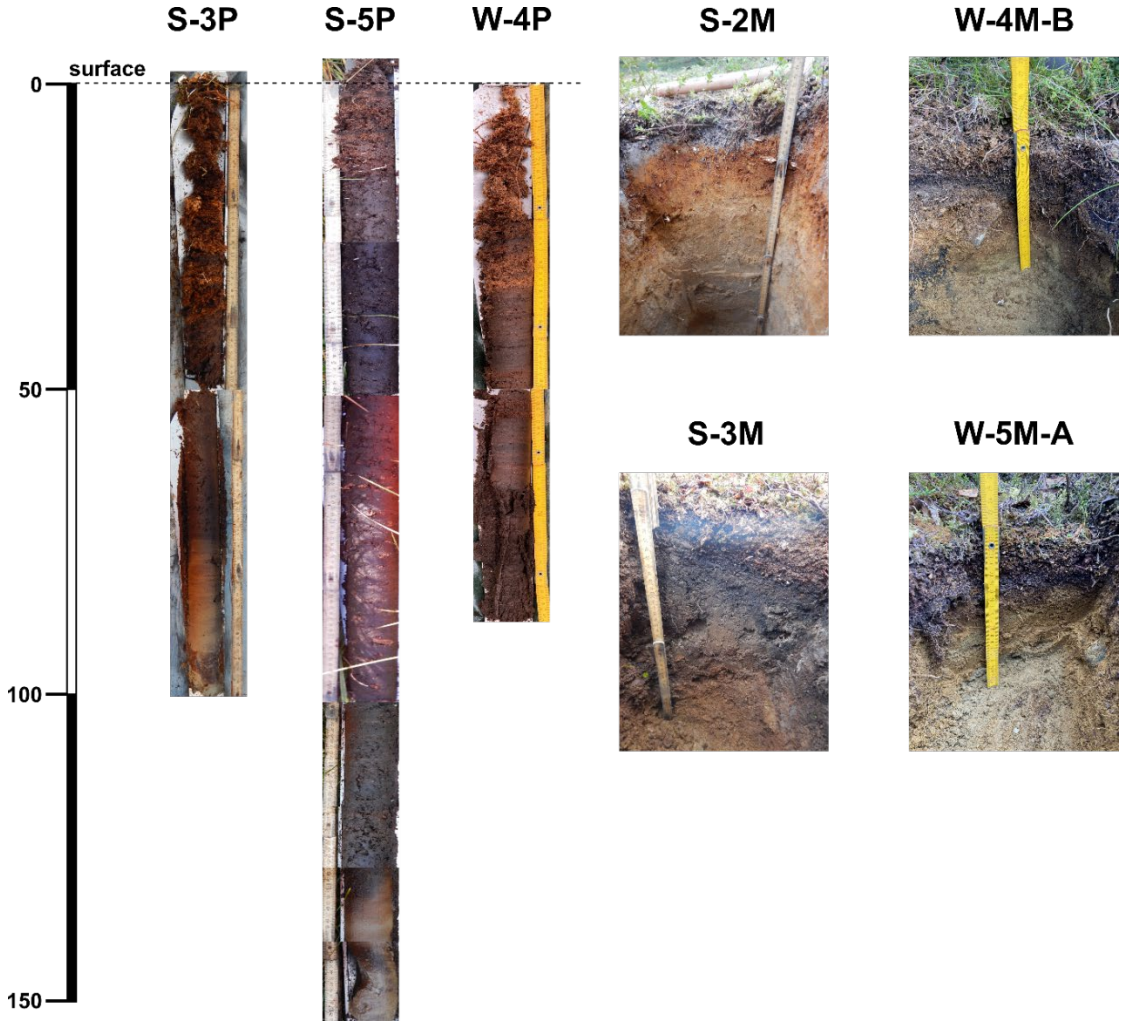

Figure 3-3 – Representative field photos of the peat cores obtained at S-3P, S-5P and W-4P, as well as soil profiles excavated at S-2M, S-3M, W-4M-B and W-5M-A; for field photos of all sites please see figures S3-2 and S3-3.

At the peat sites, the peat column (between 25 cm (W-3P) and 143 cm (S-4P)) was underlain by sandy material (Fig. 3-3). The peat column was divisible by the degradation state (table 3-2). There were differences in peat source material, which was (*Sphagnum*) moss in S-2P, PR, W-4P, W-5P-A and W-5P-B, while at the other sites the material was more heterogeneous, darker and often more decomposed. However, similar moss peat appeared deeper in the profiles at S-3P and S-5F.

3.5.2 Vegetation

We encountered four main vegetation types at our sampling locations. The first is a mixed forest mainly consisting of *Pinus sylvestris* and *Betula pubescens* ssp. *czerepanovii* trees, which was found at sites E-1M-A, S-2M, W-3M, W-4M-A and -B, W-5M and MR. There were differences in the understorey vegetation, though (table 3-2).

The second vegetation type we found is best described as a wet birch forest, consisting mainly of *B. czerepanovii*. This type, found at sites S-5F, W-4P and FR, featured a ground layer holding *Vaccinium*, and some *Sphagnum* spp. underneath (table 3-2).

The third vegetation type, found in non-forest areas, was a tundra-like mix of heath and grassland vegetation. It is predominantly covered by *Salix* sp., *Vaccinium* sp. and *Empetrum nigrum* and was found at S-2P, S-3M, S-3P, W-3P, S-4P and PR (table 3-2).

The fourth vegetation type, found only at grazing-intensive sites S-5P , W-5P-A and -B and S-5M, was a grassland with no significant shrub layer and very few species. Summer sites were strongly dominated (> 90 % coverage) by *D. cespitosa*, which grew nest- or tussock-like and reached up to 120 cm in height at S-5P and up to 70 cm in height at S-5M, while on winter sites *Eriophorum* made up the vast majority of graminoid vegetation (table 3-2). For detailed vegetation records per site, please see table 3-2.

3.5.3 Carbon parameters

3.5.3.1 Total organic carbon (TOC)

At mineral soil sites, the maximum sampling depth was reached at S-2M with 67 cm bs (Fig. 3-4a). For all mineral soil sites, TOC was highest in the uppermost sample, representing the organic top layer, and declined with depth. The highest value across mineral soil sites was found in W-3M (51.30 wt% at 10 cm bs), while the lowest value occurred in W-5M (0.44 wt% at 19.75 cm bs).

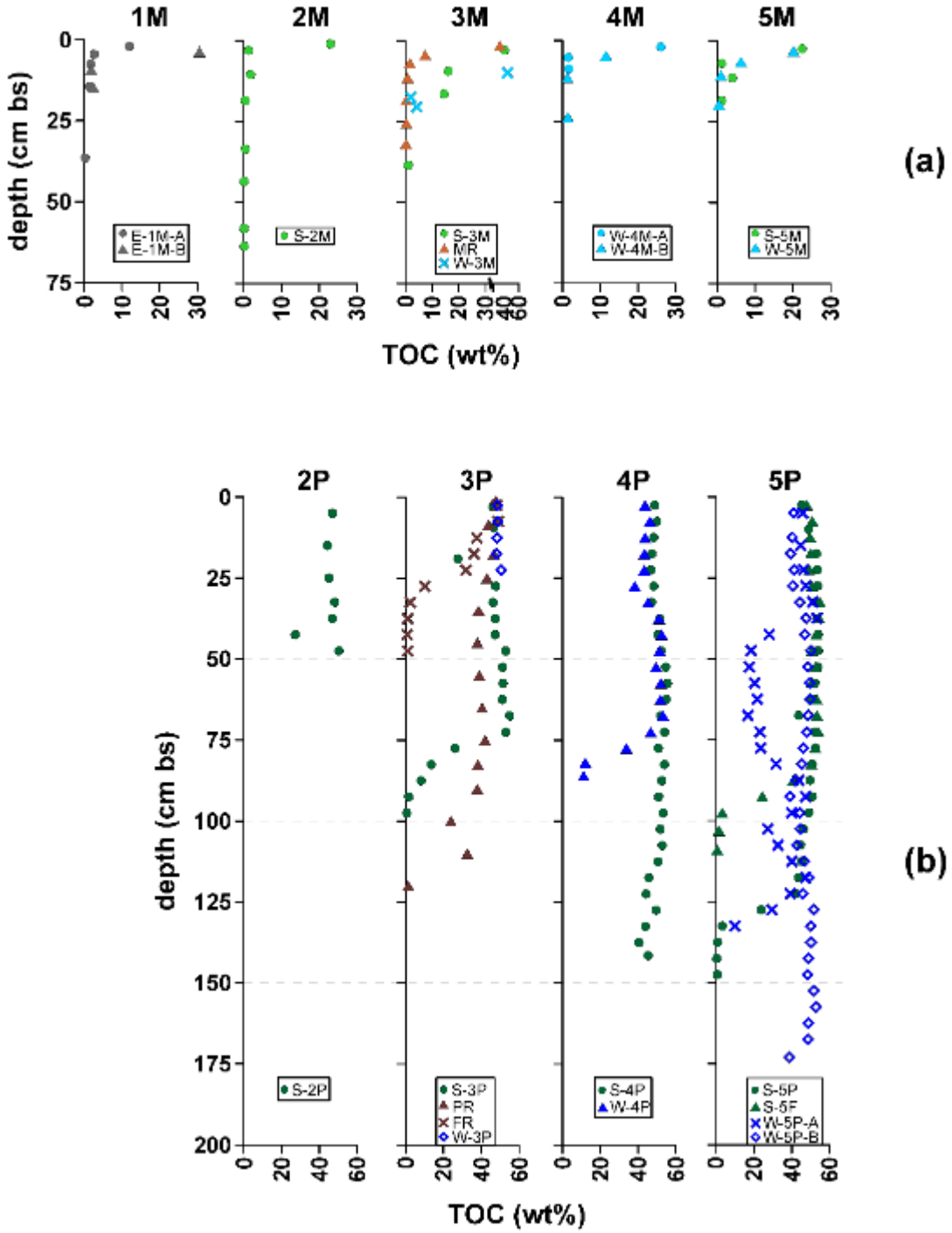

Figure 3-4 – TOC for all sites, plotted over depth; grazing intensity increases from left to right; a) mineral soil sites; b) peat sites; different symbols are for different sites within one plot; green indicates summer sites, blue winter sites, grey exclosure sites, and brown colours mark reference sites with natural grazing regime outside the reindeer fences. Note the differently scaled x-axes for mineral soil and peat sites as well as the axis break in 3M.

At peat sites, TOC was high and homogenous in the peat column, with a sharp drop in the underlying mineral soil (Fig. 3-4b). Within the peat columns, the TOC ranged between 17.62 wt% (W-5P-A at 52.5 cm bs) and 55.67 wt% (S-4P at 57.5 cm bs). In the underlying mineral soil, excluding the visible mineral soil - peat mix phase, TOC ranged between 0.24 wt%

(S-5P at 142.5 cm bs) and 1.58 wt% (S-3P at 92.5 cm bs). In general, TOC was higher in the upper core parts, in which S-4P marks an exception.

3.5.3.2 TOC/TN and $\delta^{13}C$ ratios

We calculated the TOC/TN ratio for 221 out of 255 samples. For the remaining samples (often the lowermost samples of a core, and only mineral soil samples) the TN was below the detection limit of 0.1 wt%. As excluding these samples would cause a systematic bias we decided to set the TN values to 0.05 wt% (half the detection limit). This was the case for 34 samples. For four samples (E-1M-A-5, S-2M-6, -7, and -8), $\delta^{13}C$ measurement was not successful, as a result of low TOC content. Therefore, we excluded these four samples from TOC/TN - $\delta^{13}C$ analysis (Fig. S3-4).

For the mineral soil sites, we found highest TOC/TN values at intensity 3 with 43.76 (S-3M; 3 cm bs), with similar values occurring in intensities 1 and 2 (summer) as well as 5 (winter) (Fig. S3-4). The lowest TOC/TN value in mineral soils is found in S-5M (11.28 at 7 cm bs), indicating a less decomposed state of the OM. With $\delta^{13}C$, all values range between -29.99 (S-3M; 3 cm bs) and -25.99 ‰ vs. VPDB (W-5M at 19.75 cm bs). At the peat sites, we found much higher TOC/TN values, with a maximum value of 109.37 at intensity 2 (S-2P; 15 cm bs) (Fig. S3-4). The lowest value occurred in FR (intensity 3; 4.88 at 32.5 cm bs). The TOC/TN maximum found in PR also features the highest $\delta^{13}C$ values with -25.44 ‰ vs. VPDB. In general, values for all peat cores lie between -29.87 ‰ vs. VPDB (W-5P-B at 173 cm bs) and -26.33 ‰ vs. VPDB (PR at 17.5 cm bs). Grazing intensity 3 shows the greatest range $\delta^{13}C$ values, while the strongest spread in TOC/TN ratios is found in summer peat sites at intensity 2.

3.5.3.3 SOC density

SOC stocks in total as well as in the upper 30 cm show no trend across either seasonality or grazing intensity (table 3-3). However, using their mean values across soil types and seasonality or soil type and grazing intensity allows for easier comparison between sites. Highest SOC value was found at site PR (26.47 kg m^{-2}), lowest value occurred in W-4M-A (3.45 kg m^{-2}) with values ranging between 4.95 and 26.47 kg m^{-2} for peat, and 3.45 and 19.4 kg m^{-2}) for mineral soils. Due to missing bulk density values for site W-3M, we did not calculate SOC density here. Based on the station premises' coverage with peatlands (16.9 %, 7.5 km^2) and mineral soil (77.0 %, 34.4 km^2) we calculated 83.08 ± 37.92 kilotons (kt) of carbon for the top 30 cm of peat sites across the station area, and 256.21 ± 177.11 kt for mineral soil sites, omitting areas covered by lakes and rock. This gives us a total SOC stock of 339.29 ± 215.03 kt for the uppermost 30 cm of soil for the 44.6 km^2 station area (7.61 ± 4.82 kt km^{-2}).

3.5.4 Bulk density

At all mineral soil sites, dry bulk density shows a converse behaviour in relation to TOC, resulting in highest bulk density values for those samples with the lowest TOC (Fig. S3-5a). Bulk density was lowest in the organic top layer with values between 0.09 g cm^{-3} (MR, 1.5 cm bs) and 0.39 g cm^{-3} (W-4M-B, 4.75 cm bs). The maximum bulk density was found in W-4M-A with 1.77 g cm^{-3} (8.75 cm bs). Bulk density could not be measured for site W-3M due to equipment restraints in the field.

Sampling also did not allow for bulk density measurement in samples S-4P-7 (32.5 cm bs) and W-3P-5 (22.5 cm bs). At peat sites, bulk density values within the peat column ranged between 0.004 g cm^{-3} (W-5P-B, 12.5 cm bs) and 0.54 g cm^{-3} (W-5P-A, 67.5 cm bs) and reached a maximum of 2.49 g cm^{-3} in the underlying mineral soil at S-5P (147.5 cm bs) (Fig. S3-5b).

3.5.5 Radiocarbon ages

For radiocarbon ages, we used macro-organic remains, especially moss and grass root remains for 42 samples. However, due to low content of such remains in the mineral soils sampled, we also used bulk TOC of 12 additional samples for dating mineral sediments.

In the dated samples closest to the surface, we found modern material (younger than 1950 AD) at some sites. This was the case, in mineral soils, for E-1M-A (7.5 cm bs), E-1M-B (9.25 cm bs and 14.75 cm bs), S-3M (9.5 cm bs), S-5M (11.5 cm bs), W-3M (20.5 cm bs), W-4M-A (8.75 cm bs) and W-4M-B (23.75 cm bs), and W-5M (6.5 cm bs and 19.75 cm bs). Age-depth relations show similar radiocarbon ages at similar depth, giving 3239 cal yr BP in E-1M-A (36.5 cm bs), 3283 cal yr BP in MR (32 cm bs) and 3853 cal yr BP in S-3M (38.5 cm bs). The oldest material in mineral soil sites was found in S-2M with 4738 cal yr BP (63.5 cm bs). For full radiocarbon dating details, pleasesee table S3-1.

For peat sites, modern material was encountered at site FR for samples at 7.5 cm bs and 22.5 cm bs as well as at site S-2P (25 cm bs). In general, we found older ages at peat sites. Again, age-depth relations are similar across some sites with 7650 cal yr BP in S-4P (57.5 cm bs), 7589 cal yr BP in S-5F (52.5 cm bs) and 7698 cal yr BP in S-5P (82.5 cm bs) and 7397 cal yr BP in W-5P-A (82.5 cm bs). W-5P-B held much younger material, reaching 6332 cal yr BP at 173 cm bs. The maximum ages within the peat column are also similar across some cores, with 8650 cal yr BP in W-5P-A (132.5 cm bs), 8714 cal yr BP in PR (110 cm bs), 9815 cal yr BP in S-4P (141.5 cm bs), 9643 cal yr BP in S-5F (92.5 cm bs) and 9147 cal yr BP in S-5P (127.5 cm bs). In S-5P, an age inversion is found between the peat column and the underlying sand, which was dated to 5584 cal yr BP at 147.5 cm bs.

3.5.6 Comparative data analysis

When visualising the data, the differences in TOC concentration range and median between migration route sites and pasture sites is clearly visible (Fig. 3-5). The range of these TOC

data is similar for grazing intensity-corresponding summer and winter sites. For mineral soil sites, the uppermost and organic-rich sample shows much higher TOC values compared to the underlying samples, increasing the range. For mineral soils, we found a range from 1.06 to 49.01 wt% TOC in summer migration route (intensity 3 summer; *n* = 4 samples, median of 15.25 wt%), and a range from 1.98 to 51.23 wt% TOC in winter migration route (intensity 3 winter; *n* = 3 samples, median of 4.29 wt%) (Fig. 3-5 mineral soil). For pasture sites on mineral soil, we found a range of 1.17 to 22.47 wt% TOC for summer (intensity 5 summer; *n* = 4 samples, median of 2.59 wt%) and a range of 0.44 to 20.19 wt% TOC for winter (intensity 5 winter; *n* = 4 samples, median of 3.61 wt%).

The median for non-grazed mineral soil sites (intensity 1, *n* = 8 samples) is 6.7 wt%.

Comparing the samples from peat sites, we found a range of 0.56 to 52.91 wt% TOC for summer migration route (intensity 3 summer; *n* = 18 samples, median of 46.92 wt%) and a range of 47.98 to 50.59 wt% TOC for winter migration route (intensity 3 winter; *n* = 5 samples, median of 48.60 wt%) (Fig. 3-5 peat). On pasture / feeding peat sites, we found a range of 0.24 to 54.90 wt% TOC for summer pastures (intensity 5 summer; *n* = 51 samples, median of 50.57 wt%), and a range of 9.91 to 53.38 wt% TOC for winter feeding sites (intensity 5 winter; *n* = 59 samples, median of 44.70 wt%). For the peat reference sites outside the station area, we found a range from 0.78 to 49.00 wt% TOC (*n* = 24 samples, median of 37.94 wt%).

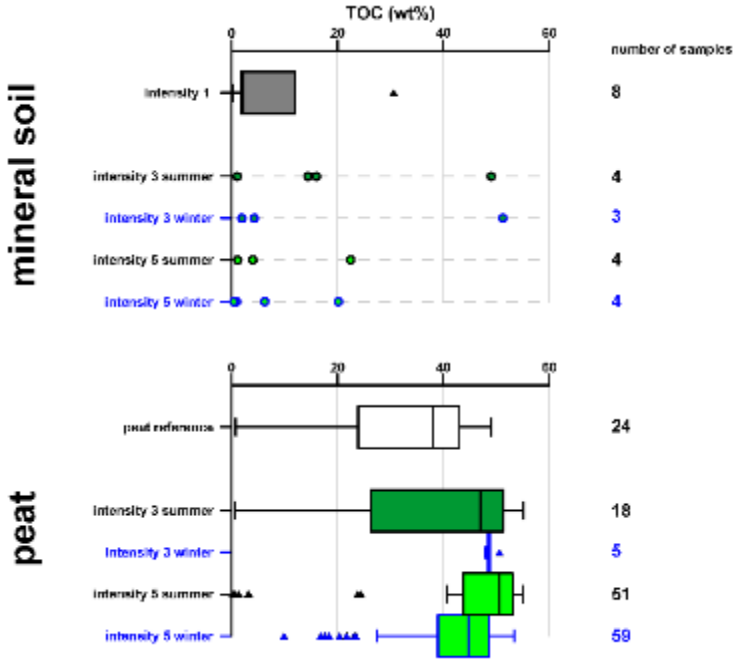

Figure 3-5 – Boxplots of TOC concentration of all non-grazed (E-1M-A, E-1M-B; grey), summer migration route (grazing intensity 3: S-3M, S-3P; dark green, black line), winter migration route (grazing intensity 3: W-3M, W-3P; dark green, blue line), summer pasture (grazing intensity 5: S-5F, S-5P, S-5M; light green, black line) and winter pasture (grazing intensity 5: W-5P-A, W-5P-B, W-5M; light green, blue line) sites, differentiated by soil type; peat reference sites (PR, FR) were additionally added; for mineral soils, intensity 1 (exclosures) are used as reference; median indicated by vertical line in the boxes; box margins show the upper and lower quartile; whiskers mark the range of the data; outliers (outside 1.5 time the interquartile range) are marked by black triangles; the number of samples per plot is given in each box; if less than 5 samples are in one group, no boxplot was created but the individual samples were plotted instead, using a dashed line for orientation.

Comparing the mean TOC values of the top 30 cm across grazing intensities, soil types and seasonalities, we see an increase for summer peat sites with increasing grazing intensity (Fig. 3-6).

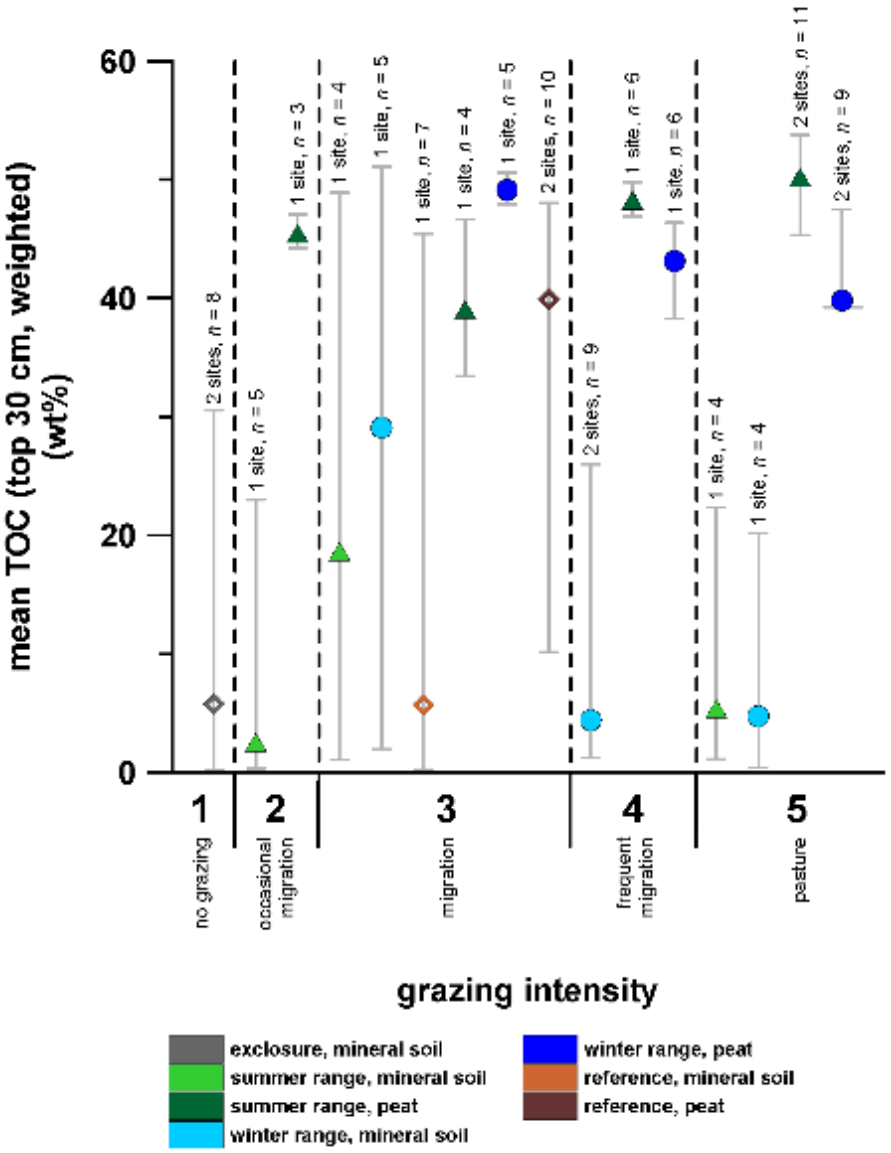

Figure 3-6 – Mean TOC for the top 30 cm, summarised for sites with identical grazing intensity, soil type and seasonality; triangles indicate summer sites, dots indicate winter sites, rhombuses indicate sites with no seasonality; the TOC value range of the samples used in these mean values is given as grey error bars.

Contrary to this, values decrease for summer mineral soil, winter mineral soil and winter peat sites. Under grazing intensities 2, 4 and 5, we see similar values as found at the exclosure sites, with the mineral soil at intensity 3 which was not affected by a clear grazing seasonality (MR) showing a similar mean TOC. The peat reference sites PR and FR (intensity 3, no seasonality) is in line with the value for intensity 3 summer peat, justifying our understanding of these sites as intensity 3 (migration route).

PCA revealed a stretch along bulk density among samples of the top 30 cm of all sites (Fig. 3-7). TOC and water content are correlating. The combination of $\delta^{13}C$ ratios and TOC/TN ratios as markers of OM degradation shows a spread on the Y-axis.

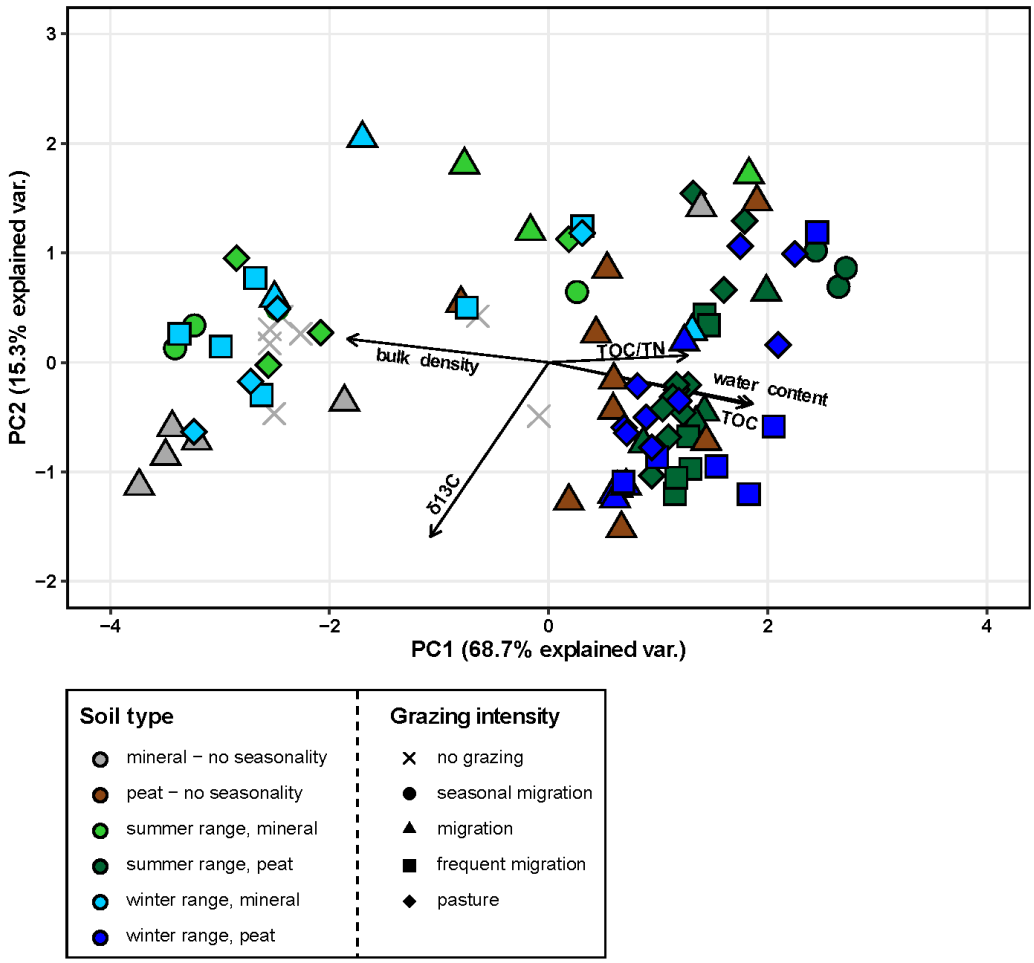

Figure 3-7 – Principal component analysis of the top 30 cm of all sites across the parameters bulk density, $\delta^{13}C$ ratios, TOC/TN ratio, soil type, water content and TOC; shapes encode different grazing intensities; colours indicate seasonality and soil type.

3.6 Discussion

3.6.1 Reindeer impact on soil carbon storage

For this study, seasonality at the sites was expected to be crucial. On the one hand in summer, grazing effects including trampling, fertilisation via faeces, and browsing in summer affect mainly vegetation. On the other hand, in winter the animal effects on the snow cover are more important. High grazing intensity in summer shifts vegetation towards graminoid-dominated and mainly light-coloured vegetation, increasing albedo and hence leading to a relatively lower heat transfer into the ground as with short tundra-like vegetation (te Beest et al. 2016). In contrast, winter grazing reduces snow cover, baring the ground to cold air, inducing a cooling effect on the soil (Beer et al. 2020).

Looking at our data, like TOC, all median values are close together when comparing peat sites across grazing intensities. We found the interquartile ranges of migration and pasture sites overlapping largely, regardless of seasonality (Fig. 3-5 peat). For mineral soils, the median differences are much larger, but since this is a comparison of individual sites (1 site per grazing

intensity and seasonality, except for the exclosures), this difference is mainly due to the TOC content in the uppermost sample, taken from organic-rich soil horizons, and therefore most likely depending on the vegetation growing on top. No clear trend along grazing intensity was found. Also, SOC densities of the top 30 cm show no clear trend along grazing intensity or grazing seasonality (table 3-3). Thus, following our research question if reindeer grazing increases soil carbon storage, and under which grazing intensity and seasonality this effect is greatest, we found no clear evidence for strong differences in TOC between grazing intensities. As TOC is slightly higher on summer pastures compared to summer migration route sites, artificially intensified grazing appears to increase soil carbon storage in comparison to natural grazing intensities (Fig. 3-4 3M and 3P). In winter sites, this effect is not visible, but the animal impact on snow might be relevant here: At the feeding sites (intensity 5) on the winter ranges, supplementary feeding is practiced, so there is less need for the animals to dig through snow. Instead, the animals will compact the snow, while snow removal and breakup is more likely along migration tracks in this case. The proposed effect of ground cooling via snow removal would therefore not be in place at our study sites, but might occur at winter pastures without supplementary feeding.

The small differences in TOC we observed are likely related to the pre-existing and general soil conditions, resulting in similar TOC values across mineral soil sites as well as across peat sites (Fig. 3-4). The differences in TOC range between migration route sites versus pasture sites in peat (Fig. 3-5 peat) are likely originating from the presence of underlying TOC-poor mineral soil in some of the sampled cores, lowering the median value. Other options are that the differences in grazing intensity or frequency, reindeer stock size or grazing duration were not strong enough to see differences in SOC in our study area. Opposing to this, findings from a similar study in a permafrost area with only 25 years of intensive grazing history already show differences in soil TOC storage (Windirsch et al. 2022a). Yet, our results agree with findings from other studies conducted on boreal forest sites in northern Fennoscandia that also found no effect of reindeer presence on soil carbon storage (Stark et al. 2008, Köster et al. 2015). This leads to the assumption that frozen ground would have a major impact and the increased carbon storage under grazing pressure observed in permafrost is linked to the animals maintaining a frozen ground state, hence reducing OM degradation. Therefore, our hypothesis of intensive grazing leading to higher soil carbon storage was not proven for this study site on seasonally frozen ground. We state that an increase of soil carbon storage as a result of intensive animal grazing occurs only in permafrost-affected landscapes, where the ground underneath the active layer can be kept frozen by animal activity, hence reducing OM degradation (Windirsch et al. 2022a).

3.6.2 Reindeer impact on vegetation

We found strong contrasts in vegetation cover between grazing intensities. While the exclusion of reindeer promotes an increase or rather preservation of *Cladonia rangiferina* (Inga 2009), summer pasture sites are more likely to be transformed into grasslands dominated by *Deschampsia cespitosa* (Rosef et al. 2004), with a reduced or missing shrub layer. On winter pastures where the animals trample down the snow cover but hardly feed on the local vegetation due to supplementary feeding, vegetation is also graminoid-dominated but still features common tundra vegetation such as *Vaccinium* ssp. and *Empetrum nigrum*. Studies conducted in the same study area have shown that the biomass of *Empetrum nigrum* has increased substantially over the recent decades (Stark et al. 2021).The gradual transformation from tundra vegetation towards graminoid-dominated vegetation as a result of animal impacts is best seen by comparing the shrubby vegetation found at migration route sites of this study, the tundra-like vegetation at sites with high revisiting frequency (intensity 4) featuring some *D. cespitosa* (summer; S-4P) or *Eriophorum* (W-4P) and the vast grasslands found at the pasture sites. The x-axis spread in TOC/TN - $\delta^{13}C$ analysis (Fig. S3-4) is therefore most likely not an indicator of different degrees of OM decomposition, but a source signal produced by different vegetation communities found at the different sites. The very high TOC/TN values at S-2P, W-4P and W-5M are likely a result of the presence of mosses and lichen that would disappear under more intensive animal impact.

Vegetation change effects with increasing grazing intensity are less visible at winter sites. Thermal aspects of the animals' physical impacts on winter sites (snow removal, snow compaction), resulting in a proposed cooling effect on the ground and hence increased carbon storage (Sturm et al. 2005, Falk et al. 2015) or rather reduced OM decomposition (Davidson and Janssens 2006, Walz et al. 2017) could not be confirmed in this study.

However, the vegetation composition and structure shows no signs of shrubification on the studied pasture sites. In contrast to this, shrub expansion is a prominent process in many high-latitude non-forest ecosystems (Mekonnen et al. 2021). Intensive herbivory might slow down this process, thereby reducing two main effects of shrub expansion: (1) increased localised snow trapping and warming of the ground underneath (Beer et al. 2020), and (2) increased carbon uptake from the soil, which adds carbon to the more active part of the carbon cycle by biomass increase, litter production and above-ground litter decomposition (Vowles and Björk 2019, Verma et al. 2020, Parker et al. 2021).

3.6.3 Reindeer impact on ground characteristics

The shallow peat and relatively young basal peat age (table S3-1) at migration sites (sites S-3P and W-3P) indicate that peat formation started later than at the other peat sites. The older ages found at the pasture sites indicate a difference in peat accumulation, compared to S-3P. The

age inversion at the bottom of the pasture (site S-5P) shows that there was rearrangement of organic carbon at approximately 130 cm bs. However, this rearrangement must have taken place after peat formation started on top. An option would be relocation of carbon inside the soil column caused by lateral water flow (Kramer et al. 2004). The bottom ages of most peat columns (table S3-1) match the beginning of peat formation after the deglaciation of northern Fennoscandia around 9700 cal yr BP (Stroeven et al. 2016).

The organic top layer of the mineral soil sites indicates two things: undisturbed growth of moss and lichen at the exclusion sites (E-1M-A and -B) on the one hand and animal action such as trampling and therefore turbation as well as the soil structure, consisting of an eluvial and an illuvial horizon, at mineral sites (S-3M, S-5M, W-3M, W-4M-A and W-4M-B) on the other hand bring newly formed organic material into the ground (table S1). This is most likely enhanced by the formation of roots. This might be a result of grassland formation featuring plants that tend to develop deeper roots than tundra vegetation, as a result of high grazing pressure.

Bulk density of the peatland sites slightly decreases with increasing grazing intensity (Fig. S3-5b), especially from intensities 3 to 5. While this is not a common result, as animal trampling usually compresses the ground (Tuomi et al. 2021), we reckon that the previously mentioned vegetation shift towards graminoid-dominated vegetation produced a less compressible peat compared to peat produced by mosses and shrubby tundra vegetation. This lower compressibility is likely caused by larger and more stable vegetation pieces in the peat, such as roots and grass stalks compared to mosses, as can be seen in root-intervened peat in other locations (Carlton 1974, van Asselen et al. 2010). This less-dense peat on intensity 5-sites means more spaces inside the ground, that would insulate underlying material from intruding air temperature and reduce cooling effects on the soil in winter, if air-filled. Taking that into account, our hypothesis suggests colder ground temperatures and therefore less carbon decomposition in intensity 3-sites, where bulk density is higher. As we do not see any clear trend in the carbon data pointing towards this hypothesis, we assume that, independent of bulk density, all examined peats feature high water contents throughout the year, allowing for temperature exchanges between air and deeper soil layers, eliminating the insulation effects that air-filled spaces would cause.

3.6.4 SOC density and stocks across the Kutuharju station area

While we did not find obvious correlations between reindeer grazing intensity and soil TOC storage, we used our dataset to calculate mean SOC stocks for the premises of the Kutuharju Field Research Station. We calculated mean SOC stocks for peatlands and mineral soil areas separately, as well as for summer and winter ranges, again classified by soil type. While there was only little difference for uppermost 30 cm of the peatlands (summer mean: 11.36 ± 6.07 kg m^{-2}; winter mean: 10.61 ± 3.23 kg m^{-2}; overall mean: 11.02 ± 5.03 kg m^{-2}), mineral soils showed a larger difference between reindeer ranges (summer mean: 10.14 ± 6.73 kg m^{-2}; winter mean: 4.49 ± 1.18 kg m^{-2}; overall mean: 7.45 ± 5.15 kg m^{-2}) (table 3-3). Separate calculations grouped by grazing intensity revealed highest mean SOC values for regular migration route sites (intensity 3) for both mineral (19.40 ± 0.00 kg m^{-2}) and peat (13.09 ± 2.84 kg m^{-2}) sites, but no clear trend across grazing intensities. These values are likely a result of vegetation composition at these sites, keeping in mind that for mineral soils only one site (S-3M) was available for SOC stock calculation.

3.6.5 Methodological limitations of the pilot study design

Our pilot study design mainly aimed at identifying if there are TOC differences between grazing intensities that need to be investigated further. For this reason, we did not collect multiple replicates of our samples. This leaves us with an extendable dataset that does not allow for significance testing, as e.g. in unfrozen soil conditions samples from different depths within a core are not independent in terms of TOC, due to seeping water possibly relocating carbon, which would require using every core as a single sample.

While summer is the best sampling period to allow for full area access, ensuring fully unfrozen conditions in seasonally frozen ground, the limitation to separate summer and winter pastures does not provide direct insights into animal effects year-round.

3.6.6 Implications of the pilot study for future research

Due to only seasonally frozen soil conditions and soil parts staying unfrozen during the whole year, carbon relocation via seeping water as well as year-round decomposition processes are likely to take place in our study area. Contrary to a similar study on permafrost (Windirsch et al. 2022a), this might be the reason for non-visible trends found in this study. However, to record the full impact of grazing on seasonally frozen soils, sampling a year-round reindeer enclosure that has been grazed by large numbers of animals for several decades is needed.

A key element for estimating animal-induced effects on both vegetation and soil is also a sufficient availability of reference sites where animals are excluded. In this study, there was no exclosure site featuring peat soils available. These exclosures would also be vital for creating a baseline for all parameters, measured repeatedly throughout the duration of the experiment.

3.7 Conclusion

In conclusion we found no clear evidence that reindeer alter the soil organic carbon storage capacities in seasonally frozen ground in the studied setting. However, while putting no detectable effects on mineral soils, they do affect bulk density in peat under heavy grazing influence. This is most likely a result of their effect on vegetation communities, increasing root production by transforming tundra into species-poor grasslands.

Thus, we found no analogue effects of herbivores like in permafrost-affected landscapes, where intensive animal grazing likely promotes an increase of soil carbon storage. If these results for our studied seasonally frozen Arctic soils is caused by lower herbivory pressure, higher winter temperatures or other aspects could not be answered in our pilot study. Increasing the number of reference sites for also covering peat soils and analysing soils of year-round reindeer pastures needs to be addressed in order to assess the potential for long-term carbon storage in high-latitude soils by changing grazing regimes.

3.8 Data availability

All measurement data are available via the PANGAEA data repository under DOI 10.1594/PANGAEA.941930 (Windirsch *et al.* 2022c) and DOI 10.1594/PANGAEA.952470 (Windirsch *et al.* 2022b).

3.9 Author contribution

TW, GG, MU and JS designed the study. TW, MU, JS and MF prepared the field work. TW and MF carried out the field work. Lab work was done by TW, supported by JS and JW. BF, SS and JO provided expertise on herbivory in northern Fennoscandia. BF, SS, JO and MM-F provided knowledge on ecosystem interactions. TW, JW, CT and MU analysed the data statistically. SS and TK provided expertise on the study area. CT, BF and MM-F provided knowledge on peatlands. JW worked on radiocarbon dating. GG and TK worked on remote sensing data and compiled the maps. TW and JS compiled the figures and the manuscript structure. All authors contributed to writing and editing the manuscript.

3.10 Competing interests

The authors declare no conflict of interests.

3.11 Acknowledgements

We thank the Kutuharju Field Research Station team for station access and support during the field campaigns. Special thanks go out to the Reindeer Herders' Association of Finland (paliskunnat.fi) for organisational help and insights into the station's research. We are especially thankful to Jouko Kumpula (Natural Resources Institute Finland, Inari) for providing detailed knowledge on the reindeer numbers and migration processes at the Kutuharju Field Research

Station. We thank Johanna Schwarzer for great field assistance and extremely helpful knowledge on vegetation.

We would like to thank Metsähallitus, namely Katja Sandgren, for providing help with research permits and regular updates on the SARS-Cov-19 pandemic situation in the study area.

We acknowledge Justin Lindemann, Jonas Sernau, Angelique Opitz, Flavio Maggioni, Alena Kalitzki and Jonas Kaltschmidt (Permafrost Carbon and Nitrogen Lab (CarLa)) as well as Mikaela Weiner and Hanno Meyer (ISOLAB facility), the Micadas facility at AWI and the Stable Isotopes working group at GFZ, namely Birgit Plessen, for measurements and laboratory assistance. We want to thank the AWI logistics for helping in planning these field campaigns. We also thank J. Otto Habeck (Universität Hamburg) for his help in designing this study.

3.12 Funding

The field campaigns were carried out as part of the PeCHEc (Permafrost Carbon Stabilization by Recreating a Herbivore-Driven Ecosystem) project funded by the Potsdam Graduate School, with additional support from the Geo.X research network (SO_087_GeoX). The field campaigns were funded by AWI and the Permafrost Research section baseline funding. Additional funding was provided by European Commission Research and Innovation Action no. 869471 (CHARTER).

Table 3-1 – Description of the sampling sites, including location, sampling depth, soil, relief and vegetation type description; E marks exclosure sites, S marks reindeer summer ranges, W marks reindeer winter ranges.

site	latitude (°N)	longitude (°E)	grazing intensity (during season)	sampling depth [cm bs]	soil type	relief	vegetation type
E-1M-A	69.159500	26.991278	no grazing (~ 50 yrs)	40	mineral	flat, dry	mixed forest, mosses
E-1M-B	69.154113	26.971089	no grazing (~ 50 yrs)	17.5	mineral	slight slope, dry	open mixed forest, mosses
S-2M	69.159861	26.991250	seldom	67	mineral	flat, dry	mixed forest, mosses
S-2P	69.152357	26.971650	seldom	50	peat, bedrock below	slope, wet	mixed forest / bog edge
S-3M	69.139250	26.984000	regularly	42	mineral	valley edge, dry	heath / grassland
S-3P	69.139944	26.983778	regularly	100	peat (0-92 cm), mineral (92-100 cm)	valley, wet	heath / grassland
S-4P	69.143500	26.990000	frequently	143	peat	valley, wet	heath / grassland
S-5F	69.145806	26.994306	very often	112	peat (0-92 cm), mineral (92-112 cm)	valley, wet	birch forest, grassy understorey
S-5P	69.146722	26.993306	very often	150	peat (0-135 cm), mineral (135-150 cm)	valley, semi-dry	grassland
S-5M	69.147222	26.991528	very often	22	mineral	valley edge, dry	grassland

W-3M	69.107441	27.015753	regularly	22	mineral	slope plateau	birch forest, shrubby understorey
W-3P	69.103456	27.019161	regularly	25	peat, bedrock below	valley, wet (meltwater run)	heath / grassland
W-4M-A	69.109031	27.013619	frequently	11	mineral	bog edge, dry	birch forest
W-4M-B	69.109079	27.013550	frequently	26.5	mineral	bog edge, dry	birch forest
W-4P	69.119953	27.030306	frequently	88	peat (0-66 cm), mineral content (66-88 cm)	slight slope	bog in a mixed forest clearing
W-5M	69.120851	27.026792	very often	22.5	mineral	dry, flat	forest edge
W-5P-A	69.109076	27.012831	very often	135	peat (0-133 cm), mineral (133-135 cm)	valley, wet	fenn / grassland
W-5P-B	69.120867	27.026270	very often	176	peat	valley, wet	fenn / grassland
MR	69.229750	26.795806	regularly	35	mineral	flat, dry	mixed forest, shrubby understorey
PR	69.226778	26.810111	regularly	125	peat (0-115 cm), mineral (115-125 cm)	lakeside peatland, wet	heath / grassland, mosses
FR	69.226000	26.833417	regularly	50	peat (0-30 cm), mineral (30-50 cm)	valley, semi-dry	birch forest, grassy understorey

Table 3-2 – Detailed soil and vegetation descriptions of the sampling sites; vegetation coverage identifies only the most abundant species; soil horizons given as "eh" mark eluvial horizons, "ih" marks illuvial horizons.

site	soil layers (depth, given in cm bs)	vegetation composition and coverage (% of 1 m²)
E-1M-A	organic layer (0-4); eh (4-5); ih (5-10); transition (10-19); pale sand with gravel (19-41)	*Cladonia rangiferina* (76 %); *Vaccinium uliginosum* (12 %); *Empetrum nigrum* (6 %); *Vaccinium myrtillus* (2 %); *Vaccinium vitis-idaea* (1 %)
E-1M-B	organic layer (0-4); organic-rich soil (4-7); eh (7-10); ih (10-25); gravel/bedrock	*Cladonia rangiferina* (36 %); *Empetrum nigrum* (28 %); *Vaccinium myrtillus* (6 %); *Vaccinium uliginosum* (4 %); *Ledum palustre* (3 %); brown moss
S-2M	organic layer (0-2); eh (2-4); ih (4-15); transition (15-25); pale sand (25-70)	*Cladonia arbuscula* (38 %); *Vaccinium vitis-idaea* (17 %); *Vaccinium uliginosum* (16 %); mossy understorey
S-2P	fresh moss peat (0-30); light-brown moss peat, hardly decomposed (30-41); brown, decomposed peat (41-50)	*Eriophorum* (43 %); *Vaccinium uliginosum* (14 %); *Rubus chamaemorus* (11 %); *Ledum palustre* (10 %); *Betula nana* (8 %); *Empetrum nigrum* (8 %); *Vaccinium myrtillus* (2 %); *Vaccinium vitis-idaea* (2 %); *Calluna vulgaris* (1 %); *Andromeda polifolia* (1 %); mossy understorey
S-3M	organic layer (0-6); organic-rich soil (6-13); greyish silty sand with gravel (13-23); brownish sand (23-40); gravel/bedrock	*Salix* (shrubs) (46 %); *Betula nana* (24 %); *Empetrum nigrum* (13 %); *Vaccinium uliginosum* (9 %); *Vaccinium myrtillus* (8 %); *Ledum palustre* (4 %); mossy understorey

site	soil layers (depth, given in cm bs)	vegetation composition and coverage (% of 1 m²)
S-3P	organic layer (0-6); dark, undecomposed peat (6-13); light-brown moss peat, hardly decomposed (13-37); dark, sandy peat (37--92); greyish sand with gravel (92-100)	*Eriophorum* (52 %); *Empetrum nigrum* (28 %); *Vaccinium uliginosum* (18 %); *Rubus chamaemorus* (6 %); *Ledum palustre* (3 %); other grasses (2-3 %)
S-4P	organic layer (0-2); dark, undecomposed peat (2-19); light-brown moss peat (19-33); dark peat (33-81); dark peat with macro organics (81-133); dark, compact peat (133-143)	*Sphagnum* (33 %); *Empetrum nigrum* (32 %); *Vaccinium myrtillus* (17 %); *Vaccinium uliginosum* (9 %); *Betula nana* (4 %)
S-5F	organic layer (0-4); dark, undecomposed peat (4-19); light-brown moss peat (19-22); dark peat (22-45); dark peat, hardly decomposed (45-57); dark peat (57-82); sandy transition (82-92); organic-rich sand (92-101); grey sand (101-112)	*Eriophorum* (57 %); *Vaccinium uliginosum* (22 %); *Rubus chamaemorus* (6 %); *Vaccinium vitis-idaea* (5 %); *Equisetum arvense L.* (1 %); mossy understorey
S-5P	peat, hardly decomposed (0-15); peat (15-60); peat with macro organics (60-125); sandy transition (125-135); grey sand (135-150)	*Deschampsia cespitosa* (> 95 %)
S-5M	organic layer (0-5); eh (5-6); ih (6-15); pale sand with gravel (15-25); gravel/bedrock	*Deschampsia cespitosa* (> 95 %)

site	soil layers (depth, given in cm bs)	vegetation composition and coverage (% of 1 m²)
W-3M	organic layer (0-4); organic-rich soil (4-16); eh (16-19); ih (19-22); gravel/bedrock	*Vaccinium myrtillus* (48 %); *Vaccinium uliginosum* (23 %); *Empetrum nigrum* (12 %); *Vaccinium vitis-idaea* (9 %); *Eriophorum* (6 %); other grasses (1-2 %); mossy understorey
W-3P	dark peat (0-25); gravel/bedrock	*Eriophorum* (72 %); *Sphagnum* (19 %); *Equisetum* (3 %); *Carex appendiculata* (2 %); *Andromeda polifolia* (1 %); *Potentilla palustris* (1 %); *Vaccinium uliginosum* (1 %)
W-4M-A	organic layer (0-4); eh (4-6.5); ih (6.5-12); gravel/bedrock	*Empetrum nigrum* (49 %); *Vaccinium uliginosum* (34 %); *Vaccinium myrtillus* (11 %); *Eriophorum* (5 %); *Cladonia rangiferina* (3 %); *Vaccinium vitis-idaea* (2 %); mossy understorey
W-4M-B	organic layer (0-8); eh (8-9); ih (9-14); yellowish sand (14-28); gravel/bedrock	*Eriophorum* (previous year) (51 %); *Empetrum nigrum* (31 %); *Vaccinium myrtillus* (11 %); *Vaccinium vitis-idaea* (6 %)
W-4P	moss peat (0-33); dark, compact, decomposed peat (33-52); moss peat (52-55); dark, brown peat (55-66); dark, sandy peat (66-88)	*Eriophorum* (17 %); *Empetrum nigrum* (16 %); *Vaccinium uliginosum* (11 %); *Betula nana* (5 %); *Rubus chamaemorus* (4 %); *Ledum palustre* (1 %); *Vaccinium macrocarpon* (1 %); mossy understorey

site	soil layers (depth, given in cm bs)	vegetation composition and coverage (% of 1 m²)
W-5M	organic-rich soil (0-6); eh (6-7); ih (7-17); pale sand with gravel (17-22.5)	*Empetrum nigrum* (47 %); *Phyllodoce caerulea* (9 %); *Vaccinium myrtillus* (8 %); *Cladonia rangiferina* (7 %); *Vaccinium uliginosum* (5 %); *Ledum palustre* (4 %); *Vaccinium vitis-idaea* (2 %); mossy understorey
W-5P-A	fresh peat (0-20); brown, decomposed peat (20-133); grey silty sand (133-135)	*Eriophorum* (previous year) (63 %); *Vaccinium uliginosum* (11 %); *Betula nana* (9 %); *Empetrum nigrum* (8 %); *Rubus chamaemorus* (2 %); mossy understorey
W-5P-B	fresh peat (0-10); dark, decomposed peat (10-145); dark, very fine peat (145-165); light-brown peat (165-176)	*Eriophorum* (previous year) (60 %); *Eriophorum* (20 %); *Potentilla palustris* (8 %); *Andromeda polifolia* (1 %); *Equisetum arvense L.* (1 %); *Viola epipsila* (1 %); mossy understorey
MR	organic layer (0-3); organic-rich, sandy soil (3-6); eh (6-8); ih (8-18); pale sand (18-35); gravel/bedrock	*Cladonia stellaris* (21 %); *Vaccinium vitis-idaea* (13 %); mosses
PR	organic layer (0-2); moss peat, hardly decomposed (2-15); dark peat (15-115); yellowish sand (115-125)	*Empetrum nigrum* (27 %); *Cladonia stellaris* (16 %); *Salix* (shrubs) (14 %); *Vaccinium uliginosum* (8 %); *Ledum palustre* (7 %); *Vaccinium vitis-idaea* (3 %); mossy understorey
FR	organic layer (0-5); dark peat with roots (5-25); sandy peat (25-30); grey sand with gravel (30-50)	*Vaccinium uliginosum* (43 %); *Empetrum nigrum* (22 %); *Vaccinium vitis-idaea* (16 %); *Salix* (13 %); *Betula nana* (11 %); *Eriophorum* (10 %); *Ledum palustre* (2 %); mossy understorey

Table 3-3 – SOC stocks calculated for the top 30 cm of each site, given in kg m^{-2}, SOC density range per cm depth of the samples used for SOC stock calculation, given in g cm^{-3}, and the number of samples in the top 30 cm (*n*).

site	SOC 0-30 cm (kg m^{-2})	SOC density range (g cm^{-3})	*n*	site	SOC 0-30 cm (kg m^{-2})	SOC density range (g cm^{-3})	*n*
E-1M-A	4.39	0.06 – 2.98	5	W-3M	n/a	n/a	n/a
E-1M-B	11.32	0.36 – 1.86	3	W-3P	15.92	1.19 – 1.46	5
S-2M	3.60	0.09 – 2.18	5	W-4M-A	3.45	0.66 – 0.82	3
S-2P	4.95	0.13 – 0.19	3	W-4M-B	6.14	0.23 – 0.81	3
S-3M	19.40	0.24 – 1.86	4	W-4P	10.19	0.23 – 1.17	6
S-3P	10.25	0.21 – 1.71	4	W-5M	3.88	0.09 – 10.17	4
S-4P	7.56	0.63 – 1.39	6	W-5P-A	8.99	0.15 – 1.22	4
S-5M	7.43	0.16 – 1.14	4	W-5P-B	7.32	0.03 – 0.98	5
S-5P	22.66	0.76 – 2.77	5	MR	4.51	0.04 – 1.93	7
S-5F	11.36	0.71 – 2.18	6	PR	26.47	0.51 – 2.20	4
				FR	19.21	0.73 – 4.19	6

Chapter 4: Lipid Biomarker Screening to Trace Recent Large Herbivore Influence on Soil Carbon in Permafrost and Seasonally Frozen Arctic Ground

A Pilot Study of Lipid Biomarkers to Trace Recent Large Herbivore Influence on Soil Carbon in Permafrost and Seasonally Frozen Arctic Ground

Windirsch, T.[1,2], Mangelsdorf, K.[3], Grosse, G.[1,2], Wolter, J.[4], Jongejans, L. L.[1,#], and Strauss, J.[1]

[1]Alfred Wegener Institute Helmholtz Centre for Polar and Marine Research, Potsdam, Germany

[2]Institute for Geosciences, University of Potsdam, Potsdam, Germany

[3]German Research Centre for Geosciences, Helmholtz Centre Potsdam, Organic Geochemistry Section, Potsdam, Germany

[4]Institute of Biochemistry and Biology, University of Potsdam, Potsdam, Germany

[#]now at Ruhr-University Bochum, Institute of Geography, Bochum, Germany

Submitted to: Arctic Science

4.1 Abstract

This study investigates the impact of large herbivores on soil organic matter (OM) stability in Arctic permafrost and seasonally frozen ground ecosystems, focusing on the potential preservation effect of grazing. Soil samples were collected from Siberian and Finnish permafrost and non-permafrost areas, analysing organic carbon content, carbon-to-nitrogen ratio, stable carbon isotopes, *n*-alkane, and n-alcohol contents to assess OM stability. The results suggest that grazing activity, particularly in permafrost environments, preserves soil OM by reducing decomposition. Permafrost soils exhibit higher functionalized to non-functionalized biomarker ratios, indicating better preservation under frozen conditions. While differences in grazing intensities had minor effects, the data also showed variability due to soil heterogeneity, especially in seasonally frozen ground ecosystems. Nevertheless, there are slight trends towards enhanced OM preservation with increasing grazing intensity, especially in permafrost, emphasizing the potential role of grazing in locally preserving Arctic soil OM. This pilot study offers initial insights into the impact of large herbivores on OM stability in cold-region ecosystems, suggesting that significant effects may require prolonged, intensive grazing pressure.

4.2 Introduction

Global warming is directly related to continuously rising carbon dioxide levels in the Earth's atmosphere (IPCC 2021). In addition to direct anthropogenic emissions from human fossil fuel burning, land cover change has been identified as a large source of emissions as soil organic carbon may become more vulnerable to mineralization (Kaplan *et al.* 2010). Large quantities of organic carbon are stored in soils and can partially be mobilised and mineralised to greenhouse gases by microbial activity following soil warming (van Groenigen *et al.* 2011) and surface erosion (Lal 2022). Hence, it is important to study in detail how soils and soil organic matter (OM) behave under various environmental conditions, land cover changes, and land

use scenarios (Ramesh *et al.* 2019). A better understanding of soil carbon characteristics may then help to identify pitches for emission reductions. A large portion of global soil organic carbon is found in the terrestrial Arctic (Hugelius *et al.* 2020, Strauss *et al.* 2021), with a large share currently still stored in perennially frozen ground termed permafrost (Schuur *et al.* 2015, 2022). Due to Arctic amplification, ongoing climate warming leads to especially strong warming in the Arctic (Previdi *et al.* 2021), which results in permafrost warming and widespread thaw (Bowen *et al.* 2020). As a consequence, newly thawed OM becomes bioavailable for microbial decomposition, finally leading to carbon release to the atmosphere in the form of the greenhouse gases CO_2 and CH_4 (Turetsky *et al.* 2019, Bowen *et al.* 2020). In addition to organic carbon, other temperature-stabilised soil element inventories such as nitrogen (Strauss *et al.* 2022), various mineral elements (Monhonval *et al.* 2021, Stimmler *et al.* 2023), or contaminants like mercury (Schuster *et al.* 2018, Rutkowski *et al.* 2021) are also affected by thaw.

Land cover change can promote active layer deepening and permafrost thaw by changing insulating layers of vegetation and organic soil layers, affecting snow distribution, and changing soil wetness and surface hydrology. For example, deforestation can cause deepening of the active layer and loss of soil carbon (Peplau et al. 2022), and shrubification can cause ground warming via snow trapping, and therefore also active layer deepening (Mekonnen et al. 2021). Surface disturbances, either natural or anthropogenic, can hereby affect soil carbon storage on short or long time scales (Forbes et al. 2001, Grosse et al. 2011). In particular, permafrost can be severely affected by wildfires via post-fire permafrost thaw (Jones et al. 2015, Zhang et al. 2023), which also affects soil carbon storage (Harden et al. 2006, Genet et al. 2013). Anthropogenic-driven land use change, in particular deforestation and intensifying agricultural activities in some permafrost regions, can also have large effects on permafrost thermal conditions, active layer deepening, and also soil carbon stability. Land use pressure might even increase further in the Arctic with shifting climate and agricultural zones (Bradley and Stein 2022). Some land use practices might, however, also help stabilising permafrost and therefore soil carbon.

In particular, large-mammal herbivory has been hypothesised to influence soil OM composition and stability for cold-region ecosystems (Olofsson and Post 2018, Ylänne *et al.* 2018, Kristensen *et al.* 2022). Zimov *et al.* (1995) suggested that the late-Pleistocene stable cold-environment ecosystem, called the Mammoth steppe, with its substantial presence of large herbivorous animals, impacted snow and vegetation conditions and resulted in enhanced preservation of permafrost and soil OM. Large herbivores browsing for food in winter trample, compress, and partially remove snow, which leads to more effective contact between winter air and the ground and thus soil cooling (Zimov *et al.* 2009, Park *et al.* 2015, Beer *et al.* 2020). In addition, animal density results in varying degrees of trampling damage and nutrient availability from animal faeces (Grellmann 2002, Schuur *et al.* 2008), and selective grazing throughout the year

results in vegetation changes through food and habitat preferences. As these two processes under high animal densities can reduce soil insulation against low winter temperatures during the long season of freezing degree days, they are thought to contribute to stabilising permafrost conditions. In contrast, the vegetation shift from sturdy and shrubby tundra vegetation towards graminoid-dominated landscapes reduces shadowing effects of vegetation in summer, leading to increased summer soil warming. However, due to the substantially longer winters, these less-insulated surfaces compensate for the slightly enhanced summer warming by enhanced winter cooling, producing an annual net-negative soil temperature relative to a shrub-covered surface. This is due to the fact that, unlike shrubs, graminoids tend to fall over underneath the snow and do not form an insulating, air pocket-filled layer (Blok *et al.* 2010, Macias-Fauria *et al.* 2020). Adding to this, graminoid-dominated vegetation is comparably light-coloured, increasing the albedo and therefore reflection of energy from solar radiation. The cold ground conditions, reinforced in that way in widespread permafrost regions during the late Pleistocene, prevented OM from decomposition and continued accumulation of soil OM by maintaining a frozen state with low microbial activity (Turetsky *et al.* 2019, Windirsch *et al.* 2022a).

Focusing on herbivory, previous studies (Windirsch *et al.* 2022a, Windirsch *et al.* 2023c) on the same sites in regard to sediment and OM characteristics revealed that large herbivore activity likely reduces permafrost thaw by snow compaction and alteration of the vegetation community, but has no significant effect on the amount of carbon stored within the soil, as the experimental herbivore density increase happened only quite recently (23 years on permafrost, 50 years on seasonally frozen ground). In seasonally frozen ground, no clear trends for carbon storage increase along with increasing grazing intensity were found. However, these previous studies only looked at total carbon storage. In this study we aimed to find out whether the degradational state of soil OM varies in relation to the influence of large-mammal herbivory. Therefore, we investigated in situ carbon quality - meant as the degree of ‘freshness’ or ‘state-of-decomposition’. Our main research question is: how does the degradational state of soil OM vary in relation to the influence of large-mammal herbivory? In order to answer this, our two specific objectives were to investigate whether (1) large herbivore activity at various grazing intensities alters biomarker signals of the soil OM, and whether (2) biomarker signals are affected by the local thermal regime of the ground (i.e., permafrost vs. seasonally frozen ground). First, we analysed bulk total organic carbon (TOC) characteristics as well as functionalized (n-alcohols) versus non-functionalized (n-alkanes) biomarkers in sediment samples along grazing intensity transects. These lipid biomarkers provide semi-specific information on OM sources such as vegetation types, as well as on OM decomposition levels (Strauss et al. 2015, Jongejans et al. 2021). Secondly, we compared permafrost sites to study sites with seasonally frozen ground (SFG) to gain insights into the carbon storage processes in a warming Arctic

where permafrost will increasingly transition to seasonally frozen ground. We hypothesise that under high grazing impact biomarker indices for degradation (Higher Plant Alcohol index (HPA) and Carbon Preference Index (CPI)) are higher compared to non-grazed sites with warmer soil conditions and therefore more degraded OM. Thirdly, we determined whether large herbivore grazing leads to reduced OM decomposition or increased OM input. We did this in a pilot study approach, collecting a set of samples with large spatial spread to capture different landscape and soil types, as well as different degrees of herbivore activity, to test if and under which circumstances significant effects can be found.

4.3 Study area

We collected sediment samples from permafrost and non-permafrost sites from two terrestrial Arctic study areas that are exposed to a range of large-herbivore grazing intensities at the local scale.

The first study area is located in the continuous permafrost zone in the floodplains of the Kolyma River in northeastern Siberia, approximately 100 km inland from the Arctic Ocean (Fig. 4-1a) (Fuchs *et al.* 2021). The landscape is characterised by Yedoma permafrost deposits and thermokarst lake basins (Palmtag *et al.* 2015, Veremeeva *et al.* 2021). The climate is continental with large temperature amplitudes (average of -33 °C in January; average of 12 °C in July) and low mean annual precipitation of less than 200 mm (Göckede *et al.* 2017), most of which usually falls in winter as snow. As a consequence, meltwater is the main water source for soil wetness in this region. Sediments are mainly silt-sized with additional clayish content, in drained thermokarst basins often topped with peat or peat-mixed sediment. Active layer depth ranges between 38 and 80 cm, depending on animal activity and vegetation type (Windirsch *et al.* 2022a). The drained thermokarst basins are covered by tussock grasses (*Carex appendiculata*) and short tundra vegetation (dwarf-shrub dominated with *Betula nana*, *Empetrum nigrum* and *Vaccinium* and *Salix* species being common), following wetness gradients from seasonally flooded areas to snowmelt affected areas. Wet areas feature tall grasses such as *Calamagrostis canadensis* (Corradi *et al.* 2005). On the surrounding uplands, tundra vegetation, interspersed with willow shrubs, is found.

The second study area, featuring seasonally frozen ground, is located in the glacially imprinted area of northern Finland (Fig. 4-1b and c) (Windirsch *et al.* 2021a, Windirsch *et al.* 2023c). In this area, glacial sands provide the main soil substrate for the formation of shallow podzols on top of glacial gravel and debris deposits. Relief mainly consists of glacial features such as eskers and moraines (Paoli *et al.* 2018). In depressions, peat mires formed on top of the sandy material. *Pinus sylvestris* and *Betula pubescens* ssp. *tortuosa* form vast forests in which wetlands covered by typical tundra vegetation and graminoids form more open areas. Underneath, bryophytes and ground lichen form the lowermost vegetation layer in this area (Oksanen and Virtanen 1995, Maliniemi *et al.* 2018). A subarctic and continental climate provides an annual

air temperature amplitude of approximately 26 °C in humid conditions (Finnish Meteorological Institute 2021).

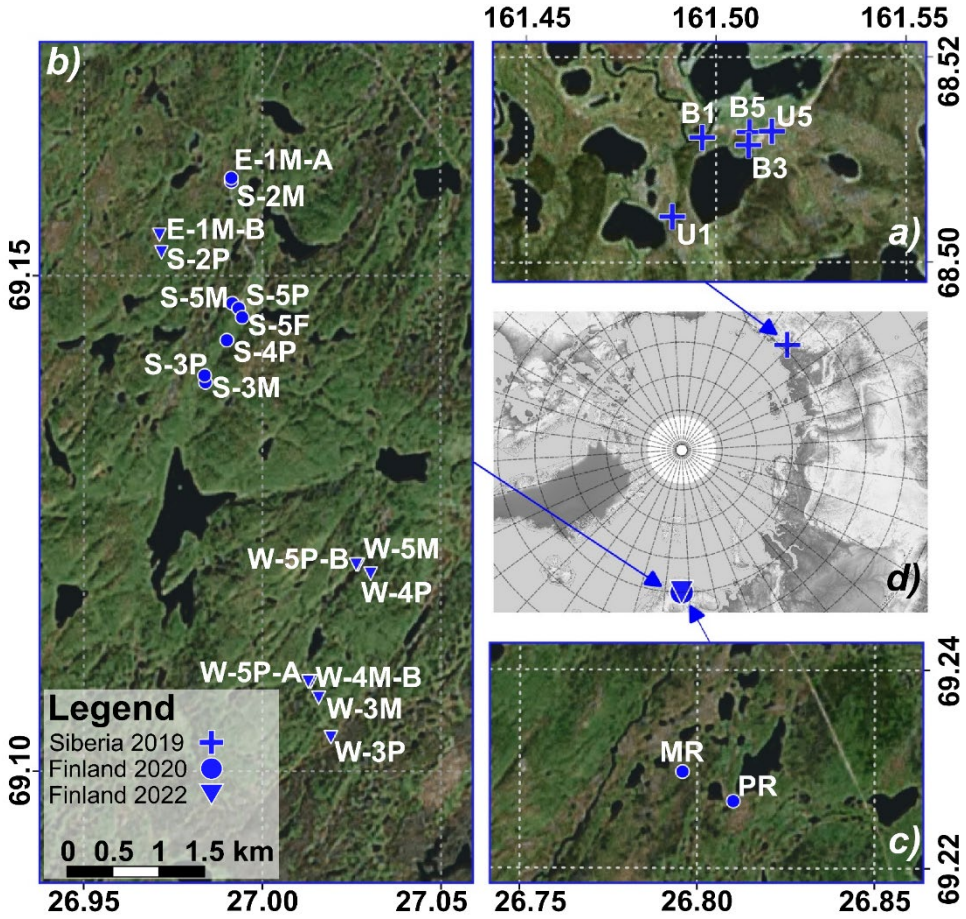

Figure 4-1 – Study site map indicating locations of all sampled sites; all detail maps are oriented with North up; scale bar applies for all detail maps; a) Sampling sites in Pleistocene Park, northeastern Siberia; b) Sampling sites at the Kutuharju Field Research Station, northern Finland; c) Reference sampling sites in northern Finland outside the Kutuharju Field Research Station; d) Overview map (circumpolar) showing the study areas and their position in the Arctic; E: Exclosure site, S: Reindeer summer range sites, W: Reindeer winter range sites, B: Drained thermokarst lake basin sites, U: Yedoma upland sites, M: Mineral soil sites, P: Peat sites; Numbers 1 to 5 state the grazing intensity (1: no grazing to 5: intensive grazing/pasture/supplementary feeding site); imagery provided by ESRI and Arctic SDI; coordinate system: EPSG:3067 – ETRS89 / TM35FIN(E,N).

4.4 Methods

4.4.1 Sampling approach

We collected the lipid biomarker samples during field campaigns in northeastern Siberia (2019) (Windirsch *et al.* 2022a) and northern Finland (2020 and 2022) (Windirsch *et al.* 2023c) (Fig. 4-1). The exact coordinates of all sampling locations are reported in the datasets available on the PANGAEA repository (Windirsch *et al.* 2021b, Windirsch *et al.* 2022c; b). During these campaigns, we sampled transects along gradients of large-mammal grazing intensity, spanning across 5 identified grazing intensities (Fig. 4-1). In each study area, several transects, each within a single landform or soil type, were selected, covering exclosure sites (intensity 1;

3 sites in total), occasional seasonal migration routes (intensity 2; 3 sites in total), daily migration routes (seasonal in Finland) (intensity 3; 6 sites in total), high-frequency seasonal daily migration routes (intensity 4; 3 sites in total), and pasture or supplementary feeding sites (intensity 5; 7 sites in total). These intensities are based on manipulation, such as fences around exclosures and across the landscape to guide migration or seasonal supplementary feeding, and long-term observation by research station staff, combined with our own observations for several days in the beginning of each sampling campaign. For final site selection, we also used dung abundance and the animal-induced shift in vegetation composition to identify the intensity of animal activity. In Siberia, the intermediate intensities 2 and 4 were omitted as identification was unclear. This sampling approach was applied in a pilot study design, capturing a large variety of soil and vegetation types as well as landscape forms but not having a balanced set of sampling sites. Also, due to limited resources and the objective to test our methods for finding differences between grazing intensities at all, we did not take any replicate samples, though we collected dung samples as a reference for the pure animal signal. A list of all sampling sites is provided in table 4-1.

In Siberia, we sampled permafrost-affected soils and the active layer in 3 sites along a transect in a partially drained thermokarst basin (sites B) with increasing grazing intensity towards the basin centre, as well as two sites along a transect on the surrounding Yedoma uplands (sites U) in the Pleistocene Park experimental area (68.51 °N, 161.50 °E) (Zimov 2005). The local herbivore species are Yakutian horses (*Equus ferus caballus*), Kalmykian cows (*Bos primigenius taurus*), sheep (*Ovis* sp.), reindeer (*Rangifer tarandus tarandus*), musk oxen (*Ovibos moschatus*), yaks (*Bos mutus*), moose (*Alces alces*), European bisons (*Bos bonasus*) and American bisons (*Bos bison*), which access the pasture sites year-round.

In Finland, we sampled a series of locations at the Kutuharju Field Research Station (69.15 °N, 27.00 °E) in a forest tundra area in a glacially imprinted landscape. The glacial retreat from these surfaces was estimated to 9,700 cal yr BP (Stroeven et al. 2016). The sample series consists of 8 mineral soil sites (M) and 10 peat sites (P) which seasonally freeze from the surface in winter, but are not underlain by permafrost. In addition, three reference sites outside the managed station area were sampled during this campaign, which we identified as grazing intensity 3 (migration routes with occasional grazing, representing the natural or most common state in northern Finland). There, we sampled a mineral soil, a peatland soil, and a peat soil underneath a birch forest to cover the predominant landscape types. The predominant large herbivore species in this area is reindeer, along with moose.

For comparison to the soil sample contents, we took a fresh faecal sample of the predominant herbivore species in each study area. In Siberia, we sampled fresh horse dung at the location U5. In Finland, we took a sample of fresh reindeer dung at site S-2M.

We sampled a total of 23 sites, with either one core or one soil profile each, reaching depths between 11 and 176 cm. From the material collected, we selected 58 subsamples for biomarker analysis. In frozen ground, we obtained soil cores using a SIPRE permafrost auger (Jon's Machine Shop, Alaska). In unfrozen peat soils, we used a peat corer (Eijkelkamp), and in unfrozen mineral soils we sampled within a soil profile using fixed-volume stainless steel cylinders. Frozen cores were transported intact to the labs, where they were subsampled for biomarker analysis, while unfrozen material was subsampled directly in the field. To avoid contamination with fresh vegetation material, the uppermost sections that held living plant roots from the soil cores and soil profiles were excluded. For the lower sections, we specifically sampled visibly separable stratigraphic units and the freeze-thaw interface, if visible.
Biomarker samples were taken exclusively using metal instruments and transported in sterile and annealed glass jar sample containers. The samples were frozen directly after sampling and kept frozen until further laboratory analysis started.

4.4.2 Laboratory analysis

All samples were freeze-dried using a Zirbus Sublimator 15. After drying, the samples were powdered and homogenised using a Fritsch Pulverisette 5 mill equipped with corundum jars.
For lipid biomarker extraction, we followed the procedures presented by Jongejans et al. (2021). Lipids were extracted from approximately 5 g of the homogenised samples using accelerated solvent extraction (ASE) with dichloromethane / methanol (DCM / MeOH 99:1 v/v) using a ThermoFisher Scientific Dionex ASE 350. The samples were each held in a static phase (5 min heating) for 20 min (75 °C, 5 MPa). Samples were subsequently concentrated using a Genevac SP Scientific Rocket Synergy evaporator at 42 °C.
We added internal standards for compound quantification: 5α-androstane as a reference for *n*-alkanes and 5α-androstan-17-one for *n*-alcohols. After removal of the asphaltenes (*n*-hexane-insoluble fraction) by asphaltene precipitation, we separated the resulting maltene fraction (*n*-hexane soluble compounds) by medium pressure liquid chromatography (MPLC) (Radke et al. 1980) into aliphatic, aromatic and NSO (nitrogen, sulphur, and oxygen containing) components using *n*-hexane. The NSO fraction was additionally separated into an acidic and neutral polar compound fraction. For this, each NSO fraction was transferred to an potassium hydroxide impregnated silica column where the acidic components were trapped as their potassium salts and the neutral polar components were washed through. Afterwards, the potassium salts were protonated again using DCM / formic acid (98:2 v/v) and the acidic fraction was washed off the column. Before measurements, the neutral polar fraction (containing the alcohols) was silyllated by adding 100 µl DCM / MSTFA (N-Methyl-N-(trimethylsilyl)trifluoroacetamide; 50:50 v/v) and heating the samples at 75 °C for one hour.

n-Alkanes from the aliphatic fraction as well as alcohols from the NSO fraction were measured using a Thermo Scientific ISQ 7000 Single Quadrupole Mass Spectrometer equipped with a Thermo Scientific Trace 1310 Gas Chromatograph (capillary column from BPX5, 2 mm x 50 m, 0.25 mm) as used by Jongejans et al. (2018), measuring with a MS transfer line temperature of 320 °C and an ion source temperature of 300 °C with an ionisation energy of 70 eV at 50 µA. Compound identification and quantification in relation to the internal standards from full-scan mass spectra (m/z 50-600 Da, 2.5 scans s^{-1}) were carried out using the software Xcalibur.
In addition, we analysed the samples for total organic carbon content (TOC), using an Elementar soliTOC cube analyser, and total nitrogen (TN), using an Elementar rapidMAX N analyser. From these measurements we calculated the TOC to TN (C/N) ratio.
We measured stable carbon isotope ratios ($\delta^{13}C$) after removing carbonates from our samples, using hydrochloric acid at 50 °C for three hours. The samples were measured with a Delta V Advantage Isotope Ratio MS supplement equipped with a Flash 2000 Organic Elemental Analyser, and results are provided in ‰ relative to the Vienna Pee Dee Belemnite (VPDB) standard (Coplen et al. 2006). Both C/N ratio and $\delta^{13}C$ ratio can be used as an indication for the quality and source of OM (Biester et al. 2014, Strauss et al. 2015). In fresh organic-rich samples, microbial activity is the main factor for OM decomposition, and the microorganisms prefer the consumption of ^{12}C over ^{13}C, which leads to higher $\delta^{13}C$ values of the remaining OM (Golubtsov et al. 2022). However, in recently deposited OM, the source of the OM, produced from different vegetation types, has a strong impact on the $\delta^{13}C$ signatures, complicating the use of this parameter as a decomposition indicator (Wynn 2007).

4.4.3 Lipid biomarker indices

Three indices from the measured lipid concentrations were calculated: (1) the average chain length (ACL) of *n*-alkanes with *i* carbon numbers as a measure of the dominating chain length distribution (Poynter and Eglinton 1990), providing information on the respective OM sources, (2) the carbon preference index (CPI) of *n*-alkanes as a measure of the OM degradation level (Bray and Evans 1961, Marzi et al. 1993) and (3) the higher-plant alcohol index (HPA) as a measure of leaf wax component degradation (Poynter 1989) applying the following equations:

(Eq. 1) $$ACL_{23-33} = \frac{\Sigma\, i\, C_i}{\Sigma\, C_i}$$

(Eq. 2) $$CPI_{23-33} = \frac{\Sigma\, odd\ C_{23-31} + \Sigma\, odd\ C_{25-33}}{2 * \Sigma\, even\ C_{24-32}}$$

(Eq. 3) $$HPA = \frac{\Sigma\, (alcohols\ C24, C26, C28)}{\Sigma\, (alcohols\ C24, C26, C28) + \Sigma\, (n-alkanes\ C27, C29, C31)}$$

following the methods applied by Jongejans et al. (2021). Lower CPIs indicate a higher degradation state of OM (Glombitza *et al.* 2009, Strauss *et al.* 2015). The same holds true for lower

HPA values (Poynter 1989). High HPA values express a high content of *n*-alcohols vs. *n*-alkanes, and thus of functionalized to non-functionalized biomarkers. During decomposition it is suggested that aliphatic functionalized biomarkers are degraded to non-functionalized aliphatics (Poynter 1989). However, in fresh OM both parameters are affected by the biomarker composition of the initial source material (Jongejans *et al.* 2021). Thus, to use these parameters to assess different degradation stages, the initial source material should be comparable.

4.4.4 Statistics

We tested for statistical significance of the differences in all parameters. Due to independence of our samples, when separated by grazing intensity and therefore location, and unequal sample amounts within the groups, we chose to run a Kruskal-Wallis H test. We did this in the R environment using the 'stats' package (R Core Team 2021) and used a confidence level of 0.95. Therefore, if the resulting *p*-value is smaller than 0.05, the differences are statistically significant.

We further run mixed effect models in the R environment ('lme4' package) for the biomarker indices, using 'grazing intensity' as a fixed variable and 'site' as a random variable to identify random effects between sites, accounting for the spatial heterogeneity of the analysed soils. Positive random interception values indicate that the respective biomarker index baseline value at one site is higher than the overall baseline, while negative values indicate the opposite.

4.5 Results

Here, we report the TOC, C/N, $\delta^{13}C$, $ACL_{23\text{-}33}$ (for *n*-alkane chain lengths with 23 to 33 carbon atoms), $CPI_{23\text{-}33}$ (for *n*-alkane chain lengths with 23 to 33 carbon atoms), total *n*-alkane concentration and HPA values for all permafrost-affected and seasonally frozen ground samples. We distinguish between the seasonally thawed samples (top 38 cm of all study sites; Fig. 4-2) and the full sampling depth from all sites (Fig. 4-3). All data will be published in PANGAEA. Missing values for C/N ratio are due to very low TN values below the instrument detection limit of 0.1 wt%. In the following, all samples are referred to by using the site name and the mean sample depth.

4.5.1 TOC

In permafrost-affected samples TOC ranges between 0.81 wt% (CH19-B1 26.25 cm bs) and 21.13 wt% (CH19-B3 71.5 cm bs) with a mean value of 7.53 wt%. For seasonally frozen ground, the TOC range is between 0.42 wt% (FI20-S-2M 18.5 cm bs) and 53.99 wt% (FI20-S-4P 82.5 cm bs) with a mean of 28.54 wt%. There are no general trends with depth across sites visible (Fig. S1). Many TOC values are in the same range for the permafrost and seasonally frozen ground samples, with exception of the peat samples from seasonally frozen

ground showing much higher TOC values, similar to the reference dung samples with 37.66 wt% (horse, Siberia) and 44.69 wt% (reindeer, Finland). When comparing grazing intensities, values are lowest in grazing intensity 1 and seem to increase to grazing intensity 5 at least at the permafrost sites (Fig. 4-2).

4.5.2 C/N ratio

For the permafrost-affected samples, values range from 11.40 (CH19-U5 49 cm bs) to 29.27 (CH19-U1 65 cm bs) with a mean of 17.79. For the seasonally frozen ground samples, the C/N ratio range is between 13.77 (FI20-S-3P 92.5 cm bs) and 51.20 (FI20-S-3P 9.5 cm bs) with a mean of 29.78. C/N values most often show a decrease over depth (Fig. S4-1), but are similar across grazing intensities.

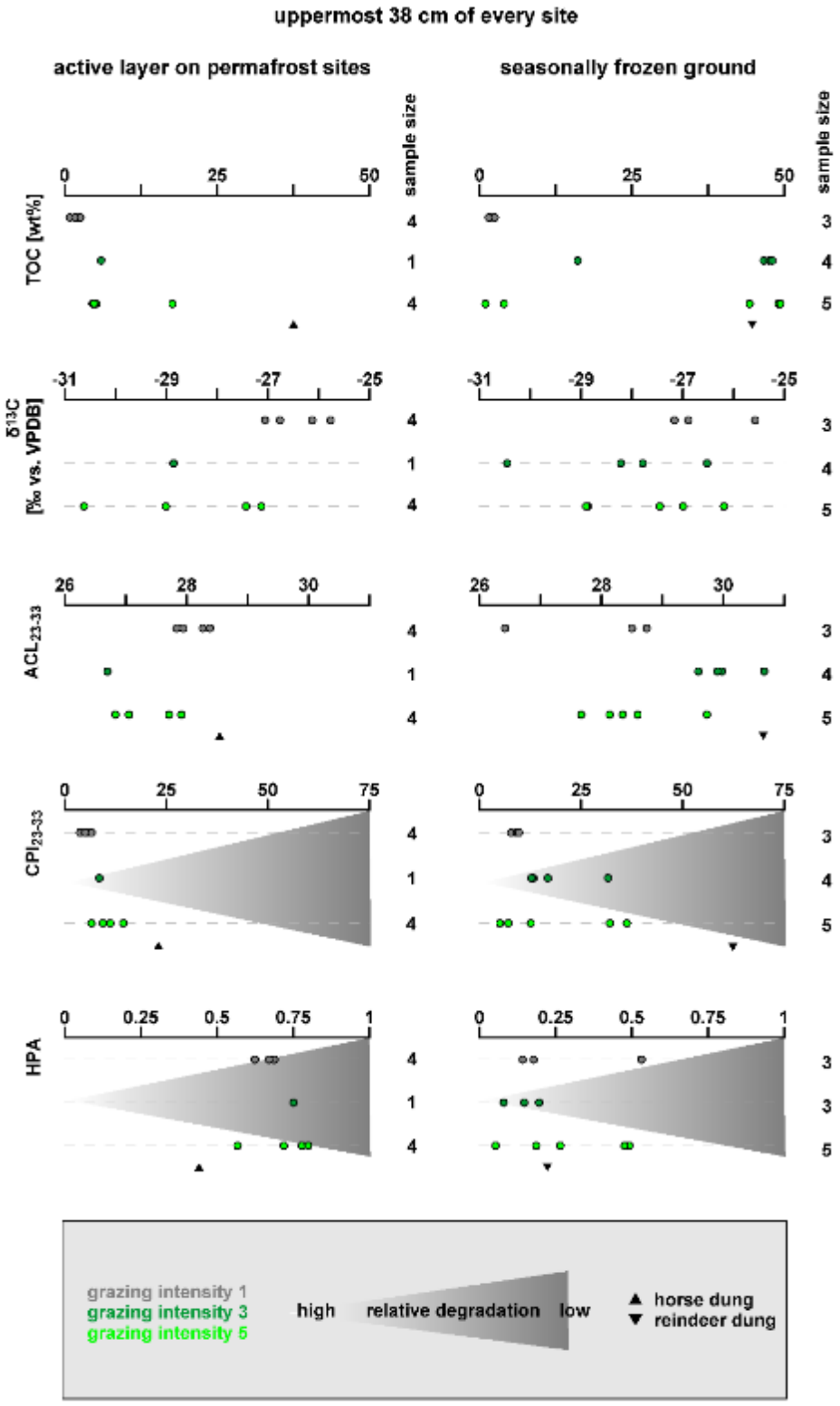

Figure 4-2 – Carbon and biomarker characteristics for the uppermost 38 cm for grazing intensities 1 (exclosure / no grazing; grey), 3 (migration route / occasional grazing; dark green) and 5 (pasture / supplementary feeding site; light green); from top to bottom: distribution plots of total organic carbon content (TOC), stable carbon isotopes ($\delta^{13}C$), *n*-alkane average chain length (ACL_{23-33}), carbon preference index (CPI_{23-33}) and higher-plant alcohol index (HPA); left: active layers (top 38 cm) from permafrost study sites; right: top 38 cm samples of sites with seasonally frozen ground; sample size for each category is listed on the right for each plot; for better readability; values for the dung reference samples are added as triangles.

4.5.3 Stable carbon isotope ratio

Stable carbon isotope ratios ($\delta^{13}C$) values range from -30.61 ‰ (CH19-B5 5.75 cm bs) to -23.49 ‰ (CH19-U5 49 cm bs) with a mean of -27.43 ‰ for the permafrost-affected samples. For seasonally frozen ground samples, the range is -28.93 ‰ (FI20-S-5P 127.5 cm bs) to -26.44 ‰ (FI20-S-3M 38.5 cm bs) with a mean of -27.52 ‰. Values are generally similar over depth at each site, but different across sites (Fig. S4-1). At the permafrost sites, a general trend to lighter $\delta^{13}C$ values can be observed with increasing grazing intensity, which is less clear for the seasonally frozen ground.

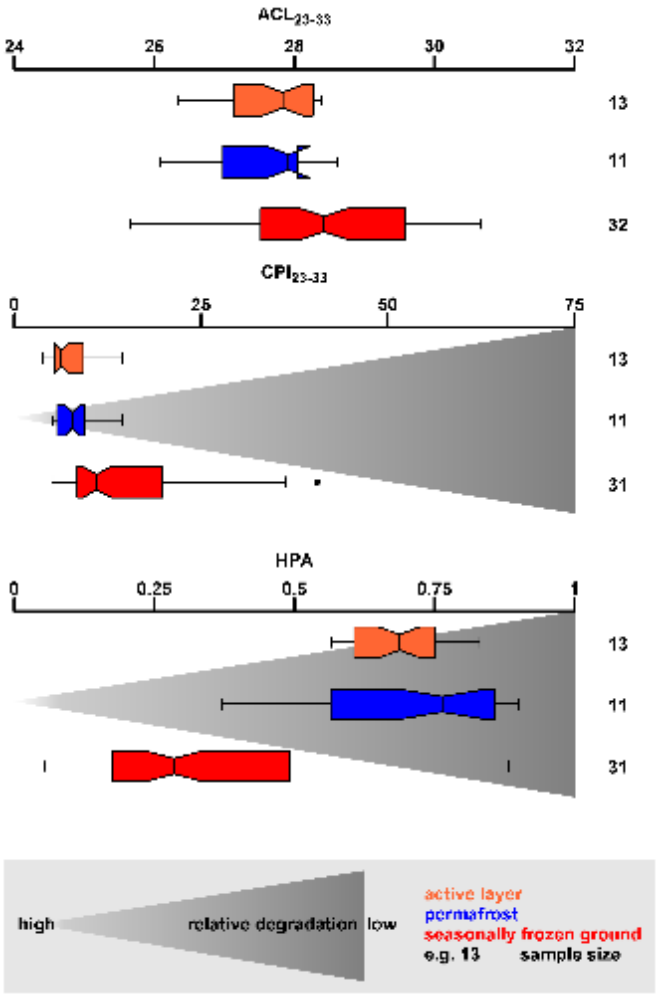

Figure 4-3 – Boxplots of ACL_{23-33}, CPI_{23-33} and HPA comparing all active layer samples (Siberia; orange), permafrost samples (Siberia; blue) and seasonally frozen ground sites (Finland; red); dots mark outliers (more than 1.5 box lengths away from the median).

4.5.4 Absolute *n*-alkane concentration

The absolute lipid concentration of the *n*-alkanes in permafrost-affected samples range from 1.5 $\mu g/g_{TOC}$ (CH19-B3 71.5 cm bs) to 170.3 $\mu g/g_{TOC}$ (CH19-B1 124 cm bs). With a large share of samples having rather low concentrations, the mean value is 36.5 $\mu g/g_{TOC}$ with a median of 26.2 $\mu g/g_{TOC}$. In seasonally frozen ground samples, the *n*-alkane concentration varies between 1.7 $\mu g/g_{TOC}$ (FI20-S-5F 22.5 cm bs) and 117.8 $\mu g/g_{TOC}$ (FI22-W-5P-A 47.5 cm bs). The mean value is 22.2 $\mu g/g_{TOC}$, the median is 8.1 $\mu g/g_{TOC}$.

Concentrations follow no general pattern over depth across sites (Fig. S4-1), but are generally lower at sites in grazing intensity 3. Dung reference samples show values of 2.3 $\mu g/g_{TOC}$ (horse) and 14.3 $\mu g/g_{TOC}$ (reindeer). The individual *n*-alkane concentrations for carbon numbers 23 to 33 are reported in figure S4-2 for each sample.

4.5.5 Average chain length

Across permafrost-affected sites, ACL_{23-33} of the *n*-alkanes ranges between 26.1 (CH19-B1 87.5 cm bs) and 28.6 (CH19-U5 93 cm bs) with a mean value of 27.65. For seasonally frozen ground, the ACL_{23-33} range is 25.7 (sample FI-S-2M 18.5 cm bs) to 30.7 (FI22-W-3P 17.5 cm

bs) with a mean of 28.3. The values for our reference dung samples are 28.5 for horse dung and 30.7 for reindeer dung (Fig. 4-2 and 4-3).

4.5.6 Carbon preference index

For permafrost-affected samples, the CPI_{23-33} ranges from 3.8 (CH19-B1 26.25 cm bs) to 14.5 (CH19-U1 65 cm bs) and a mean value of 7.9. The median is 7.7.

The CPI_{23-33} for seasonally frozen ground samples ranges from 5.0 (FI20-S-5M 11.5 cm bs) to 40.5 (FI22-W-3P 17.5 cm bs) with a mean value of 15.9 and a median of 11.1. There is no general trend visible (Fig. S4-1). CPI for the horse dung reference sample is 23.3, and for reindeer dung 62.2 (Fig. 4-2).

For one sample from seasonally frozen ground (FI20-S-2M 18.5 cm bs), we were not able to calculate the CPI_{23-33} due to the absence of *n*-alkanes with even carbon lengths between 24 and 32. The CPI_{23-33} data indicate a slight trend to higher values with increasing grazing intensity at the permafrost and less clear also at the seasonally frozen ground sites (Fig. 4-2).

4.5.7 Higher-plant alcohol index

HPA of permafrost-affected samples ranges from 0.37 (CH19-B1 87.5 cm bs) to 0.90 (CH19-B5 106 cm bs) with a mean of 0.69 and a median of 0.70. For seasonally frozen ground samples, HPA ranges between 0.05 (FI20-S-5P 10 cm bs) and 0.88 (FI20-S-2M 18.5 cm bs) with a mean value of 0.34 and a median of 0.29. No general trend is visible over depth (Fig. S4-1). Values are generally higher for intensively grazed sites (Fig. 4-2). The dung reference samples show values of 0.44 (horse) and 0.23 (reindeer). For one seasonally frozen ground sample (FI20-S-3P 9.5 cm bs), we could not calculate the HPA index due to measurement issues.

4.5.8 Statistical results

We found no distinct differences between permafrost sites (Siberia) and seasonally frozen sites (Finland) that are consistent throughout all parameters. However, for individual parameters, and especially the HPA index, some differences were evident from our data. We found positive correlation for C/N ratio and CPI_{23-33} ($R = 0.60$) as well as for ACL_{23-33} and $\delta^{13}C$ ($R = 0.37$). At the same time, we found a strong negative correlation for HPA and TOC ($R = -0.57$). We tested for statistically significant differences in biomarker parameters, comparing the permafrost-affected samples and the samples from seasonally frozen ground. We found a statistically significant difference for the HPA index between all samples from the permafrost environment (Siberia) and the seasonally frozen ground study area (Finland) (p-value < 0.001). For CPI_{23-33} we found a significant difference comparing the same set of samples (p-value < 0.001). For ACL_{23-33} and absolute *n*-alkane concentration, the differences were not significant (p-value > 0.05).

However, when comparing HPA and $CPI_{23\text{-}33}$ between grazing intensities, the differences were not significant.

To identify random effects in our dataset, especially spatial variation of the soil composition, and to identify if grazing intensity plays a role in parameter changes across our data, we run mixed effects models that showed positive interception values for HPA from permafrost sites in general, and for seasonally frozen sites with high grazing intensity. However, for seasonally frozen ground, this observation was not consistent, even though only negative values were returned for all seasonally frozen ground sites with a grazing intensity below 5. Repeating this procedure for $CPI_{23\text{-}33}$ produced clearly negative values for permafrost sites, and a range of values between -2.00 and 4.50 for seasonally frozen ground sites with no particular trend along grazing intensities or across soil types. The same holds for $ACL_{23\text{-}33}$, where the range for seasonally frozen ground sites is -0.78 and 1.04.

4.6 Discussion

4.6.1 Effects of grazing intensity on biomarker signals

Since animal activity influences OM storage and likely also OM decomposition in permafrost-affected areas (Windirsch et al. 2022a), we expected to find differences in the stored OM between different animal grazing intensities. We summarised our findings from *n*-alkane and *n*-alcohol analysis in figure 4-2, separated by grazing intensities, and limited the comparison to samples taken from the top 38 cm of soil for two specific reasons. Firstly, during our sampling at sites with permafrost, we found that the active layer depth was a minimum of 38 cm (Windirsch et al. 2022a). This means that the material down to this depth is unfrozen during the summer season, but frozen during winter. Secondly, given that the introduction of large-mammal herbivores at the Siberian site was only 23 years ago and at the Finland site approximately 50 years ago, it is important to note that herbivory influence primarily affects the soil surface and upper soil section. As a result, the top soil samples are most likely to exhibit noticeable changes induced by grazing, making them more suitable for comparison across different grazing intensities.

When examining HPA values of the surface samples affected by different grazing intensities, a slight trend towards higher values with increasing grazing intensity can be observed for permafrost-affected soils (Fig. 4-2). While in grazing intensity 3 only one sample is present, this sample's HPA value aligns between intensities 1 and 5. For the seasonally frozen soils, this trend is not as strong with one higher HPA value at grazing intensity 1. Nevertheless, three of the four highest HPA values can be observed at grazing intensity 5. This suggests that the OM stored at sites of higher grazing intensity often shows a lower degradation level. This supports our hypothesis that animal grazing can have a preserving effect on soil OM. The reason for this could be that intense grazing reduces the soil cover of sturdy and snow-catching shrub

vegetation, in favour of graminoid-dominated vegetation types, leading to faster and stronger soil cooling when air temperatures drop in autumn/winter causing reduced OM degradation in surface soils. In the permafrost-affected environment, this also appears to have an impact on the total carbon storage (Fig. 4-2 TOC), since highest OC contents were observed at the sites of grazing intensity 3 and 5. We did not see this for the seasonally frozen ground sites, with partly very high TOC values at grazing intensity 3 and 5 due to the fact that they are peat deposits, which makes them hardly comparable to the mineral soil sites found in grazing intensity 1 in terms of TOC content. Further, soil compression from animal trampling often plays an important role on peat soils, leading to higher bulk densities and therefore OC stocks. However, this was not the case in this specific study area, as bulk density was not increasing under animal trampling on these study sites but in fact decreasing, as reported in Windirsch *et al.* (2023c). The CPI23-33 data also show a slight trend towards higher values (less decomposed) with increasing grazing intensity especially at the permafrost sites. For the seasonally frozen ground samples, the data show a lot more variation which is most likely related to a higher heterogeneity of the source OM (including peat samples) in this area. Previous studies showed that increased degradation within soils can also lead to an increase of the δ13C values of the remaining organic biomass (Fig. 4-2) due to the fact that isotopically lighter OM is preferentially degraded by microorganisms (Barker and Fritz 1981). Thus, δ13C values are often used as an additional parameter for OM degradation (Bonanomi et al. 2013, Biester et al. 2014, Strauss et al. 2015). Here, the $\delta^{13}C$ values of the soil OM show a trend towards lighter values and therefore less degraded OM with increased grazing intensity for both areas. This would additionally support our hypothesis that higher grazing intensity leads to lower OM decomposition in the soils due to the increased exposure of the soils to the winter cold. As mentioned before, $\delta^{13}C$ values can also be influenced by the $\delta^{13}C$ signal of the source OM, however in this case a change from shrub-dominated ($\delta^{13}C$ values around -28 ‰ (Pattison and Welker 2014)) environment at lower grazing intensity to a graminoid-dominated ($\delta^{13}C$ values around -26 ‰ (Pattison and Welker 2014)) environment at higher grazing intensity should lead to an opposite trend. This suggests that the $\delta^{13}C$ signal of the source OM is not the determining factor of the bulk $\delta^{13}C$ signal of the deposited OM at least for the permafrost sites. This might be different for the seasonally frozen ground sites where some of the samples at grazing intensities 3 and 5 are organic-rich peat samples. Peats in this area are for instance dominated by *Sphagnum* species with $\delta^{13}C$ signals around -29 ‰ (Preis et al. 2018) and might be responsible for the higher variability of bulk $\delta^{13}C$ signals in the Finland dataset. While the ACL values exhibit clear differences between different grazing intensities, which is also in support of different vegetation compositions, we cannot state if these differences originate from any recent vegetation shifts triggered by grazing activity of from the original soil OM itself.

At the seasonally frozen ground sites in Finland, one HPA value at grazing intensity 1 is exceptionally high compared to the other values being even slightly higher than at grazing intensity 5. While the effects on the pasture sites (soil cooling via animal activity and hence reduced OM decomposition) are a possible explanation for increased OM stability at grazing intensity 5, the stable and undisturbed growth of ground-covering and therefore insulating species such as *Cladonia rangiferina* observed at the Finland site (Windirsch *et al.* 2023c) might be a plausible explanation for the low decomposition state of this specific sample at grazing intensity 1 (Porada et al. 2016). While such a layer insulates the ground against low winter temperatures, it also insulates against summer heat to some degree, in contrast to graminoid vegetation. Therefore, in artificially undisturbed areas where such a layer can form, the summer shadowing effects and generally lower soil temperature amplitudes might partially compensate for the total absence of the positive large-mammal herbivore effect on the OM preservation, leading to colder ground conditions compared to the disturbed sites with intermediate grazing intensity (intensity 3), but not as well as in the highly disturbed and now graminoid-dominated areas of grazing intensity 5. However, this only works in areas where herbivores can be excluded (e.g. by fences) and also where environmental characteristics are enabling such a vegetation type to grow. At the grazing intensity 3 sites, animal impact is too strong for such an insulating lichen layer to form, but too weak for animal-induced vegetation shifts towards graminoid-dominated vegetation and effective soil cooling by snow trampling and mentioned vegetation change leading to intermediate OM degradation.

4.6.2 Effects of ground thermal regime on soil OM degradation

When comparing permafrost-affected deposits in Siberia with the seasonally frozen ground deposits in Finland, both depositional areas can clearly be distinguished by the CPI, ACL and HPA index data (Fig. 4-3). While the active layer and deeper permafrost deposits show variations within a similar range, the seasonally frozen ground samples show a distinct offset. The ACL and CPI for the Finland sites are notably higher, which is due to differences of the vegetation composition of both sites. As shown before with the dung samples, the permafrost sites are dominated by *Calamagrostis* ssp. which shows a lower ACL (28) (Berke et al. 2019) than *Deschampsia cespitosa* (ACL 30.3) (Gamarra and Kahmen 2015) mixed with *Sphagnum* ssp. (ACL 25.9) (Huang et al. 2012) at the Finland sites. Additionally, the seasonal frozen ground also contains a high number of peat samples (21 out of 32) supporting the assumption of different OM compositions. When examining the HPA index, a significant difference (with a *p*-value of 1.08^{-7}) between these deposits or rather study areas is found. The samples from the examined permafrost and active layer have a median HPA of 0.70, while the seasonally frozen ground has a significantly lower median HPA of 0.27. Generally, HPA values are lower than 0.50 in the seasonally frozen ground samples, while samples from the permafrost study area are higher than 0.50 (Fig. 4-3). Thus, the HPA data, generally, indicate a higher level of OM

preservation for the permafrost deposits, which can be related to the reduced annual time of OM degradation which is limited to the period when the soil is not frozen (Schuur *et al.* 2008, Strauss *et al.* 2015, Walz *et al.* 2017).

Whether direct digestion of the OM by the local herbivore community may contribute to the overall degradation pattern is difficult to say, since the proportion of the digested OM relative to the total OM is unknown. However, such a contribution might be indicated when comparing the HPA values of the horse (HPA of 0.44) and reindeer dung (HPA of 0.23) (Fig. 4-2 HPA), showing a higher degree of degradation of the OM at the Finland site in the reindeer sample. When comparing the reindeer dung sample with ACL values from literature, it can be observed that the dung signal and the mean signal of the most abundant graminoid species are quite similar. The sampled reindeer dung (Finland) had one of the highest values found in our study (30.7, Fig. 4-2), which is close to the ACL value of *Deschampsia cespitosa* (30.3), the predominant species on the sampled seasonally frozen pasture sites (Gamarra and Kahmen 2015, Windirsch *et al.* 2023c). For the horse dung (Siberia), which is expected to contain mainly locally predominating *Calamagrostis* material, we found an ACL value of 28.5. In the literature, an ACL value of 28 was reported for another species of the *Calamagrostis* genus with a similar distribution of *n*-alkane chains as in our horse dung sample (Berke *et al.* 2019), although slightly shifted towards shorter chains. Thus, the horse dung from the Siberian study area likely contains mainly *Calamagrostis* material with a minor content of other plant material. However, the ACL values of the dung samples from both sites do not fit to the ACL values in the soils at grazing intensity 5, which suggests that our soil samples must contain a wider mix of plant species signals than present in the dung sample. Although only one dung sample has been investigated in each study area, and therefore cannot be considered representative, the measured dung samples seem to reflect the source OM signal rather than deposited OM. Nevertheless, in terms of OM degradation, an effect of herbivore digestion on the HPA values of the soil OM cannot be excluded. For the permafrost sites, where the active layer shows a slightly lower HPA value than the underlying permafrost, we can therefore assume that in the active layer we have a mixed signal between the original substrate, preserved below in the permafrost, and the recent vegetation, either directly or via animal faeces. This mixing could also explain the low HPA values in grazing intensity 5 in seasonally frozen ground samples, where the low reindeer dung HPA, either representing the current vegetation or the animal influence, could lower the overall HPA value of a sample.

4.6.3 Impact of herbivory on permafrost OM storage

The bulk $\delta^{13}C$, $CPI_{23\text{-}33}$ and HPA values suggest that intensive grazing (intensity 5) tends to lead to less decomposed OM (Fig. 4-2). However, partly variable data at the permafrost but particularly at the seasonally frozen ground site indicate that also other processes such as

composition of the organic source material must have an impact on the level of OM decomposition. We also found hints that degradation of functionalized OM might generally be lower in permafrost-affected soils (Fig. 3 HPA). This leads to the conclusion that ground thermal regimes have an impact on biomarker signals and OM degradation. If ground thermal regimes can be influenced by animal activity via snow trampling and grazing-induced vegetation changes, which ultimately would result in altered degradation conditions, is not clear from our pilot study dataset, but our findings indicate that further studies on this topic are advised.

The differences between grazing intensities that can be observed in this pilot study are mainly trends and due to the data variability statistically not well supported. Furthermore, it has to be kept in mind that the observed differences are attributed to relatively short time spans between the beginning of grazing and sampling (23 years for permafrost-affected sites, 50 years for seasonally frozen ground sites) and that they also depend on the animal densities to observe these effects across a whole area. Also, differences between grazing intensities in seasonally frozen ground could be due to random effects caused by spatial variability. While there are differences observed, and these differences approximately match our expectations of less degraded material under high grazing impact, our mixed effects modelling revealed that variability between sites even within grazing intensities is high. On the other hand, the model confirmed that HPA and $CPI_{23\text{-}33}$, which we used as degradation proxies, indicate a generally less decomposed state of soil OM for the permafrost-affected sites, reporting highest interception values for the permafrost sites, clearly above the interception baseline of the complete dataset.

Also, at our study sites, these herbivore densities are unnaturally increased, and still grazing-related effects are rather small. Actively utilising herbivory to reduce OM decomposition might therefore only be feasible on a very local scale where animals can be herded and controlled over longer periods of time. We are not able to make a precise statement on how long grazing pressure needs to be applied in order to produce significant effects, if at all, but estimating from the data presented, where some differences are already seen, the target period on permafrost sites should exceed 50 years of grazing activity. At the same time, detailed measurements of each site's preconditions and a higher spatial resolution of sampling points as well as replicate sampling are advised to account for confounding factors.

4.7 Conclusion

Building upon the hypothesis that large herbivore activity contributes to colder ground temperatures by keeping the soil vegetation low and thereby slowing down OM decomposition, we have found indications that both permafrost-affected and to a smaller extend also seasonally frozen Arctic ground tend to exhibit better-preserved soil OM under high grazing intensity. Based on our lipid biomarker screening data we also observed, in addition to the grazing effect, an overall lower degradation level of the permafrost OM compared to OM in the seasonally frozen ground. The grazing effect on the OM preservation was evident in data trends but was

not statistically confirmable. This was most likely due to high spatial variability of the examined soil material (including source OM) and little expressed changes in the biomarker signals.
Hence, we see indications that intensive herbivory tends to have a positive impact on soil carbon storage in permafrost, while in seasonally frozen ground an effect is not clearly visible or more strongly masked by random effects such as soil material differences and overall spatial heterogeneity (i.e. micro-topography, vegetation, hydrology etc.). At the same time, we also found no negative impact of herbivory on soil carbon storage in seasonally frozen ground. These results need to be evaluated in future studies with a more dense sampling approach. We still suggest that the implementation of intensive herbivory practices may offer localised opportunities for mitigating OM decomposition and subsequently reducing carbon emissions originating from permafrost and should be further examined in climate change strategy development.

4.8 Acknowledgements

The authors gratefully acknowledge Anke Kaminski and Cornelia Karger from the GFZ Organic Geochemistry laboratory facilities for their invaluable guidance and assistance in lipid biomarker sample preparation and measurement. They would also like to express their appreciation to the AWI's Permafrost Carbon and Nitrogen Lab, especially Justin Lindemann for his expert assistance with sample preparation. Furthermore, the authors extend their gratitude to J. Otto Habeck (Universität Hamburg) for his valuable contributions to the design of this study.

4.9 Competing interests

The authors declare no conflict of interests, neither commercial nor financially nor ethical.

4.10 Author contribution

TW and JS designed this pilot study. KM, LJ and JS provided expertise in biomarker analysis and interpretation. TW, GG, JW and JS put the data into local environment context. All authors contributed to writing and editing the manuscript.

4.11 Funding

This research was carried out as part of the PeCHEc (Permafrost Carbon Stabilisation by Recreating a Herbivore-Driven Ecosystem) project. This project was funded by the Potsdam Graduate School, supported by the AWI Permafrost Research section and the Geo.X research network (SO_087_GeoX).
Field campaigns were financed by the CACOON (Changing Arctic Carbon Cycle in the Coastal Ocean Near-Shore) project (#03F0806A (German Federal Ministry of Education and Research)) and the AWI and the Permafrost Research section baseline and expedition funding.

4.12 Data availability

The biomarker measurement data are available from the PANGAEA repository (Windirsch *et al.* 2023a; b). All other data used in this manuscript are available from the PANGAEA repository (Windirsch *et al.* 2021b, Windirsch *et al.* 2022c; b).

Table 4-1 – Study sites in active layer (AL) and permafrost (PF) samples in permafrost-affected soils in Cherskiy (CH), northeastern Siberia, from 2019, and in seasonally frozen ground (SFG) in Finland (FI) from 2020 and 2022; grazing intensity defined from 1 (exclosure) to 5 (pasture).

study area	site	sampling year	sampling size analysed	grazing intensity	ground thermal regime	soil type
Siberia	CH19-B1	2019	5	1	AL, PF	mineral, peat
	CH19-U1	2019	4	1	AL, PF	mineral
	CH19-B3	2019	4	3	AL, PF	mineral
	CH19-B5	2019	5	5	AL, PF	mineral, peat
	CH19-U5	2019	6	5	AL, PF	mineral
Finland	FI20-E-1M-A	2020	2	1	SFG	mineral
	FI22-E-1M-B	2022	1	1	SFG	mineral
	FI20-S-2M	2020	2	2	SFG	mineral
	FI22-S-2P	2022	1	2	SFG	peat
	FI20-S-3M	2020	2	3	SFG	mineral
	FI20-S-3P	2020	3	3	SFG	peat
	FI22-W-3P	2022	1	3	SFG	peat
	FI20-MR	2020	1	natural	SFG	mineral
	FI20-PR	2020	1	natural	SFG	peat
	FI22-W-4M	2022	1	4	SFG	mineral
	FI20-S-4P	2020	3	4	SFG	peat
	FI22-W-4P	2022	2	4	SFG	peat
	FI20-S-5M	2020	1	5	SFG	mineral
	FI22-W-5M	2022	1	5	SFG	mineral
	FI20-S-5P	2020	3	5	SFG	peat
	FI22-W-5P-A	2022	2	5	SFG	peat
	FI22-W-5P-B	2022	2	5	SFG	peat
	FI20-S-5F	2020	3	5	SFG	peat

Chapter 5: Synthesis

The main objective of this dissertation project was to determine the impact of large herbivore activity, such as trampling, browsing, snow removal, and fertilization, on the storage of soil organic carbon in Arctic regions. Based on the hypothesis that the mammoth steppe represents a stable carbon storage system self-sustained by intensive herbivory in cold environments, my findings indicate that animal activity does indeed affect soil carbon storage in permafrost environments locally (chapter 2). Such effects were not clearly visible in seasonally frozen ground, where apparently other soil factors play a larger role compared to permafrost, giving a rather weak correlation between animal abundance and soil carbon reservoirs (chapter 3). Concerning the degradation state of the belowground OM (chapter 4), I encountered lower degradation at sites with high grazing intensity. This effect is clearly visible in permafrost-affected soils, and findings from seasonally frozen ground indicate a similar but less intense effect of grazing on soil OM preservation.

5.1 Ecosystem changes under the impact of large herbivores

An important driver of Arctic soil warming, and a key element to the Arctic amplification (Zhang *et al.* 2013, Previdi *et al.* 2021), is the establishment of larger and more perennial vegetation, mainly in the form of shrubs colonising tundra areas and exceeding the former northern treeline (Parker *et al.* 2021). While numerous studies found that grazing pressure by large herbivores reduces the extent of shrubification (Olofsson *et al.* 2009, te Beest *et al.* 2016, Mekonnen *et al.* 2021), this thesis reveals the complete transformation of Arctic open-landscape vegetation by intensive herbivory towards graminoid-dominated vegetation communities, including the reduction of shrubification (chapters 2.5.1 and 3.5.2). The research showed that tundra areas exposed to high animal activity transformed into species-poorer and graminoid-dominated vegetation types (table 3-2), while with decreasing animal activity the abundance of shrubs increased. While it is conceivable that animals simply avoid shrubby

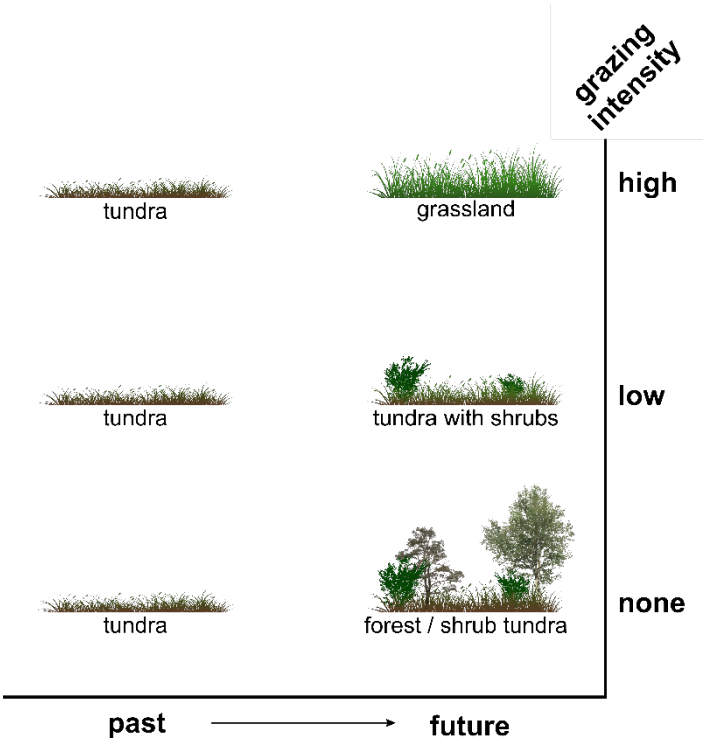

Figure 5-1 – Graphic representation of Arctic tundra vegetation development under different grazing pressures, accounting for ongoing shrubification under climate warming.

areas – leading to high animal activity in shrub-poor areas – it was shown in other studies that shrubs vanish in the presence of large animal numbers, most likely due to browsing pressure (Olofsson *et al.* 2009, Verma *et al.* 2020). This supports the assumption of the future vegetation pathways under grazing pressure as depicted in figure 5-1.

However, reindeer prefer open landscapes for insect avoidance, as the insects are exposed to wind in such areas (Skarin *et al.* 2010, Bezard *et al.* 2015). Nevertheless, this leads to reindeer maintaining such open landscapes as described above.

5.2 Grazing effects on soil organic matter decomposition

While the data presented in chapter 2 show that soil carbon storage is higher under intensively grazed conditions in a permafrost-affected area, this seems to be true only for the active layer, the seasonally thawed top part of the soil. Therefore it is plausible to expect the same effect in seasonally frozen ground (chapter 3), where the top layer undergoes the same winter-freezing summer-thawing cycle. However, the findings from chapter 3 were inconclusive in this regard. An explanation to this would be that even in the seasonally thawed active layer, the general existence of permafrost underneath plays an important role, as it prevents vertical water movement below the permafrost table (Smith *et al.* 2012), and therefore also the vertical wash-out of carbon (Mueller *et al.* 2015). This frozen water-impermeable layer does not exist in seasonally frozen ground, so even if animal presence increases carbon input, it maybe is not visible in the upper soil part due to removal processes. Another explanation to why increased carbon contents are only found in the active layer on top of permafrost might be the relatively short time span of intensive grazing (~ 23 yr) in my permafrost study area, while present-day permafrost was deposited in times where mammoths were still around. This is visible from the range of the permafrost radiocarbon ages, reaching from approximately 2300 to 34600 cal yr BP (chapter 2, appendix III table S2-1).

If we investigate the decomposition state of soil organic matter via lipid biomarker analysis (chapter 4), it is revealed that the decomposition state is indeed different between grazing intensities also in seasonally frozen ground (Fig. 4-2). This means that there is not necessarily more carbon stored in ground affected by intensive grazing, but that OM shows signs of lower decomposition under intensive grazing influence. This is especially true for alcohol compounds. When comparing all the samples taken for lipid biomarker analysis from both study areas, the alcohol compounds showed enhanced decomposition in seasonally frozen ground compared to permafrost-affected ground, including the active layer (Fig. 4-3).

Therefore, in line with the hypothesis of this thesis, the ground temperature regime affected by animal activity via snow removal, compression and vegetation change is the key influence of animals on soil OM storage. To prevent soil OM from further and, as a result of climate warming and Arctic amplification, accelerated decomposition, and hence carbon release, the ground must be kept as cold as possible (Conant *et al.* 2011). The findings presented in the previous

chapters and indicated by others (Olofsson and Post 2018, Beer *et al.* 2020, Macias-Fauria *et al.* 2020, Tuomi *et al.* 2021) show that the process of keeping carbon in the ground in general is feasible if applying intensive grazing pressure to permafrost-affected soils.

5.3 Feasibility of utilising herbivory in the Arctic

The fact that previously named animal-induced effects on soil OM occur under artificially high grazing intensities and are therefore feasible only on local scale pushes any future approaches into the direction of grazing management, e.g. herding. This means that human action is required to apply these affects to locations in the Arctic.

Since preservative effects of animal grazing on permafrost and therefore permafrost-bound OM are indicated from the findings of chapter 2, this provides a valid argument for indigenous land users, who historically herded animals such as reindeer, to increase their stock sizes or even return to the herding practises at all (Fig. 5-2). Nowadays, society often hinders traditional lifestyles in favour of other interests such as forestry or mineral resource exploitation (Tuisku 2002, Berg *et al.* 2008, Persson *et al.* 2017).

In a similar way, society can revive or expand animal herding on seasonally frozen ground, while accounting for the vegetation changes described in chapters 2 and 3. Graminoid vegetation is more productive in regard to carbon fixation than tundra vegetation (Zimov *et al.* 2012). Here, the conflict with forestry interests might be even less of a problem, as potentially already harvested high-latitude forest areas could be used for herding, preventing the establishment of tundra and shrub vegetation (Olofsson *et al.* 2009), transforming such places into graminoid-dominated landscapes (chapters 2.6.1 and 3.6.2) with high productivity. However, it might be necessary to prepare such areas by e.g. removing tree stumps to make them favourable for migratory grazers like reindeer (Bezard *et al.* 2015).

However, when thinking about grazing as a solution to circumarctic permafrost thaw, we must consider the required animal numbers for such an impact. Zimov *et al.* (2012) calculated a required animal density of 10.5 t/km² herbivore biomass to transform tundra into steppe-like biomes (based on fossil findings from the Pleistocene). Considering a total Arctic tundra area of 5 070 000 km² (Zona *et al.* 2016), this results in a total of 53 235 000 t animal biomass required to reach the needed animal density for this transformation across the terrestrial Arctic. Following Zimov *et al.* (2012), this means that approximately 25.4 million bison, 38.1 million horses, 76.1 million reindeer, 1.3 million lions, 5.3 million wolves, 5.1 million mammoths or an equivalent of other large herbivores, and additionally 2.6 million tons of smaller herbivores are needed to create permafrost-stabilising ecosystem conditions throughout the Arctic tundra. If using only reindeer, the Arctic would need a total of 532 million animals. Compared to a recent global reindeer population of approximately 7 million animals (World Animal Foundation 2023), including wild and semi-domesticated reindeer (*Rangifer tarandus*; reindeer and caribou), these high numbers show that utilising herbivory for permafrost stabilisation is only feasible on

small and local scales, where such high animal densities could be reached under controlled conditions.

Finally, if domesticated or semi-domesticated animals increase in the Arctic, society could use this population as a share of global meat production (Fig. 5-2). While taking into account the lower carbon footprint of free-roaming animals, as a result of their varying and seasonally diverse diet (Hansen 2012), and cutting back at industrial cattle farming, meat availability on the global market could be kept at an equal level while reducing meat production's climate impact at the same time.

However, such implications are not part of the research presented in this thesis, and require additional research. However, we should explore this concept when considering the overall impact of intensifying herbivory in the Arctic.

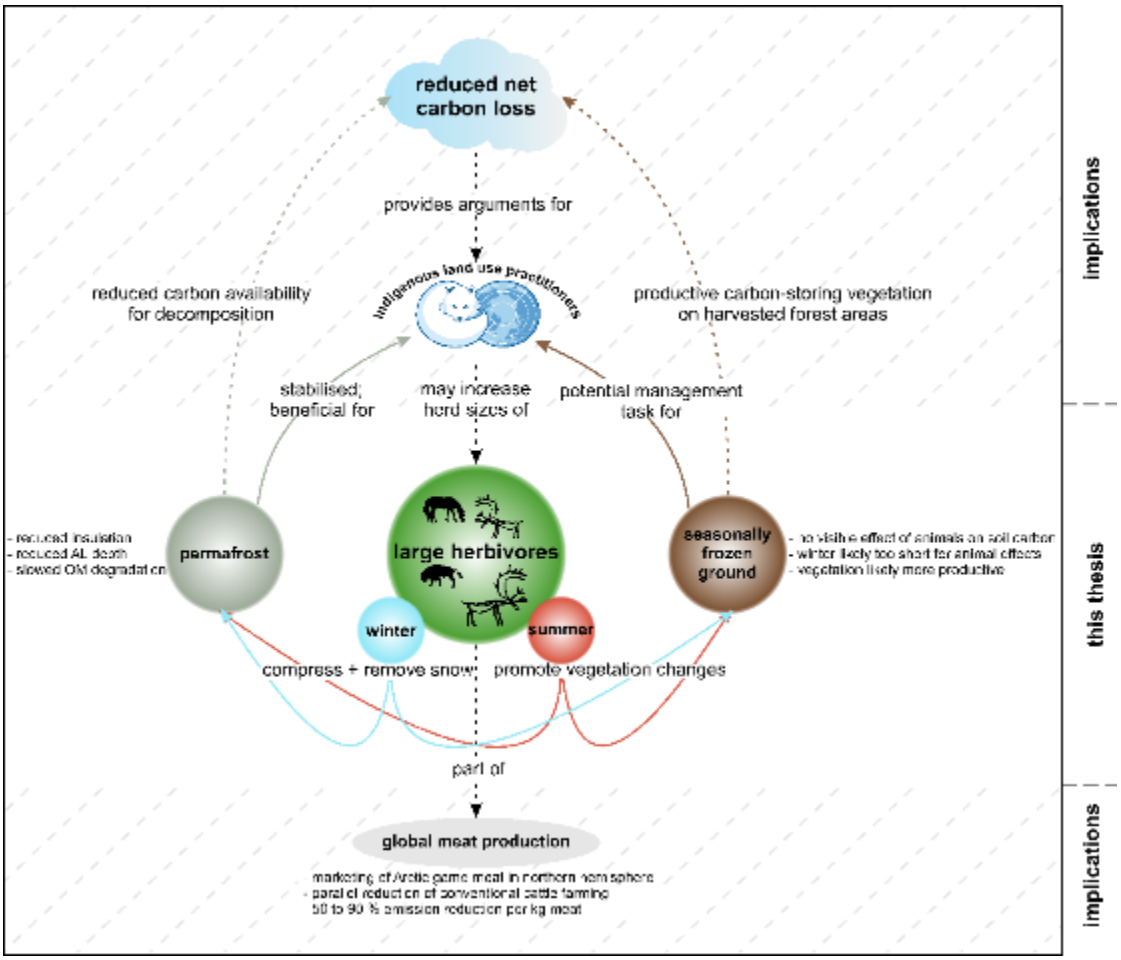

Figure 5-2 – Summarising graph for the key findings of this thesis (centre; white), potential implications for grazing and herding practices (top; grey-dashed) and speculative further implications (bottom; grey-dashed).

5.4 Research implications for successful planning and use of Arctic herbivory

In the face of global warming, it is imperative to take advantage of every available technique to mitigate carbon emissions. Preventing further and avoidable human-caused carbon emissions (Peñuelas and Carnicer 2010, IPCC 2021) or even stop them (Abbott *et al.* 2022) is

crucial to stop climate warming, but the active removal of CO_2 from the atmosphere is an important piece to mitigate the warming. One promising tool to achieve these goals is the management of Arctic large-mammal herbivory, as demonstrated in figure 5-2. However, in order to implement and monitor the efficiency of this approach, we need to address specific knowledge gaps through extensive experimental and monitoring sites across the Arctic (chapters 2.6.3 and 3.6.5). These sites would require exclosures that are repeatedly sampled and evaluated, permanent sensors for soil temperature and moisture, detailed assessments of vegetation community composition and status, detection of albedo changes, continuous gas flux measurements, areas with varying animal numbers and species composition, annual snow measurements, and a monitoring of at least decades, as illustrated in figure 5-3. While such experiments may affect local carbon inventories already (chapter 2.7), the findings could be extended to broader coverage in the future.

While time is running out to find and implement ways of carbon removal and long-term storage, I immediately advise setting up larger numbers of such experimental sites based on the findings in this thesis. With strong hints on the usefulness of large-herbivore grazing on permafrost stability and hence slowing down soil carbon loss (chapter 2), such experimental sites in the circumpolar terrestrial Arctic would double as research sites to test effectiveness, and permafrost stabilisation sites where at least some extent of OM decomposition reduction is already in place. At the same time, such sites provide the opportunity for future adjustments based on ongoing research to maximise emission reduction from Arctic ground.

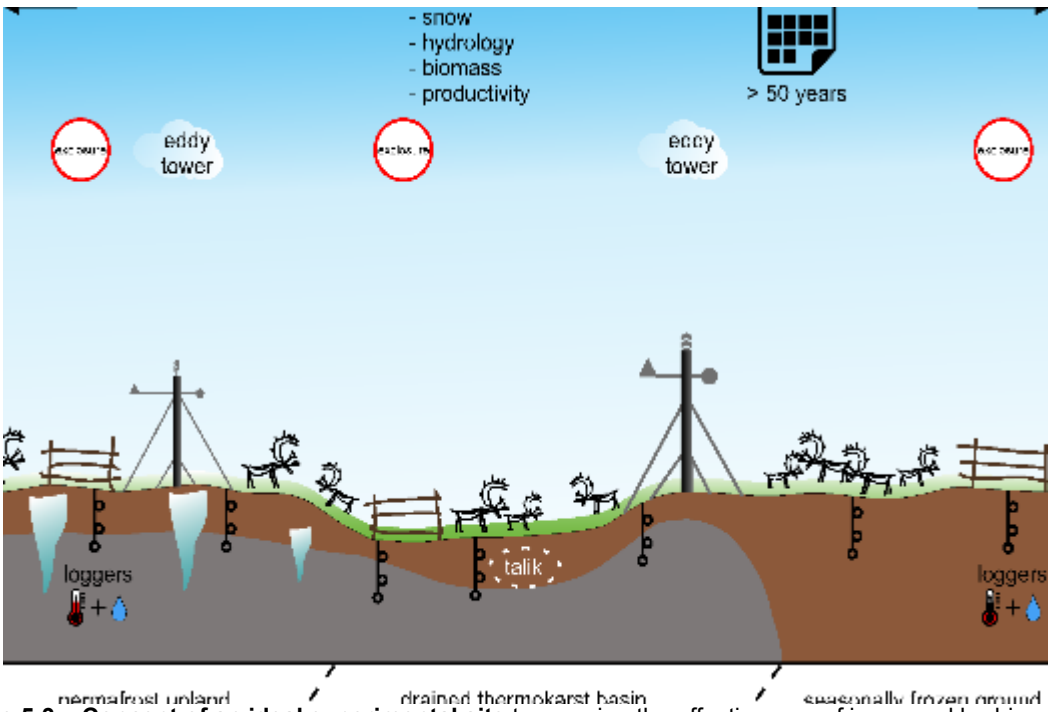

Figure 5-3 – Concept of an ideal experimental site to examine the effectiveness of increased herbivore numbers in the Arctic; this concept includes gas flux measurements, soil moisture and temperature measurements, snow measurements, albedo measurements, repeated biomass and vegetation assessments and the setup of exclosure sites; further different grazing intensities, different ground types representative across the Arctic and long project times are needed.

References

(including supplement references)

Abbott, B. W., Brown, M., Carey, J. C., Ernakovich, J., Frederick, J. M., Guo, L., Hugelius, G., Lee, R. M., Loranty, M. M., Macdonald, R., Mann, P. J., Natali, S. M., Olefeldt, D., Pearson, P., Rec, A., Robards, M., Salmon, V. G., Sayedi, S. S., Schädel, C., Schuur, E. A. G., Shakil, S., Shogren, A. J., Strauss, J., Tank, S. E., Thornton, B. F., Treharne, R., Turetsky, M., Voigt, C., Wright, N., Yang, Y., Zarnetske, J. P., Zhang, Q. & Zolkos, S. 2022. *We Must Stop Fossil Fuel Emissions to Protect Permafrost Ecosystems*. Frontiers in Environmental Science 10 doi:10.3389/fenvs.2022.889428.

Abramov, A., Davydov, S., Ivashchenko, A., Karelin, D., Kholodov, A., Kraev, G., Lupachev, A., Maslakov, A., Ostroumov, V., Rivkina, E., Shmelev, D., Sorokovikov, V., Tregubov, O., Veremeeva, A., Zamolodchikov, D. & Zimov, S. 2019. *Two decades of active layer thickness monitoring in northeastern Asia*. Polar Geography: 1-17, doi:10.1080/1088937X.2019.1648581.

Akayuli, C., Ofosu, B., Nyako, S. O. & Opuni, K. O. 2013. *The influence of observed clay content on shear strength and compressibility of residual sandy soils*. International Journal of Engineering Research and Applications 3 (4): 2538-2542.

Anderson, R. S., Sørensen, M. & Willetts, B. B. 1991. A review of recent progress in our understanding of aeolian sediment transport. In: Barndorff-Nielsen O.E., and Willetts, B.B. (ed.), *Aeolian Grain Transport 1,* Acta Mechanica Supplementum, Springer, Vienna, pp. 1-19 doi:10.1007/978-3-7091-6706-9_1.

Ashastina, K., Schirrmeister, L., Fuchs, M. & Kienast, F. 2017. *Palaeoclimate characteristics in interior Siberia of MIS 6–2: first insights from the Batagay permafrost mega-thaw slump in the Yana Highlands*. Clim. Past 13 (7): 795-818, doi:10.5194/cp-13-795-2017.

Ballantyne, A. P., Alden, C. B., Miller, J. B., Tans, P. P. & White, J. W. C. 2012. *Increase in observed net carbon dioxide uptake by land and oceans during the past 50 years*. Nature 488 (7409): 70-72, doi:10.1038/nature11299.

Barker, J. F. & Fritz, P. 1981. *Carbon isotope fractionation during microbial methane oxidation*. Nature 293 (5830): 289-291, doi:10.1038/293289a0.

Batey, T. 2009. *Soil compaction and soil management – a review*. Soil Use and Management 25 (4): 335-345, doi:10.1111/j.1475-2743.2009.00236.x.

Beer, C., Zimov, N., Olofsson, J., Porada, P. & Zimov, S. 2020. *Protection of Permafrost Soils from Thawing by Increasing Herbivore Density*. Scientific Reports 10 (1): 4170, doi:10.1038/s41598-020-60938-y.

Berg, A., Östlund, L., Moen, J. & Olofsson, J. 2008. *A century of logging and forestry in a reindeer herding area in northern Sweden*. Forest Ecology and Management 256 (5): 1009-1020, doi:10.1016/j.foreco.2008.06.003.

Berke, M. A., Cartagena Sierra, A., Bush, R., Cheah, D. & O'Connor, K. 2019. *Controls on leaf wax fractionation and δ2H values in tundra vascular plants from western Greenland*. Geochimica et Cosmochimica Acta 244: 565-583, doi:10.1016/j.gca.2018.10.020.

Bezard, P., Brilland, S. & Kumpula, J. 2015. *Composition of late summer diet by semi-domesticated reindeer in different grazing conditions in northernmost Finland*. Rangifer 35 (1): 39-52, doi:10.7557/2.35.1.2942.

Biester, H., Knorr, K. H., Schellekens, J., Basler, A. & Hermanns, Y. M. 2014. *Comparison of different methods to determine the degree of peat decomposition in peat bogs*. Biogeosciences 11 (10): 2691-2707, doi:10.5194/bg-11-2691-2014.

Biskaborn, B. K., Smith, S. L., Noetzli, J., Matthes, H., Vieira, G., Streletskiy, D. A., Schoeneich, P., Romanovsky, V. E., Lewkowicz, A. G., Abramov, A., Allard, M., Boike, J., Cable, W. L., Christiansen, H. H., Delaloye, R., Diekmann, B., Drozdov, D., Etzelmüller, B., Grosse, G., Guglielmin, M., Ingeman-Nielsen, T., Isaksen, K., Ishikawa, M., Johansson, M., Johannsson, H., Joo, A., Kaverin, D., Kholodov, A., Konstantinov, P., Kröger, T., Lambiel, C., Lanckman, J.-P., Luo, D., Malkova, G., Meiklejohn, I., Moskalenko, N., Oliva, M., Phillips, M., Ramos, M., Sannel, A. B. K., Sergeev, D., Seybold, C., Skryabin, P., Vasiliev, A., Wu, Q., Yoshikawa, K., Zheleznyak, M. & Lantuit, H. 2019. *Permafrost is warming at a global scale*. Nature Communications 10 (1): 264, doi:10.1038/s41467-018-08240-4.

Blaauw, M. & Christen, J. A. 2011. *Flexible paleoclimate age-depth models using an autoregressive gamma process*. Bayesian Anal. 6 (3): 457-474, doi:10.1214/11-BA618.

Blok, D., Heijmans, M. M. P. D., Schaepman-Strub, G., Kononov, A. V., Maximov, T. C. & Berendse, F. 2010. *Shrub expansion may reduce summer permafrost thaw in Siberian tundra*. Global Change Biology 16 (4): 1296-1305, doi:10.1111/j.1365-2486.2009.02110.x.

Blott, S. J. & Pye, K. 2001. *GRADISTAT: a grain size distribution and statistics package for the analysis of unconsolidated sediments*. Earth Surface Processes and Landforms 26 (11): 1237-1248, doi:10.1002/esp.261.

Bonanomi, G., Incerti, G., Giannino, F., Mingo, A., Lanzotti, V. & Mazzoleni, S. 2013. *Litter quality assessed by solid state 13C NMR spectroscopy predicts decay rate better than C/N and Lignin/N ratios*. Soil Biology and Biochemistry 56: 40-48, doi:10.1016/j.soilbio.2012.03.003.

Bosikov, N. 1998. *Wetness variability and dynamics of thermokarst processes in Central Yakutia*. In: *Proceedings of the 7th International Permafrost Conference,* pp. 71-74.

Bowen, J. C., Ward, C. P., Kling, G. W. & Cory, R. M. 2020. *Arctic Amplification of Global Warming Strengthened by Sunlight Oxidation of Permafrost Carbon to CO2*. Geophysical Research Letters 47 (12): e2020GL087085, doi:10.1029/2020GL087085.

Bradley-Cook, J. I. & Virginia, R. A. 2018. *Landscape variation in soil carbon stocks and respiration in an Arctic tundra ecosystem, west Greenland*. Arctic, Antarctic, and Alpine Research 50 (1): S100024, doi:10.1080/15230430.2017.1420283.

Bradley, H. & Stein, S. 2022. *Climate opportunism and values of change on the Arctic agricultural frontier*. Economic Anthropology 9 (2): 207-222, doi:10.1002/sea2.12251.

Bray, E. E. & Evans, E. D. 1961. *Distribution of n-paraffins as a clue to recognition of source beds*. Geochimica et Cosmochimica Acta 22 (1): 2-15, doi:10.1016/0016-7037(61)90069-2.

Butler, R. F. 1992. *Paleomagnetism: magnetic domains to geologic terranes*. Blackwell Scientific Publications Boston.

Chadburn, S. E., Burke, E. J., Cox, P. M., Friedlingstein, P., Hugelius, G. & Westermann, S. 2017. *An observation-based constraint on permafrost loss as a function of global warming*. Nature Climate Change 7 (5): 340-344, doi:10.1038/nclimate3262.

Chlachula, J. 2003. *The Siberian loess record and its significance for reconstruction of Pleistocene climate change in north-central Asia*. Quaternary Science Reviews 22 (18): 1879-1906, doi:10.1016/S0277-3791(03)00182-3.

Cole, J. J., Cole, J. J., Caraco, N. F. & Caraco, N. F. 2001. *Carbon in catchments: connecting terrestrial carbon losses with aquatic metabolism*. Marine and Freshwater Research 52 (1): 101-110, doi:10.1071/MF00084.

Conant, R. T., Ryan, M. G., Ågren, G. I., Birge, H. E., Davidson, E. A., Eliasson, P. E., Evans, S. E., Frey, S. D., Giardina, C. P., Hopkins, F. M., Hyvönen, R., Kirschbaum, M. U. F., Lavallee, J. M., Leifeld, J., Parton, W. J., Megan Steinweg, J., Wallenstein, M. D., Martin Wetterstedt, J. Å. & Bradford, M. A. 2011. *Temperature and soil organic matter decomposition rates – synthesis of current knowledge and a way forward*. Global Change Biology 17 (11): 3392-3404, doi:10.1111/j.1365-2486.2011.02496.x.

Copernicus Climate Change Service, European State of the Climate. 2020. *Surface temperature anomaly for 2020*. accessed 05.05.2023. https://climate.copernicus.eu/esotc/2020/arctic-temperatures.

Coplen, T. B., Brand, W. A., Gehre, M., Gröning, M., Meijer, H. A. J., Toman, B. & Verkouteren, R. M. 2006. *New Guidelines for δ13C Measurements*. Analytical Chemistry 78 (7): 2439-2441, doi:10.1021/ac052027c.

Corradi, C., Kolle, O., Walter, K., Zimov, S. A. & Schulze, E.-D. 2005. *Carbon dioxide and methane exchange of a north-east Siberian tussock tundra*. Global Change Biology 11 (11): 1910-1925, doi:10.1111/j.1365-2486.2005.01023.x.

Crate, S., Ulrich, M., Habeck, J. O., Desyatkin, A. R., Desyatkin, R. V., Fedorov, A. N., Hiyama, T., Iijima, Y., Ksenofontov, S., Mészáros, C. & Takakura, H. 2017. *Permafrost livelihoods: A transdisciplinary review and analysis of thermokarst-based systems of indigenous land use*. Anthropocene 18: 89-104, doi:10.1016/j.ancene.2017.06.001.

Crawley, M. 2015. *Statistics: An Introduction using R*. 2nd ed. Wiley.

Dearing, J. 1999. *Magnetic susceptibility*. Environmental magnetism: A practical guide 6: 35-62.

Diekmann, B., Pestryakova, L., Nazarova, L., Subetto, D., Tarasov, P. E., Stauch, G., Thiemann, A., Lehmkuhl, F., Biskaborn, B. & Kuhn, G. J. P. 2017. *Late Quaternary lake dynamics in the Verkhoyansk Mountains of Eastern Siberia: implications for climate and glaciation history*. Polarforschung 86 (2): 97-110, doi:10.2312/polarforschung.86.2.97.

Diochon, A. & Kellman, L. 2008. *Natural abundance measurements of 13C indicate increased deep soil carbon mineralization after forest disturbance*. Geophysical Research Letters 35 (14) doi:10.1029/2008GL034795.

Domine, F., Barrere, M. & Morin, S. 2016. *The growth of shrubs on high Arctic tundra at Bylot Island: impact on snow physical properties and permafrost thermal regime*. Biogeosciences 13 (23): 6471-6486, doi:10.5194/bg-13-6471-2016.

Falk, J. M., Schmidt, N. M., Christensen, T. R. & Ström, L. 2015. *Large herbivore grazing affects the vegetation structure and greenhouse gas balance in a high arctic mire*. Environmental Research Letters 10 (4) doi:10.1088/1748-9326/10/4/045001.

Fedorov, A. & Konstantinov, P. 2003a. *Observations of surface dynamics with thermokarst initiation, Yukechi site, Central Yakutia*. In: Phillips, Springman S.M. & Arenson L.U. (eds.), *Proceedings of the 8th International Conference on Permafrost, 21-25 July 2003, Zurich, Switzerland,* AA Balkema, Lisse, the Netherlands, pp. 239-243.

Fedorov, A. N. 2006. *Present post-disturbance dynamics of permafrost in Central Yakutia*. Symptom of Environmental Change in Siberian Permafrost Region: 225-231.

Fedorov, A. N. & Konstantinov, P. 2003b. *Observations of surface dynamics with thermokarst initiation, Yukechi site, Central Yakutia*. In: Phillips M., Springman S.M. & Arenson L.U. (eds.), *8th International Conference On Permafrost,* University of Zurich, Zurich, Switzerland.

Finnish Meteorological Institute. 2021. *Observation data (monthly observations) for station 102047 Inari Kaamanen, 2008-2020*. accessed 17.09.2021. https://en.ilmatieteenlaitos.fi/download-observations.

Finnish-Reindeer-Herders'-Association. 2022. *TOKAT data*.

Fischer, W., Thomas, C. K., Zimov, N. & Göckede, M. 2022. *Grazing enhances carbon cycling but reduces methane emission during peak growing season in the Siberian Pleistocene Park tundra site*. Biogeosciences 19 (6): 1611-1633, doi:10.5194/bg-19-1611-2022.

Forbes, B. C. 2006. *The challenges of modernity for reindeer management in northermost Europe*. Ecological Studies, Springer, Berlin, Heidelberg.

Forbes, B. C., Ebersole, J. J. & Strandberg, B. 2001. *Anthropogenic Disturbance and Patch Dynamics in Circumpolar Arctic Ecosystems*. Conservation Biology 15 (4): 954-969, doi:10.1046/j.1523-1739.2001.015004954.x.

French, H. & Shur, Y. 2010. *The principles of cryostratigraphy*. Earth-Science Reviews 101 (3): 190-206, doi:10.1016/j.earscirev.2010.04.002.

Friedlingstein, P., Jones, M. W., O'Sullivan, M., Andrew, R. M., Hauck, J., Peters, G. P., Peters, W., Pongratz, J., Sitch, S., Le Quéré, C., Bakker, D. C. E., Canadell, J. G., Ciais, P., Jackson, R. B., Anthoni, P., Barbero, L., Bastos, A., Bastrikov, V., Becker, M., Bopp, L., Buitenhuis, E., Chandra, N., Chevallier, F., Chini, L. P., Currie, K. I., Feely, R. A., Gehlen, M., Gilfillan, D., Gkritzalis, T., Goll, D. S., Gruber, N., Gutekunst, S., Harris, I., Haverd, V., Houghton, R. A., Hurtt, G., Ilyina, T., Jain, A. K., Joetzjer, E., Kaplan, J. O., Kato, E., Klein Goldewijk, K.,

Korsbakken, J. I., Landschützer, P., Lauvset, S. K., Lefèvre, N., Lenton, A., Lienert, S., Lombardozzi, D., Marland, G., McGuire, P. C., Melton, J. R., Metzl, N., Munro, D. R., Nabel, J. E. M. S., Nakaoka, S. I., Neill, C., Omar, A. M., Ono, T., Peregon, A., Pierrot, D., Poulter, B., Rehder, G., Resplandy, L., Robertson, E., Rödenbeck, C., Séférian, R., Schwinger, J., Smith, N., Tans, P. P., Tian, H., Tilbrook, B., Tubiello, F. N., van der Werf, G. R., Wiltshire, A. J. & Zaehle, S. 2019. *Global Carbon Budget 2019*. Earth Syst. Sci. Data 11 (4): 1783-1838, doi:10.5194/essd-11-1783-2019.

Frost, G. V., Epstein, H. E., Walker, D. A., Matyshak, G. & Ermokhina, K. 2013. *Patterned-ground facilitates shrub expansion in Low Arctic tundra*. Environmental Research Letters 8 (1): 015035, doi:10.1088/1748-9326/8/1/015035.

Fuchs, M., Bolshiyanov, D., Grigoriev, M. N., Morgenstern, A., Pestryakova, L., Tsibizov, L. & Dill, A. 2021. *Russian-German Cooperation: Expeditions to Siberia in 2019*. Alfred Wegener Institute for Polar and Marine Research, Bremerhaven, available at https://epic.awi.de/id/eprint/53575/.

Gamarra, B. & Kahmen, A. 2015. *Concentrations and δ2H values of cuticular n-alkanes vary significantly among plant organs, species and habitats in grasses from an alpine and a temperate European grassland*. Oecologia 178 (4): 981-998, doi:10.1007/s00442-015-3278-6.

Gao, Q., Schwartz, M. W., Zhu, W., Wan, Y., Qin, X., Ma, X., Liu, S., Williamson, M. A., Peters, C. B. & Li, Y. 2016. *Changes in Global Grassland Productivity during 1982 to 2011 Attributable to Climatic Factors*. Remote Sensing 8 (5) doi:10.3390/rs8050384.

Genet, H., McGuire, A. D., Barrett, K., Breen, A., Euskirchen, E. S., Johnstone, J. F., Kasischke, E. S., Melvin, A. M., Bennett, A., Mack, M. C., Rupp, T. S., Schuur, E. A. G., Turetsky, M. R. & Yuan, F. 2013. *Modeling the effects of fire severity and climate warming on active layer thickness and soil carbon storage of black spruce forests across the landscape in interior Alaska*. Environmental Research Letters 8 (4): 045016, doi:10.1088/1748-9326/8/4/045016.

Gisnås, K., Etzelmüller, B., Lussana, C., Hjort, J., Sannel, A. B. K., Isaksen, K., Westermann, S., Kuhry, P., Christiansen, H. H., Frampton, A. & Åkerman, J. 2017. *Permafrost Map for Norway, Sweden and Finland*. Permafrost and Periglacial Processes 28 (2): 359-378, doi:10.1002/ppp.1922.

Glombitza, C., Mangelsdorf, K. & Horsfield, B. 2009. *Maturation related changes in the distribution of ester bound fatty acids and alcohols in a coal series from the New Zealand Coal Band covering diagenetic to catagenetic coalification levels*. Organic geochemistry 40 (10): 1063-1073, doi:10.1016/j.orggeochem.2009.07.008.

Göckede, M., Kwon, M. J., Kittler, F., Heimann, M., Zimov, N. & Zimov, S. 2019. *Negative feedback processes following drainage slow down permafrost degradation*. Global Change Biology 25 (10): 3254-3266, doi:10.1111/gcb.14744.

Göckede, M., Kittler, F., Kwon, M. J., Burjack, I., Heimann, M., Kolle, O., Zimov, N. & Zimov, S. 2017. *Shifted energy fluxes, increased Bowen ratios, and reduced thaw depths linked with drainage-induced changes in permafrost ecosystem structure*. The Cryosphere 11 (6): 2975-2996, doi:10.5194/tc-11-2975-2017.

Golubtsov, V. A., Vanteeva, Y. V., Voropai, N. N., Vasilenko, O. V., Cherkashina, A. A. & Zazovskaya, E. P. 2022. *Stable Carbon Isotopic Composition (δ13C) as a Proxy of Organic Matter Dynamics in Soils on the Western Shore of Lake Baikal*. Eurasian Soil Science 55 (12): 1700-1713, doi:10.1134/S1064229322700041.

Grellmann, D. 2002. *Plant responses to fertilization and exclusion of grazers on an arctic tundra heath*. Oikos 98 (2): 190-204, doi:10.1034/j.1600-0706.2002.980202.x.

Grosse, G., Jones, B. & Arp, C. 2013. 8.21 Thermokarst Lakes, Drainage, and Drained Basins. In: Shroder J.F. (ed.), *Treatise on Geomorphology,* Academic Press, San Diego, pp. 325-353 doi:10.1016/B978-0-12-374739-6.00216-5.

Grosse, G., Harden, J., Turetsky, M., McGuire, A. D., Camill, P., Tarnocai, C., Frolking, S., Schuur, E. A. G., Jorgenson, T., Marchenko, S., Romanovsky, V., Wickland, K. P., French, N., Waldrop, M., Bourgeau-Chavez, L. & Striegl, R. G. 2011. *Vulnerability of high-latitude soil organic carbon in North America to disturbance*. Journal of Geophysical Research: Biogeosciences 116 (G4) doi:10.1029/2010JG001507.

Halcomb, S. & Sjostedt, S. 2019. Surcharge Embankment on Marine Clayey Silt Case Study and Lessons Learned. In: *Geo-Congress 2019,* pp. 119-130 doi:10.1061/9780784482070.012.

Hansen, K. K. 2012. *Methane emissions from reindeer.* Master thesis, Faculty of Biosciences, Fisheries and Economics, Department of Arctic and Marine Biology, University of Tromsø, Tromsø, Norway.

Harden, J. W., Manies, K. L., Turetsky, M. R. & Neff, J. C. 2006. *Effects of wildfire and permafrost on soil organic matter and soil climate in interior Alaska*. Global Change Biology 12 (12): 2391-2403, doi:10.1111/j.1365-2486.2006.01255.x.

Horita, J., Ueda, A., Mizukami, K. & Takatori, I. 1989. *Automatic δD and δ18O analyses of multi-water samples using H2- and CO2-water equilibration methods with a common equilibration set-up*. International Journal of Radiation Applications and Instrumentation. Part A. Applied Radiation and Isotopes 40 (9): 801-805, doi:10.1016/0883-2889(89)90100-7.

Huang, X., Xue, J., Zhang, J., Qin, Y., Meyers, P. A. & Wang, H. 2012. *Effect of different wetness conditions on Sphagnum lipid composition in the Erxianyan peatland, central China*. Organic geochemistry 44: 1-7, doi:10.1016/j.orggeochem.2011.12.005.

Hugelius, G., Loisel, J., Chadburn, S., Jackson, R. B., Jones, M., MacDonald, G., Marushchak, M., Olefeldt, D., Packalen, M., Siewert, M. B., Treat, C., Turetsky, M., Voigt, C. & Yu, Z. 2020. *Large stocks of peatland carbon and nitrogen are vulnerable to permafrost thaw*. PNAS 117 (34): 20438-20446, doi:10.1073/pnas.1916387117.

Hugelius, G., Strauss, J., Zubrzycki, S., Harden, J. W., Schuur, E. a. G., Ping, C. L., Schirrmeister, L., Grosse, G., Michaelson, G. J., Koven, C. D., O'Donnell, J. A., Elberling, B., Mishra, U., Camill, P., Yu, Z., Palmtag, J. & Kuhry, P. 2014. *Estimated stocks of circumpolar permafrost carbon with quantified uncertainty ranges and identified data gaps*. Biogeosciences 11 (23) doi:10.5194/bg-11-6573-2014.

Huh, Y., Tsoi, M.-Y., Zaitsev, A. & Edmond, J. M. 1998. *The fluvial geochemistry of the rivers of Eastern Siberia: I. tributaries of the Lena River draining the sedimentary platform of the Siberian Craton*. Geochimica et Cosmochimica Acta 62 (10): 1657-1676, doi:10.1016/S0016-7037(98)00107-0.

IPCC. 2019. *Summary for Policymakers*. IPCC Special Report on the Ocean and Cryosphere in a Changing Climate [H.-O. Pörtner, D.C. Roberts, V. Masson-Delmotte, P. Zhai, M. Tignor, E. Poloczanska, K. Mintenbeck, M. Nicolai, A. Okem, J. Petzold, B. Rama, N. Weyer (eds.)], In press, available.

IPCC. 2021. *Climate Change 2021: The Physical Science Basis. Contribution of Working Group I to the Sixth Assessment Report of the Intergovernmental Panel on Climate Change*. IPCC, Cambridge University Press, available.

Jackson, R. B., Lajtha, K., Crow, S. E., Hugelius, G., Kramer, M. G. & Piñeiro, G. 2017. *The Ecology of Soil Carbon: Pools, Vulnerabilities, and Biotic and Abiotic Controls*. Annual Review of Ecology, Evolution, and Systematics 48 (1): 419-445, doi:10.1146/annurev-ecolsys-112414-054234.

Johansson, M., Callaghan, T. V., Bosiö, J., Åkerman, H. J., Jackowicz-Korczynski, M. & Christensen, T. R. 2013. *Rapid responses of permafrost and vegetation to experimentally increased snow cover in sub-arctic Sweden*. Environmental Research Letters 8 (3): 035025.

Jones, B. M., Grosse, G., Arp, C. D., Miller, E., Liu, L., Hayes, D. J. & Larsen, C. F. 2015. *Recent Arctic tundra fire initiates widespread thermokarst development*. Scientific Reports 5 (1): 15865, doi:10.1038/srep15865.

Jones, M. C., Grosse, G., Jones, B. M. & Walter Anthony, K. 2012. *Peat accumulation in drained thermokarst lake basins in continuous, ice-rich permafrost, northern Seward Peninsula, Alaska*. Journal of Geophysical Research: Biogeosciences 117 (G2) doi:10.1029/2011JG001766.

Jongejans, L. L. & Strauss, J. 2020. *Bootstrapping approach for permafrost organic carbon pool estimation*. Zenodo doi:10.5281/zenodo.3734247.

Jongejans, L. L., Strauss, J., Lenz, J., Peterse, F., Mangelsdorf, K., Fuchs, M. & Grosse, G. 2018. *Organic matter characteristics in yedoma and thermokarst deposits on Baldwin Peninsula, west Alaska*. Biogeosciences 15 (20): 6033-6048, doi:10.5194/bg-15-6033-2018.

Jongejans, L. L., Liebner, S., Knoblauch, C., Mangelsdorf, K., Ulrich, M., Grosse, G., Tanski, G., Fedorov, A. N., Konstantinov, P. Y., Windirsch, T., Wiedmann, J. & Strauss, J. 2021. *Greenhouse gas production and lipid biomarker distribution in Yedoma and Alas thermokarst lake sediments in Eastern Siberia*. Global Change Biology 27 (12): 2822-2839, doi:10.1111/gcb.15566.

Kaiser, C., Meyer, H., Biasi, C., Rusalimova, O., Barsukov, P. & Richter, A. 2007. *Conservation of soil organic matter through cryoturbation in arctic soils in Siberia*. Journal of Geophysical Research: Biogeosciences 112 (G2) doi:10.1029/2006JG000258.

Kaplan, J. O., Krumhardt, K. M., Ellis, E. C., Ruddiman, W. F., Lemmen, C. & Goldewijk, K. K. 2010. *Holocene carbon emissions as a result of anthropogenic land cover change*. The Holocene 21 (5): 775-791, doi:10.1177/0959683610386983.

Katasonov, E. M. 1975. *Frozen-ground and facial analysis of Pleistocene deposits and paleogeography of Central Yakutia*. Biuletyn Peryglacjalny 24: 33-40.

Katasonov, E. M. & Ivanov, M. S. 1973. Cryolothology of central Yakutia (excursion on the Lena and Aldan Rivers). In: *Guidebook, Second International Conference on Permafrost,* U.S.S.R. Academy of Sciences, Yakutsk,

Keuper, F., van Bodegom, P. M., Dorrepaal, E., Weedon, J. T., van Hal, J., van Logtestijn, R. S. P. & Aerts, R. 2012. *A frozen feast: thawing permafrost increases plant-available nitrogen in subarctic peatlands*. Global Change Biology 18 (6): 1998-2007, doi:https://doi.org/10.1111/j.1365-2486.2012.02663.x.

Köster, K., Berninger, F., Köster, E. & Pumpanen, J. 2015. *Influences of Reindeer Grazing on Above- and Belowground Biomass and Soil Carbon Dynamics*. Arctic, Antarctic, and Alpine Research 47 (3): 495-503, doi:10.1657/AAAR0014-062.

Kristensen, J. A., Svenning, J.-C., Georgiou, K. & Malhi, Y. 2022. *Can large herbivores enhance ecosystem carbon persistence?* Trends in Ecology & Evolution 37 (2): 117-128, doi:10.1016/j.tree.2021.09.006.

Kropp, H., Loranty, M. M., Natali, S. M., Kholodov, A. L., Rocha, A. V., Myers-Smith, I., Abbot, B. W., Abermann, J., Blanc-Betes, E., Blok, D., Blume-Werry, G., Boike, J., Breen, A. L., Cahoon, S. M. P., Christiansen, C. T., Douglas, T. A., Epstein, H. E., Frost, G. V., Goeckede, M., Høye, T. T., Mamet, S. D., O'Donnell, J. A., Olefeldt, D., Phoenix, G. K., Salmon, V. G., Sannel, A. B. K., Smith, S. L., Sonnentag, O., Vaughn, L. S., Williams, M., Elberling, B., Gough, L., Hjort, J., Lafleur, P. M., Euskirchen, E. S., Heijmans, M. M. P. D., Humphreys, E. R., Iwata, H., Jones, B. M., Jorgenson, M. T., Grünberg, I., Kim, Y., Laundre, J., Mauritz, M., Michelsen, A., Schaepman-Strub, G., Tape, K. D., Ueyama, M., Lee, B.-Y., Langley, K. & Lund, M. 2020. *Shallow soils are warmer under trees and tall shrubs across Arctic and Boreal ecosystems*. Environmental Research Letters 16 (1): 015001, doi:10.1088/1748-9326/abc994.

Kuhry, P., Bárta, J., Blok, D., Elberling, B., Faucherre, S., Hugelius, G., Jørgensen, C. J., Richter, A., Šantrůčková, H. & Weiss, N. 2020. *Lability classification of soil organic matter in the northern permafrost region*. Biogeosciences 17 (2) doi:10.5194/bg-17-361-2020.

Kuznetsova, L. V., Zakharova, V. I., Sosina, N. K., Nikolin, E. G., Ivanova, E. I., Sofronova, E. V., Poryadina, L. N., Mikhalyova, L. G., Vasilyeva, I. I., Remigailo, P. A., Gabyshev, V. A., Ivanova, A. P. & Kopyrina, L. I. 2010. Flora of Yakutia: Composition and Ecological Structure. In: Troeva E.I., Isaev A.P., Cherosov M.M. & Karpov N.S. (eds.), *The Far North: Plant Biodiversity and Ecology of Yakutia,* Springer Netherlands, Dordrecht, pp. 24-140 doi:10.1007/978-90-481-3774-9_2.

Lal, R. 2022. Biophysical Controls That Make Erosion-Transported Soil Carbon a Source of Greenhouse Gases. *Applied Sciences* 12, 16, 10.3390/app12168372.

Macias-Fauria, M., Jepson, P., Zimov, N. & Malhi, Y. 2020. *Pleistocene Arctic megafaunal ecological engineering as a natural climate solution?* Philosophical Transactions of the Royal Society B: Biological Sciences 375 (1794): 20190122, doi:10.1098/rstb.2019.0122.

Magnússon, R. Í., Hamm, A., Karsanaev, S. V., Limpens, J., Kleijn, D., Frampton, A., Maximov, T. C. & Heijmans, M. M. P. D. 2022. *Extremely wet summer events enhance permafrost thaw for multiple years in Siberian tundra*. Nature Communications 13 (1): 1556, doi:10.1038/s41467-022-29248-x.

Maliniemi, T., Kapfer, J., Saccone, P., Skog, A. & Virtanen, R. 2018. *Long-term vegetation changes of treeless heath communities in northern Fennoscandia: Links to climate change trends and reindeer grazing*. Journal of Vegetation Science 29 (3): 469-479, doi:10.1111/jvs.12630.

Malone, E. T., Abbott, B. W., Klaar, M. J., Kidd, C., Sebilo, M., Milner, A. M. & Pinay, G. 2018. *Decline in Ecosystem δ13C and Mid-Successional Nitrogen Loss in a Two-Century Postglacial Chronosequence*. Ecosystems 21 (8): 1659-1675, doi:10.1007/s10021-018-0245-1.

Martin, A. C., Jeffers, E. S., Petrokofsky, G., Myers-Smith, I. & Macias-Fauria, M. 2017. *Shrub growth and expansion in the Arctic tundra: an assessment of controlling factors using an evidence-based approach*. Environmental Research Letters 12 (8): 085007, doi:10.1088/1748-9326/aa7989.

Marzi, R., Torkelson, B. E. & Olson, R. K. 1993. *A revised carbon preference index*. Organic geochemistry 20 (8): 1303-1306, doi:10.1016/0146-6380(93)90016-5.

Mekonnen, Z. A., Riley, W. J., Berner, L. T., Bouskill, N. J., Torn, M. S., Iwahana, G., Breen, A. L., Myers-Smith, I. H., Criado, M. G., Liu, Y., Euskirchen, E. S., Goetz, S. J., Mack, M. C. & Grant, R. F. 2021. *Arctic tundra shrubification: a review of mechanisms and impacts on ecosystem carbon balance*. Environmental Research Letters 16 (5): 053001, doi:10.1088/1748-9326/abf28b.

Meyer, H., Schönicke, L., Wand, U., Hubberten, H. W. & Friedrichsen, H. 2000. *Isotope studies of hydrogen and oxygen in ground ice-experiences with the equilibration technique*. Isotopes in Environmental and Health Studies (36): 133-149, doi:10.1080/10256010008032939.

Meyer, H., Schirrmeister, L., Andreev, A., Wagner, D., Hubberten, H.-W., Yoshikawa, K., Bobrov, A., Wetterich, S., Opel, T., Kandiano, E. & Brown, J. 2010. *Lateglacial and Holocene isotopic and environmental history of northern coastal Alaska – Results from a buried ice-wedge system at Barrow*. Quaternary Science Reviews 29 (27): 3720-3735, doi:10.1016/j.quascirev.2010.08.005.

Meyers, P. A. 1997. *Organic geochemical proxies of paleoceanographic, paleolimnologic, and paleoclimatic processes*. Organic geochemistry 27 (5-6): 213-250, doi:10.1016/S0146-6380(97)00049-1.

Mishra, U., Hugelius, G., Shelef, E., Yang, Y., Strauss, J., Lupachev, A., Harden, J. W., Jastrow, J. D., Ping, C.-L., Riley, W. J., Schuur, E. A. G., Matamala, R., Siewert, M., Nave, L. E., Koven, C. D., Fuchs, M., Palmtag, J., Kuhry, P., Treat, C. C., Zubrzycki, S., Hoffman, F. M., Elberling, B., Camill, P., Veremeeva, A. & Orr, A. 2021. *Spatial heterogeneity and environmental predictors of permafrost region soil organic carbon stocks*. Science Advances 7 (9): eaaz5236, doi:10.1126/sciadv.aaz5236.

Mod, H. K. & Luoto, M. 2016. *Arctic shrubification mediates the impacts of warming climate on changes to tundra vegetation*. Environmental Research Letters 11 (12): 124028, doi:10.1088/1748-9326/11/12/124028.

Mollenhauer, G., Grotheer, H., Gentz, T., Bonk, E. & Hefter, J. 2021. *Standard operation procedures and performance of the MICADAS radiocarbon laboratory at Alfred Wegener Institute (AWI), Germany*. Nuclear Instruments and Methods in Physics Research Section B: Beam Interactions with Materials and Atoms 496: 45-51, doi:10.1016/j.nimb.2021.03.016.

Monhonval, A., Mauclet, E., Pereira, B., Vandeuren, A., Strauss, J., Grosse, G., Schirrmeister, L., Fuchs, M., Kuhry, P. & Opfergelt, S. 2021. *Mineral Element Stocks in the Yedoma Domain: A Novel Method Applied to Ice-Rich Permafrost Regions*. Frontiers in Earth Science 9 doi:10.3389/feart.2021.703304.

Monteath, A. J., Gaglioti, B. V., Edwards, M. E. & Froese, D. 2021. *Late Pleistocene shrub expansion preceded megafauna turnover and extinctions in eastern Beringia*. Proceedings of the National Academy of Sciences 118 (52): e2107977118, doi:10.1073/pnas.2107977118.

Morgenstern, A., Grosse, G., Günther, F., Fedorova, I. & Schirrmeister, L. 2011. *Spatial analyses of thermokarst lakes and basins in Yedoma landscapes of the Lena Delta*. The Cryosphere Discussions 5: 1495-1545, doi:10.5194/tcd-5-1495-2011.

Mudge, P. L., Wallace, D. F., Rutledge, S., Campbell, D. I., Schipper, L. A. & Hosking, C. L. 2011. *Carbon balance of an intensively grazed temperate pasture in two climatically contrasting years*. Agriculture, Ecosystems & Environment 144 (1): 271-280, doi:10.1016/j.agee.2011.09.003.

Mueller, C. W., Rethemeyer, J., Kao-Kniffin, J., Löppmann, S., Hinkel, K. M. & G. Bockheim, J. 2015. *Large amounts of labile organic carbon in permafrost soils of northern Alaska*. Global Change Biology 21 (7): 2804-2817, doi:10.1111/gcb.12876.

Murchie, T. J., Monteath, A. J., Mahony, M. E., Long, G. S., Cocker, S., Sadoway, T., Karpinski, E., Zazula, G., MacPhee, R. D. E., Froese, D. & Poinar, H. N. 2021. *Collapse of the mammoth-steppe in central Yukon as revealed by ancient environmental DNA*. Nature Communications 12 (1): 7120, doi:10.1038/s41467-021-27439-6.

Murton, J. B., Edwards, M. E., Lozhkin, A. V., Anderson, P. M., Savvinov, G. N., Bakulina, N., Bondarenko, O. V., Cherepanova, M. V., Danilov, P. P., Boeskorov, V., Goslar, T., Grigoriev, S., Gubin, S. V., Korzun, J. A., Lupachev, A. V., Tikhonov, A., Tsygankova, V. I., Vasilieva, G. V. & Zanina, O. G. 2017. *Preliminary paleoenvironmental analysis of permafrost deposits at Batagaika megaslump, Yana Uplands, northeast Siberia*. Quaternary Research 87 (2): 314-330, doi:10.1017/qua.2016.15.

Myers-Smith, I. H., Forbes, B. C., Wilmking, M., Hallinger, M., Lantz, T., Blok, D., Tape, K. D., Macias-Fauria, M., Sass-Klaassen, U., Lévesque, E., Boudreau, S., Ropars, P., Hermanutz, L., Trant, A., Collier, L. S., Weijers, S., Rozema, J., Rayback, S. A., Schmidt, N. M., Schaepman-Strub, G., Wipf, S., Rixen, C., Ménard, C. B., Venn, S.,

Goetz, S., Andreu-Hayles, L., Elmendorf, S., Ravolainen, V., Welker, J., Grogan, P., Epstein, H. E. & Hik, D. S. 2011. *Shrub expansion in tundra ecosystems: dynamics, impacts and research priorities*. Environmental Research Letters 6 (4): 045509, doi:10.1088/1748-9326/6/4/045509.

Nazarova, L., Lüpfert, H., Subetto, D., Pestryakova, L. & Diekmann, B. 2013. *Holocene climate conditions in central Yakutia (Eastern Siberia) inferred from sediment composition and fossil chironomids of Lake Temje*. Quaternary International 290-291: 264-274, doi:10.1016/j.quaint.2012.11.006.

Nitzbon, J., Westermann, S., Langer, M., Martin, L., Strauss, J., Laboor, S. & Boike, J. 2020. *Fast response of cold ice-rich permafrost in northeast SIberia to a warming climate*. Nature Communications 11 (2201) doi:10.1038/s41467-020-15725-8.

Nitze, I., Grosse, G., Jones, B. M., Romanovsky, V. E. & Boike, J. 2018. *Remote sensing quantifies widespread abundance of permafrost region disturbances across the Arctic and Subarctic*. Nature Communications 9 (1): 1-11, doi:10.1038/s41467-018-07663-3.

Obu, J., Westermann, S., Bartsch, A., Berdnikov, N., Christiansen, H. H., Dashtseren, A., Delaloye, R., Elberling, B., Etzelmüller, B., Kholodov, A., Khomutov, A., Kääb, A., Leibman, M. O., Lewkowicz, A. G., Panda, S. K., Romanovsky, V., Way, R. G., Westergaard-Nielsen, A., Wu, T., Yamkhin, J. & Zou, D. 2019. *Northern Hemisphere permafrost map based on TTOP modelling for 2000–2016 at 1 km2 scale*. Earth-Science Reviews 193: 299-316, doi:10.1016/j.earscirev.2019.04.023.

Oksanen, L. & Virtanen, R. 1995. Topographic, altitudinal and regional patterns in continental and suboceanic heath vegetation of northern Fennoscandia. In: *Acta Botanica Fennica,* Finnish Zoological and Botanical Publishing Board, Helsinki, pp. 1-80

Olofsson, J. 2006. *Short- and long-term effects of changes in reindeer grazing pressure on tundra heath vegetation*. Journal of Ecology 94 (2): 431-440, doi:10.1111/j.1365-2745.2006.01100.x.

Olofsson, J. & Post, E. 2018. *Effects of large herbivores on tundra vegetation in a changing climate, and implications for rewilding*. Philosophical Transactions of the Royal Society B: Biological Sciences 373 (1761): 20170437, doi:10.1098/rstb.2017.0437.

Olofsson, J., Stark, S. & Oksanen, L. 2004. *Reindeer influence on ecosystem processes in the tundra*. Oikos 105 (2): 386-396, doi:10.1111/j.0030-1299.2004.13048.x.

Olofsson, J., Oksanen, L., Callaghan, T., Hulme, P. E., Oksanen, T. & Suominen, O. 2009. *Herbivores inhibit climate-driven shrub expansion on the tundra*. Global Change Biology 15 (11): 2681-2693, doi:10.1111/j.1365-2486.2009.01935.x.

Opel, T., Meyer, H., Wetterich, S., Laepple, T., Dereviagin, A. & Murton, J. 2018. *Ice wedges as archives of winter paleoclimate: A review*. Permafrost and Periglacial Processes 29 (3): 199-209, doi:10.1002/ppp.1980.

Opel, T., Murton, J. B., Wetterich, S., Meyer, H., Ashastina, K., Günther, F., Grotheer, H., Mollenhauer, G., Danilov, P. P. & Boeskorov, V. 2019. *Past climate and continentality inferred from ice wedges at Batagay megaslump in the Northern Hemisphere's most continental region, Yana Highlands, interior Yakutia*. Climate of the Past 15 (4): 1443-1461, doi:10.5194/cp-15-1443-2019.

Palmtag, J., Hugelius, G., Lashchinskiy, N., Tamstorf, M. P., Richter, A., Elberling, B. & Kuhry, P. 2015. *Storage, Landscape Distribution, and Burial History of Soil Organic Matter in Contrasting Areas of Continuous Permafrost*. Arctic, Antarctic, and Alpine Research 47 (1): 71-88, doi:10.1657/AAAR0014-027.

Palmtag, J., Obu, J., Kuhry, P., Richter, A., Siewert, M. B., Weiss, N., Westermann, S. & Hugelius, G. 2022. *A high spatial resolution soil carbon and nitrogen dataset for the northern permafrost region based on circumpolar land cover upscaling*. Earth Syst. Sci. Data 14 (9): 4095-4110, doi:10.5194/essd-14-4095-2022.

Paoli, A., Weladji, R. B., Holand, Ø. & Kumpula, J. 2018. *Winter and spring climatic conditions influence timing and synchrony of calving in reindeer*. PLOS ONE 13 (4): e0195603, doi:10.1371/journal.pone.0195603.

Papina, T., Malygina, N., Eirikh, A., Galanin, A. & Zheleznyak, M. 2017. *Isotopic composition and sources of atmospheric precipitation in Central Yakutia*. Earth's Cryosphere 21 (2): 52-61, doi:10.21782/EC2541-9994-2017-1(52-61).

Park, H., Fedorov, A. N., Zheleznyak, M. N., Konstantinov, P. Y. & Walsh, J. E. 2015. *Effect of snow cover on pan-Arctic permafrost thermal regimes*. Climate Dynamics 44 (9): 2873-2895, doi:10.1007/s00382-014-2356-5.

Parker, T. C., Thurston, A. M., Raundrup, K., Subke, J.-A., Wookey, P. A. & Hartley, I. P. 2021. *Shrub expansion in the Arctic may induce large-scale carbon losses due to changes in plant-soil interactions*. Plant and Soil 463 (1): 643-651, doi:10.1007/s11104-021-04919-8.

Pattison, R. R. & Welker, J. M. 2014. *Differential ecophysiological response of deciduous shrubs and a graminoid to long-term experimental snow reductions and additions in moist acidic tundra, Northern Alaska*. Oecologia 174 (2): 339-350, doi:10.1007/s00442-013-2777-6.

Pearson, R. G., Phillips, S. J., Loranty, M. M., Beck, P. S. A., Damoulas, T., Knight, S. J. & Goetz, S. J. 2013. *Shifts in Arctic vegetation and associated feedbacks under climate change*. Nature Climate Change 3: 673, doi:10.1038/nclimate1858.

Peñuelas, J. & Carnicer, J. 2010. *Climate Change and Peak Oil: The Urgent Need for a Transition to a Non-Carbon-Emitting Society*. Ambio 39 (1): 85-90, doi:10.1007/s13280-009-0011-x.

Peplau, T., Schroeder, J., Gregorich, E. & Poeplau, C. 2022. *Subarctic soil carbon losses after deforestation for agriculture depend on permafrost abundance*. Global Change Biology 28 (17): 5227-5242, doi:10.1111/gcb.16307.

Persson, S., Harnesk, D. & Islar, M. 2017. *What local people? Examining the Gállok mining conflict and the rights of the Sámi population in terms of justice and power*. Geoforum 86: 20-29, doi:10.1016/j.geoforum.2017.08.009.

Péwé, T. L. & Journaux, A. 1983. *Origin and character of loesslike silt in unglaciated south-central Yakutia, Siberia, USSR*. Professional Paper, USGPO, available.

Péwé, T. L., Journaux, A. & Stuckenrath, R. 1977. *Radiocarbon Dates and Late-Quaternary Stratigraphy from Mamontova Gora, Unglaciated Central Yakutia, Siberia, U.S.S.R*. Quaternary Research 8 (1): 51-63, doi:10.1016/0033-5894(77)90056-4.

Phillips, C. A. & Wurzburger, N. 2019. *Elevated rates of heterotrophic respiration in shrub-conditioned arctic tundra soils*. Pedobiologia 72: 8-15, doi:10.1016/j.pedobi.2018.11.002.

Planet. 2017. *Planet Application Program Interface: In Space for Life on Earth*. San Francisco, CA.

Popp, S., Diekmann, B., Meyer, H., Siegert, C., Syromyatnikov, I. & Hubberten, H.-W. 2006. *Palaeoclimate signals as inferred from stable-isotope composition of ground ice in the Verkhoyansk foreland, Central Yakutia*. Permafrost and Periglacial Processes 17 (2): 119-132, doi:10.1002/ppp.556.

Porada, P., Ekici, A. & Beer, C. 2016. *Effects of bryophyte and lichen cover on permafrost soil temperature at large scale*. The Cryosphere 10 (5): 2291-2315, doi:10.5194/tc-10-2291-2016.

Poynter, J. 1989. *Molecular stratigraphy: The recognition of palea-climatic signals in organic geochemical data.* School of Chemistry, University of Bristol, Bristol.

Poynter, J. & Eglinton, G. 1990. *14. Molecular composition of three sediments from hole 717c: The Bengal fan*. In: Cochran J.R., Stow, D. A. V., et al. (ed.), *The Ocean Drilling Program, Scientific Results*.

Preis, Y. I., Simonova, G. V., Voropay, N. N. & Dyukarev, E. A. 2018. *Estimation of the influence of hydrothermal conditions on the carbon isotope composition in Sphagnum mosses of bogs of Western Siberia*. IOP Conference Series: Earth and Environmental Science 211 (1): 012031, doi:10.1088/1755-1315/211/1/012031.

Previdi, M., Smith, K. L. & Polvani, L. M. 2021. *Arctic amplification of climate change: a review of underlying mechanisms*. Environmental Research Letters 16 (9): 093003, doi:10.1088/1748-9326/ac1c29.

Pye, K. 1995. *The nature, origin and accumulation of loess*. Quaternary Science Reviews 14 (7): 653-667, doi:10.1016/0277-3791(95)00047-X.

Radke, M., Willsch, H. & Welte, D. H. 1980. *Preparative hydrocarbon group type determination by automated medium pressure liquid chromatography*. Analytical Chemistry 52 (3): 406-411, doi:10.1021/ac50053a009.

Ramesh, T., Bolan, N. S., Kirkham, M. B., Wijesekara, H., Kanchikerimath, M., Srinivasa Rao, C., Sandeep, S., Rinklebe, J., Ok, Y. S., Choudhury, B. U., Wang, H., Tang, C., Wang, X., Song, Z. & Freeman Ii, O. W. 2019. Chapter One - Soil organic carbon dynamics: Impact of land use changes and management practices: A review. In: Sparks D.L. (ed.), *Advances in Agronomy,* Academic Press, pp. 1-107 doi:https://doi.org/10.1016/bs.agron.2019.02.001.

R Core Team. 2021. *R: A language and environment for statistical computing*, *v4.1.1*. R Foundation for Statistical Computing, Vienna, Austria. https://www.R-project.org/.

Regmi, P., Grosse, G., Jones, M. C., Jones, B. M. & Anthony, K. W. 2012. *Characterizing Post-Drainage Succession in Thermokarst Lake Basins on the Seward Peninsula, Alaska with TerraSAR-X Backscatter and Landsat-based NDVI Data*. Remote Sensing 4 (12): 3741-3765, https://www.mdpi.com/2072-4292/4/12/3741.

Reimer, P. J., Bard, E., Bayliss, A., Beck, J. W., Blackwell, P. G., Ramsey, C. B., Buck, C. E., Cheng, H., Edwards, R. L., Friedrich, M., Grootes, P. M., Guilderson, T. P., Haflidason, H., Hajdas, I., Hatté, C., Heaton, T. J., Hoffmann, D. L., Hogg, A. G., Hughen, K. A., Kaiser, K. F., Kromer, B., Manning, S. W., Niu, M., Reimer, R. W., Richards, D. A., Scott, E. M., Southon, J. R., Staff, R. A., Turney, C. S. M. & Plicht, J. v. d. 2013. *IntCal13 and Marine13 Radiocarbon Age Calibration Curves 0–50,000 Years cal BP*. Radiocarbon 55 (4): 1869-1887, doi:10.2458/azu_js_rc.55.16947.

Reimer, P. J., Austin, W. E. N., Bard, E., Bayliss, A., Blackwell, P. G., Bronk Ramsey, C., Butzin, M., Cheng, H., Edwards, R. L., Friedrich, M., Grootes, P. M., Guilderson, T. P., Hajdas, I., Heaton, T. J., Hogg, A. G., Hughen, K. A., Kromer, B., Manning, S. W., Muscheler, R., Palmer, J. G., Pearson, C., van der Plicht, J., Reimer, R. W., Richards, D. A., Scott, E. M., Southon, J. R., Turney, C. S. M., Wacker, L., Adolphi, F., Büntgen, U., Capano, M., Fahrni, S. M., Fogtmann-Schulz, A., Friedrich, R., Köhler, P., Kudsk, S., Miyake, F., Olsen, J., Reinig, F., Sakamoto, M., Sookdeo, A. & Talamo, S. 2020. *The IntCal20 Northern Hemisphere Radiocarbon Age Calibration Curve (0–55 cal kBP)*. Radiocarbon 62 (4): 725-757, doi:10.1017/RDC.2020.41.

Reineck, H.-E. & Singh, I. B. 1980. *Depositional sedimentary environments*. 2nd ed. Springer-Verlag New York Berlin Heidelberg.

Reineck, H. E. & Singh, I. B. 2012. *Depositional Sedimentary Environments: With Reference to Terrigenous Clastics*. Springer Science & Business Media.

Romanovskii, N. 1993. *Fundamentals of cryogenesis of lithosphere*. Moscow University Press, Moscow.

Ruosteenoja, K., Räisänen, J. & Pirinen, P. 2011. *Projected changes in thermal seasons and the growing season in Finland*. International Journal of Climatology 31 (10): 1473-1487, doi:10.1002/joc.2171.

Rutkowski, C., Lenz, J., Lang, A., Wolter, J., Mothes, S., Reemtsma, T., Grosse, G., Ulrich, M., Fuchs, M., Schirrmeister, L., Fedorov, A., Grigoriev, M., Lantuit, H. & Strauss, J. 2021. *Mercury in Sediment Core Samples From Deep Siberian Ice-Rich Permafrost*. Frontiers in Earth Science 9 doi:10.3389/feart.2021.718153.

Sannel, A. B. K. 2020. *Ground temperature and snow depth variability within a subarctic peat plateau landscape*. Permafrost and Periglacial Processes 31 (2): 255-263, doi:https://doi.org/10.1002/ppp.2045.

Santoro, M. & Strozzi, T. 2012. *Circumpolar digital elevation models > 55_N with links to geotiff images, ESA data user element - permafrost*. doi:10.1594/PANGAEA.779748.

Schirrmeister, L., Froese, D., Tumskoy, V., Grosse, G. & Wetterich, S. 2013. Yedoma: Late Pleistocene ice-rich syngenetic permafrost of Beringia. In: *Encyclopedia of Quaternary Science,* 2 ed. Elsevier, pp. 542-552 doi:10.1016/B978-0-444-53643-3.00106-0.

Schirrmeister, L., Grosse, G., Wetterich, S., Overduin, P. P., Strauss, J., Schuur, E. A. G. & Hubberten, H.-W. 2011. *Fossil organic matter characteristics in permafrost deposits of the northeast Siberian Arctic*. Journal of Geophysical Research: Biogeosciences 116 (G2) doi:10.1029/2011JG001647.

Schirrmeister, L., Siegert, C., Kuznetsova, T., Kuzmina, S., Andreev, A., Kienast, F., Meyer, H. & Bobrov, A. 2002. *Paleoenvironmental and paleoclimatic records from permafrost deposits in the Arctic region of Northern Siberia*. Quaternary International 89 (1): 97-118, doi:10.1016/S1040-6182(01)00083-0.

Schuster, P. F., Schaefer, K. M., Aiken, G. R., Antweiler, R. C., Dewild, J. F., Gryziec, J. D., Gusmeroli, A., Hugelius, G., Jafarov, E., Krabbenhoft, D. P., Liu, L., Herman-Mercer, N., Mu, C., Roth, D. A., Schaefer, T., Striegl, R. G., Wickland, K. P. & Zhang, T. 2018. *Permafrost Stores a Globally Significant Amount of Mercury*. Geophysical Research Letters 45 (3): 1463-1471, doi:10.1002/2017GL075571.

Schuur, E. A. G., McGuire, A. D., Schädel, C., Grosse, G., Harden, J. W., Hayes, D. J., Hugelius, G., Koven, C. D., Kuhry, P., Lawrence, D. M., Natali, S. M., Olefeldt, D., Romanovsky, V. E., Schaefer, K., Turetsky, M. R., Treat, C. C. & Vonk, J. E. 2015. *Climate change and the permafrost carbon feedback*. Nature 520: 171, doi:10.1038/nature14338.

Schuur, E. A. G., Bockheim, J., Canadell, J. G., Euskirchen, E., Field, C. B., Goryachkin, S. V., Hagemann, S., Kuhry, P., Lafleur, P. M., Lee, H., Mazhitova, G., Nelson, F. E., Rinke, A., Romanovsky, V. E., Shiklomanov, N., Tarnocai, C., Venevsky, S., Vogel, J. G. & Zimov, S. A. 2008. *Vulnerability of Permafrost Carbon to Climate Change: Implications for the Global Carbon Cycle*. BioScience 58 (8): 701-714, doi:10.1641/B580807.

Schuur, E. A. G., Abbott, B. W., Commane, R., Ernakovich, J., Euskirchen, E., Hugelius, G., Grosse, G., Jones, M., Koven, C., Leshyk, V., Lawrence, D., Loranty, M. M., Mauritz, M., Olefeldt, D., Natali, S., Rodenhizer, H., Salmon, V., Schädel, C., Strauss, J., Treat, C. & Turetsky, M. 2022. *Permafrost and Climate Change: Carbon Cycle Feedbacks From the Warming Arctic*. Annual Review of Environment and Resources 47 (1): 343-371, doi:10.1146/annurev-environ-012220-011847.

Shmelev, D., Cherbunina, M., Rogov, V., Opfergelt, S., Monhonval, A. & Strauss, J. 2021. *Reconstructing Permafrost Sedimentological Characteristics and Post-depositional Processes of the Yedoma Stratotype Duvanny Yar, Siberia*. Frontiers in Earth Science 9 (961) doi:10.3389/feart.2021.727315.

Shmelev, D., Veremeeva, A., Kraev, G., Kholodov, A., Spencer, R. G. M., Walker, W. S. & Rivkina, E. 2017. *Estimation and Sensitivity of Carbon Storage in Permafrost of North-Eastern Yakutia*. Permafrost and Periglacial Processes 28 (2): 379-390, doi:10.1002/ppp.1933.

Siewert, M. B., Hanisch, J., Weiss, N., Kuhry, P., Maximov, T. C. & Hugelius, G. 2015. *Comparing carbon storage of Siberian tundra and taiga permafrost ecosystems at very high spatial resolution*. Journal of Geophysical Research: Biogeosciences 120 (10): 1973-1994, doi:10.1002/2015JG002999.

Skarin, A., Danell, Ö., Bergström, R. & Moen, J. 2010. *Insect avoidance may override human disturbances in reindeer habitat selection*. Rangifer 24 doi:10.7557/2.24.2.306.

Skarin, A., Verdonen, M., Kumpula, T., Macias-Fauria, M., Alam, M., Kerby, J. T. & Forbes, B. C. 2020. *Reindeer use of low Arctic tundra correlates with landscape structure*. Environmental Research Letters doi:10.1088/1748-9326/abbf15.

Smith, L. C., Beilman, D. W., Kremenetski, K. V., Sheng, Y., MacDonald, G. M., Lammers, R. B., Shiklomanov, A. I. & Lapshina, E. D. 2012. *Influence of permafrost on water storage in West Siberian peatlands revealed from a new database of soil properties*. Permafrost and Periglacial Processes 23 (1): 69-79, doi:10.1002/ppp.735.

Soloviev, P. 1973. *Guidebook: alass thermokarst relief of central Yakutia*. In: *Second International Conference on Permafrost, Yakutsk,* pp. 13-28.

Soloviev, P. A. 1959. *Cryolithic Zone of the Northern Part of Lena-Amga Interfluve*. Academy of Sciences of the USSR press, Moscow.

Stevenson, F. J. 1994. *Humus chemistry: genesis, composition, reactions*. John Wiley & Sons.

Stimmler, P., Goeckede, M., Elberling, B., Natali, S., Kuhry, P., Perron, N., Lacroix, F., Hugelius, G., Sonnentag, O., Strauss, J., Minions, C., Sommer, M. & Schaller, J. 2023. *Pan-Arctic soil element bioavailability estimations*. Earth Syst. Sci. Data 15 (3): 1059-1075, doi:10.5194/essd-15-1059-2023.

Strauss, J., Schirrmeister, L., Wetterich, S., Borchers, A. & Davydov, S. P. 2012. *Grain-size properties and organic-carbon stock of Yedoma Ice Complex permafrost from the Kolyma lowland, northeastern Siberia*. Global Biogeochemical Cycles 26 (3) doi:10.1029/2011GB004104.

Strauss, J., Schirrmeister, L., Mangelsdorf, K., Eichhorn, L., Wetterich, S. & Herzschuh, U. 2015. *Organic-matter quality of deep permafrost carbon – a study from Arctic Siberia*. Biogeosciences 12 (10.5194/bg-12-2227-2015): 2227-2245, doi:10.5194/bg-12-2227-2015.

Strauss, J., Schirrmeister, L., Grosse, G., Wetterich, S., Ulrich, M., Herzschuh, U. & Hubberten, H.-W. 2013. *The deep permafrost carbon pool of the Yedoma region in Siberia and Alaska*. Geophysical Research Letters 40 (23): 6165-6170, doi:10.1002/2013GL058088.

Strauss, J., Abbott, B. W., Hugelius, G., Schuur, E., Treat, C., Fuchs, M., Schädel, C., Ulrich, M., Turetsky, M. & Keuschnig, M. 2021. 9. Permafrost. In: *Recarbonizing global soils–A technical manual of recommended management practices: Volume 2–Hot spots and bright spots of soil organic carbon,* p. 130

Strauss, J., Schirrmeister, L., Grosse, G., Fortier, D., Hugelius, G., Knoblauch, C., Romanovsky, V., Schädel, C., Schneider von Deimling, T., Schuur, E. A. G., Shmelev, D. & Veremeeva, A. 2017. *Deep Yedoma permafrost: A synthesis of depositional characteristics and carbon vulnerability*. Earth-Science Reviews (172): 75-86, doi:10.1016/j.earscirev.2017.07.007.

Strauss, J., Biasi, C., Sanders, T., Abbott, B. W., von Deimling, T. S., Voigt, C., Winkel, M., Marushchak, M. E., Kou, D., Fuchs, M., Horn, M. A., Jongejans, L. L., Liebner, S., Nitzbon, J., Schirrmeister, L., Walter Anthony, K., Yang, Y., Zubrzycki, S., Laboor, S., Treat, C. & Grosse, G. 2022. *A globally relevant stock of soil nitrogen in the Yedoma permafrost domain*. Nature Communications 13 (1): 6074, doi:10.1038/s41467-022-33794-9.

Stroeven, A. P., Hättestrand, C., Kleman, J., Heyman, J., Fabel, D., Fredin, O., Goodfellow, B. W., Harbor, J. M., Jansen, J. D., Olsen, L., Caffee, M. W., Fink, D., Lundqvist, J., Rosqvist, G. C., Strömberg, B. & Jansson, K. N.

2016. *Deglaciation of Fennoscandia*. Quaternary Science Reviews 147: 91-121, doi:10.1016/j.quascirev.2015.09.016.

Stuenzi, S. M., Boike, J., Gädeke, A., Herzschuh, U., Kruse, S., Pestryakova, L. A., Westermann, S. & Langer, M. 2021. *Sensitivity of ecosystem-protected permafrost under changing boreal forest structures*. Environmental Research Letters 16 (8): 084045, doi:10.1088/1748-9326/ac153d.

2018. *CALIB 7.1 [WWW program]*, http://calib.org.

Stuiver M., Reimer P.J., Reimer R.W. 2021. *CALIB 8.2 [WWW program]*, http://calib.org.

Sundqvist, M. K., Moen, J., Björk, R. G., Vowles, T., Kytöviita, M.-M., Parsons, M. A. & Olofsson, J. 2019. *Experimental evidence of the long-term effects of reindeer on Arctic vegetation greenness and species richness at a larger landscape scale*. Journal of Ecology 107 (6): 2724-2736, doi:10.1111/1365-2745.13201.

Suominen, O. & Olofsson, J. 2000. *Impacts of semi-domesticated reindeer on structure of tundra and forest communities in Fennoscandia: a review*. Annales Zoologici Fennici 37 (4): 233-249, http://www.jstor.org/stable/23735717.

te Beest, M., Sitters, J., Ménard, C. B. & Olofsson, J. 2016. *Reindeer grazing increases summer albedo by reducing shrub abundance in Arctic tundra*. Environmental Research Letters 11 (12): 125013, doi:10.1088/1748-9326/aa5128.

Tuisku, T. 2002. *Nenets Reindeer Herding and Industrial Exploitation in Northwestern Russia*. Human Organization 61 (2): 147-153.

Tuomi, M., Väisänen, M., Ylänne, H., Brearley, F. Q., Barrio, I. C., Anne Bråthen, K., Eischeid, I., Forbes, B. C., Jónsdóttir, I. S., Kolstad, A. L., Macek, P., Petit Bon, M., Speed, J. D. M., Stark, S., Svavarsdóttir, K., Thórsson, J. & Bueno, C. G. 2021. *Stomping in silence: Conceptualizing trampling effects on soils in polar tundra*. Functional Ecology 35 (2): 306-317, doi:10.1111/1365-2435.13719.

Turetsky, M. R., Abbott, B. W., Jones, M. C., Walter Anthony, K., Olefeldt, D., Schuur, E. A. G., Koven, C., McGuire, A. D., Grosse, G., Kuhry, P., Hugelius, G., Lawrence, D. M., Gibson, C. & Sannel, A. B. K. 2019. *Permafrost collapse is accelerating carbon release*. Nature doi:10.1038/d41586-019-01313-4.

Turetsky, M. R., Abbott, B. W., Jones, M. C., Walter Anthony, K., Olefeldt, D., Schuur, E. A. G., Grosse, G., Kuhry, P., Hugelius, G., Koven, C., Lawrence, D. M., Gibson, C., Sannel, A. B. K. & McGuire, A. D. 2020a. *Carbon release through abrupt permafrost thaw*. Nature Geoscience 13 (2): 138-143, doi:10.1038/s41561-019-0526-0.

Turetsky, M. R., Abbott, B. W., Jones, M. C., Anthony, K. W., Olefeldt, D., Schuur, E. A. G., Grosse, G., Kuhry, P., Hugelius, G., Koven, C., Lawrence, D. M., Gibson, C., Sannel, A. B. K. & McGuire, A. D. 2020b. *Carbon release through abrupt permafrost thaw*. Nature Geoscience 13 (2): 138-143, doi:10.1038/s41561-019-0526-0.

Ulrich, M., Grosse, G., Strauss, J. & Schirrmeister, L. 2014. *Quantifying Wedge-Ice Volumes in Yedoma and Thermokarst Basin Deposits*. Permafrost and Periglacial Processes 25 (3): 151-161, doi:10.1002/ppp.1810.

Ulrich, M., Matthes, H., Schirrmeister, L., Schütze, J., Park, H., Iijima, Y. & Fedorov, A. N. 2017a. *Differences in behaviour and distribution of permafrost-related lakes in Central Yakutia and their response to climatic drivers*. Water Resources Research: 1167-1188, doi:10.1002/2016WR019267.

Ulrich, M., Wetterich, S., Rudaya, N., Frolova, L., Schmidt, J., Siegert, C., Fedorov, A. N. & Zielhofer, C. 2017b. *Rapid thermokarst evolution during the mid-Holocene in Central Yakutia, Russia*. The Holocene 27 (12): 1899-1913, doi:10.1177/0959683617708454.

Ulrich, M., Matthes, H., Schmidt, J., Fedorov, A. N., Schirrmeister, L., Siegert, C., Schneider, B., Strauss, J. & Zielhofer, C. 2019. *Holocene thermokarst dynamics in Central Yakutia - A multi-core and robust grain-size endmember modeling approach*. Quaternary Science Reviews 218 (10-33) doi:10.1016/j.quascirev.2019.06.010.

Van Everdingen, R. O. 1998. *Multi-language glossary of permafrost and related ground-ice terms in Chinese, English, French, German, Icelandic, Italian, Norwegian, polish, Romanian, Russian, Spanish, and Swedish*. International Permafrost Association, Terminology Working Group.

van Groenigen, K. J., Osenberg, C. W. & Hungate, B. A. 2011. *Increased soil emissions of potent greenhouse gases under increased atmospheric CO2*. Nature 475 (7355): 214-216, doi:10.1038/nature10176.

Veremeeva, A., Nitze, I., Günther, F., Grosse, G. & Rivkina, E. 2021. *Geomorphological and Climatic Drivers of Thermokarst Lake Area Increase Trend (1999–2018) in the Kolyma Lowland Yedoma Region, North-Eastern Siberia*. Remote Sensing 13 (2): 178, doi:10.3390/rs13020178.

Verma, M., Schulte to Bühne, H., Lopes, M., Ehrich, D., Sokovnina, S., Hofhuis, S. P. & Pettorelli, N. 2020. *Can reindeer husbandry management slow down the shrubification of the Arctic?* Journal of Environmental Management 267: 110636, doi:10.1016/j.jenvman.2020.110636.

Walker, D. A., Jia, G. J., Epstein, H. E., Raynolds, M. K., Chapin III, F. S., Copass, C., Hinzman, L. D., Knudson, J. A., Maier, H. A., Michaelson, G. J., Nelson, F., Ping, C. L., Romanovsky, V. E. & Shiklomanov, N. 2003. *Vegetation-soil-thaw-depth relationships along a low-arctic bioclimate gradient, Alaska: synthesis of information from the ATLAS studies*. Permafrost and Periglacial Processes 14 (2): 103-123, doi:10.1002/ppp.452.

Walter Anthony, K. M., Zimov, S. A., Grosse, G., Jones, M. C., Anthony, P. M., Iii, F. S. C., Finlay, J. C., Mack, M. C., Davydov, S., Frenzel, P. & Frolking, S. 2014. *A shift of thermokarst lakes from carbon sources to sinks during the Holocene epoch*. Nature 511 (7510): 452, doi:10.1038/nature13560.

Walz, J., Knoblauch, C., Böhme, L. & Pfeiffer, E.-M. 2017. *Regulation of soil organic matter decomposition in permafrost-affected Siberian tundra soils - Impact of oxygen availability, freezing and thawing, temperature, and labile organic matter*. Soil Biology and Biochemistry 110: 34-43, doi:10.1016/j.soilbio.2017.03.001.

Wang, P., Mommer, L., van Ruijven, J., Berendse, F., Maximov, T. C. & Heijmans, M. M. P. D. 2016. *Seasonal changes and vertical distribution of root standing biomass of graminoids and shrubs at a Siberian tundra site*. Plant and Soil 407 (1): 55-65, doi:10.1007/s11104-016-2858-5.

Weiss, N., Blok, D., Elberling, B., Hugelius, G., Jørgensen, C. J., Siewert, M. B. & Kuhry, P. 2016. *Thermokarst dynamics and soil organic matter characteristics controlling initial carbon release from permafrost soils in the Siberian Yedoma region*. Sedimentary Geology 340: 38-48, doi:10.1016/j.sedgeo.2015.12.004.

Wetterich, S., Herzschuh, U., Meyer, H., Pestryakova, L., Plessen, B., Lopez, C. M. L. & Schirrmeister, L. 2008. *Evaporation effects as reflected in freshwater and ostracod calcite from modern environments in Central and Northeast Yakutia (East Siberia, Russia)*. Hydrobiologia (614): 171-195, doi:10.1007/s10750-008-9505-y.

Wetterich, S., Schirrmeister, L., Andreev, A. A., Pudenz, M., Plessen, B., Meyer, H. & Kunitsky, V. V. 2009. *Eemian and Late Glacial/Holocene palaeoenvironmental records from permafrost sequences at the Dmitry Laptev Strait (NE Siberia, Russia)*. Palaeogeography, Palaeoclimatology, Palaeoecology 279 (1): 73-95, doi:10.1016/j.palaeo.2009.05.002.

Wetterich, S., Rudaya, N., Tumskoy, V., Andreev, A. A., Opel, T., Schirrmeister, L. & Meyer, H. 2011. *Last Glacial Maximum records in permafrost of the East Siberian Arctic*. Quaternary Science Reviews 30 (21): 3139-3151, doi:10.1016/j.quascirev.2011.07.020.

Wetterich, S., Tumskoy, V., Rudaya, N., Andreev, A. A., Opel, T., Meyer, H., Schirrmeister, L. & Hüls, M. 2014. *Ice Complex formation in arctic East Siberia during the MIS3 Interstadial*. Quaternary Science Reviews 84: 39-55, doi:10.1016/j.quascirev.2013.11.009.

Wetterich, S., Tumskoy, V., Rudaya, N., Kuznetsov, V., Maksimov, F., Opel, T., Meyer, H., Andreev, A. A. & Schirrmeister, L. 2016. *Ice Complex permafrost of MIS5 age in the Dmitry Laptev Strait coastal region (East Siberian Arctic)*. Quaternary Science Reviews 147: 298-311, doi:10.1016/j.quascirev.2015.11.016.

Wilcock, P. R. & Crowe, J. C. 2003. *Surface-based Transport Model for Mixed-Size Sediment*. Journal of Hydraulic Engineering 129 (2): 120-128, doi:10.1061/(ASCE)0733-9429(2003)129:2(120).

Wilcox, E. J., Keim, D., Jong, T., Walker, B., Sonnentag, O., Sniderhan, A. E., Mann, P. & Marsh, P. 2019. *Tundra shrub expansion may amplify permafrost thaw by advancing snowmelt timing*. Arctic Science 5 (4): 202-217, doi:10.1139/as-2018-0028.

Windirsch, T., Fuchs, M., Grosse, G., Habeck, J. O., Ulrich, M. & Strauss, J. 2021a. Expedition to Kutuharju Field Research Station, Northern Finland, September 2020. In: Fuchs M., van Delden L., Lehmann N. & Windirsch T. (eds.), *Expeditions to Fennoscandia in 2020,* Berichte zur Polar- und Meeresforschung = Reports on polar and marine research, Alfred Wegener Institute for Polar and Marine Research, Bremerhaven, pp. 5-12 doi:10.48433/BzPM_0752_2021.

Windirsch, T., Mangelsdorf, K., Grosse, G., Wolter, J., Jongejans, L. L. & Strauss, J. 2023a. *n-Alkane characteristics of Arctic soils, comparing different large herbivore grazing intensities under permafrost and non-permafrost conditions*. PANGAEA. doi:10.1594/PANGAEA.963258.

Windirsch, T., Mangelsdorf, K., Grosse, G., Wolter, J., Jongejans, L. L. & Strauss, J. 2023b. *n-alcohol characteristics of Arctic soils, comparing different large herbivore grazing intensities under permafrost and non-permafrost conditions*. PANGAEA. doi:10.1594/PANGAEA.963259.

Windirsch, T., Mangelsdorf, K., Grosse, G., Wolter, J., Jongejans, L. L. & Strauss, J. under review. *A Pilot Study of Lipid Biomarkers to Trace Recent Large Herbivore Influence in Permafrost and Seasonally Frozen Ground*. Arctic Science.

Windirsch, T., Grosse, G., Ulrich, M., Schirrmeister, L., Fedorov, A. N., Konstantinov, P., Fuchs, M. & Strauss, J. 2019. *Organic material, sediment and ice characteristics of two permafrost cores from Yukechi Alas, Central Yakutia*. doi:10.1594/PANGAEA.898754.

Windirsch, T., Grosse, G., Ulrich, M., Forbes, B. C., Göckede, M., Zimov, N., Macias-Fauria, M., Olofsson, J., Wolter, J. & Strauss, J. 2021b. *Large herbivores affecting terrestrial permafrost in northeastern Siberia: biogeochemical and sediment characteristics under different grazing intensities*. PANGAEA. doi:10.1594/PANGAEA.933446.

Windirsch, T., Grosse, G., Ulrich, M., Forbes, B. C., Göckede, M., Wolter, J., Macias-Fauria, M., Olofsson, J., Zimov, N. & Strauss, J. 2022a. *Large herbivores on permafrost— a pilot study of grazing impacts on permafrost soil carbon storage in northeastern Siberia*. Frontiers in Environmental Science 10 doi:10.3389/fenvs.2022.893478.

Windirsch, T., Grosse, G., Ulrich, M., Schirrmeister, L., Fedorov, A. N., Konstantinov, P., Fuchs, M., Jongejans, L. L., Wolter, J., Opel, T. & Strauss, J. 2020a. *Detailed core log of deep permafrost core YUK15-YED1*. PANGAEA. doi:10.1594/PANGAEA.914874.

Windirsch, T., Grosse, G., Ulrich, M., Schirrmeister, L., Fedorov, A. N., Konstantinov, P., Fuchs, M., Jongejans, L. L., Wolter, J., Opel, T. & Strauss, J. 2020b. *Detailed core log of deep permafrost core YUK15-Alas1*. PANGAEA. doi:10.1594/PANGAEA.914876.

Windirsch, T., Grosse, G., Ulrich, M., Schirrmeister, L., Fedorov, A. N., Konstantinov, P. Y., Fuchs, M., Jongejans, L. L., Wolter, J., Opel, T. & Strauss, J. 2020c. *Organic carbon characteristics in ice-rich permafrost in alas and Yedoma deposits, central Yakutia, Siberia*. Biogeosciences 17 (14): 3797-3814, doi:10.5194/bg-17-3797-2020.

Windirsch, T., Forbes, B. C., Grosse, G., Wolter, J., Treat, C. C., Ulrich, M., Stark, S., Fuchs, M., Olofsson, J., Macias-Fauria, M., Kumpula, T. & Strauss, J. 2022b. *Peat and sediment characteristics from Reindeer winter ranges in Northern Finland* PANGAEA. doi:10.1594/PANGAEA.952470.

Windirsch, T., Forbes, B. C., Grosse, G., Wolter, J., Treat, C. C., Ulrich, M., Stark, S., Fuchs, M., Olofsson, J., Macias-Fauria, M., Kumpula, T. & Strauss, J. 2022c. *Peat and sediment characteristics from different Reindeer grazing intensities in Northern Finland*. PANGAEA. doi:10.1594/PANGAEA.941930.

Windirsch, T., Forbes, B. C., Grosse, G., Wolter, J., Stark, S., Treat, C. C., Ulrich, M., Fuchs, M., Olofsson, J., Kumpula, J., Macias-Fauria, M. & Strauss, J. 2023c. *Impacts of reindeer on soil carbon storage in the seasonally frozen ground of northern Finland*. Boreal Environment Research https://www.borenv.net/BER/archive/pdfs/ber28/ber28-207-226.pdf.

World Animal Foundation. 2023. *Reindeer Animal Information && Interesting Facts*. accessed 12.06.2023. https://worldanimalfoundation.org/mammals/reindeers/.

Wynn, J. G. 2007. *Carbon isotope fractionation during decomposition of organic matter in soils and paleosols: Implications for paleoecological interpretations of paleosols*. Palaeogeography, Palaeoclimatology, Palaeoecology 251 (3): 437-448, doi:10.1016/j.palaeo.2007.04.009.

Ylänne, H., Olofsson, J., Oksanen, L. & Stark, S. 2018. *Consequences of grazer-induced vegetation transitions on ecosystem carbon storage in the tundra*. Functional Ecology 32 (4): 1091-1102, doi:10.1111/1365-2435.13029.

Zhang, C., Douglas, T. A., Brodylo, D. & Jorgenson, M. T. 2023. *Linking repeat lidar with Landsat products for large scale quantification of fire-induced permafrost thaw settlement in interior Alaska*. Environmental Research Letters 18 (1): 015003, doi:10.1088/1748-9326/acabd6.

Zhang, T., Barry, R. G., Knowles, K., Heginbottom, J. A. & Brown, J. 1999. *Statistics and characteristics of permafrost and ground-ice distribution in the Northern Hemisphere*. Polar Geography 23 (2): 132-154, doi:10.1080/10889379909377670.

Zhang, W., Miller, P. A., Smith, B., Wania, R., Koenigk, T. & Döscher, R. 2013. *Tundra shrubification and tree-line advance amplify arctic climate warming: results from an individual-based dynamic vegetation model*. Environmental Research Letters 8 (3): 034023, doi:10.1088/1748-9326/8/3/034023.

Zimov, N. 2020. *Pleistocene Park*. accessed 05.05.2023. https://pleistocenepark.ru/.

Zimov, N. S., Zimov, S. A., Zimova, A. E., Zimova, G. M., Chuprynin, V. I. & Chapin III, F. S. 2009. *Carbon storage in permafrost and soils of the mammoth tundra-steppe biome: Role in the global carbon budget*. Geophysical Research Letters 36 (2) doi:10.1029/2008GL036332.

Zimov, S. A. 2005. *Pleistocene Park: Return of the Mammoth's Ecosystem*. Science 308 (5723): 796-798, doi:10.1126/science.1113442.

Zimov, S. A., Zimov, N. S., Tikhonov, A. N. & Chapin, F. S. 2012. *Mammoth steppe: a high-productivity phenomenon*. Quaternary Science Reviews 57: 26-45, doi:10.1016/j.quascirev.2012.10.005.

Zimov, S. A., Chuprynin, V. I., Oreshko, A. P., Chapin III, F. S., Reynolds, R. & Chapin, M. C. 1995. *Steppe-Tundra Transition: A Herbivore-Driven Biome Shift at the End of the Pleistocene*. The American Naturalist 146 (5): 765-794, doi:10.1086/285824.

Zimov, S. A., Davydov, S. P., Zimova, G. M., Davydova, A. I., Schuur, E. A. G., Dutta, K. & Chapin, F. S. 2006. *Permafrost carbon: Stock and decomposability of a globally significant carbon pool*. Geophysical Research Letters 33 (20) doi:10.1029/2006GL027484.

Zona, D., Gioli, B., Commane, R., Lindaas, J., Wofsy, S. C., Miller, C. E., Dinardo, S. J., Dengel, S., Sweeney, C., Karion, A., Chang, R. Y.-W., Henderson, J. M., Murphy, P. C., Goodrich, J. P., Moreaux, V., Liljedahl, A., Watts, J. D., Kimball, J. S., Lipson, D. A. & Oechel, W. C. 2016. *Cold season emissions dominate the Arctic tundra methane budget*. Proceedings of the National Academy of Sciences 113 (1): 40-45, doi:10.1073/pnas.1516017113.

Financial and technical support

My PhD project was funded by a grant of the Potsdam Graduate School (PoGS) and was hosted by the Alfred Wegener Institute Helmholtz Centre for Polar and Marine Research (AWI) in Potsdam, where I had access to all facilities including laboratories.

My 2019 field campaign to Siberia was part of the CACOON (Changing Arctic Carbon Cycle in the Coastal Ocean Near-Shore) project funded by the German Federal Ministry of Education and Research (BMBF) (grant number #03F0806A).

The 2020 and 2022 field campaigns to northern Finland were funded by the AWI expedition funds, while the 2022 campaign was additionally supported by the Geo.X research network (grant number SO_087_GeoX).

The AWI base funds also funded the final phase of my PhD project.

Travel for training and conference purposes was funded by the Helmholtz Graduate School for Polar and Marine Research (POLMAR) and the PoGS.

Appendix

Appendix I Organic Carbon Characteristics in Ice-rich Permafrost in Alas and Yedoma Deposits, Central Yakutia, Siberia

This publication deals with two deep permafrost cores from an drained thermokarst basin (alas) and the adjacent Yedoma upland. Since the alas is used for hay-making and cattle farming, this paper is also relevant in the context of this thesis. It is based on studies previous to this thesis.

Organic Carbon Characteristics in Ice-rich Permafrost in Alas and Yedoma Deposits, Central Yakutia, Siberia

Windirsch, T.[1,2], Grosse, G.[1,2], Ulrich, M.[3], Schirrmeister, L.[1], Fedorov, A. N.[4,5], Konstantinov, P. Y.[4], Fuchs, M.[1], Jongejans, L. L.[1,2], Wolter, J.[1], Opel, T.[1], and Strauss, J.[1]

[1]Alfred Wegener Institute Helmholtz Centre for Polar and Marine Research, Potsdam, Germany

[2]Institute of Geosciences, University of Potsdam, Potsdam, Germany

[3]Institute for Geography, Leipzig University, Leipzig, Germany

[4]Melnikov Permafrost Institute, SB RAS, Yakutsk, Republic of Sakha, Russia

[5]BEST International Centre, North-East Federal University, Yakutsk, Republic of Sakha, Russia

Published in: Biogeosciences, Volume 17, 2020

Citation: Windirsch, T., Grosse, G., Ulrich, M., Schirrmeister, L., Fedorov, A. N., Konstantinov, P. Y., Fuchs, M., Jongejans, L. L., Wolter, J., Opel, T., and Strauss, J.: Organic Carbon Characteristics in Ice-rich Permafrost in Alas and Yedoma Deposits, Central Yakutia, Siberia, Biogeosciences 17, doi: 10.5194/bg-17-3797-2020, 2020.

IV.1 Abstract

Permafrost ground is one of the largest repositories of terrestrial organic carbon and might become or is already a carbon source in response to ongoing global warming. With this study of syngenetically frozen, ice-rich and organic carbon (OC)-bearing Yedoma and associated Alas deposits in Central Yakutia, we aimed to assess the local sediment deposition regime and its effect on permafrost carbon storage. For this purpose, we investigated the Yukechi Alas area (61.76495 °N, 130.46664 °E), a thermokarst landscape degrading into Yedoma in Central Yakutia. We retrieved two sediment cores (Yedoma upland, 22.35 m deep, and Alas basin, 19.80 m deep) in 2015 and analysed biogeochemistry, sedimentology, radiocarbon dates and stable isotope geochemistry. The laboratory analyses of both cores revealed very low total OC (TOC) contents (< 0.1 wt%) for a 12 meter section in each core, while the remaining sections ranged from 0.1 to 2.4 wt% TOC. Those core parts holding very little to no detectable OC consisted of coarser sandy material estimated to an age between 39,000 and 18,000 years before present. For this period, we assume deposition of organic-poor material. Pore water stable isotope data from the Yedoma core indicated a continuously frozen state except for the surface sample, thereby ruling out Holocene reworking. In consequence, we see evidence that no strong organic matter (OM) decomposition took place in the sediments of the Yedoma core until today. The Alas core from an adjacent thermokarst basin was strongly disturbed by lake development and permafrost thaw. Similar to the Yedoma core, some sections of the Alas core were also OC poor (< 0.1 wt%) in 17 out of 28 samples. The Yedoma deposition was likely influenced by fluvial regimes in nearby streams and the Lena River shifting with climate. With its coarse sediments with low OC content (OC mean of 5.27 kg/m³), the Yedoma deposits in the Yukechi area differ from other Yedoma sites in North Yakutia that were generally characterised by silty sediments with higher OC contents (OC mean of 19 kg/m³ for the non-ice wedge sediment). Therefore, we conclude that sedimentary composition and deposition regimes of Yedoma may differ considerably within the Yedoma domain. The resulting heterogeneity should be taken into account for future upscaling approaches on the Yedoma carbon stock. The Alas core, strongly affected by extensive thawing processes during the Holocene, indicates a possible future pathway of ground subsidence and further OC decomposition for thawing Central Yakutian Yedoma deposits.

IV.2 Introduction

Permafrost deposits represent one of the largest terrestrial carbon reservoirs. Perennial freezing largely prevents decomposition and preserves organic material. These permafrost soil conditions are found in the ground of approximately one quarter of the Northern Hemisphere's land surface (Zhang *et al.* 1999). The estimated amount of frozen and unfrozen carbon stored in the terrestrial permafrost region is 1330 to 1580 gigatons (Gt) (Hugelius *et al.* 2014, Schuur

et al. 2015), which is approximately 45 % more than what is currently present in the atmosphere (~ 864 Gt, based on 407 ppm CO_2 measured in 2018) (Ballantyne *et al.* 2012, Friedlingstein *et al.* 2019). Permafrost aggregation and conservation is highly dependent on long-term climatic conditions, both directly via air temperature and indirectly by the presence or absence of insulating vegetation and snow cover (Johansson *et al.* 2013). Currently, these permafrost conditions are under threat by rapidly increasing global, and in particular Arctic air temperatures which have resulted in widespread permafrost warming in recent years (Biskaborn *et al.* 2019). Gradual permafrost losses of up to 70 % by 2100 in the uppermost 3 m are expected in a business-as-usual climate scenario (Chadburn *et al.* 2017, IPCC 2019), and even deeper if accounting for deep thermokarst-induced rapid thaw (Nitzbon *et al.* 2020), while rapid permafrost thaw is not considered at all (Turetsky *et al.* 2020a).

A special type of permafrost is the Yedoma ice complex deposit (in the following referred to as Yedoma), formed syngenetically by late Pleistocene deposition of fine-grained sediments with large volumes of ground ice. Yedoma is ice-rich (50-90 vol% ice) and usually has organic carbon contents of 2 to 4 weight percent with an estimated deposit thickness up to 40 m (Schirrmeister *et al.* 2013, Strauss *et al.* 2013). In Central Yakutia, the cryostratigraphic characteristics of these syngenetic Late Pleistocene deposits have been previously studied by various researchers (Soloviev 1959, Katasonov and Ivanov 1973, Katasonov 1975, Péwé *et al.* 1977, Péwé and Journaux 1983). In the context of global climate change, such high ice content with intrasedimental ice and syngenetic ice wedges render Yedoma deposits highly vulnerable to thaw induced landscape changes (Schirrmeister *et al.* 2013) and ground volume loss causing surface subsidence. Thawing leads to ground subsidence that is often associated with thaw lake development (Grosse *et al.* 2013). Thaw lake development, surface subsidence, lake drainage, and refreezing of the sediments result in a thermokarst basin landform called Alas in Central Yakutia (Soloviev 1973). During these thermokarst processes, the organic material stored within the permafrost becomes exposed to decomposition in the thaw bulbs (taliks) underneath the thermokarst lakes. It is subsequently released into the atmosphere as a result of microbial activity in unfrozen and aquatic conditions in form of gases such as carbon dioxide or methane, amplifying global climate change (Schuur *et al.* 2008). After a lake drainage event, the resulting thermokarst deposits in the Alas basins refreeze and the remaining Pleistocene soil carbon, as well as carbon from new plant biomass forming in thermokarst lakes and basins, becomes protected from decomposition again. The occurrence of these draining and refreezing processes can usually be determined by higher carbon content compared to the adjacent deposits (Strauss *et al.* 2013).

The resulting landscape patterns of Yedoma uplands and Alas basins form a heterogeneous landscape mosaic (Morgenstern *et al.* 2011). The heterogeneity and carbon characteristics

within these deposit types, especially below 3 m, are still poorly studied, as only very few studies examining long Siberian permafrost cores have been conducted (Zimov *et al.* 2006, Strauss *et al.* 2013, Shmelev *et al.* 2017). Studies from this area mostly examine natural Yedoma exposures as for example in the Batagay mega thaw slump (Ashastina *et al.* 2017). In Central Yakutia, several permafrost studies have been conducted, especially on thermokarst processes, related surface dynamics and temperature changes (Fedorov and Konstantinov 2003a, Ulrich *et al.* 2017a, Ulrich *et al.* 2017b, Ulrich *et al.* 2019). Other studies show a direct relation between dense vegetation cover and low permafrost carbon storage due to warmer permafrost conditions as a result of ground insulation (Siewert *et al.* 2015). Hugelius *et al.* (2014) estimate the carbon stock in the circumarctic permafrost region to be approximately 822 Gt carbon. However, despite the still high vulnerability of deeper deposits to thaw by thermokarst and thermo-erosion (Turetsky *et al.* 2019), only very few studies report organic carbon characteristics for permafrost deposits deeper than 3 m. This lack of data results in very high uncertainties for the impact of deep thaw in ice-rich permafrost regions and consequences for the carbon cycle (Kuhry *et al.* 2020).

By investigating deeper permafrost sediments in the continuous permafrost region of Central Yakutia, we aimed to understand the processes involved in organic carbon deposition and reworking in Yedoma and thermokarst deposits of this fast changing permafrost landscape (Nitze *et al.* 2018).

Our main research questions are: (1) What are the sedimentological processes that influenced the carbon stocks found in the Yedoma and Alas deposits of the Yukechi area?, and (2) How did the sedimentological processes affect the local carbon storage?

IV.3 Study site

The Yukechi Alas landscape (61.76495 °N; 130.46664 °E) covers an area of approximately 1.4 km² and is located on the Abalakh Terrace (~ 200 m above sea level) in the Lena-Aldan interfluve of Central Yakutia (Fig. IV-1a) (Ulrich *et al.* 2019). It is characterised by Yedoma uplands and drained Alas basins indicating active thermokarst processes (Fedorov and Konstantinov 2003a). Yedoma deposits cover 66.4 % of the area. The lakes cover about 13.0 % of the Yukechi Alas landscape, and approximately 20.6 % of the area consists of basins covered by grasslands, which contain Alas deposits (Fig. S-IV-1).

Today, Central Yakutia is characterised by an extreme continental subpolar climate regime with very low winter air temperatures down to minima of -63 °C in January (Nazarova *et al.* 2013). Holocene summer climate reconstructions indicate climate settings with slightly colder conditions (TJuly for 10,000 to 8,000 yr BP and 4,800 to 0 yr BP is 15.6 ± 0.7 °C,) compared to modern climate (TJuly is 16.6 to 17.5 °C) and a mid–Holocene warming phase between about 6,000 and 4,500 yr BP (TJuly ~ 1.5 °C higher than today) (Nazarova *et al.* 2013, Ulrich *et al.* 2017b). The contemporary mean annual air temperature in Central Yakutia (measured

at Yakutsk Meteorological Station) is -9.7 °C. The modern active layer thickness in Central Yakutia is approximately 1.5 m but it can be larger in grasslands, such as within Alas basins (about 2 m and more), and smaller below the taiga forest (less than 1 m) (Fedorov 2006). For the Yukechi Alas deposits, the active layer depth can be estimated at around 2 m and therefore reaches down into an observed talik, following Fedorov (2006). Taliks form because of a recent or already drained lake that prevented winter freezing, or an incomplete refreezing of the active layer.

The Yedoma deposits in this region can be more than 30 m in thickness as was already shown by older Russian works (Soloviev 1959, 1973). Lakes are found in partially drained basins as well as on the surrounding Yedoma uplands (Fig. IV-1b). The land surface within the Alas basins is covered by grasslands while the boreal forest found on the Yedoma uplands mainly consists of *Larix cajanderi* with several *Pinus sylvestris* communities (Kuznetsova *et al.* 2010, Ulrich *et al.* 2017b). Central Yakutian Alas landscapes are characterised by extensive land use (mainly horse and cattle herding and hay farming) (Crate *et al.* 2017).

Lake dynamics have been monitored at the Yukechi Alas study site for several decades by the Melnikov Permafrost Institute in Yakutsk (Bosikov 1998, Fedorov and Konstantinov 2003b, Ulrich *et al.* 2017a) and have partially been linked to local land use (Crate *et al.* 2017).

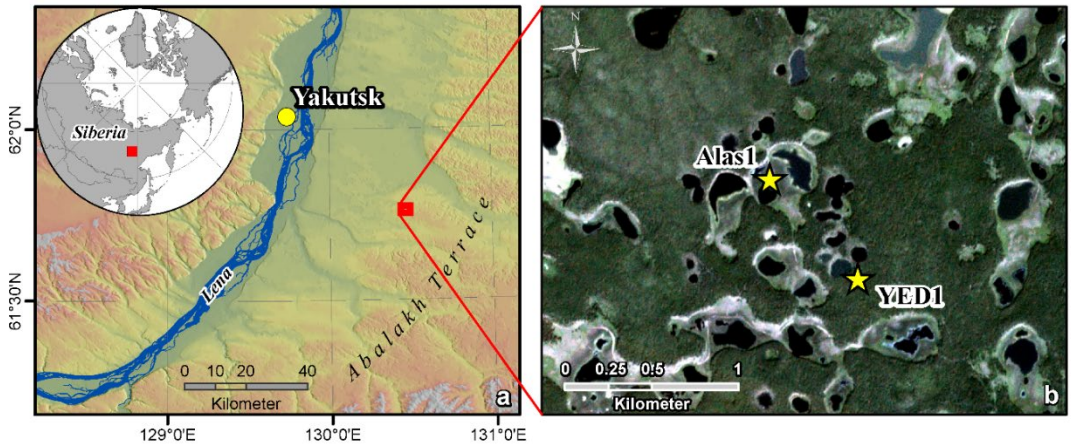

Figure IV-1 – Study site overview; a: location of the Yukechi Alas study site in Central Yakutia on the edge of the Abalakh Terrace (Circumpolar digital elevation model, Santoro and Strozzi, 2012); b: locations of the Alas1 and the YED1 coring site within the Yukechi Alas landscape (Planet OrthoTile, acquisition date: 7 July 2018; Planet Team (2017)).

IV.4 Methods

IV.4.1 Field work

Field work took place in March 2015 during a joint Russian-German drilling expedition. Two long permafrost sediment cores were obtained, one from Yedoma deposits and one from the adjacent drained Yukechi Alas basin (Fig. IV-1b). The surface of the Alas sample site (61.76490 °N, 130.46503 °E; h = 209 m above sea level) is located approximately 9 m lower than the surface of the sampled Yedoma site (61.75967 °N, 130.47438 °E; h = 218 m above

sea level) (Fig. IV-2). The distance between the two coring locations is 765 m. Both cores were drilled from dry land surface, kept frozen, and sent to Potsdam, Germany, for laboratory analysis. The Yedoma core (YED1) reached a depth of 22.35 m below surface (bs) and includes an ice wedge section from approximately 7.0 to 9.5 m bs. A talik section due to not completely refrozen active layer as identifies at 100 to 200 cm bs. The Alas core (Alas1) reached 19.80 m bs. A talik section was found in the Alas core reaching from approximately 160 down to 750 cm bs.

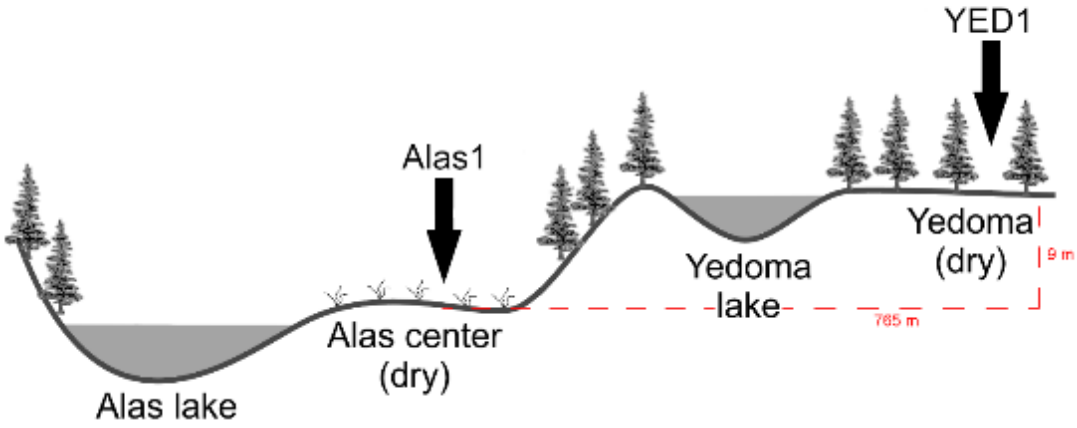

Figure IV-2 – Setting of the drilling locations for the Alas1 and YED1 cores showing distance and height difference between the locations (vertical scale exaggerated); the terms “Alas lake” and “Yedoma lake” are chosen after Ulrich et al., 2017a in accordance to the deposit type in which the thermokarst lakes are located; following Crate et al., (2017), the Yedoma lake can also be called “dyede” due to its development stage.

IV.4.2 Laboratory analysis

The frozen cores were split lengthwise using a band saw and were subsequently subsampled. Each subsample consisted of approximately 5 cm core material. Subsamples were equally distributed along the cores. According to visual changes, we covered all visible stratigraphic layers and we sampled at least every 50 cm in order to capture specific sediment properties. The samples were weighed and thawed. Intrasedimental ice or, if the sediment was unfrozen during drilling, intrasedimental water was extracted using artificial plant roots (Rhizones) consisting of porous material with a pore size of 0.15 µm and applied vacuum. In order to avoid evaporation, the samples were thawed at 4 °C inside their sample bags and sealed tightly after inserting the Rhizones. These water samples were then analysed for stable oxygen and hydrogen isotopes (see section IV.4.2.5). The ice wedge ice was subsampled using a saw for the analysis of stable oxygen and hydrogen isotopes.

IV.4.2.1 Ice content, bulk density, and subsampling

The weighed sediment samples were freeze-dried and weighed again afterwards for determining the absolute ice content in weight percent (wt%). We decided for the absolute ice content

as the gravimetric one, normalised with the dry sample weight, is not suitable for further calculations. Ice content within talik areas represents the water content, which froze after drilling. Bulk density was calculated from the absolute ice content, assuming an ice density of 0.9127 g/cm^3 at 0 °C and a mineral density of 2.65 g/cm^3 (Strauss *et al.* 2012).

IV.4.2.2 Elemental analyses

Subsamples used for elemental analyses were homogenised using a planetary mill (Fritsch Pulverisette 5). Subsamples were then weighed into tin capsules and steel crucibles for the elemental analyses. Total carbon (TC), total nitrogen (TN), and total organic (TOC) content were measured through combustion and analyses of resulting gases using a vario EL III and a varioMAX C Element Analyser. Results give the carbon and nitrogen amounts in relation to the sample mass used for analysis in wt%. The carbon nitrogen ratio (C/N) was calculated from the TN and TOC content. Besides showing an input signal, we used this ratio as a rough indicator for the state of degradation or source of organic matter. Assuming a constant source, a higher ratio indicates better-preserved organic matter (Stevenson 1994, Strauss *et al.* 2015).

IV.4.2.3 Magnetic susceptibility and grain size analysis

Subsamples taken for grain size analysis were first measured for mass specific magnetic susceptibility using a Bartington Magnetic Susceptibility Meter Model MS2 and a frequency of 0.465 kHz. This allows us to differentiate between different mineral compositions (Butler 1992, Dearing 1999). Values are given in SI units (10^{-8} m³/kg).

For grain size analysis, the samples were treated with hydrogen peroxide and put on a shaker for 28 days to remove organic material. The pH was kept at a reaction-supporting level between 6 and 8. Subsequently, the samples were centrifuged and freeze–dried. Of each sample, 1 g of each sample was mixed with tetra-Sodium Pyrophosphate 10–hydrate ($Na_4P_2O_7$*$10H_2O$) (dispersing agent) and dispersed in an ammonia solution. The grain size distribution and proportions were determined using a Malvern Mastersizer 3000 equipped with a Malvern Hydro LV wet–sample dispersion unit. Statistics of the grain size measurements were calculated using Gradistat 8.0 (Blott and Pye 2001). Results are used to identify different stratigraphic layers via material composition and to deduce sedimentary processes.

IV.4.2.4 Radiocarbon dating

Radiocarbon dating was done for nine samples using the Mini Carbon Dating System (MICADAS) at AWI Bremerhaven. We used bulk sediment samples for dating due to a lack of macro-organic remains within the deposits. The results were calibrated with the software Calib 7.1 (Stuiver *et al.* 2018) using the IntCal13 calibration curve (Reimer *et al.* 2013). Results are given in calibrated years before present (cal yr BP). The age–depth model was developed using the "Bacon" package in the R environment (Blaauw and Christen 2011) (Fig. S-IV-2).

IV.4.2.5 Stable isotopes

Besides showing a source signal (Meyers 1997), stable carbon isotopes can be used as a proxy for the degree of decomposition of organic material, as during decomposition and mineralization ^{12}C is lost, resulting in a higher share of ^{13}C and hence a higher $\delta^{13}C$ ratio (Fig. S-IV-3) (Diochon and Kellman 2008).

Twenty-three subsamples for $\delta^{13}C$ analysis were ground and carbonates were removed by treating the samples with hydrochloric acid for three hours at 97.7 °C. The samples were then vacuum-filtered, dried, and weighed into tin capsules for analysis. The stable carbon isotopes were measured using a Delta V Advantage Isotope Ratio MS supplement equipped with a Flash 2000 Organic Elemental Analyser. The results are compared to the Vienna Pee Dee Belemnite (VPDB) standard and given in per mille (‰) (Coplen *et al.* 2006) with an analytical accuracy of ≤ 0.15 ‰.

Stable hydrogen and oxygen isotopes can be used as a temperature proxy. Lower δ^2H and $\delta^{18}O$ values indicate lower temperatures during precipitation. Samples taken from the ice wedges generally yield a winter temperature signal (Opel *et al.* 2018), whereas pore ice and pore water signals are a mix of different seasons with a higher uncertainty due to alteration and fractionation during deposition and multiple freeze-thaw cycles as well as evaporation (Meyer *et al.* 2000).

Our δ^2H and $\delta^{18}O$ samples were measured at AWI Potsdam Stable Isotope Laboratory using a Finnigan MAT Delta-S mass spectrometer with the equilibration technique after Horita *et al.* (1989). In total, 29 samples were measured, of which 16 originated from YED1 pore ice, 8 originated from YED1 wedge ice, and 5 from Alas1 pore ice or pore water. The results are given in per mille related to standard mean ocean water (‰ vs. SMOW). The analytical accuracy for δ^2H was ≤ 0.8 ‰ and for $\delta^{18}O$ it was ≤ 0.1 ‰ (Meyer *et al.* 2000). The Deuterium excess (d excess) ($d=\delta^2H-8*\delta^{18}O$) was calculated as well from these values.

IV.4.2.6 Statistics and bootstrapping approach for carbon budget estimations

For the mean grain size, the mean of each core unit, consisting of several samples' mean values, is given. We estimated the carbon budget of the Yukechi Alas area after Eq. (1), using a bootstrapping approach. Bootstrapping is a statistical method to estimate the sample distribution using resampling and replacement (Crawley 2015). Resampling consists of drawing randomly selected samples from the dataset (i.e. BD and TOC) repeatedly (10,000 iterations), after which those values are fed into the formula. Replacement refers to the fact that the drawn samples in each iteration are available for all following iterations. We used combined BD and TOC values, as they are not independent. In addition, we corrected for irregular sampling by value replication according to depth interval so that values spanning larger intervals have a higher chance of being drawn. We calculated the mean and standard deviation of all iterations.

$$OC\ quantity\ (kt) = \frac{thickness \times coverage \times \frac{100-WIV}{100} \times BD \times \frac{TOC}{100}}{10^3} \quad (1)$$

with deposit thickness in m, coverage in m², wedge-ice volume (WIV) in vol%, BD in 10^3 kg/m³ and TOC in wt%. For all TOC values below the detection limit (0.1 wt%), a value of 0.05 wt% was set. Missing bulk density values, resulting from low ice contents (< 20 wt%) and therefore not fully ice-saturated sediments (Strauss *et al.* 2012), were calculated after Eq. (2), which describes the relation between TOC and bulk density in the examined cores. This had to be done for 9 samples in YED1 and 12 samples in Alas1 (see also Windirsch *et al.* (2019)).

$$bulk\ density = 1.3664^{-0.115 \times TOC} \quad (2)$$

The core length of the examined cores was assumed to represent the different ground types, resulting in a deposit thickness of 22 m for Yedoma deposits and 20 m for Alas deposits. A mean wedge-ice volume of 46.3 % for Central Yakutian Yedoma deposits and 7 % for Alas deposits of Central Yakutia was assumed following Ulrich *et al.* (2014) who determined average wedge-ice volumes for several deposit types in multiple locations in Siberia. We estimated the deposit coverage of Yedoma and Alas deposits using satellite imagery as shown in figure S-IV-1. The ice wedge in YED1 was excluded in the bootstrapping.

Bootstrapping calculations were done after Jongejans and Strauss (2020) for the upper 3 meters, the different core units as well as for the complete cores (table IV-2) using the "boot" package in the R environment. Bootstrapping included 10,000 iterations of random sampling with replacement. We used combined BD and TOC values, as they are not independent, and corrected for irregular sampling by value replication according to depth interval. We calculated the mean and standard deviation of all iterations.

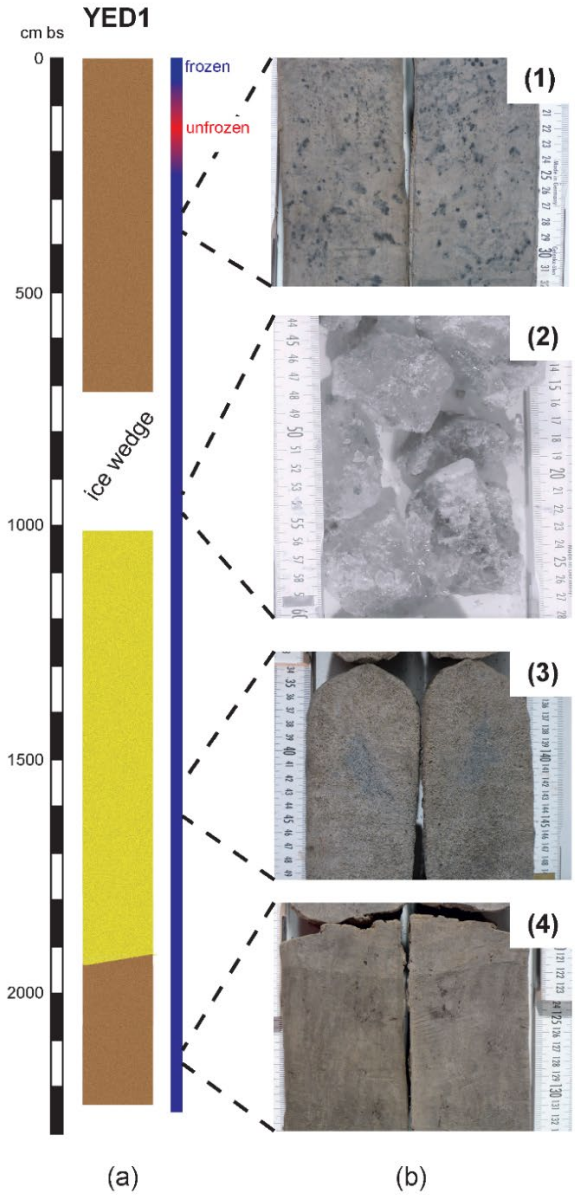

Figure IV-3 – a: overview of the Yedoma core; depth given in cm bs; state after core retrieval is given by colours: blue = frozen, red = unfrozen; location of the ice wedge is labelled; brown illustrates silty sediments, yellow represents sandy sediments; b: detailed pictures of the YED1 core; (1) 332–317 cm bs, picture of unit Y1 showing black organic-rich inclusions within the grey silty matrix; (2) 960–944 cm bs, picture of the wedge ice in Y2; (3) 1549–1532 cm bs, picture of Y3, showing the coarse sandy material with no visible cryostructures or organic material; (4) 2133–2117 cm bs, picture of Y4, showing the grey silty matrix with some dark organic dots.

IV.5 Results

IV.5.1 Characteristics of the Yedoma deposits

The Yedoma core YED1 visually appears rather heterogeneous (Fig. IV-3a) with material varying from fine gray material (Fig. IV-3b[1]) to sandy grayish brown material (Fig. IV-3b[3]) (Windirsch *et al.* 2020a). Between 2235 and 1920 cm bs and between 691 and 0 cm bs, brown to black dots up to 2 cm in diameter may be organic-rich material. Cryostructures include structureless to microlenticular ice and larger ice veins and bands. The core penetrated an ice wedge between 1005 and 691 cm bs, so we could take ice samples only. The core contains an unfrozen layer close to the surface between approximately 200 and 100 cm bs, representing a thin initiating talik layer underneath the 100 cm thick frozen active layer (Fig. IV-3a, red). All laboratory results are listed in detail in the PANGAEA repository (Windirsch *et al.* 2019).

We divided the Yedoma core into four main Yedoma units (Y) (Fig. IV-4). Y4 is the lowest (2235 to 1920 cm bs) and oldest (radiocarbon age of 49,323 cal yr BP)

stratigraphic unit. The absolute ice content slightly increased towards the surface (35.8 to 36.6 wt%, peak value of 53.6 wt% in between). MS also increased from 60.7 to 155.4 SI. The grain size was rather consistent with a mean value of 24.3 ± 3 µm and the soil texture varied between sand and silt (Fig. S-IV-4 and S-IV-5). We found TOC contents of up to 1.7 wt% (mean of 1.3 wt%). The C/N ratios within this unit varied between 9.2 and 10.6, and $\delta^{13}C$ values ranged between -25.27 and -24.66 ‰ vs. VPDB (Fig. S-IV-3). TN values only reached the detection limit of 0.1 wt% in 9 out of 36 samples in the whole YED1 core. As just these 9 samples exceeded the detection limit (highest value 0.16 wt% at 2036 cm bs), only they have been used for C/N ratio calculations.

The radiocarbon sample age of Y3 (between 1927 and 1010 cm bs) yielded an infinite age (> 49,000 yr BP) with ^{14}C below detection limit. There is a transition zone between Y4 and Y3 represented by a diagonal sediment boundary in the core between 1927 and 1920 cm bs (see Fig. IV-3a). Y3 showed distinctly lower absolute ice contents (< 32.1 wt%). MS varied between 120.5 and 285.0 SI. Higher sand contents (> 56.9 vol%) led to an increase in grain size (72.1 to 191.6 µm) with a mean grain size of 120.5 ± 35.5 µm. Grain size decreased down to 33.3 µm in the uppermost sample of Y3 and no detectable TOC was found in this unit.

Y2 (1010 to 714 cm bs) consisted of massive wedge ice, which contained very little sediment inclusions (Fig. IV-3b[2]). Thus, only water isotopes ($\delta^{2}H$ and $\delta^{18}O$) could be measured and analysed. The results are described in section IV.5.3.

Y1 (714 to 0 cm bs) is the uppermost and youngest unit with carbon ages ranging between 40,608 (589.5 cm bs) and 21,890 cal yr BP (157.5 cm bs). Ice content decreased from the ice wedge towards the surface ranging from 14.6 wt% (110 cm bs) to 57.4 wt% (688 cm bs). MS decreased towards the surface from 108.1 to 15.4 SI in the uppermost sample, with a maximum of 118.6 at 298 cm bs. This unit consisted of fine sediment with a mean grain size of 19.9 ± 4.2 µm. It contains up to 1.4 wt% TOC (298 cm bs). C/N values were in the range of 9.1 to 12.9. The lowest $\delta^{13}C$ value was found at 21 cm bs with -28.07 ‰ vs. VPDB; the lower part of this section showed a mean value of -24.42 ± 0.6 ‰ vs. VPDB.

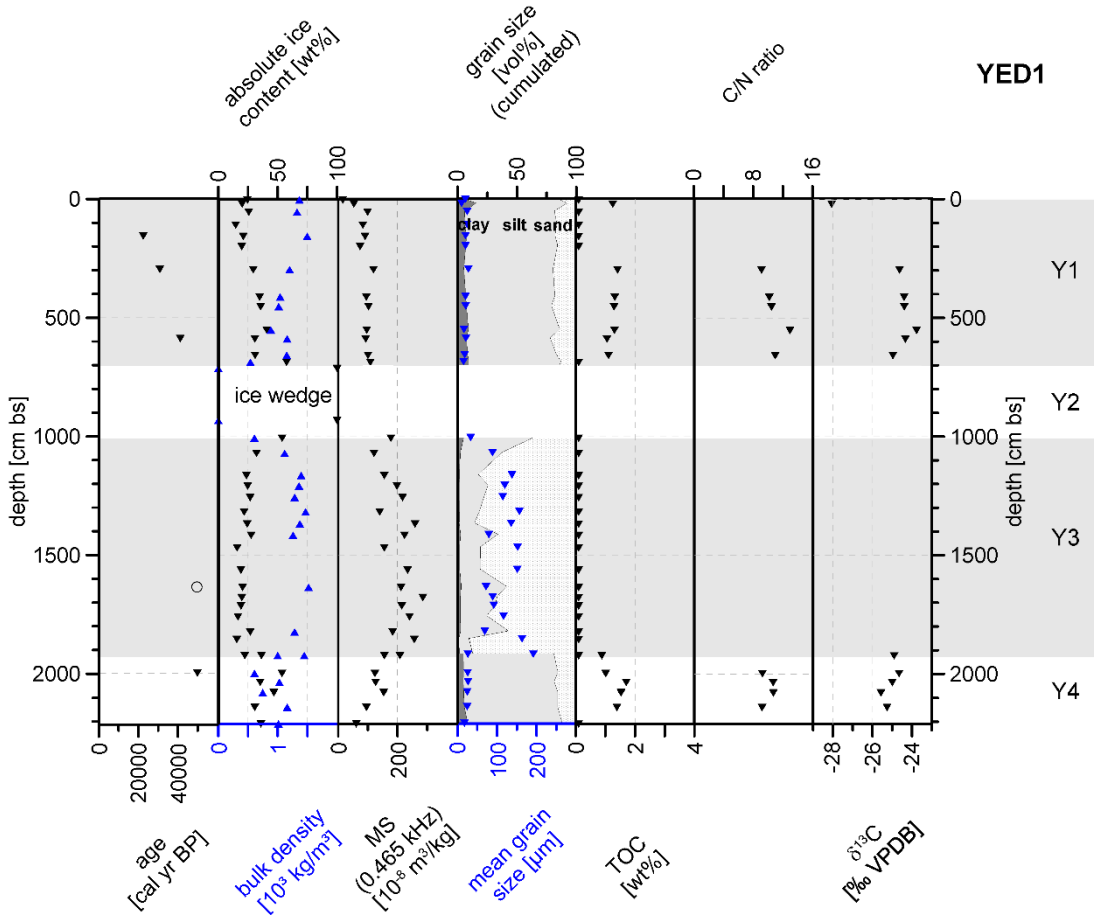

Figure IV-4 - Characteristics of the Yedoma core YED 1: radiocarbon ages, absolute ice content, bulk density, magnetic susceptibility (MS), grain size composition, mean grain size, total organic carbon (TOC) content, carbon-nitrogen (C/N) ratio and stable carbon isotope ($\delta^{13}C$) ratio; hollow circle indicates an infinite radiocarbon (dead) age; grey/white areas mark the different stratigraphic units (Y1 to Y4).

The grain size distributions (Fig. S-IV-5) illustrate the differences between the core units. Silt is the dominant grain size class in Y4 and Y1, whereas unit Y3 is dominated by sand.

The calibrated radiocarbon ages of the Yedoma deposits are listed in table IV-1 and assigned to the different core units. Our age–depth model (Fig. S-IV-2a) indicates a steep age-depth relationship from approximately 1200 to 2235 cm bs and a rather well defined, gradual age-depth relationship from 1200 cm bs towards the surface (Fig. S-IV-2a).

The bootstrapping approach resulted in a mean soil organic carbon (SOC) estimation of 4.48 ± 1.43 kg/m³ for the top 3 m of the YED1 core and a mean of 5.27 ± 1.42 kg/m³ for the entire core (table IV-2). We calculated a carbon inventory of 56.8 ± 15.2 kt for the Yukechi Yedoma deposits by upscaling the carbon storage to the complete Yedoma coverage in the Yukechi Alas landscape (66.4 %, ~ 917,000 m²) (Fig. S-IV-1).

IV.5.2 Characteristics of the Alas deposits

The Alas1 core contains a large proportion of unfrozen sediment (i.e. talik; ~ 750 to 160 cm bs) (Fig. IV-5a, red), which led to the loss of some core sections during drilling. The absolute

ice content given for samples retrieved from this zone represents absolute water content; samples were frozen directly after core recovery and field description. The core's visual appearance was more homogeneous compared to YED1 regarding colour (greyish brown) and material (clayish silt (Fig. IV-5b[2]) to sandy silt (Fig. IV-5b[4])) (Windirsch *et al.* 2020b). Cryostructures of the frozen core below 750 cm bs included horizontal ice lenses up to 5 cm thickness and structureless non-visible ice. Blackish dots and lenses (up to 1 cm in diameter) hint that organic material is included in the sediments. The frozen sediment of the uppermost 160 cm bs represents the seasonally freezing layer.

We divided the Alas1 core into four stratigraphic units (A1 to A4), according to soil texture and, if applicable, carbon content (Fig. IV-6). The oldest unit is A4 (1980 to 1210 cm bs) with radiocarbon ages of 42,865 cal yr BP (1967.5 cm bs) and 45,870 cal yr BP (1530.5 cm bs). An age inversion was detected here. Absolute ice content did not show a specific trend and ranged from 15.3 wt% at 1400.5 cm bs to 25.4 wt% at 1220 cm bs. MS ranged between 62.1 (1967.5 cm bs) and 133.9 SI (1759 cm bs) with much higher values in a sand intrusion found between 1530.5 and 1312 cm bs (266.7 at 1464 cm bs, 268.7 at 1400.5 cm bs). The mean grain size was constant (35.9 ± 36 µm) except for the sandy intrusion (152.9 µm at 1464 cm bs, 72.6 µm at 1400.5 cm bs), leading to a high standard deviation

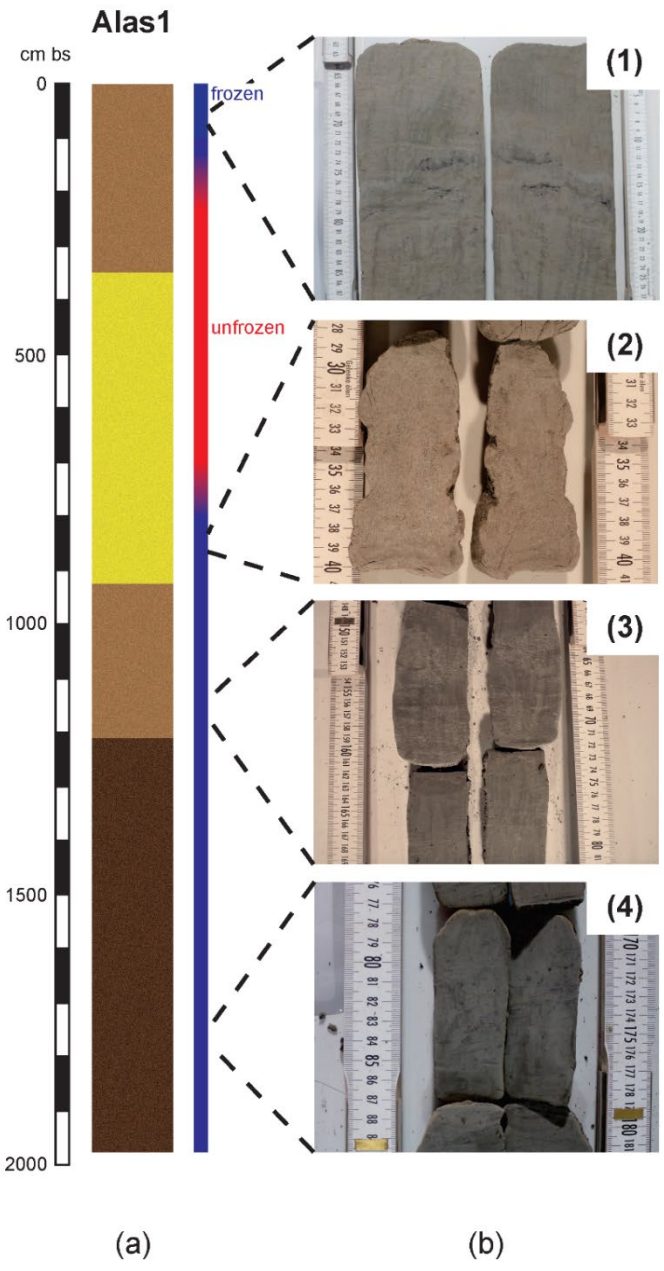

Figure IV-5 – a: overview of the Alas1 core; depth given in cm bs; state after core retrieval is given by colours: blue = frozen, red = unfrozen; light brown marks silty material, yellow marks sandy material, dark brown marks silty material containing more organic material; b: detailed pictures of the Alas1 core; (1) 88–64 cm bs, picture of A1 showing the silty grey matrix including dark organic structures; (2) 840–828 cm bs, picture of the sandy A2 unit; (3) 1169–1148 cm bs, picture of A3 showing a silty grey matrix with some darker organic dots; (4) 1781–1767 cm bs picture of the fine-grained silt-dominated A4 unit including black organic-rich inclusions.

(Fig. S-IV-4, S-IV-6). While TOC values were below detection limit within this sandy material, the other parts of A4 held TOC amounts of up to 1.8 wt% (1759 cm bs). The C/N ratio ranged between 5.8 (1274 cm bs) and 8.9 (1759 cm bs) with a mean value of 7.4 (Fig. S-IV-2). The $\delta^{13}C$ values showed a range of -25.67 to -24.06 ‰ vs. VPDB (Fig. S-IV-3). Only the TN values that exceeded the detection limit, which was the case in 8 out of 28 samples in the entire Alas1 core, have been used for C/N ratio calculations.

A3 ranged from 1210 to 925 cm bs. The absolute ice content was stable around 22.7 ± 2.9 wt%. MS increased towards the surface from 72.1 SI (1205.5 cm bs) to 122.6 SI (955 cm bs). A3 was characterised by less coarse material compared to A4 (Fig. S-IV-6), with a mean grain size of 19.7 ± 3.7 µm. All TOC values were below detection limit, so no C/N could be calculated and no $\delta^{13}C$ could be measured.

The characteristics of A2 (925 to 349 cm bs) were similar to those of the sand intrusion found in A4. A radiocarbon age of 27,729 cal yr BP was measured at 812.5 cm bs. The absolute ice content had a mean of 15.2 wt% and decreased from 16.7 wt% at 919.5 cm bs to 12.9 wt% at 395 cm bs. MS decreased upwards from 302.3 to 129.2 SI. The mean grain size at the bottom of this unit was 102.3 µm (919.5 cm bs), increased to 221.9 µm at 812.15 cm bs towards the surface, and reached the lowest value of 41.2 µm at the upper boundary of A2 (Fig. S-IV-6) with an overall mean of 108.0 ± 59.5 µm. All TOC values were below the detection limit.

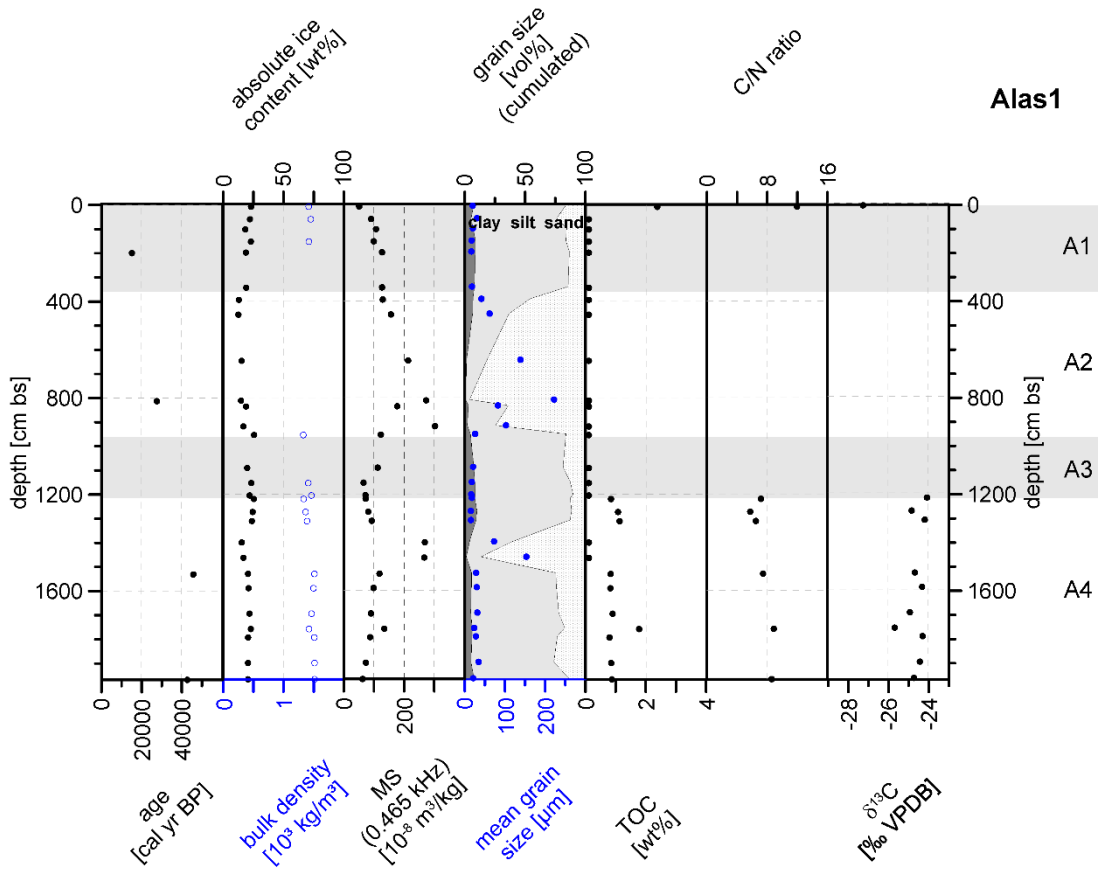

Figure IV-6 - Characteristics of the Alas1 core: radiocarbon ages, absolute ice content, bulk density, magnetic susceptibility (MS), grain size composition, mean grain size, total organic carbon (TOC) content, carbon-nitrogen (C/N) ratio and stable carbon isotope ($\delta^{13}C$) ratio; grey/white areas mark the different stratigraphic units (A1 to A4).

The uppermost stratigraphic unit A1 starts at 349 cm bs. It is the youngest unit of Alas1 with a radiocarbon sample at 199 cm bs dated to 15,287 cal yr BP. The absolute ice content slightly increased from 19.1 wt% (344.5 cm bs) to 23.1 wt% (9 cm bs) throughout this unit. MS decreased towards the surface, starting at 126.7 (344.5 cm bs) and reaching 50.8 at 9 cm bs. The mean grain size decreased again, compared to A2, representing silty material with values of $18.5^{+1.4}_{-1.6}$ µm. The mean grain size for this unit was 20.0 ± 4.6 µm. TOC was only detectable in the uppermost sample with a value of 2.4 wt% (9 cm bs). The C/N ratio for this sample was 12.0 and the $\delta^{13}C$ was -27.24 ‰ vs. VPDB.

The radiocarbon ages are listed in table IV-1. The age-depth model (Fig. S-IV-2b) shows a rather continuous slope for all calibrated ages of Alas1. Bootstrapping resulted in a mean SOC value of 6.93 ± 2.90 kg/m³ for the top 3 m of the Alas1 core (table IV-2). The calculation for the whole core resulted in a mean value of 6.07 ± 1.80 kg/m³ carbon. For the whole Alas area within the Yukechi Alas landscape (20.6 %, ~ 284,000 m²) (Fig. S-IV-1 [green]), we calculated a total organic carbon stock of 32.0 ± 9.6 kt using an estimated deposit thickness of 19.8 m.

IV.5.3 Water isotope analysis of the YED1 and Alas1 core

Stable hydrogen and oxygen isotope results are shown in figure IV-7. We found clear downward trends of $\delta^{18}O$ and $\delta^{2}H$ values becoming more negative between 1000 and 400 cm bs in the YED1 core (Fig. IV-7b). Below 1000 cm bs, both $\delta^{2}H$ and $\delta^{18}O$ become less negative with increasing depth. $\delta^{18}O$ ranged between -25.16 ‰ at the lowermost sample and -30.70 ‰ at 1071.5 cm bs with a much less negative value of -15.53 ‰ closest to the surface. While the uppermost Yedoma sample had a $\delta^{2}H$ value of -120.8 ‰, all other Yedoma samples showed much more negative values between -181.3 ‰ (2209.5 cm bs) and -221.6 ‰ (1071.5 cm bs). Values almost aligned with the global meteoric water line (GMWL), but partly also the local evaporation line (LEL) of Central Yakutia (Wetterich *et al.* 2008), except for the ice wedge samples of YED1 (Fig. IV-7a). The isotope data obtained from the ice wedge samples had more negative values for both $\delta^{2}H$ (-220.6 ‰ to -228.6 ‰) and $\delta^{18}O$ (-29.58 ‰ to -30.55 ‰) in comparison to the remaining YED1 core. The d excess values are lowest in the YED1 ice wedge (lowest value of 9.3). Other values range between 3.5 in the uppermost sample as an outlier and generally range between 14.7 and 29.5 with no clear trend visible.

Most of the Alas samples were too dry to extract pore water for water isotope analysis, resulting in a low number of water samples for this core (Fig. IV-7c). These Alas1 samples showed little variance in $\delta^{2}H$ and $\delta^{18}O$ data, ranging from -13.33 ‰ (103 cm bs) to -15.48 ‰ (1154 cm bs) for $\delta^{18}O$ and -130.4 ‰ (61 cm bs) and -137.6 ‰ (1464 cm bs) for $\delta^{2}H$. d excess values are lower towards the surface (-22.8 at 61 cm bs, -24.3 at 103 cm bs) and range from -14.1 to -12.2 in the lower core part.

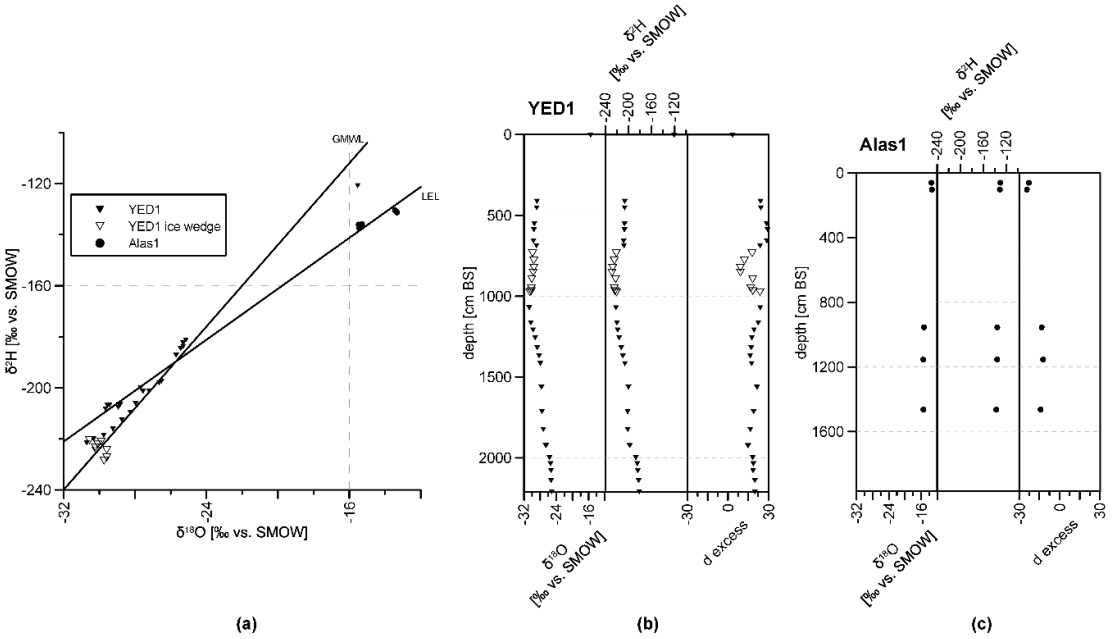

Figure IV-7 – The characteristics of water stable isotopes in the studied sediment cores; a: stable hydrogen (δ^2H) and oxygen ($\delta^{18}O$) isotope ratios of YED1 pore ice (black triangles), YED1 ice wedge ice (hollow triangles), and Alas1 pore ice and pore water (black dots) [‰ vs. SMOW]; global meteoric water line GMWL: $\delta^2H=8*\delta^{18}O+10$; local evaporation line LEL of Central Yakutia (based on data compiled until 2005 after Wetterich et al., 2008); b: oxygen isotopes, hydrogen isotopes and d excess values of YED1 plotted over depth; c: oxygen isotopes, hydrogen isotopes and d excess values of Alas1 plotted over depth.

IV.6 Discussion

IV.6.1 Carbon accumulation and loss at the Yukechi study site

We found surprisingly low TOC values in certain core sections of the Yedoma and Alas deposits. These low values appear in core sections with coarser sediments (fine sand), while the rather fine sediment layers (silt and sandy silt) store more TOC. The similarities in sediment structure and composition of the two cores, in particular between units Y1, Y4 and A4 in terms of grain size composition and OC content, and the increased accumulation rates towards the core bottoms (Fig. S-IV-2) indicate that the sedimentary sources regime was the same for both cores until approximately 35,000 cal yr BP (Fig. IV-4 and IV-6).

On the one hand, low TOC content could result from strong organic matter decomposition during accumulation or during a thawed state, especially in thermokarst deposits. On the other hand, it could reflect low carbon inputs. A suitable explanation for a low-input scenario is a change in the sedimentary regime due to fluvial transportation processes as is explained in more detail in chapter 5.2. The low stable carbon isotope data of our cores (between --24.06 and -27.24 ‰) are comparable to other studied sites from the Yedoma domain (Schirrmeister *et al.* 2013, Strauss *et al.* 2013, Jongejans *et al.* 2018). Our C/N data suggest a fairly homogeneous source signal of the organic material. Both cores show the lowest $\delta^{13}C$ values closest to the surface as the organic material is the most recent and therefore least decomposed. In deeper sections of the cores, $\delta^{13}C$ is higher (less negative) with no general

trend over depth in the Alas and Yedoma deposits. This indicates that the present material was already further decomposed when it became frozen. We see that decomposition ceased once the deposits froze; therefore $\delta^{13}C$ values do not show a clear trend at depth. The C/N ratios in both cores support this hypothesis and are in line with the results found by Strauss *et al.* (2015) and Weiss *et al.* (2016) for other Yedoma and Alas sites in Siberia. In comparison to the mean C/N ratio of 10 in YED1, the mean C/N ratio of 8 for Alas1 indicates that the Alas deposits are slightly more affected by decomposition due to their temporary thawed state during the lake phase. As the carbon was freeze-locked in the YED1 core the entire time since being frozen, it did not decomposed after deposition. The Yukechi C/N values are on the low end of C/N ratios known from other Yedoma deposits, e.g. from Bykovsky Peninsula (Schirrmeister *et al.* 2013) and Duvanny Yar (Strauss *et al.* 2012). The hypothesis of an input of organic-poor and already pre-decomposed material is supported by the fact that both cores, Alas1 and YED1, show low C/N ratios. The carbon characteristics indicate that the low carbon content results from low carbon input rather than decomposition in both cores, as no evidence for conditions favoring high decomposition rates is found. Therefore, low carbon content is likely not the result of strong decomposition during aquatic conditions of a lake-covered state, but a legacy of the source material. For a "decomposition during lake phase"-scenario, organic carbon parameters would differ largely in carbon content and isotope signature from those of the still-frozen Yedoma (Walter Anthony *et al.* 2014).

We found age inversions in both cores with similar age and depth (YED1 49,232 cal yr BP, 1998.5 cm bs; Alas1 42,865 cal yr BP, 1967.5 cm bs) (Fig. IV-4 and IV-6, Fig. S-IV-2) which is typical for many Yedoma sites (Schirrmeister *et al.* 2002). While cryoturbation might seem an obvious explanation, we suggest that this process did not play a major role here due to the long-term frozen state of YED1. Rather, we assume that the age inversions indicate a temporary shift in sediment input at approximately 35,000 cal yr BP. This could have caused some in-deposit reworking in the watershed and the incorporation of older material into younger sediments. In addition, the dating of bulk sediments very close to the maximum datable age of approximately 50,000 yr BP may cause a high uncertainty in the absolute ages of sediment layers (Reimer *et al.* 2013). Therefore, the rather small age inversions (> 49,000 cal yr BP to 49,232 yr BP in YED1, and 45,870 cal yr BP to 42,865 cal yr BP in Alas1) could be a result of material mixture in dated bulk samples. The radiocarbon ages above this age inversion align well with a simulated sedimentation rate, as shown in figure S-IV-2.

IV.6.2 Yedoma and Alas development

The differences in ice content between both cores and the homogeneous ice content throughout the whole Alas1 core indicate that thaw processes influenced the Alas deposit. As described above, this is supported by the water isotope signals, which are quite homogeneous throughout Alas1. This is the quantitative evidence that these deposits have been previously

thawed under thermokarst influence. The homogeneity in water isotopes is an outcome of percolating surface water during a thawed state. Subsequent talik refreezing in sandy sediments led to the formation of structureless pore ice, forming a taberal deposit (Wetterich *et al.* 2009). Refreezing, in our case, started from the surrounding frozen ground rather than from the surface, as a talik is still present in the upper core part. This allowed for the formation of structureless, invisible to microlenticular ice structures in the sandy material providing relatively large pore spaces (French and Shur 2010). Due to the formation of those small ice structures, no sediment mobilization by the formation of, for example, large ice bands occurred in this core, resulting in an unmixed and clearly layered sediment. This also excludes cryoturbational processes as an explanation for the age inversions that we found.

The perennially frozen conditions since incorporation into permafrost of the Yedoma deposits at YED1 are supported by the water isotope signals (Fig. IV-7) with much lower $\delta^{18}O$ values for the Yedoma pore ice in comparison to the uppermost sample (4 cm bs in YED1). The latter shows a water isotope signal reflecting very recent climate and freezing, thawing and evaporation processes in the active layer. If the Yedoma core had been thawed at some point, intruding water would have led to a more homogeneous oxygen isotope signal throughout the core as is obvious in the Alas core. Also, the intact ice wedge gives evidence for a perennially frozen state throughout the depositional history at YED1. The stable isotope ratio values of wedge ice (mean $\delta^{18}O$ of -30 ‰, mean $\delta^{2}H$ of -224 ‰) reflects winter precipitation and fits well into the regional pattern for Marine Isotope Stage (MIS) 3 ice wedges in Central and Interior Yakutia (Popp *et al.* 2006, Opel *et al.* 2019) while the d excess shows a much elevated value (16 ‰) compared to the regional pattern (Popp *et al.* 2006, Opel *et al.* 2019). The d excess values from the middle part of the ice wedge correspond well to the regional values from Mamontova Gora, Tanda and Batagay (Opel *et al.* 2019), while the others resemble those of the host sediments and are potentially overprinted by exchange processes between wedge ice and pore ice (Meyer *et al.* 2010). Due to the low number of datapoints, no meaningful co-isotopic regression was calculated. The stable isotope composition of pore ice shows a co-isotopic regression of $\delta^{2}H = 6.61\ \delta^{18}O - 18.0$ ($R^2 = 0.97$, $n = 23$), which is typical for Yedoma intrasedimental ice (Wetterich *et al.* 2011, 2014, 2016). The isotope values plot well above the regional Local Meteoric Water Line of the cold season (Papina *et al.* 2017), suggesting a substantial proportion of (early) winter precipitation – usually characterised by high d excess values – for the pore ice, which is also evident for some units of the Batagay megaslump (Opel *et al.* 2019). The decreasing trend of pore ice isotopic δ values from the bottom to the top indicates a general cooling in Central Yakutia during the time span covered by our study. However, as it is accompanied by an opposite increasing trend in d excess, these values may be overprinted by secondary freeze-thaw processes in the active layer and rather reflect the intensity of these fractionation processes (Wetterich *et al.* 2014).

The age-depth models of both cores show steep curves and higher sedimentation rates at the bottom of both cores, which slow down towards the surface (Fig. IV-4 and IV-6, Fig. S-IV-2). This indicates that during the early phase of the sediment accumulation (~ 45,000 to 35,000 cal yr BP), the depositional environment at Alas1 was the same as at YED1. The steepness of the age–depth model suggests an upward decrease in the accumulation rate or can be interpreted as an increase in surface erosion towards the top of the YED1 core (Figure S-IV-3a). Especially the sandy core part (Y3) accumulated rapidly, as indicated by the radiocarbon sample below dated to 49,232 cal yr BP (71.5 cm below the bottom of Y3) and the next radiocarbon sample above dated to 40,608 cal yr BP (420 cm above the top of Y3). These 917 cm of Y3 therefore accumulated in less than 8,600 years, while in Y1, the accumulation of 714 cm took more than 18,700 years (40,608 cal yr BP at 589.5 cm bs, 21,890 cal yr BP at 157.5 cm bs) (table IV-1). The continuous steepness of the age-depth model of Alas1 (Fig. S-IV-2b) suggests a rather constant accumulation rate throughout the deposition of these sediments.

Due to the alternation of coarse and carbon-poor material (i.e. Y3 and A2, see Fig. IV-4 and IV-6) with fine carbon-rich material (i.e. Y1 and Y4 in Fig. IV-4, A4 in Fig. IV-6), we suggest shifts in the sedimentary regime at the Yukechi study site (Soloviev 1973, Ulrich *et al.* 2017a, Ulrich *et al.* 2017b). This hypothesis is supported by the MS results, which give higher values for sandy core parts, hinting at a different material source, compared to the silty and carbon-bearing core units. Due to the great thickness of those sandy layers (core units 1 to 4, Fig. IV-4 and IV-6), the most suitable explanation is material transport by tributaries on top of the (former) Yedoma uplands of the Abalakh Terrace. We interpret this to mean that the sandy material in the studied cores was deposited during the river-connected flooding phases at our study site. Moreover, fluvial transport gives a suitable explanation for low carbon content as organic matter decomposition is often much higher under aquatic conditions (Cole *et al.* 2001). Furthermore, high flow velocity allow larger particles to be deposited, but keeps lighter particles, like organic material, in suspension (Anderson *et al.* 1991, Wilcock and Crowe 2003, Reineck and Singh 2012).

Another explanation for the occurrence of these carbon-poor sandy layers are shifts in wind direction and wind speed and therefore the sediment carrying capacity of the wind (Pye 1995). A shift in eastern Siberian climate during the beginning of the Kargin interstadial (MIS 3, ~ 50,000 yr BP) resulted in higher winter temperatures (Diekmann *et al.* 2017) and therefore higher pressure gradients within the atmosphere, leading to greater wind speeds. This in turn resulted in higher sediment carrying capacity of the wind which provides a suitable explanation for the sediment differences. Also, sand dunes of the Lena River valley (Huh *et al.* 1998) could have provided sufficient sandy material throughout the formation of the sand layers found in the Yukechi deposits (Y3 and A2 in Fig. IV-4 and IV-6). The radiocarbon ages of these coarser core segments (Y3 and A2 in Fig. IV-4 and IV-6) dated between 39,000 and 18,000 cal yr BP

match the timing of these climatic changes. Increased wind speeds at the beginning of a warmer interstadial phase during the MIS 3 (Karginian climate optimum, 50,000 to 30,000 yr BP) and a subsequent decrease in wind speed during the colder stadial MIS 2 are a suitable explanation (Diekmann *et al.* 2017). Those increased wind speeds could have led to further transport of the coarser material from the source area, enabling these materials to reach our study area (Anderson *et al.* 1991).

From our data we see that the sandy layers were deposited in approximately 7,000 yr (radiocarbon dates below and above these layers). As the sediments are rather coarse (115.3 µm mean grain size), a fluvial deposition is more likely than an aeolian deposition (Strauss *et al.* 2012). Moreover, the lack of organic material makes fluvial deposition the more plausible process. Thus, we think that periodic flooding events of Lena River tributaries near our study area are a more likely source for the sediments. The original Yedoma deposits of the Yukechi area were most likely formed by deposition of silty sediments and fine organic material during seasonal alluvial flooding. The climatic changes (Diekmann *et al.* 2017, Murton *et al.* 2017) and the resulting higher water availability during the deposition period of the sandy layers may have caused changes in fluvial patterns on the Abalakh Terrace. More water could cause higher flow velocities under warmer climatic conditions and therefore increased erosive power, leading to the formation of new flow channels (Reineck and Singh 1980).

With a climatic backshift to colder conditions during MIS 2, water availability decreased and silty organic-bearing material was again deposited by seasonal flooding on top of the sandy layers. This likely led to lake initiation on top of the Yedoma deposits. The underlying ground began to thaw and subside, forming the Yukechi Alas basin. During this process, ice was lost from the sediment and the ground subsided by at least 9 m (height difference of 9 m between YED1 and Alas1 surface). Surface or lake water was able to percolate through the unfrozen sediments. This is revealed by the homogeneous water isotope signal that is similar to the YED1 surface sample (Fig. IV-7). Under the unfrozen aquatic conditions in the sediment, microbial activity started, resulting in the decomposition of the already small amount of organic material (Cole *et al.* 2001). When the lake drained, the sediments started to refreeze both upward from the underlying permafrost and downward from the surface, leaving a talik in between (Fig. IV-5). The subsided ground indicates that core unit A4 (Fig. IV-6) lies beneath the lowest unit of the Yedoma core, Y4 (Fig. IV-4), while units A1 to A3 shrank due to thawing from approximately 2200 to 1200 cm length. The presence of large ice wedges in the area supports this theory of ground subsidence during thaw as it hints to large excess ice contents of the ground (see Fig. S-IV-7) (Soloviev 1959). These subsidence processes might represent the future path of the Yukechi Yedoma deposits, as already an initiating talik of approximately 150 cm thickness was found at the YED1 site (Fig. IV-3a). This is caused by ground temperature

warming which itself is affected by snow layer thickness and air temperatures and more, and could lead to Alas development (Ulrich *et al.* 2017a).

IV.6.3 Central Yakutian Yedoma deposits in a circumarctic and regional context

Strauss *et al.* (2017) report a mean organic carbon density for the upper 3 m of Yedoma deposits in the Lena-Aldan interfluve of 25 to 33 kg/m³ based on data of Romanovskii (1993) and Hugelius *et al.* (2014). Using a bootstrapping approach (Jongejans and Strauss 2020) we found a much lower organic carbon density of 4.48 ± 1.43 kg/m³ for the top 3 m of the YED1 core. For Alas1, an organic carbon density of 6.93 ± 2.90 kg/m³ was calculated for the top 3 m. Taking both the area covered by each deposit type within the Yukechi Alas landscape and the ice wedge volumes estimated by Ulrich *et al.* (2014) (see section IV-3 and Fig. S-IV-2) into account, we find a mean organic carbon density of only 4.40 kg/m³ for the top 3 m of dry soil at the Yukechi study site. This landscape scale carbon stock density includes the entire study area (1.4 km²), including all water bodies (approximately 0.18 km²), which we assumed to contain no soil carbon. This means that both the average Yukechi site carbon density and our individual cores' carbon densities are substantially below the range (25 to 33 kg/m³) reported by Strauss *et al.* (2017). This strong difference between previously published and our new data from the same region can only be explained by high depositional heterogeneity of the Central Yakutian permafrost landscapes that was not represented in the earlier dataset of Strauss *et al.* (2017) in sufficient detail. Geographically, the Yukechi area is located in one of the southernmost Yedoma areas in the Yedoma domain, which could be a reason for the differences to previously studied Arctic deposits (Schirrmeister *et al.* 2013, Strauss *et al.* 2013, Jongejans *et al.* 2018). Results of Siewert *et al.* (2015) for the Spasskaya Pad/Neleger site in a similar setting also differ greatly from our findings at the Yukechi site, showing carbon densities of approximately 19.3 kg/m³ for the top two meters of larch forest-covered Yedoma deposits and approximately 21.9 kg/m³ for the top two meters of grassland-covered Alas deposits in a setting similar to the Yukechi site.

In general, Yedoma deposits are estimated to hold 10 +7/-6 kg/m³ for the whole column within the Pleistocene Yedoma deposits (approximate depth of 25 m) (Strauss *et al.* 2013). Jongejans *et al.* (2018) calculated a larger organic carbon stock of 15.3 ± 1.6 kg/m³ for Yedoma deposits found on the Baldwin Peninsula in Alaska. Another study by Shmelev *et al.* (2017) stated a Yedoma carbon stock of 14.0 ± 23.5 kg/m³ for a study region in northeastern Siberia between the Indigirka River and the Kolyma River.

Assessing the carbon inventory of the full-length Central Yakutian cores examined in this study, we estimated an organic carbon density of 5.27 ± 1.42 kg/m³ for the sediments of the YED1 core down to a depth of 22.12 m bs, excluding the ice wedge. The organic carbon density within the Yukechi Yedoma is approximately two to three times lower than estimated in previous studies of deep Yedoma deposits (Strauss *et al.* 2013, Shmelev *et al.* 2017, Jongejans *et*

al. 2018). Even when including roughly 10 m of organic carbon-free material, the higher carbon densities for the whole cores (compared to the carbon densities of the first 3 m) show that large portions of organic carbon are stored below 3 m. The Alas1 core contains slightly more organic carbon with a mean value of 6.07 ± 1.80 kg/m³ organic carbon for the whole core (19.72 m), which is about 20 % of the mean thermokarst deposit carbon content of 31 +23/-18 kg/m³ stated by Strauss *et al.* (2017). Within the Alas core, organic carbon storage is slightly higher in the top 3 m (approximately 14 % more than below). This likely is a result of former lake coverage that led to accumulation of organic-richer lake sediments found in the upper part of Alas1. Most likely there was enhanced growth of aquatic plants along with a reduction in decomposition of the input organic material due to anaerobic conditions during the lake phase.

IV.7 Conclusions

We conclude that low organic carbon contents encountered in sections of both cores are not caused by decomposition of originally high organic matter contents but rather are a legacy of the accumulation of organic-poor material during the late Pleistocene MIS 3 and MIS 2 periods. The most likely landscape scenario causing the differences in sediment and organic carbon characteristics during the Pleistocene deposition is the temporary existence of tributary rivers on the Abalakh Terrace with varying flow velocities and alternating paths as a result of climatic changes or local landscape dynamics. While with the onset of the Holocene the sedimentation on the Yedoma upland ceased, the Alas was affected by thaw, subsidence and lake formation processes, resulting in a compaction of sediments in situ as well as causing higher C inputs under lacustrine conditions in the upper parts of the sediments.

We further show that the Yedoma deposits at this site down to a depth of 22 m are characterised by rather low organic carbon contents, often less than 1 wt% TOC, resulting in a mean C density of only ~ 5 kg/m³.

Hence, the studied Yukechi Yedoma deposits store less carbon than other, comparable Yedoma Ice Complex deposits in the Central Yakutian area. However, there have been comparatively few studies on this so far. The biogeochemical impact of permafrost thawing in the Yukechi area might therefore be smaller than generally assumed for Yedoma deposits, as this area does not feature the high carbon stock estimates and high ice contents of other previously studied localities in Central Yakutia and elsewhere in the Arctic.

The permafrost characteristics found in the Alas core reveal that its composition and stratigraphy before lake formation and disappearance was very similar to the Yedoma core material. Its past development including thaw, the loss of old ice and surface subsidence, along with sediment compaction, shows a possible pathway for the Central Yakutian Yedoma deposits under the influence of global climate change.

IV.8 Data availability

The measurement data and laboratory results are available via PANGAEA at https://doi.org/10.1594/PANGAEA.898754 (Windirsch *et al.* 2019). A detailed core log is available for YED1 at https://doi.org/10.1594/PANGAEA.914874 and for Alas1 at https://doi.org/10.1594/PANGAEA.914876 (Windirsch *et al.* 2020a; b).

IV.9 Author contribution

JS designed the study concept. TW conducted the laboratory work, analysed the laboratory results, prepared the graphics, and led the writing of this paper. GG and AF led the drilling expedition in 2015. JS, MU, and PK participated in the drilling fieldwork. GG and JS supervised the data analyses and provided expertise on thermokarst processes and cryostratigraphy. LS provided expertise on grain size characteristics and Central Yakutian permafrost genesis. MF designed the maps and provided expertise on Yedoma and thermokarst-affected carbon. LJ developed the bootstrapping routine and provided expertise on carbon stock upscaling. JW developed the age-depth models and worked on age calibration and contextualization. TO interpreted the water isotope results and provided context for the isotope data. JS took part in the laboratory work and provided expertise in permafrost carbon processes. All authors contributed to commenting and editing the manuscript.

IV.10 Competing interests

The authors declare no conflict of interests.

IV.11 Acknowledgements

This study is based on a joint field campaign of the ERC PETA-CARB project (Starting Grant #338335) and the DFG project UL426/1-1 and was carried out in cooperation with the Melnikov Permafrost Institute, Siberian Branch of Russian Academy of Sciences. TW was funded by the PoGS and LJ was funded by the DBU. The field campaign was supported by Avksentry P. Kondakov. We thank Dyke Scheidemann (Carbon and Nitrogen Lab [CarLa]) as well as Mikaela Weiner and Hanno Meyer (Stable Isotope Lab) from AWI for assistance in the laboratory. Planet data were provided freely through Planet's Education and Research program. We thank Candace O'Connor for language correction.

Table IV-1 – Radiocarbon measurement data and calibrated ages for YED1 and Alas1 bulk organic material samples.

core	mean sample depth [cm bs]	^{14}C age [yr BP]	± [yr]	$F^{14}C$	± [%]	calibrated ages (2 σ)* [cal yr BP]	mean age [cal yr BP]	core unit	AWI no.
YED1	157.5	18064	104	0.1055	0.83	21582-22221	21890	Y1	1543.1.1
	298	25973	88	0.0394	1.09	29822-30640	30268	Y1	1544.1.1
	589.5	35965	184	0.0114	2.29	40116-41118	40608	Y1	1545.1.1
	1636	>49000	n/a	0.0017	6.66	n/a	n/a	Y3	1547.1.1
	1998.5	45854	501	0.0033	6.23	48202-calib. limit	49232	Y4	1548.1.1
Alas1	199	12826	57	0.2026	0.70	15144-15548	15287	A1	1549.1.1
	812.5	23615	151	0.0529	1.88	27478-27976	27729	A2	1550.1.2
	1530.5	42647	364	0.0049	4.53	45172-46619	45870	A4	1551.1.1
	1967.5	39027	251	0.0078	3.12	42478-43262	42865	A4	1552.1.1

* calibrated using Calib 7.1 (Stuiver *et al.* 2018) equipped with IntCal 13 (Reimer *et al*. 2013)

Table IV-2 – SOC contents for the individual core units, based on the bootstrapping results; calculations were done for 1 m²; the measurement data used in the bootstrapping approach (bulk density, TOC density) are provided in the data sheet in the PANGAEA repository; * refers to samples with TOC content < 0.1 wt%; for organic carbon pool calculations, we assumed a TOC of 0.05 wt% for these samples; note: we excluded unit Y2 in the calculations.

core	depth [cm bs]	number of samples used in bootstrapping	mean dry bulk density [10^3 kg/m³]	mean TOC content [wt%]	mean SOC content (bootstrapping results) [kg/m³]
YED1	0 – 300	7	1190	0.42	4.48 ± 1.43
	0 – 714 (unit Y1)	13	1090	0.59	8.31 ± 1.41
	1010 – 1927 (unit Y3)	18	1172	0.10	0.86 ± 0.32
	1927 – 2235 (unit Y4)	5	910	1.14	11.50 ± 1.36
	total core	36	1105	0.46	5.27 ± 1.42
Alas1	0 – 300	5	1257	0.51	6.93 ± 2.90
	0 – 349 (unit A1)	6	1214	0.44	5.00 ± 2.55
	349 – 925 (unit A2)	6	998	0.05*	0.50 ± 0
	925 – 1210 (unit A3)	4	1299	0.05*	0.66 ± 0.01
	1210 – 1980 (unit A4)	12	1377	0.83	11.03 ± 1.62
	total core	28	1250	0.47	6.07 ± 1.80

Appendix II What are the effects of herbivore diversity on tundra ecosystems? A systematic review (Abstract)

This manuscript assesses the effects of herbivory and herbivore diversity on tundra ecosystems in form of an excessive systematic literature review. It was initiated by researchers from the CHARTER and the TUNDRAsalad project.

What are the effects of herbivore diversity on tundra ecosystems? A systematic review

Barbero-Palacios, L.[1], Barrio, I. C.[1], Axmacher, J. C.[1,2], Bartra, L.[3], Björnsdóttir, K.[4], Bjørkås, R.[3], Deforneaux, M.[1], García Criado, M.[5], Gilg, O.[6,7], den Herder, M.[8], Hik, D. S.[9], Hwang, B. C.[10], Kaarlejärvi, E.[11], Kater, I.[12], Kolari, T. H. M.[13], Kristensen, J. A.[14], Kuoppamaa, M.[15,16], Lameris, T. K.[17], Leffler, A. J.[18], Myers-Smith, I.[5], Pagneux, E. P.[1], Petit Bon, M.[19], Ramsay, J. S.[20], Serrano, E.[21], Skarin, A.[22], Soininen, E. M.[23], Sokolova, N.[24,25], Speed, J. D. M.[26], Tuomi, M.[23,27], Wheeler, H.[20], Windirsch, T.[28]

[1]Faculty of Environmental and Forest Sciences, Agricultural University of Iceland, Árleyni 22, Keldnaholt, IS-112 Reykjavík, Iceland

[2]UCL Department of Geography, University College London, London, UK

[3]Centre for Biodiversity Dynamics, Department of Biology, Norwegian University of Science and Technology, 7491 Trondheim, Norway

[4]Department of Biological and Environmental Sciences, University of Gothenburg, P.O. Box 461, 405 30 Gothenburg, Sweden

[5]School of GeoSciences, University of Edinburgh, Edinburgh, Scotland, UK

[6]UMR 6249 Chrono-environnement, CNRS, Université de Franche-Comté, 16 route de Gray, 25000 Besançon, France

[7]Groupe de Recherche en Ecologie Arctique, 16 rue de Vernot, 21440 Francheville, France

[8]European Forest Institute, Joensuu, Finland

[9]Department of Biological Sciences, Simon Fraser University, Burnaby, BC, V5A 1S6, Canada

[10]Department of Physical Geography and Ecosystem Science, Lund University, Sölvegaten 12, 22362 Lund, Sweden

[11]Organismal and Evolutionary Research Programme, University of Helsinki, FI-00014 Helsinki, Finland

[12]Scott Polar Research Institute, University of Cambridge, Cambridge, UK

[13]Department of Environmental and Biological Sciences, University of Eastern Finland, P.O. Box 111, FI-80101, Joensuu, Finland

[14]Environmental Change Institute, School of Geography and the Environment, University of Oxford, Uxford, UK

[15]School of Environmental Sciences, University of Liverpool, Liverpool, UK

[16]Arctic Centre, University of Lapland, Rovaniemi, Finland

[17]Department of Coastal Systems, Royal Netherlands Institute for Sea Research (NIOZ), Den Burg, The Netherlands
[18]Department of Natural Resource Management, South Dakota State University, Brookings, South Dakota, USA
[19]Department of Wildland Resources, Quinney College of Natural Resource and Ecology Center, Utah State University, UT-84322 Logan, Utah, USA
[20]Anglia Ruskin University, East Road, Cambridge, CB1 1PT, UK
[21]Wildlife Ecology & Health Group (WE&H) and Servei d'Ecopatologia de Fauna Salvatge (SEFaS), Departament de Medicina I Cirurgia Animals, Facultat de Veterinària, Universitat Autònoma de Barcelona (UAB), 08193 Bellaterra, Barcelona, Spain
[22]Department of Animal Nutrition and Management, Swedish University of Agricultural Sciences, Uppsala, Sweden
[23]Department of Arctic and Marine Biology, UiT The Arctic University of Norway, Tromsø, Norway
[24]Arctic Research Station, Institute of Plant and Animal Ecology, Ural Branch of Russian Academy of Sciences, Zelenaya Gorka Str. 21, 629400 Labytnangi, Russia
[25]Arctic Research Center of the Yamal-Nenets Autonomous District, Salekhard, Russia
[26]Department of Natural History, NTNU University Museum, Norwegian University of Science and Technology, 7491 Trondheim, Norway
[27]Section of Ecology, Department of Biology, University of Turku, Turku, Finland
[28]Alfred Wegener Institute Helmholtz Centre for Polar and Marine Research, Permafrost Research Section, Potsdam, Germany

In preparation for Environmental Evidence, planned submission in 10/2023

VI.1 Abstract

Northern ecosystems are strongly influenced by herbivores, but differences in their diet composition, behaviour and energy requirements lead to contrasting impacts on ecosystem functioning by different species of herbivores. In some cases, the effects of herbivores can compensate each other but in others, the combined effects of herbivores can lead to stronger, directional changes. However, until recently, the diversity of herbivore assemblages has been largely overlooked when assessing plant-herbivore-soil interactions. Considering the rapid changes in Arctic herbivore communities in response to ongoing environmental and land use changes, with increased influx of boreal species and changes in the distribution and abundance of arctic herbivores, a better understanding of the consequences of changes in the diversity of herbivore assemblages is needed. This systematic review synthesises available evidence on the effects of herbivore diversity on different ecosystem processes, functions, and properties of tundra ecosystems.

This systematic review followed a published protocol and includes primary field studies retrieved from databases, search engines and specialist websites, that compare responses of

tundra ecosystems to different levels of herbivore diversity, including vertebrate and invertebrate herbivores. We used the richness of functional groups of herbivores as a measure of the diversity of the herbivore assemblages. Studies were screened at title, abstract and full-text, and inclusion followed pre-defined eligibility criteria based on their target population, exposure, comparator and study design. The review covered terrestrial Arctic ecosystems including the forest-tundra ecotone, and outcomes included multiple processes, functions and properties of tundra ecosystems. The validity of the studies was critically appraised and meta-analysis was performed where studies reported similar outcomes.

The searches retrieved 5944 articles. After screening titles, abstracts and full texts, 205 articles including 3992 studies (i.e., separate comparisons) were considered relevant for the systematic review. The distribution of studies across the tundra biome was geographically biased, with most studies concentrated around well-established research locations. Most studies focused on the effects of a single herbivore species, while only a few studies specifically addressed the separate and combined effects of different herbivore species. The majority of studies focused on impacts of vertebrate herbivores on different aspects of arctic tundra vegetation, while other ecosystem processes, functions and properties have received less attention.

The available knowledge on the effects of herbivore diversity is relatively limited, and mainly refers to their impacts on vegetation, so the consequences of ongoing changes in herbivore communities on tundra ecosystems may be difficult to forecast. Future studies should explicitly address the role of herbivore diversity to understand the responses of tundra ecosystems to ongoing environmental changes.

Appendix III Supplementary material to chapter 2: Large Herbivores on Permafrost – a Pilot Study of Grazing Impacts on Permafrost Soil Carbon Storage in Northeastern Siberia

Supplementary table S2-1 – Radiocarbon measurement data and dates.

site	mean sample depth [cm bs]	material	^{14}C age [yr BP]	± [yr]	$F^{14}C$	± [abs]	calibrated ages (2σ)* [cal yr BP]	mean age [cal yr BP]	AWI no.
B3	27.75	plant/wood	141	16	0.9826	0.002	58 – 118	111	6742.1.1
	45.5	plant/wood	899	18	0.8941	0.002	733 – 801	789	6743.1.1
	64	plant/wood	3157	18	0.675	0.0015	3350 – 3412	3384	6744.1.1
	106	plant/wood	9356	24	0.312	0.0009	10499 – 10609	10568	6745.1.1
B2	21.25	plant/wood	2081	17	0.7717	0.0017	1993 – 2110	2038	6746.1.1
	64	plant/wood	2300	17	0.751	0.0016	2311 – 2351	2338	6747.1.1
	77	plant/wood	2765	18	0.7088	0.0016	2782 – 2886	2854	6748.1.1
	106	plant/wood	3382	18	0.6564	0.0014	3569 – 3664	3616	6749.1.1
B1	26.25	plant/wood	modern		1.0263	0.002			6750.1.1
	76	plant/wood	3487	18	0.6479	0.0014	3695 – 3781	3761	6751.1.1
	112.5	plant/wood	3879	18	0.617	0.0014	4242 – 4407	4327	6752.1.1
	124	plant/wood	4533	20	0.5688	0.0014	552 – 5188	5154	6753.1.1
U3	26.25	plant/wood	modern		1.0262	0.002			6754.1.1
	58.5	plant/wood	8643	23	0.341	0.001	9539 – 9633	9588	6755.1.1
	82.5	bulk	27748	417	0.0316	0.0016	31105 – 32971	31779	6756.1.1
	112	bulk	30099	563	0.0236	0.0017	33267 – 35673	34564	6757.1.1
U1	27	plant/wood	191	16	0.9766	0.0019	162 – 218	183	6758.1.1
	71	plant/wood	6355	21	0.4533	0.0012	7251 - 7323	7278	6759.1.1

*calibrated using Calib 8.2 (Stuiver et al., 2021) equipped with IntCal20 (Reimer et al., 2020)

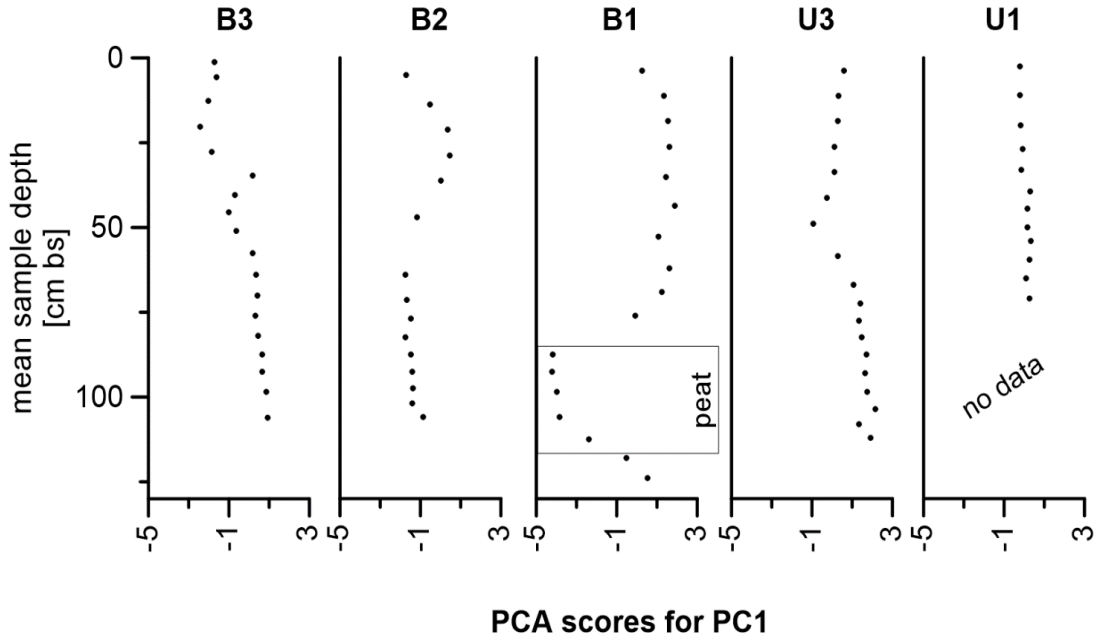

Supplementary figure S2-1 – PCA scores (PC1) for all five sampling sites plotted over depth; the peat layer in B1 is marked to underline the strong differences in score values for this core section.

Supplementary table S2-2 – PCA scores of all samples for PC1, PC2 and PC3.

sample	PC1	PC2	PC3
B3 0 - 2.5 cm	-1.72828936822952	0.79456126167141	-0.61482725290452
B3 2.5 - 9 cm	-1.61378417246138	0.836613877279835	-0.460232049621469
B3 9 - 16.5 cm	-2.02584215117961	0.484916847416413	-0.408520198467624
B3 16.5 - 24 cm	-2.43468671841201	0.360133437721508	-0.182853221506374
B3 24 - 31.5 cm	-1.85797896541634	0.586104578654619	0.0297473834549391
B3 31.5 - 38 cm	0.164611578748646	-1.26416459186833	-0.159666354741859
B3 38 - 43 cm	-0.703894321779553	-0.617433511767476	-0.36363440711776
B3 43 - 48 cm	-0.99578554193291	-0.479524510773411	-0.446574157450325
B3 48 - 54 cm	-0.641363436186067	-0.427401531216055	-0.366574393341726
B3 54 - 61 cm	0.185884511833234	-0.962729545593494	-0.192424664678638
B3 61 - 67 cm	0.355426430987167	-0.714847292891141	-0.018408454962224
B3 67 - 73 cm	0.429112041353264	-0.936623045473872	-0.10401930408524
B3 73 - 79 cm	0.307608019729899	-0.832450805588648	-0.120188574399396
B3 79 - 85 cm	0.459362568752285	-0.181038028611709	-0.178746260767103
B3 85 - 90 cm	0.63793931760529	1.53566392195926	-0.538563646706518
B3 90 - 95 cm	0.641733865886682	1.63558097293812	-0.552565321875372
B3 95 - 102 cm	0.849147307721511	1.40945744441639	-0.359610680433202
B3 102 - 110 cm	0.924561472069458	1.27711042771241	-0.199862869999766
B2 0 - 10 cm	-1.72762316025062	0.390676828058753	0.297209904020113
B2 10 - 17.5 cm	-0.53819655312725	-0.581711069453459	-0.701840319118469
B2 17.5 - 25 cm	0.350673788342737	-0.66628617482599	-0.107534641361183
B2 25 - 32.5 cm	0.450272628084469	-0.299805406658183	0.0534447836235677
B2 32.5 - 40 cm	0.0198590420979712	-0.0760137345866076	-0.0873251220091136
B2 43 - 51 cm	-1.17353471363093	0.191288603769064	0.0391197112132075
B2 59 - 69 cm	-1.74232931899253	0.0781975224372	0.867226685807276
B2 69 - 74 cm	-1.66144771812034	0.282643184151303	-0.0544025140929912
B2 74 - 80 cm	-1.46125612498465	0.278792377486865	-0.560629050457609
B2 80 - 85 cm	-1.7383131145873	0.249213647145052	-0.528605161092288
B2 85 - 90 cm	-1.45756920175365	0.201278245454611	-0.57323916622093
B2 90 - 95 cm	-1.39559390729031	0.215245091344257	-0.707091355941216
B2 95 - 100 cm	-1.35954009338321	0.0940292736766472	-0.448091246315404
B2 100 - 104 cm	-1.41570413047677	0.220282504139758	-0.645202273858343
B2 104 - 108 cm	-0.86791286475283	-0.200144811836961	-0.583093400796626
B1 0 - 7.5 cm	0.271191995263323	0.1116022739381	0.24721001304744
B1 7.5 - 15 cm	1.35823964620241	-0.24985296102967	0.350571453641561
B1 15 - 22.5 cm	1.53823060930171	-0.116225987934259	0.446758112296384
B1 22.5 - 30 cm	1.61721067149005	-0.330255037299748	0.405292357865951
B1 31.5 - 39 cm	1.44184358336806	-0.595279417693444	0.297877675702354
B1 40 - 47.5 cm	1.88269301331624	0.0785621673086083	0.570397430619768
B1 47.5 - 58 cm	1.07729181556172	-0.982049357621838	0.0855606476439327
B1 58 - 66 cm	1.60382518090042	-0.145085247672119	0.45960579195335
B1 66 - 72 cm	1.22653863363841	-0.465379468151475	0.269677984166531
B1 72 - 80 cm	-0.0876267751171507	-0.899492602046968	-0.116425503609968
B1 85 - 90 cm	-4.19253237028427	-0.34259657133402	1.28448942061627
B1 90 - 95 cm	-4.22061991065372	-0.380821987059903	1.41709531144882
B1 95 - 102 cm	-3.986318924247	-0.518552919675533	1.34933137634462
B1 102 - 110 cm	-3.84721155104831	-0.0686628123322466	0.0999809540727091
B1 110 - 115 cm	-2.39152503189249	1.96229184821575	0.827343538088331
B1 115 - 121 cm	-0.512355979270665	0.572181840552919	-0.530468506753881
B1 121 - 127 cm	0.519180870204634	-0.176361252223538	-0.398142957558924
U3 0 - 7.5 cm	0.581270466420169	-1.13685115968999	0.0900988431775815
U3 7.5 - 15 cm	0.332624869558444	-0.835526318737297	-0.248548826301236

U3 15 - 22.5 cm	0.280785462423725	-1.28203982724231	-0.19504449577392
U3 22.5 - 30 cm	0.116041280221733	-1.14058402162561	-0.303268194100373
U3 30 - 37.5 cm	0.131581545975197	-1.01479664660951	-0.254708106829293
U3 37.5 - 45 cm	-0.263301152106179	-0.846955543702143	-0.45712094543485
U3 45 - 53 cm	-0.936104657574038	-0.382671479680713	-0.585476638750803
U3 53 - 64 cm	0.285526110933803	-0.171023993251327	-0.457959694085462
U3 64 - 70 cm	1.07241301714104	-0.0557197077818492	0.0396872028329865
U3 70 - 75 cm	1.41416169896124	0.111198995078279	0.254857411542177
U3 75 - 80 cm	1.32534689627241	-0.255492113495384	0.221697583455245
U3 80 - 85 cm	1.48746929544828	-0.366853225977491	0.333920001529216
U3 85 - 90 cm	1.71068315222418	-0.316640114615832	0.502477501562614
U3 90 - 96 cm	1.63343219618652	-0.248005711594269	0.439227112733296
U3 96 - 101 cm	1.74210268355141	0.234884519857074	0.459035954943547
U3 101 - 106 cm	2.16218539485719	1.19051534784052	0.671268571114924
U3 106 - 110 cm	1.33518986869115	0.335344189733196	0.133115786202302
U3 110 - 114 cm	1.9116241492708	1.18138469808452	0.495705147857055
U1 0 - 5 cm	0.803971303920385	0.52865626398542	-0.209705539744404
U1 7 - 15 cm	0.811072882040621	0.255210299617119	-0.201173882672043
U1 17 - 23 cm	0.800601202496243	0.580422989782014	-0.170521832386132
U1 23 - 31 cm	0.85270437931884	0.17985457311159	-0.0686505950979235
U1 31 - 35 cm	0.922791296544158	0.0589824232203635	-0.138482685886514
U1 37 - 42 cm	1.49299239008226	0.145700297207129	0.311740062987035
U1 42 - 47 cm	1.24443876058526	-0.196806371334027	0.152275276659587
U1 47 - 53 cm	1.29170760757515	0.209982440856021	0.170979270812145
U1 53 - 55 cm	1.51250325642168	0.28437487218781	0.321257500444112
U1 57 - 62 cm	1.35019081717204	0.705325339266223	0.25784362193826
U1 62 - 68 cm	0.869939211008574	0.593246979757409	0.0769617970198236
U1 70 - 72 cm	1.19045214137952	1.31924351152433	0.269935286869985

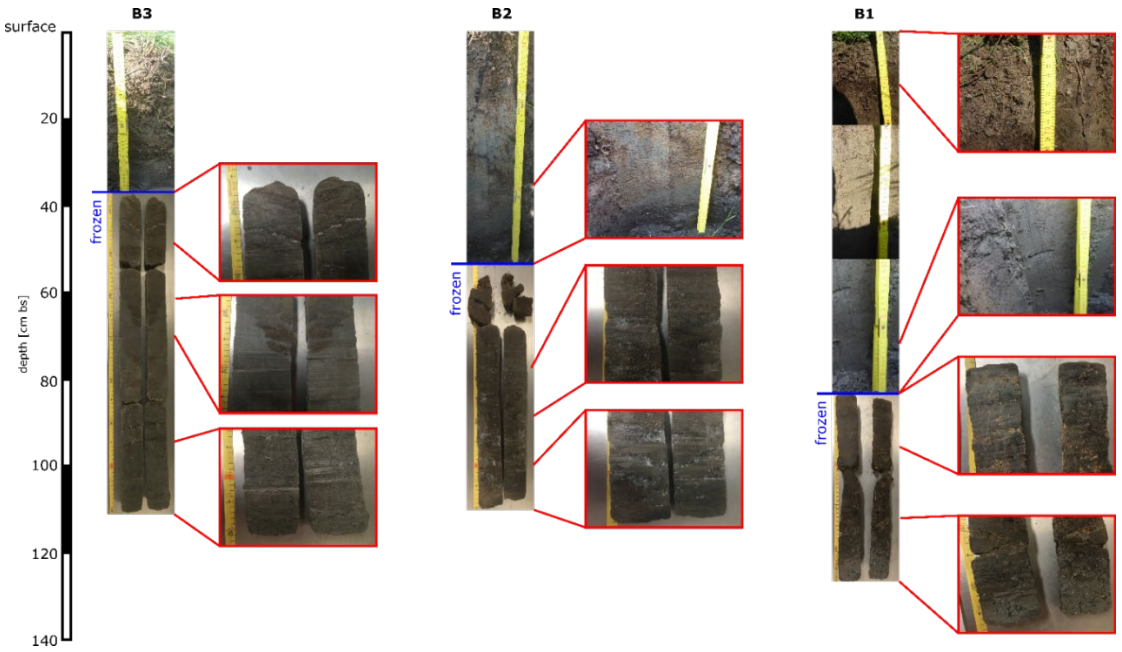

Supplementary figure S2-2 – Cores obtained from the partially drained thermokarst basin.

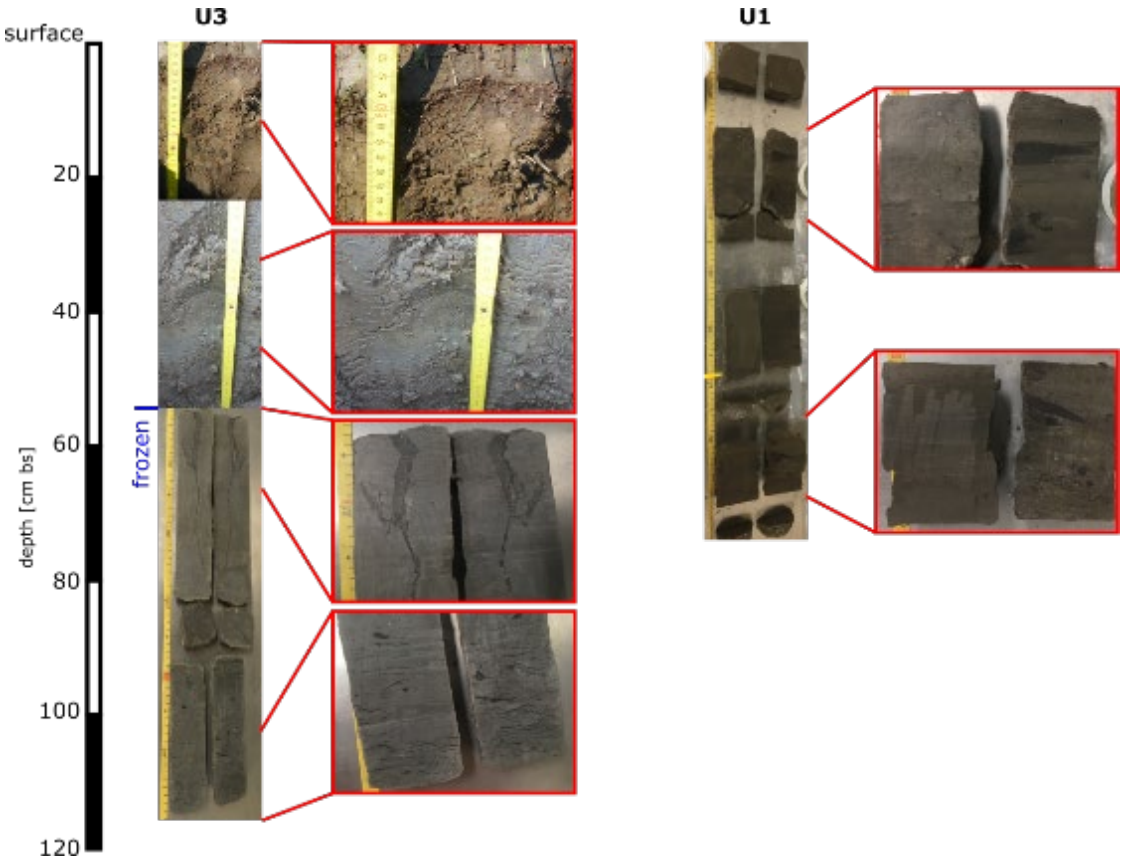

Supplementary figure S2-3 – Cores obtained from the Yedoma upland.

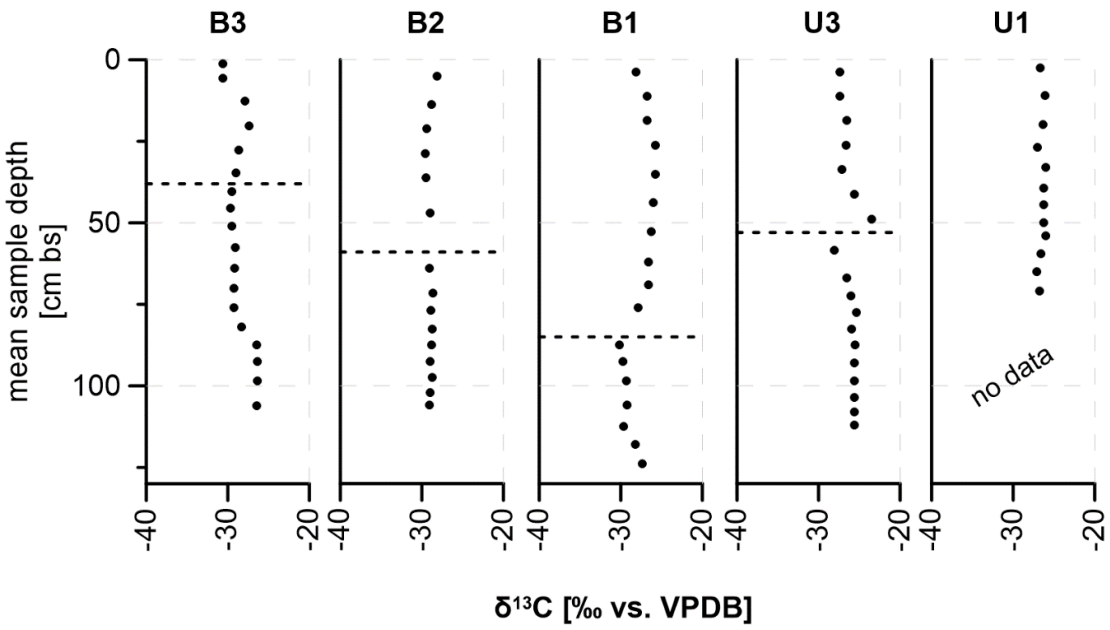

Supplementary figure S2-4 – $\delta^{13}C$ values, given in ‰ vs. VPDB, plotted over depth for all sampling sites; higher values indicate a less degraded state of the organic material; dashed lines mark the thaw depth found in July 2019.

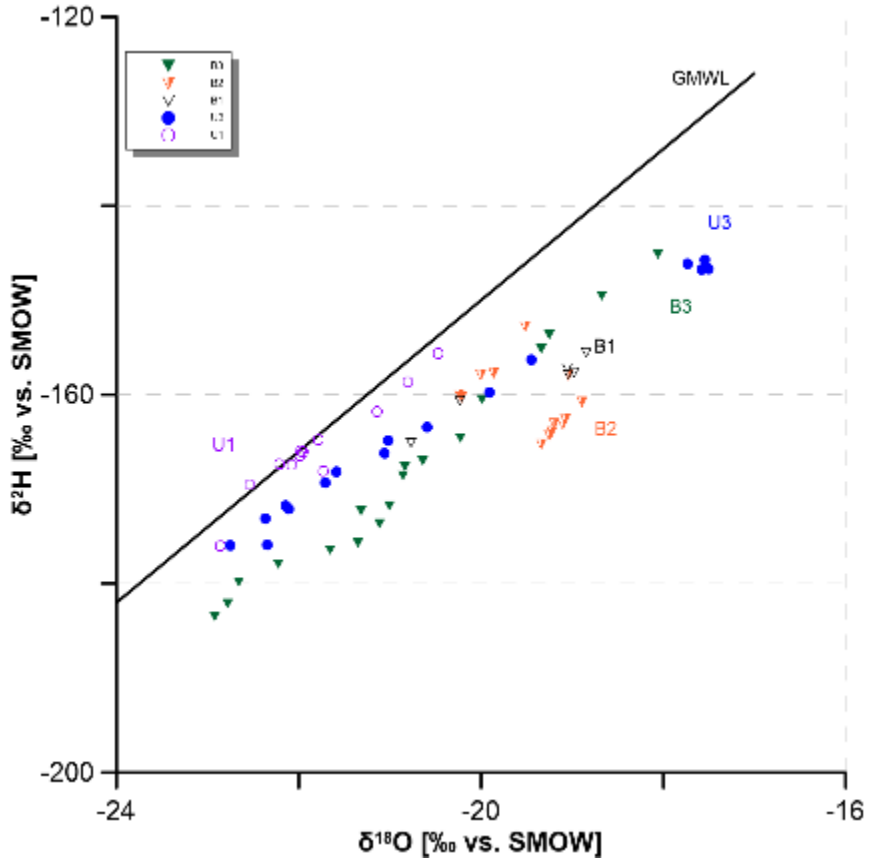

Supplementary figure S2-5 – $\delta^{18}O$ (stable oxygen isotopes) plotted versus $\delta^{2}H$ (stable hydrogen isotopes) along the global meteoric water line (GMWL, $\delta^{2}H=8*\delta^{18}O+10$); these measurements derive from pore water that was extracted from the samples using artificial plant roots (Rhizones) with a pore size of 0.15 µm and applied vacuum; not all samples could be analysed due to low water content.

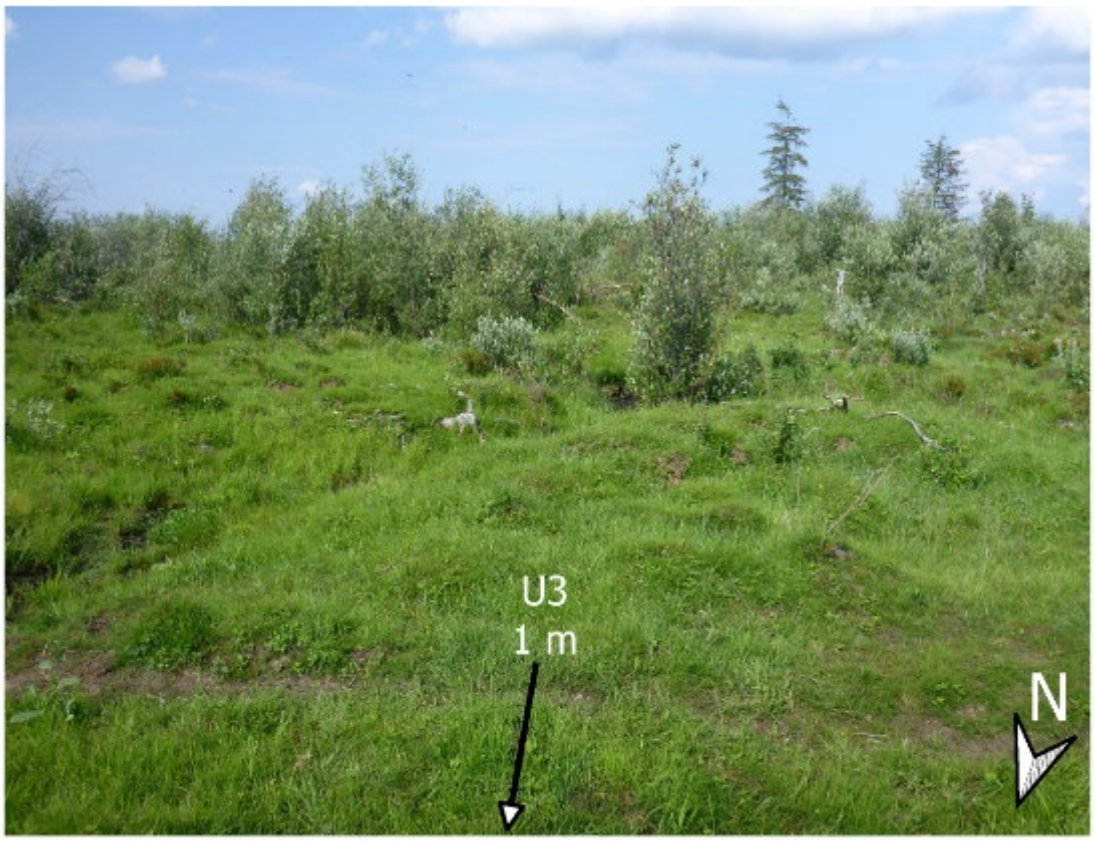

Supplementary figure S2-6 – Photograph of the surrounding landscape, taken from site U3; view direction is SSE; foreground: grasses and other short vegetation along with an animal path; background: willow shrubs with up to 2.5 m in height in the occasionally grazed neighborhood of the intensively grazed site U3.

Appendix IV Supplementary material to chapter 3: Impacts of Reindeer on Soil Carbon Storage in the Seasonally Frozen Ground of Northern Finland: a Pilot Study

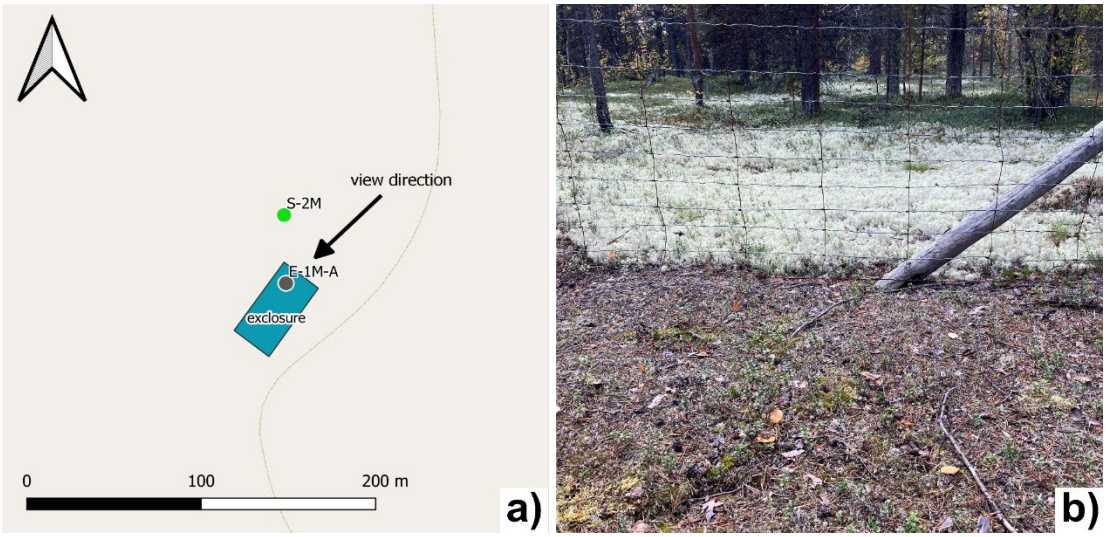

Supplementary figure S3-1 – a) Location of the exclosure site (E-1M-A) and adjacent site S-2M (© GoogleEarth); b) view of the fence surrounding the non-grazed exclosure site E-1M, with visible difference in vegetation, especially *Cladonia rangiferina*, as a result of reindeer presence/absence.

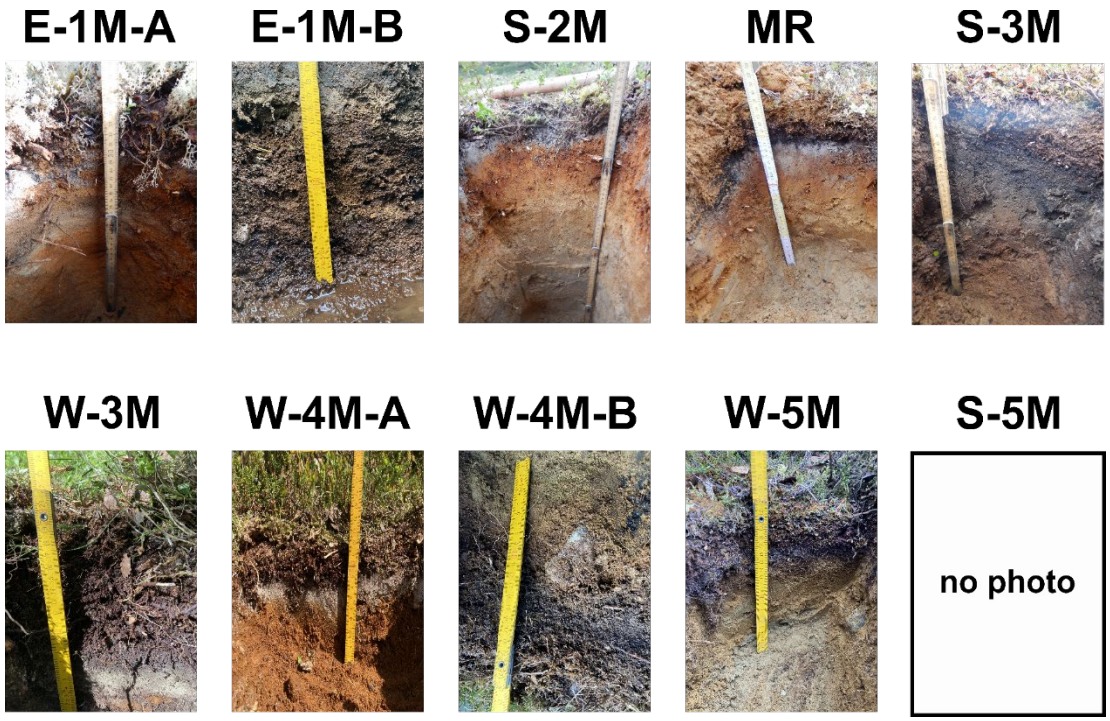

Supplementary figure S3-2 – Soil profiles at E-1M-A, E-1M-B, S-2M, MR, S-3M, W-3M, W-4M-A, W-4M-B, W-5M and S-5M.

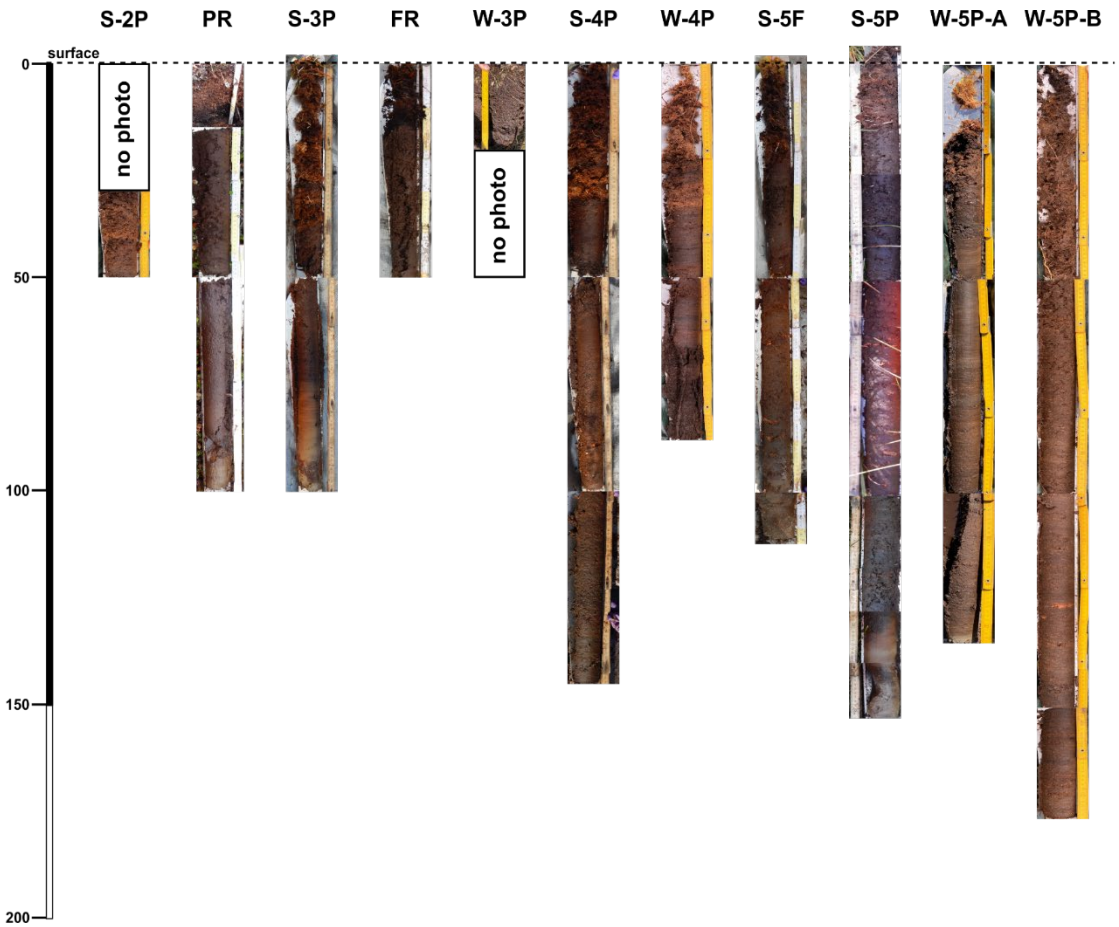

Supplementary figure S3-3 – Peat cores obtained from sites S-2P, PR, S-3P, FR, W-3P, S-4P, W-4P, S-5F, S-5P, W-5P-A and W-5P-B; depth is given in cm bs.

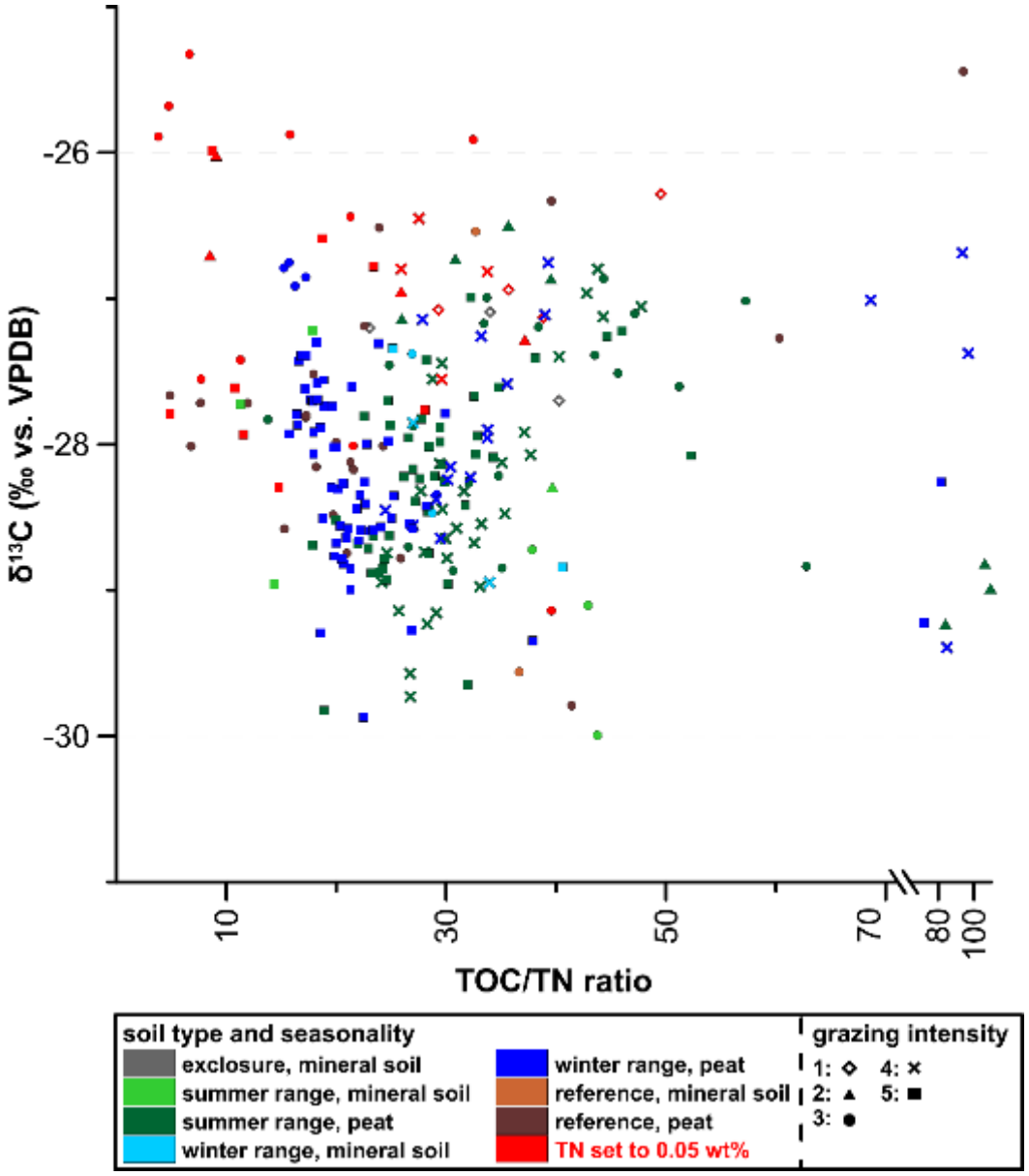

Supplementary figure S3-4 – TOC/TN ratios plotted versus $\delta^{13}C$ values for all samples with measurable $\delta^{13}C$; for calculating TOC/TN ratios, TN was set to 0.05 wt% if measurement was below detection limit (0.1 wt%) in order to show $\delta^{13}C$ values (samples marked in red); samples identified by grazing intensity (symbol), seasonality and soil type (colour).

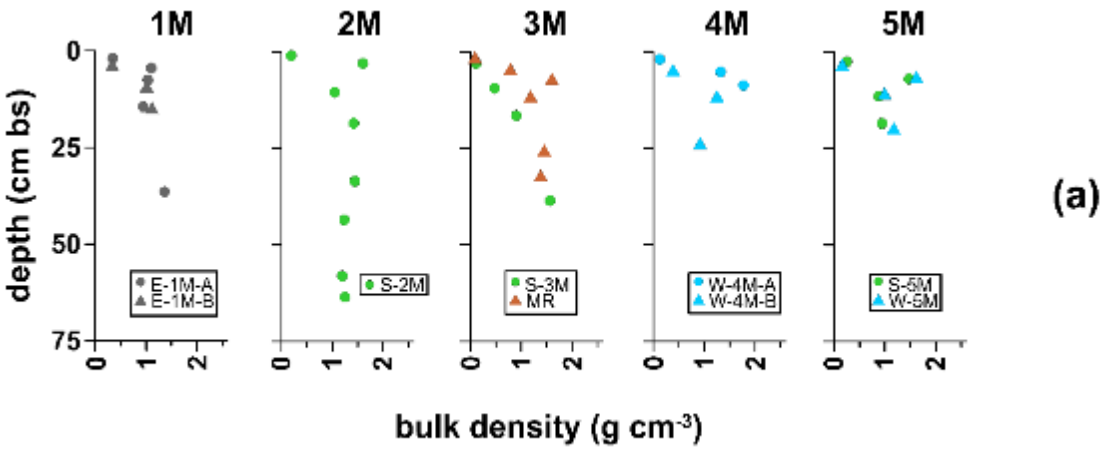

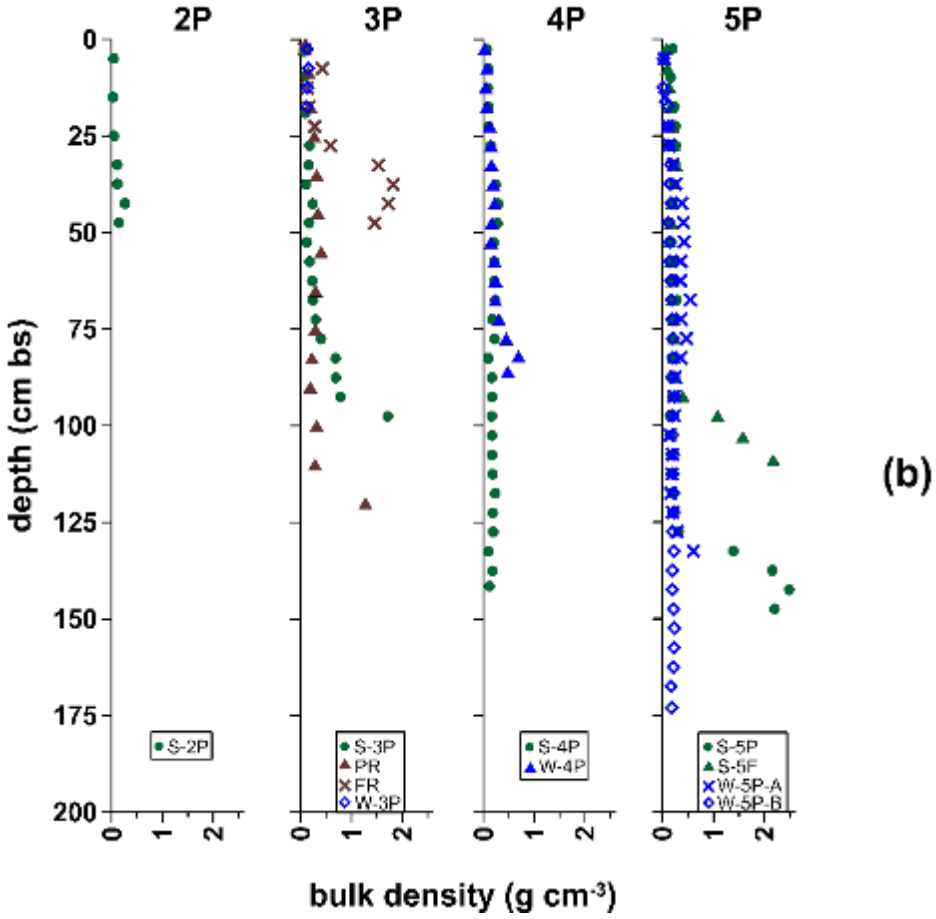

Supplementary figure S3-5 – Dry bulk density for all sampling sites except W-3M, plotted over depth; a) mineral soil sites; b) peat sites; green colours indicate summer sites, blue indicates winter sites, grey indicates exclosure sites, brown colours mark reference sites with natural grazing regime outside the reindeer fences.

Supplementary table S3-1 – Radiocarbon measurement data and calibrated ages.

site	mean sam-ple depth [cm bs]	material	^{14}C age [yr BP]	+/- [yr]	$F^{14}C$	+/- (abs)	calibrated ages (2σ)* [cal yr BP]	mean age* [cal yr BP]	soil layer
E-1M-A	7.5	plant / wood	modern		1.0217	0.0027			illuvial horizon
	36.5	bulk	3033	31	0.6855	0.0026	3150-3352	3239	pale sand
E-1M-B	9.25	plant / wood	modern		1.0179	0.0028			eluvial horizon
	14.75	plant / wood	modern		1.0930	0.0078			illuvial horizon
S-2M	10.5	bulk	592	23	0.9290	0.0026	585-645	605	illuvial horizon
	63.5	bulk	4209	33	0.5921	0.0025	4687-4762	4738	pale sand
S-2P	25	plant / wood	modern		1.1228	0.0031			fresh moss peat
	47.5	plant / wood	325	22	0.9603	0.0027	347-458	387	decomposed peat
S-3M	9.5	plant / wood	modern		1.0174	0.0026			organic-rich soil
	38.5	bulk	3555	24	0.6424	0.0019	3822-3922	3853	brownish sand
S-3P	19.0	plant / wood	102	21	0.9874	0.0026	30-141	113	light moss peat
	42.5	plant / wood	1747	22	0.8045	0.0022	1572-1706	1639	dark sandy peat
	67.5	plant / wood	3468	22	0.6494	0.0018	3687-3778	3750	dark sandy peat
	87.5	bulk	4519	25	0.5698	0.0018	5051-5193	5155	dark sandy peat
S-4P	27.5	plant / wood	694	21	0.9173	0.0024	646-674	660	light moss peat

	57.5	plant / wood	6823	24	0.4277	0.0013	7602-7692	7650	dark peat
	97.5	plant / wood	8152	25	0.3625	0.0011	8999-9126	9063	dark peat + macro organics
	141.5	plant / wood	8798	26	0.3344	0.0011	9684-9913	9815	dark, compact peat
S-5F	22.5	plant / wood	864	21	0.8980	0.0023	723-793	759	moss peat / dark peat transition
	52.5	plant / wood	6724	24	0.4330	0.0013	7566-7621	7589	peat + macro organics
	82.5	plant / wood	8593	25	0.3431	0.0011	9526-9559	9543	peat / sand transition
	92.5	plant / wood	8714	26	0.3380	0.0011	9549-9763	9643	organic-rich sand
S-5P	17.5	plant / wood	1213	21	0.8598	0.0023	1066-1170	1129	peat
	82.5	plant / wood	6872	24	0.4251	0.0013	7661-7781	7698	peat + macro organics
	127.5	plant / wood	8201	25	0.3603	0.0011	9163-9275	9147	peat / sand transition
	132.5	plant / wood	8197	25	0.3604	0.0011	9026-9150	9137	peat / sand transition
	147.5	bulk	4841	25	0.5474	0.0029	5571-5602	5584	greyish sand
S-5M	11.5	bulk	modern		1.0192	0.0029			illuvial horizon
	18.5	bulk	776	23	0.9079	0.0027	673-725	697	pale sand
W-3P	12.5	plant / wood	155	22	0.9809	0.0027	0-283	153	dark peat
	22.5	plant / wood	1038	23	0.8788	0.0025	917-972	943	dark peat
W-3M	20.5	plant / wood	modern		1.0189	0.0028			illuvial horizon
W-4P	27.5	plant / wood	128	22	0.9841	0.0027	11-150	108	moss peat

	57.5	plant / wood	2604	48	0.7231	0.0043	2693-2788	2736	dark, brown peat
	86.0	plant / wood	4256	48	0.5887	0.0035	4792-4888	4828	dark, sandy peat
W-4M-A	8.75	plant / wood	modern		1.0072	0.0089			illuvial horizon
W-4M-B	23.75	plant / wood	modern		1.0121	0.0037			pale / yellowish sand
W-5P-A	32.5	plant / wood	536	48	0.9355	0.0056	503-566	550	brown peat
	82.5	plant / wood	7397	50	0.3982	0.0025	8161-8344	8230	brown peat
	132.5	plant / wood	8650	50	0.3407	0.0021	9532-9746	9613	peat / sand transition
W-5P-B	47.5	plant / wood	1567	60	0.8228	0.0061	1342-1548	1453	dark peat
	92.5	plant / wood	2458	48	0.7364	0.0044	2362-2622	2541	dark peat
	137.5	plant / wood	4282	48	0.5868	0.0035	4804-4979	4852	dark peat
	173.0	plant / wood	6332	49	0.4546	0.0028	7160-7337	7256	light-brown peat
W-5M	6.5	plant / wood	modern		1.0298	0.0061			eluvial horizon
	19.75	plant / wood	modern		1.0141	0.0060			pale sand
MR	7.0	bulk	281	23	0.9656	0.0028	361-430	381	eluvial horizon
	32.0	bulk	3067	34	0.6827	0.0029	3206-3366	3283	pale sand
PR	17.5	plant / wood	176	21	0.9783	0.0026	162-225	184	dark peat
	65.0	plant / wood	5606	24	0.4976	0.0015	6308-6410	6364	dark peat
	110.0	bulk	7909	27	0.3736	0.0013	8599-8782	8714	dark peat, decomposed

FR	7.5	plant / wood	modern		1.3858	0.0034			dark peat + roots
	22.5	plant / wood	modern		1.0857	0.0028			dark peat + roots
	47.5	bulk	3224	25	0.6694	0.0021	3383-3469	3427	greyish sand

*calibrated using Calib 8.2 (Stuiver *et al*. 2021) equipped with IntCal20 (Reimer *et al*. 2020)

Appendix V Supplementary material to chapter 4: A Pilot Study of Lipid Biomarkers to Trace Recent Large Herbivore Influence on Soil Carbon in Permafrost and Seasonally Frozen Arctic Ground

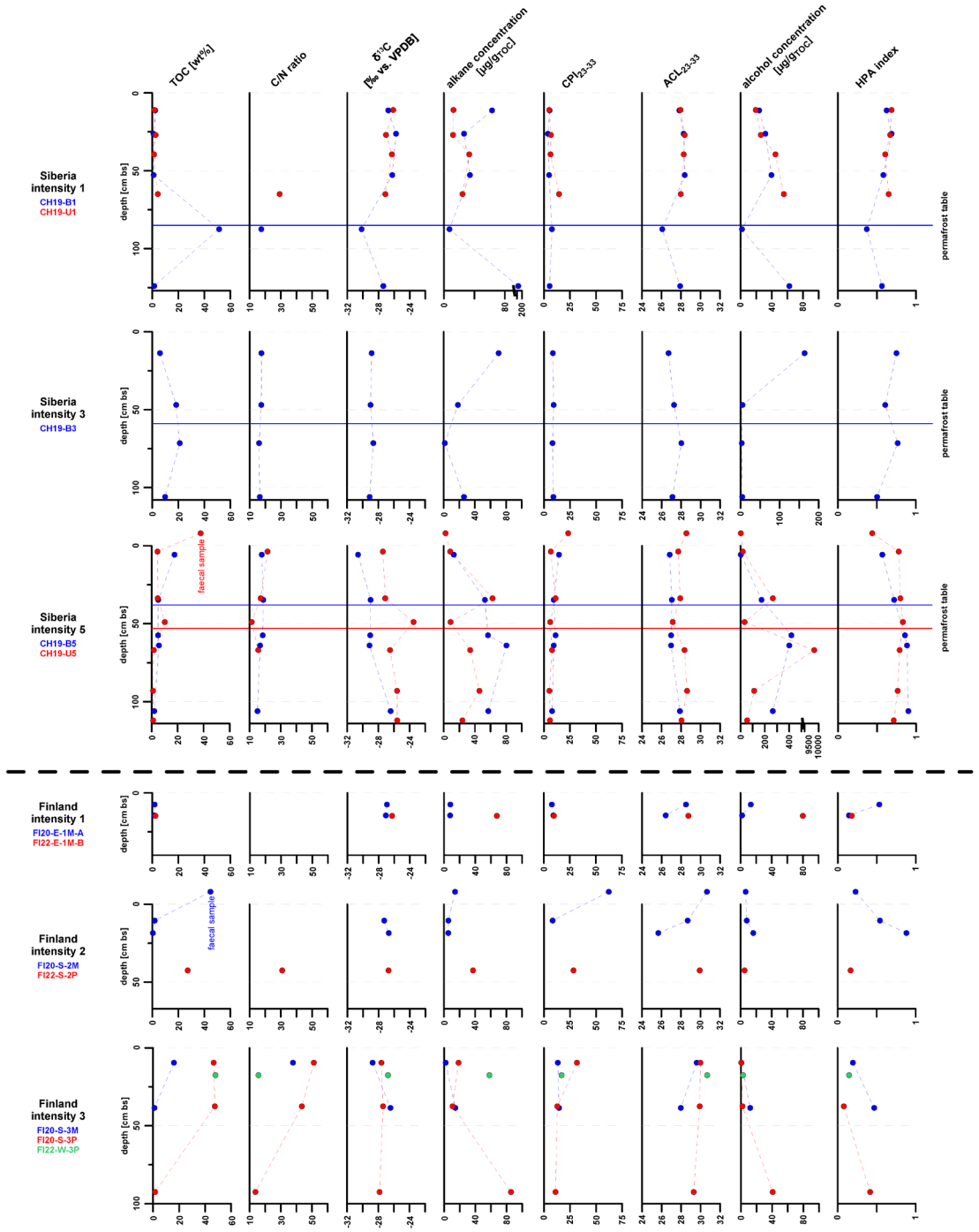

Figure S4-1a – Sites CH19-B1 to FI22-W-3P: parameters total organic carbon (TOC), carbon-to-nitrogen ratio (C/N), stable carbon isotope ratio ($\delta^{13}C$), total *n*-alkane concentration, carbon preference index for *n*-alkane chain lengths between 23 and 33 carbon atoms ($CPI_{23\text{-}33}$), average chain length for *n*-alkanes with chain length between 23 and 33 carbon atoms ($ACL_{23\text{-}33}$), total *n*-alcohol concentration and higher plant alcohol index (HPA), plotted over depth for each site, grouped by study area and grazing intensity; horizontal lines mark the permafrost table, if applicable.

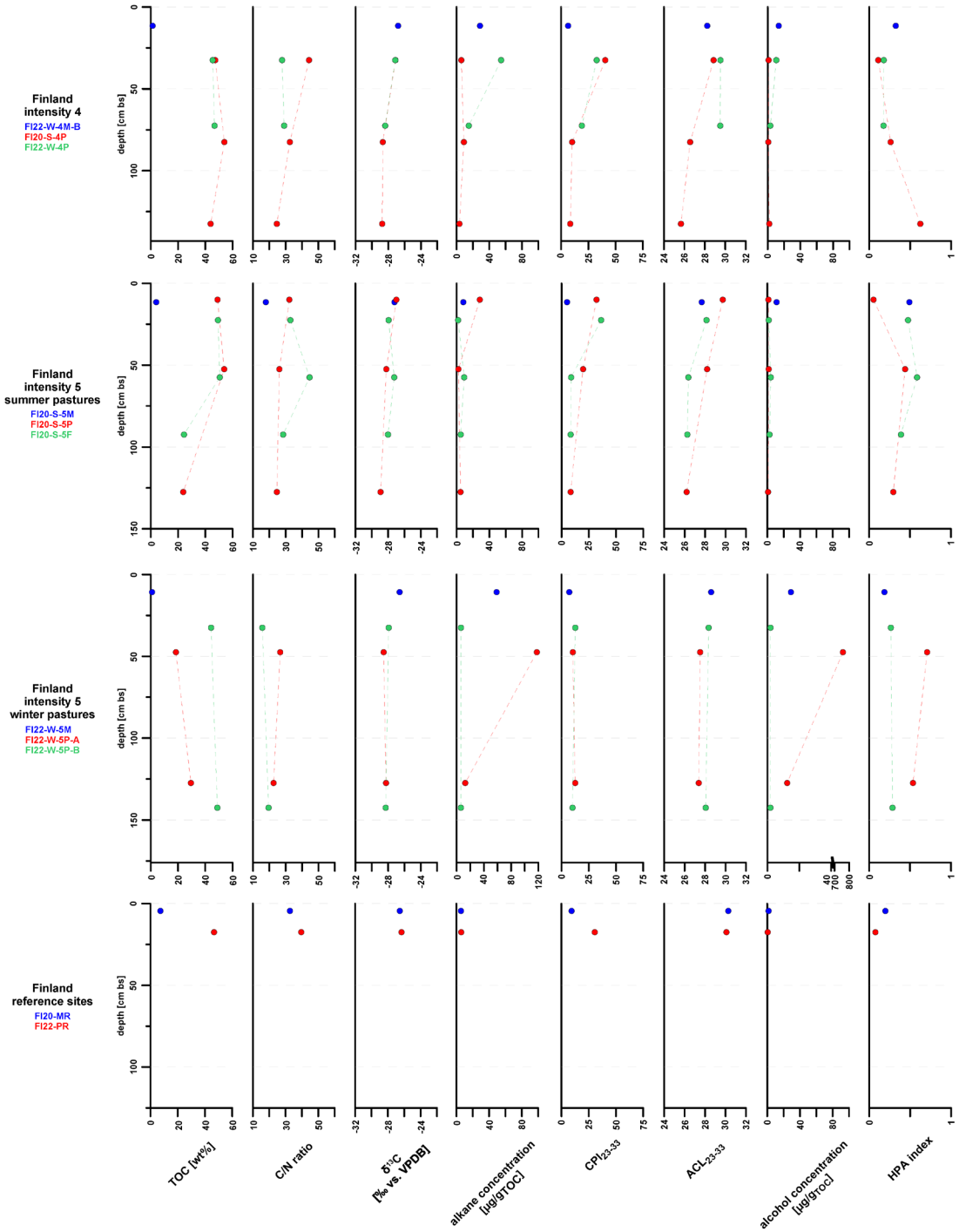

Figure S4-1b – Sites FI22-W-4M-B to FI20PR: parameters total organic carbon (TOC), carbon-to-nitrogen ratio (C/N), stable carbon isotope ratio ($\delta^{13}C$), total *n*-alkane concentration, carbon preference index for *n*-alkane chain lengths between 23 and 33 carbon atoms ($CPI_{23\text{-}33}$), average chain length for *n*-alkanes with chain length between 23 and 33 carbon atoms ($ACL_{23\text{-}33}$), total *n*-alcohol concentration and higher plant alcohol index (HPA), plotted over depth for each site, grouped by study area and grazing intensity; horizontal lines mark the permafrost table, if applicable.

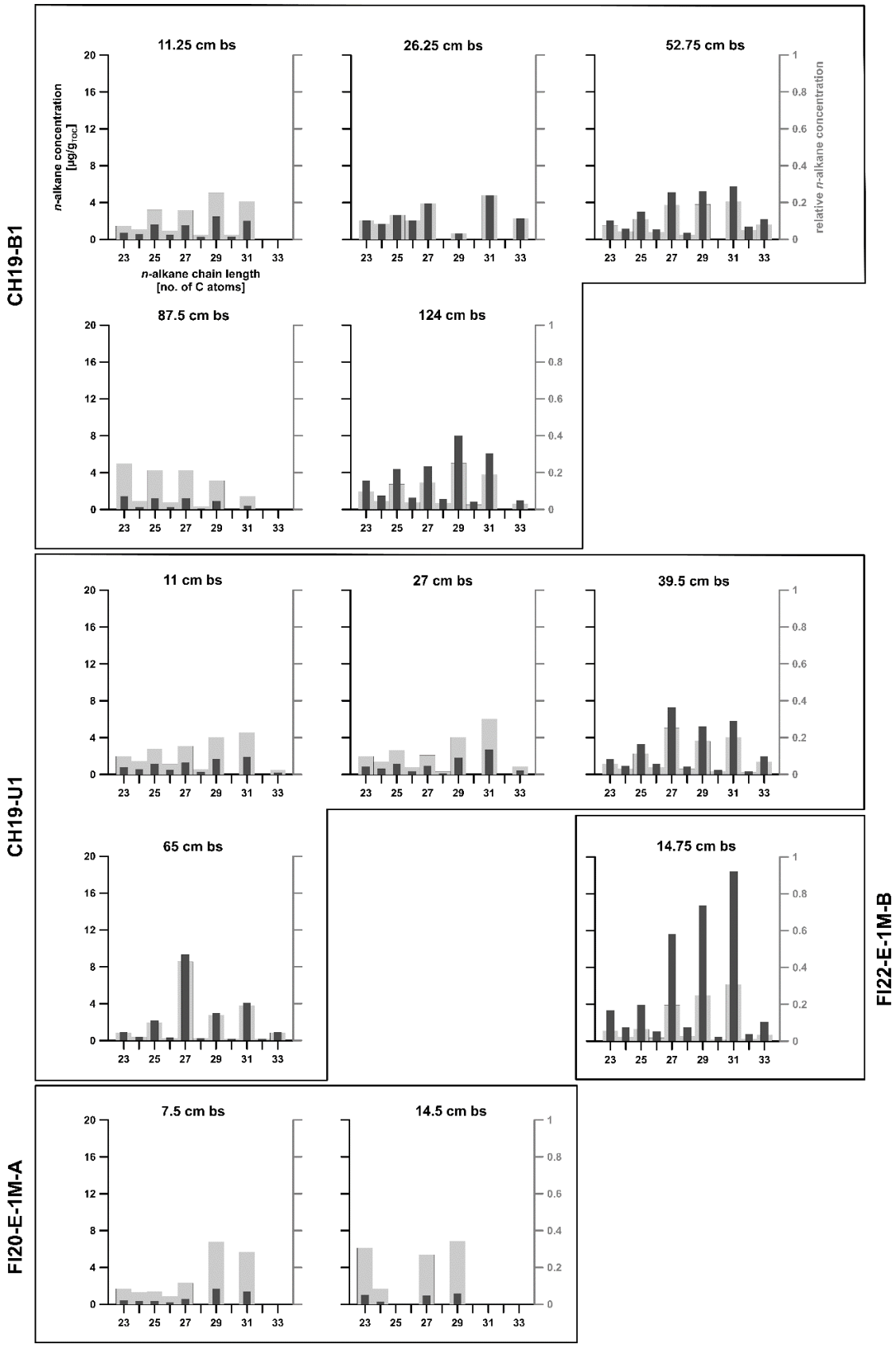

Figure S4-2.1 – *n*-alkane concentrations (left y-axis: absolute concentration in µg/g_{TOC}; right y-axis: relative concentration) for chain lengths 23 to 33 for grazing intensity 1-sites.

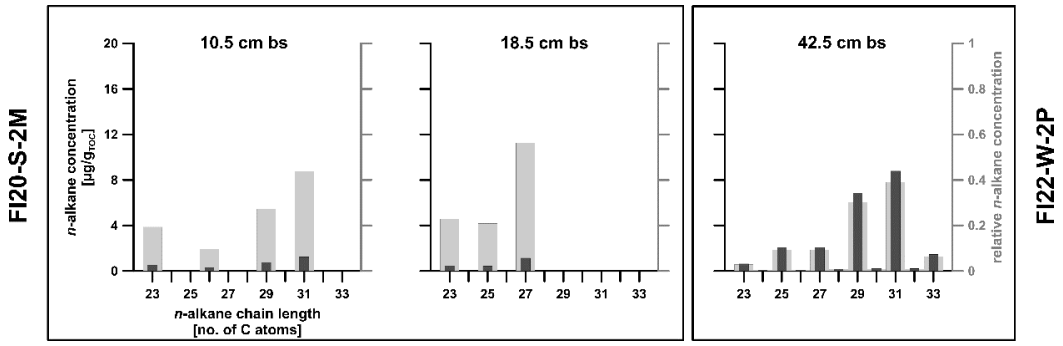

Figure S4-2.2 – *n*-alkane concentrations (left y-axis: absolute concentration in µg/g_{TOC}; right y-axis: relative concentration) for chain lengths 23 to 33 for grazing intensity 2-sites.

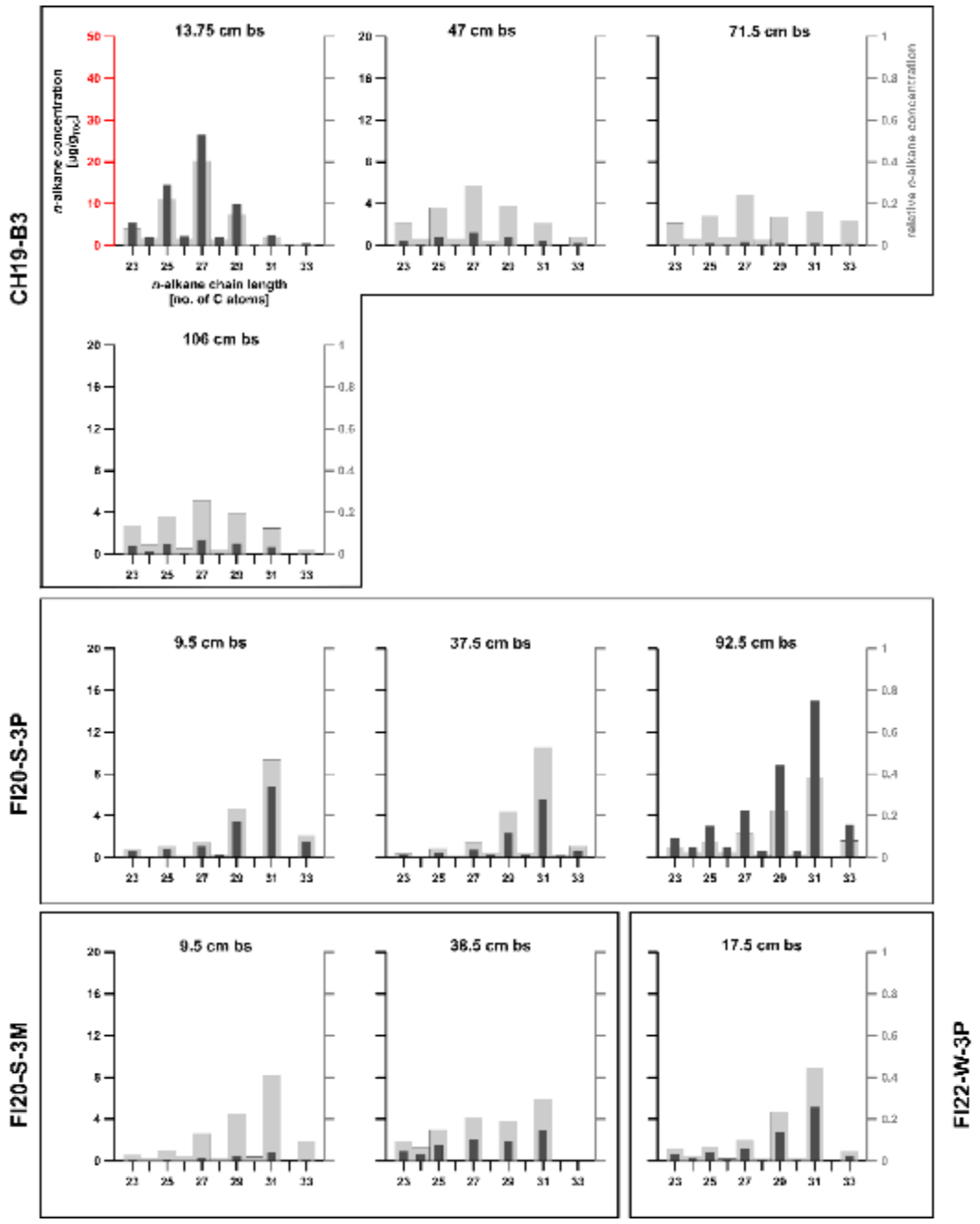

Figure S4-2.3 – *n*-alkane concentrations (left y-axis: absolute concentration in µg/g_{TOC}; right y-axis: relative concentration) for chain lengths 23 to 33 for grazing intensity 3-sites.

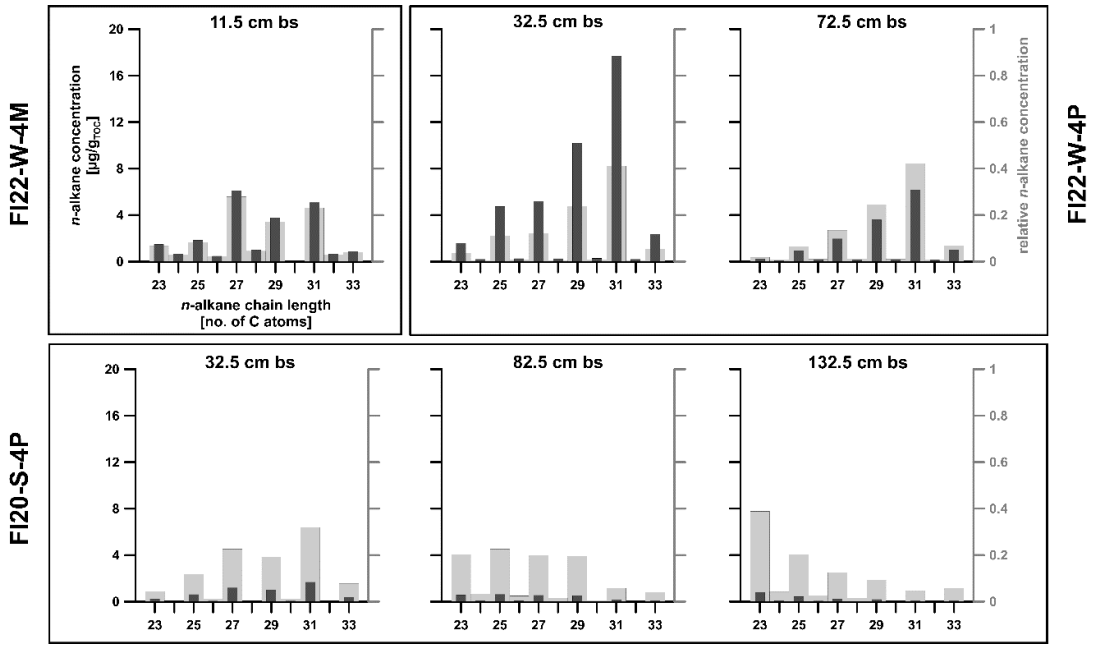

Figure S4-2.4 – *n*-alkane concentrations (left y-axis: absolute concentration in µg/g_{TOC}; right y-axis: relative concentration) for chain lengths 23 to 33 for grazing intensity 4-sites.

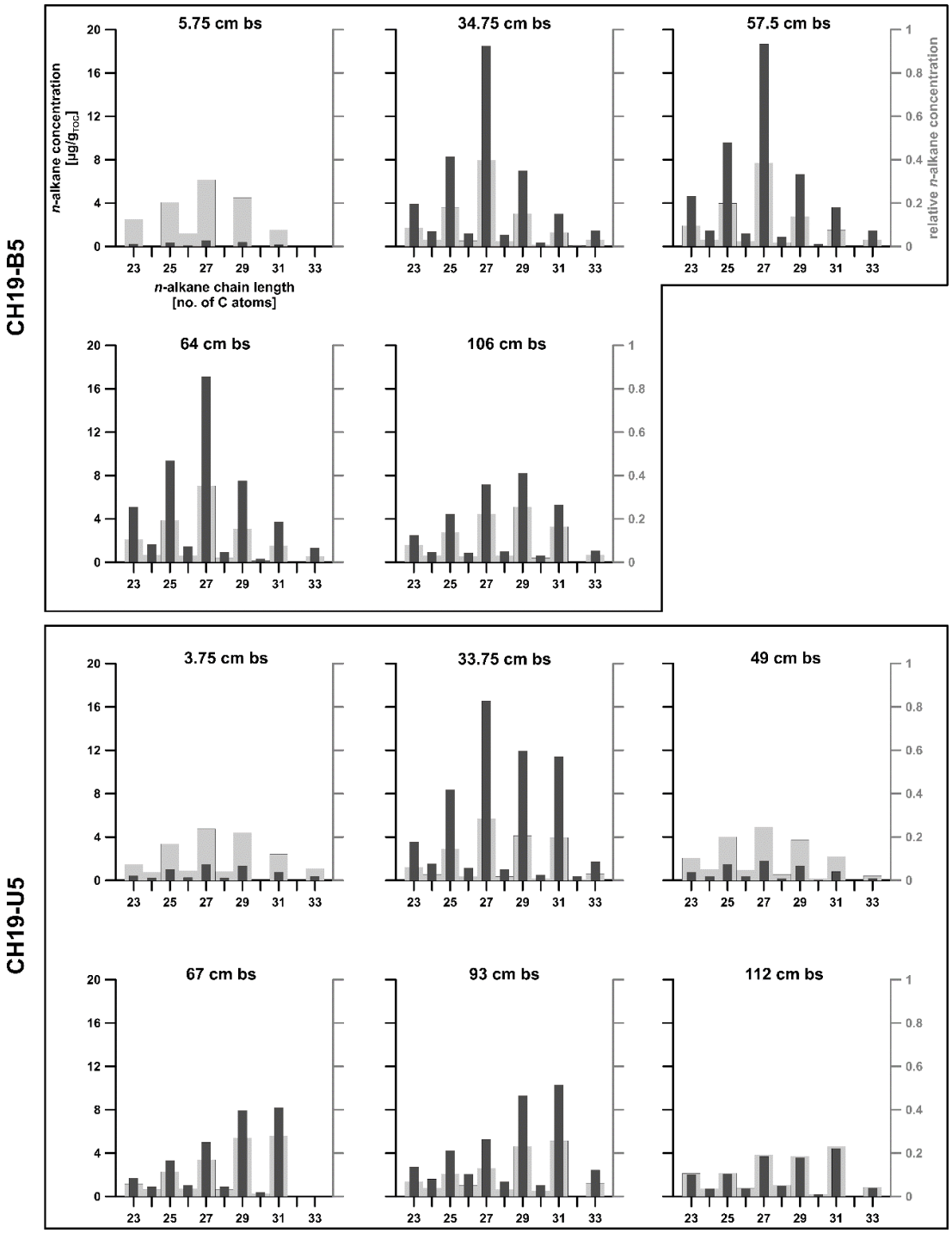

Figure S4-2.5 – *n*-alkane concentrations (left y-axis: absolute concentration in µg/g_{TOC}; right y-axis: relative concentration) for chain lengths 23 to 33 for **permafrost-affected** grazing intensity 5-sites.

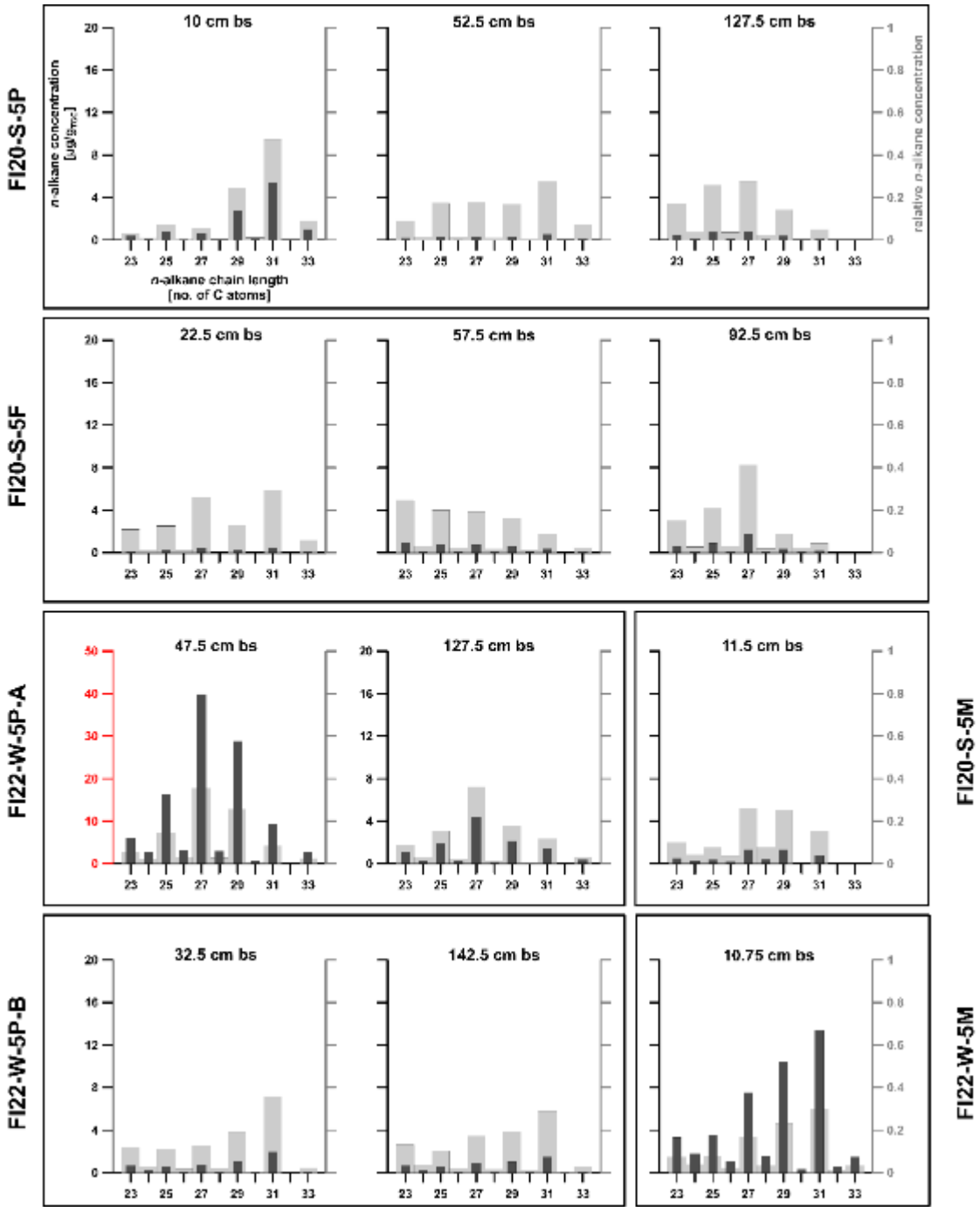

Figure S4-2.6 – *n*-alkane concentrations (left y-axis: absolute concentration in µg/g_{TOC}; right y-axis: relative concentration) for chain lengths 23 to 33 for **seasonally frozen ground** grazing intensity 5-sites.

Appendix VI Supplementary material to Appendix IV: Organic Carbon Characteristics in Ice-rich Permafrost in Alas and Yedoma Deposits, Central Yakutia, Siberia

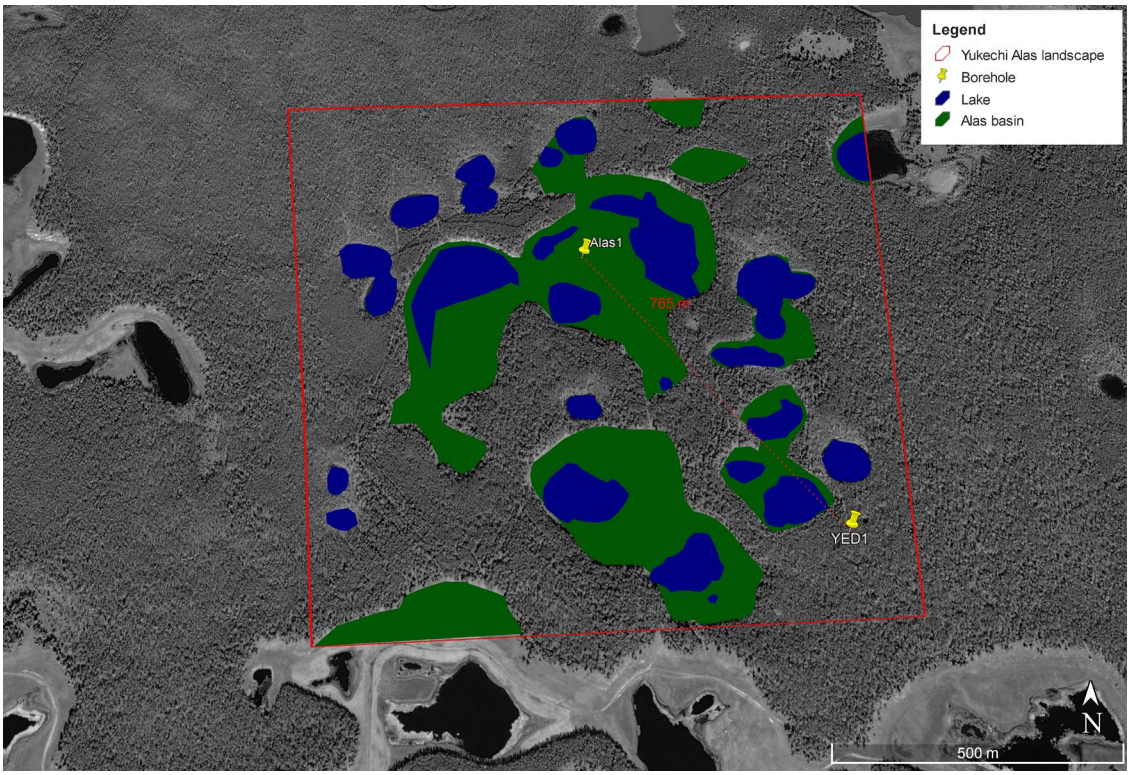

Figure S-IV-1 – Digital mapping of the Yukechi Alas landscape (red); lakes were digitalised in blue, Alas basins were digitalised in green; sampling locations Alas1 and YED1 marked in yellow; the 765 m distance between YED1 and Alas1 is marked by a red dotted line; satellite image: © Google Earth.

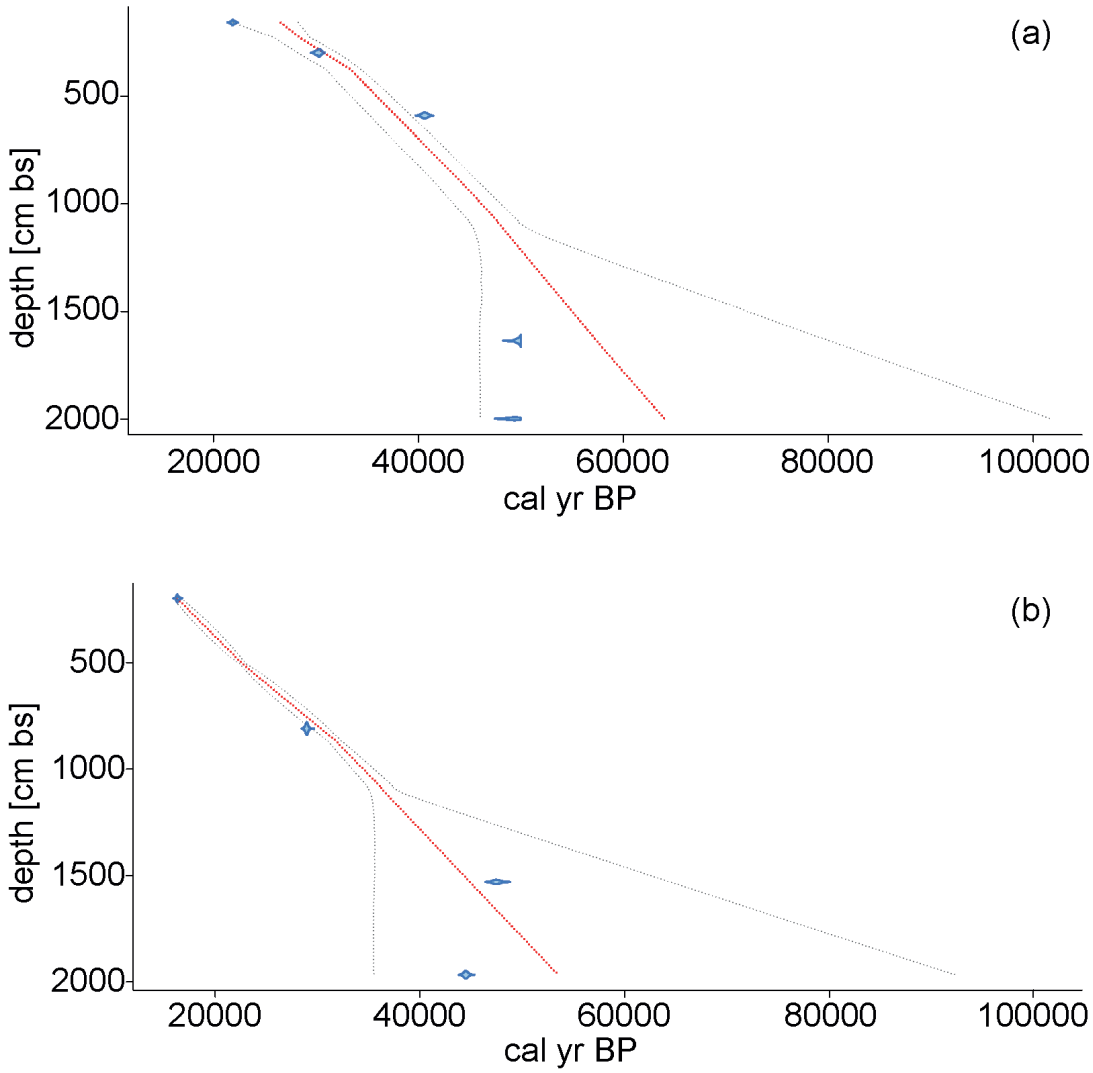

Figure S-IV-2 – Age-depth model for YED1 (a) and Alas1 (b); radiocarbon ages in blue with uncertainties; median in red; model range indicated by grey dotted lines; created with the Bacon package in the R environment.

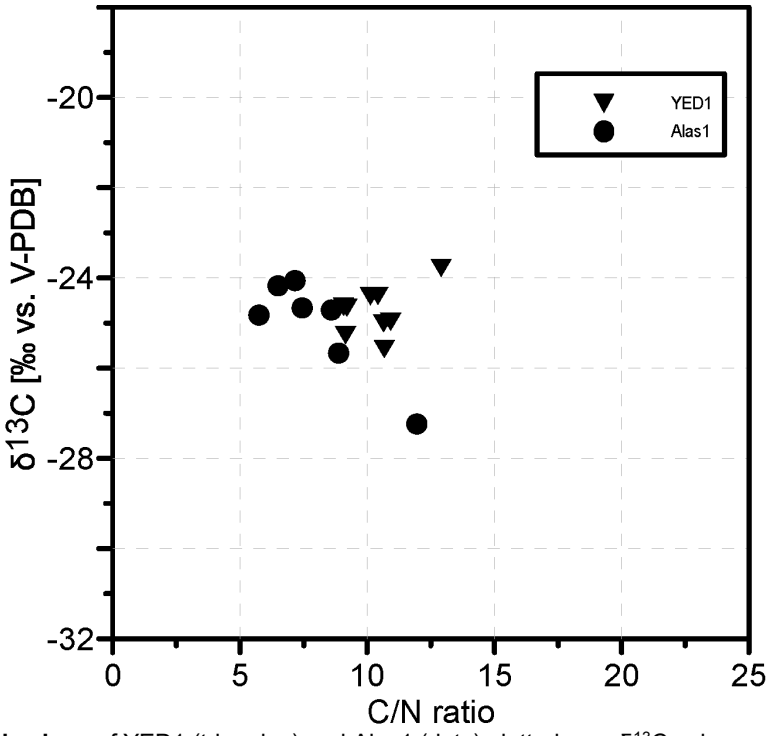

Figure S-IV-3 – C/N values of YED1 (triangles) and Alas1 (dots) plotted over $\delta^{13}C$ values.

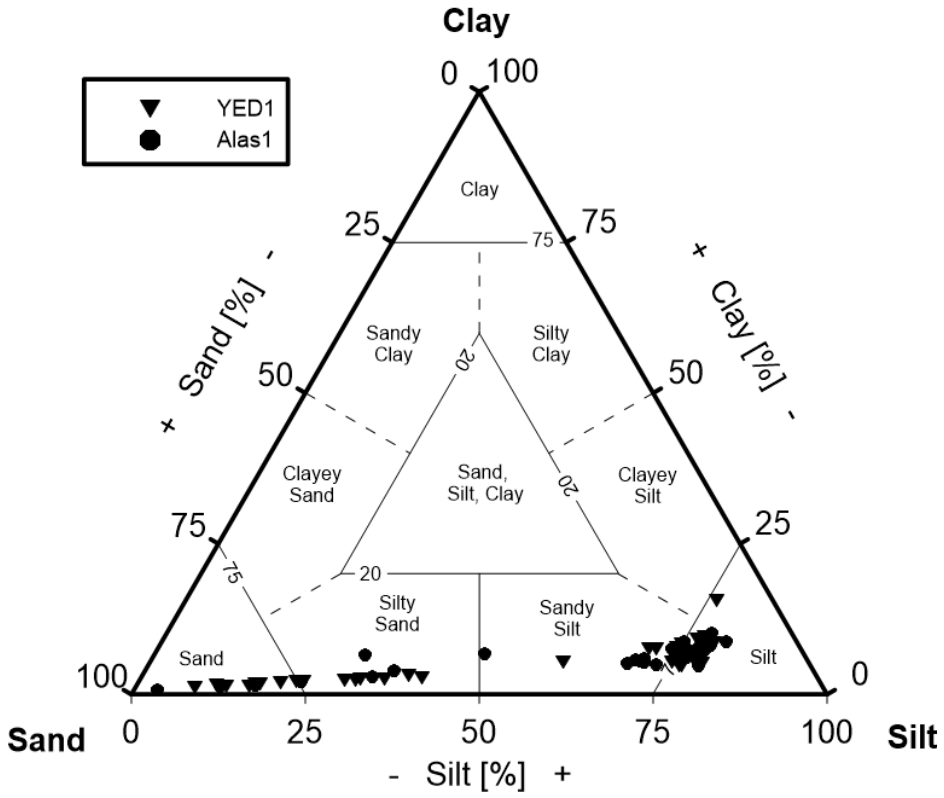

Figure S-IV-4 – Sediment triangle after Shepard showing the grain size composition.

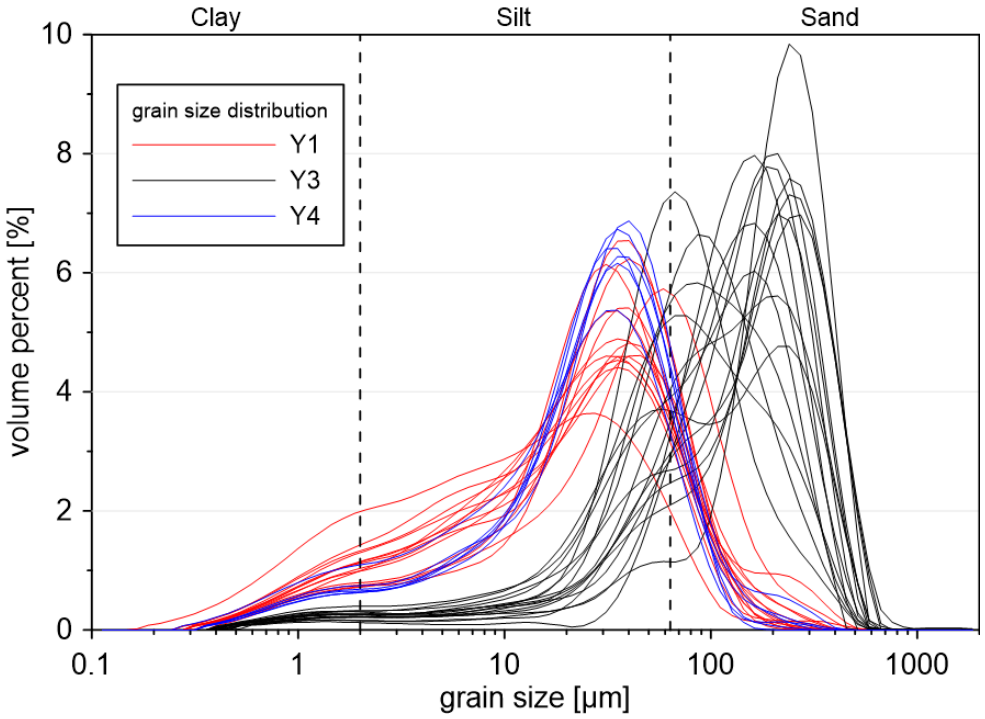

Figure S-IV-5 – Grain size distribution for the YED1 core; Y1 to Y4 indicate the different stratigraphic units; core unit Y2 did not hold enough sediment.

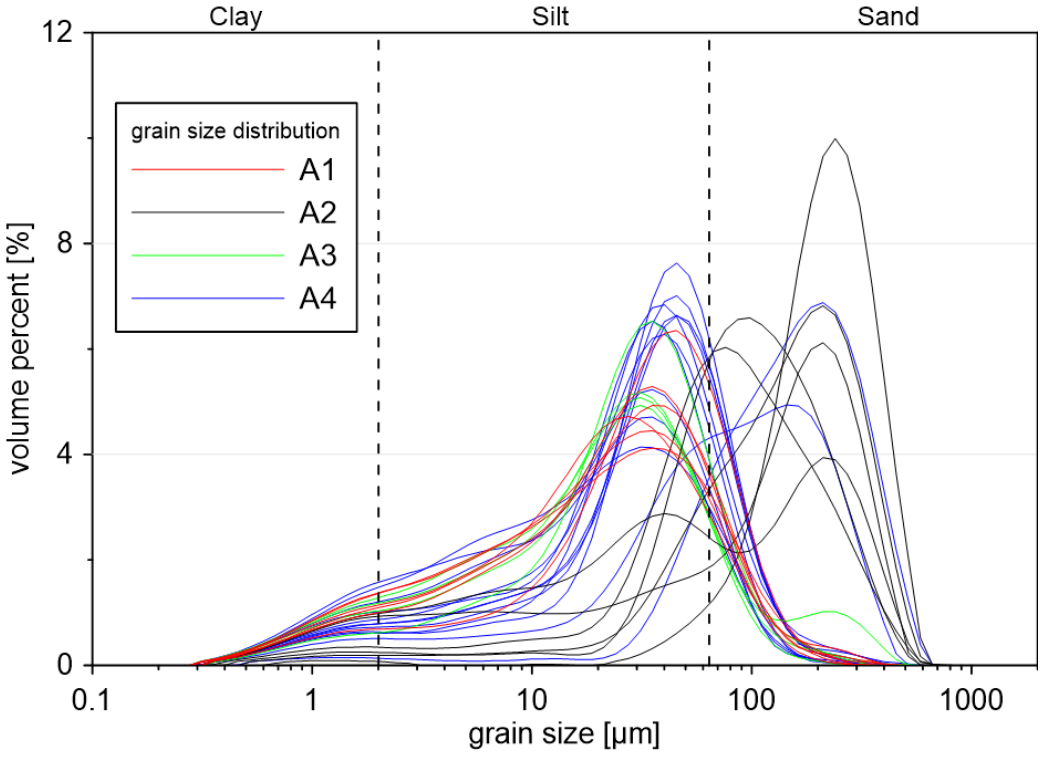

Figure S-IV-6 – Grain size distribution for the Alas1 core; A1 to A4 mark the different stratigraphic units.

Figure S-IV-7 – Photo of a large ice wedge found on the Abalakh Terrace, Central Yakutia, approximately 30 km east of the Yukechi Alas landscape; photo by Mathias Ulrich.

Acknowledgements - Danksagung

While this dissertation is my own work, it would not be possible to do such work without great support from a number of people around me.

First, I would like to thank my PhD committee, namely **Dr. Jens Strauss, Prof. Dr. Guido Grosse, Prof. Dr. J. Otto Habeck, Dr. Mathias Ulrich** and **Dr. Kai Mangelsdorf**.

Staying in this order, my special thanks goes to **Dr. Jens Strauss** for being my mentor, helper, motivator, guide and teacher. Already during my Master thesis he provided incredible valuable advice and helped me navigating through academia both scientifically and in formal and bureaucratic regards. When I lost focus during writing or ran out of ideas, he was always there with a fresh perspective to help me move on. His guidance involved a lot of personal advice for building networks and managing scientific work and having a young family at the same time. I felt a great balance between support, if needed, and independence. Writing this thesis would have simply not been possible at all without him.

Prof. Dr. Guido Grosse did a great job as my supervisor and I am really thankful that he provided the opportunity to work at Alfred Wegener Institute. He always helped me to keep an eye on the greater picture and realising the impact and value that my work could have. He pushed me to make potentially important personal contacts, and provided such contacts when necessary.

There are things I never thought about when planning this thesis, and I am really grateful to **Prof. Dr. J. Otto Habeck** for bringing these things to the table when discussing my work progress. Not only did I not have expertise in social science, but I never thought about how and in which way my research might be valuable to people. He made me realise that working in the Arctic also brings a type of responsibility towards Arctic communities and their ways of life, which I swear to always consider in my future endeavours.

I want to thank **Dr. Mathias Ulrich** for being an incredible backup contact. By backup I mean that he never pushed into discussions, but whenever I needed another opinion, help, expertise etc. he was just there. Emphasizing details everyone else had overseen is an incredible ability of him that helped me consider such details, providing a more complete picture in my research.

A great thanks goes to **Dr. Kai Mangelsdorf**, who guided me through the field of organic geochemistry and provided exceptionally valuable input in discussing and understanding lipid biomarker signals.

I would further like to thank the **Potsdam Graduate School** for funding my PhD project and the **Geo.X network** and **POLMAR** (Graduate School for Polar and Marine Research) for providing additional resources for travel and training, which both helped me to gain a more complete insight into a scientist's life.

Special thanks go to **Dr. Mathias Göckede**, **Dr. Juri Palmtag**, **Dr. Matthias Fuchs** and **Johanna Schwarzer** who were the key to my three field campaigns within this project. For all

of them, their enthusiasm and detailed knowledge on various topics enabled me to collect all the samples I needed for and used in this thesis.

For successful research, it is extremely important to have great logistical support, namely **Volkmar Aßmann**, who ensured optimal preparation and safe return for all samples and material needed in the field.

I am also very grateful to **Dr. Michael Angelopoulos** for last-minute language checks.

Along with practical support, I feel that very different levels of discussion are needed for successful and meaningful research. Apart from discussions among co-authors while working on a manuscript, off-desk discussions about general ideas or interesting questions are vital. For such discussions I would like to thank my colleagues at AWI, and especially **Dr. Juliane Wolter**, **Maren Jenrich**, **Dr. Lona van Delden**, **Dr. Claire Treat**, **Dr. Loeka Jongejans**, and **Tabea Rettelbach**. But of course, such discussions were never limited to AWI, so I would also like to thank **Dr. Nina Döring**, **Prof. Dr. Bruce C. Forbes** and **Dr. Jeppe A. Kristensen**.

Treating and analysing large sets of samples in several laboratories requires a lot of helping hands, namely **Justin Lindemann**, **Jonas Sernau**, **Angelique Opitz**, **Dyke Scheidemann**, **Jonas Kaltschmidt**, **Alena Kalitzki**, **Antje Eulenburg**, **Flavio Maggioni**, **Cornelia Karger**, **Anke Kaminsky** and **Mikaela Weiner**. I am very thankful for their invaluable support throughout these past years.

Mein größter Dank geht an meine Frau **Josephine**, die mich geduldig in den unterschiedlichsten Phasen der vergangenen Jahre unterstützt hat, an meinen Sohn **Jonne**, der mein absoluter Ruhepol und Motivator für diese Arbeit war, sowie an meine Eltern **Kerstin** und **Hajü**, die nach wie vor ein großartiges Auffangnetz für alle Eventualitäten sind.